RHENIUM AND TECHNETIUM RADIO-ISOTOPE COMPLEXES LINKED TO BIOLOGICALLY ACTIVE MOLECULES

1240/8

by

AMANDA-LEE VOLMINK

A thesis submitted to meet the requirements for the degree of
MAGISTER SCIENTIAE

In the
DEPARTMENT OF CHEMISTRY
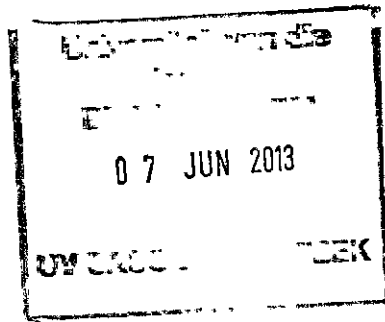## FACULTY OF SCIENCE

at the

UNIVERSITY OF THE FREE STATE

Supervisor: Prof. Hendrik G. Visser
Co-Supervisor: Prof. Andreas Roodt

JULY 2012

I can do all things through Christ who strengthens me. Phil: 4 *v* 13

Acknowledgements

CHAPTER 3

THEORY OF IR, ^{1}H- AND ^{13}C NMR, UV/VIS, X-RAY DIFFRACTION AND CHEMICAL KINETICS

CHAPTER 4

SYNTHESIS OF COMPOUNDS

CHAPTER 5

CRYSTALLOGRAPHY STUDY OF RHENIUM COMPLEXES

CHAPTER 6

KINETIC INVESTIGATION ON RHENIUM (I) COMPLEXES

CHAPTER 7

IN VITRO CANCER SCREENING OF COMPOUNDS

CHAPTER 8

CRITICAL EVALUATION

-

ABBREVIATIONS AND SYMBOLS

Acac	Acetylacetone
α	Alpha
Å	Angstrom
β	Beta
L,L'-Bid	Bidentate ligand
BFCA	Bifunctional chelating agent
BBB	Blood brain barrier
k_B	Boltzmann constant
v_{CO}	Carbonyl stretching frequencies
CNS	Central Nervous System
CT	Computer tomography
°	Degrees
DTPA	Dieethyltriamine pentaacetic acid
$\Delta H^{\neq}$	Enthalpy of activation
$\Delta S^{\neq}$	Entropy of activation
K_1	Equilibrium constant
fac	Facial
FDG	Fluorodeoxyglucose
k_1	Forward reaction rate constant
γ	Gamma
$t_{1/2}$	Half-life
HFA	Hexafluoroacetylacetone
8-Quin	8-Hydroxyquinoline
IR	Infrared
LET	Linear energy transfer
MRI	Magnetic Resonance Imaging
MRI	Magnetic Resonance Imaging
mAbs	Monoclonal antibodies

M	mol.dm^{-3}
NCA	No-carrier added state
NMR	Nuclear Magnetic Resonance spectroscopy
k_{obs}	Observed pseudo first order rate constant
ppm	Parts per million (Chemical shift unit)
ppb	Parts per billion
h	Planck constant
π	Pi
PET	Positron Emission Tomography
Py	Pyridine
k_{-1}	Reverse reaction rate constant
θ	Sigma
SPECT	Single Photon Emission Computed Tomograpghy
TFA	Trifluoroacetylacetone
UV/VIS	Ultraviolet/ Visible Spectroscopy
λ	Wavelength

ABSTRACT

Keywords: Radiopharmaceutical, cell study, aqua substitution, biologically active, X-ray crystallography, rhenium tricarbonyl, O,O'-donor bidentate ligands, stretching frequencies, technetium-99m

Rhenium is the third row congener and 5d analogue of technetium. Technetium is the most widely used radionuclide in diagnostic imaging, thus it would be advantageous to explore the use of rhenium as a possible therapeutic radiopharmaceutical. The advantage of using rhenium instead, is that it is non-radioactive in its natural form, possessing similar properties as technetium. Their (rhenium and technetium) chemical behaviour is so similar that it is almost impossible for biological systems to differentiate between them. These similarities include size, shape, lipophillicity, dipole moment, charge and ionic mobility, thus forming complexes of the same geometry.

The main attraction in the use of rhenium as a potential radiopharmaceutical agent is the *fac*-$[Re(CO)_3]^+$ moiety. Only a few crystal structures of the form, *fac*-$[Re(O-O')(CO)_3X]$, (O-O' = bidentate ligands and X being halides, monodentate ligands etc.) has been published. In 2012 only ten crystal structures containing O,O'- donor bidentate ligands have been introduced. Substitution kinetic studies using rhenium tricarbonyl complexes is still an under explored field.

The principle aim in this study, was to synthesise complexes of the form, *fac*-$[M(L,L')_3(CO)_3X]$ (M = Re, Tc; L,L' = O,O'- and N,O-donor bidentate ligands; X = Br^-, Py, H_2O). These bidentate ligands include compounds that are biologically active. In synthesising these complexes, two new rhenium(I) crystal structures, containing O,O'-donor bidentate ligands have been introduced. The bidentate ligand systems, used in this study was O,O' -donor ligand systems, acetylacetone (Acac), trifluoroacetylacetone (TFA), hexafluoroacetylacetone (HFA) and N,O-donor ligands, ephedrine (Eph) and 8-hydroxyl-quinoline (8-Quin).

The following three ^{99m}Tc complexes were synthesised, *fac*-$[^{99m}Tc(Acac)(CO)_3(H_2O)]$, *fac*-$[^{99m}Tc(TFA)(CO)_3(H_2O)]$ and *fac*-$[^{99m}Tc(HFA)(CO)_3(H_2O)]$ and their formation was established, using reverse phase thin layer chromatography (TLC). Their R_f values increased in the following

order: *fac*-[^{99m}Tc(Acac)(CO)$_3$(H$_2$O)] (0.227) > *fac*-[^{99m}Tc(TFA)(CO)$_3$(H$_2$O)] (0.392) > *fac*-[^{99m}Tc(HFA)(CO)$_3$(H$_2$O)] (0.537), indicative of their solubility in 0.1 % trifluoroacetic acid.

In the substitution kinetic study, pyridine was used as the entering ligand to substitute the methanol ligand. Chapter 4 describes the characterisation of the synthesised compounds, using IR, UV/VIS, ^{1}H-NMR as well as ^{13}C-NMR. The complexes that were characterised by X-ray crystallography are: *fac*-[Re(TFA)(CO)$_3$(Py)] and *fac*-[Re(HFA)(CO)$_3$(Py)]. Both complexes crystallised out in the *P*2$_1$/*c* space group, with their Re-O,O' bond distances at 2.135(3) Å and 2.117(3) Å, for *fac*-[Re(TFA)(CO)$_3$(Py)], and 2.127 (2) Å and 2.1376 (19) Å for *fac*-[Re(HFA)(CO)$_3$(Py)].

A trend was observed in the IR data in terms of the stretching frequencies (v_{co}), with an increase in the v_{co} (caused by the influence of the electron withdrawing fluorine atoms) in the following order: *fac*-[Re(Acac)(CO)$_3$(OH$_2$)] (2015 cm^{-1}, 1907 cm^{-1}, 1879 cm^{-1}) < *fac*-[Re(TFA)(CO)$_3$(OH$_2$)] (2018 cm^{-1}, 1895 cm^{-1}, 1878 cm^{-1}) < *fac*-[Re(HFA)(CO)$_3$(OH$_2$)] (2025 cm^{-1}, 1917 cm^{-1}, 1888 cm^{-1}), indicating a decrease in the electron density surrounding the metal centre and thus a decrease in the CO π-back bonding, causing the Re-OH$_2$ bond to shorten. The kinetic rate for the substitution of the methanol ligand (at 25 °C) yielded the following results: *fac*-[Re(Acac)(CO)$_3$(CH$_3$OH)] (k_1 = 13.7(1) x 10^{-3} M^{-1}.s^{-1}) > *fac*-[Re(TFA)(CO)$_3$(CH$_3$OH)] (k_1 = 0.35(3) x 10^{-3} M^{-1}.s^{-1}) > *fac*-[Re(HFA)(CO)$_3$(CH$_3$OH)] (k_1 = 0.17(3) x 10^{-3} M^{-1}.s^{-1}). This difference in the kinetic rate is highly affected by the electron withdrawing fluorine atoms, attached to the coordinated bidentated ligands of *fac*-[Re(TFA)(CO)$_3$(CH$_3$OH)] and *fac*-[Re(HFA)(CO)$_3$(CH$_3$OH)]. The activation parameters obtained were as follows: $\Delta H^{\neq}$ = 64(1) kJ mol^{-1} and $\Delta S^{\neq}$ = -65(5) J K^{-1} mol^{-1}, with the negative $\Delta S^{\neq}$ value indicating towards an interchange associative type mechanism.

A cell study performed on oesophageal cancer cell lines with *fac*-[Re(Acac)(CO)$_3$(Py)] (IC$_{50}$ = 14.92) and *fac*-[Re(TFA)(CO)$_3$(Py)] (IC$_{50}$ = 16.13), using the MTT assay protocol did not yield promising results.

OPSOMMING

Sleutelwoorde: Radiofarmaseutiesemiddel, sel studie, akwa substitusie, biologies aktief, X-straal kristallografie, renium trikarboniel, O,O'-skenking bidentate ligande, strekkingsfrekwensies, tegnesium-99m

Tegnesium is die radionuklied wat die meeste gebruik word in diagnostiese beelding. Renium kom voor in dieselfde groep (Groep VII) as tegnesium en is sy 5d analoog, daarom sal dit voordelig wees om die gebruik van renium as 'n moontlike terapeutiese radiofarmaseutiesemiddel te bestudeer. Renium en tegnesium het dieselfde eienskappe, en omdat renium nie radioaktief is in sy natuurlike vorm nie, sal dit beter wees om dit te gebruik in plaas van tegnesium. Hulle chemiese gedrag is soortgelyk en dit maak dit amper onmoontlik vir biologiese sisteme om tussen die twee te kan onderskei. Hierdie ooreenkomste sluit hulle grootte, lipofilisiteit, dipool moment, lading en ioniese mobiliteit in, daarom vorm hulle ook komplekse van dieselfde geometrie.

Die grootste aantrekking vir die gebruik van renium as a moontlike radiofarmaseutiese agent, is die fac-[Re(CO)$_3$]$^+$ moïeteit. Min kristal strukture met die vorm fac-[Re(O-O')(CO)$_3$X], (O-O' = bidentate ligande en X halide, monodentate ligande ens.) is gepubliseer. In 2012 is net tien kristal strukture, wat O,O'-bidentate ligande bevat, alreeds gepubliseer. Baie min werk is gedoen op die renium trikarboniel komplekse, met betrekking tot substitusie kinetika.

Die doel van hierdie studie was om komplekse met die volgende vorm, fac-[M(L,L')$_3$(CO)$_3$X] (M = Re, Tc; L,L' = O,O'- en N,O-skenkende bidentate ligande; X = Br$^-$, Py, H$_2$O), te sintetiseer. Die bidentate ligande wat gebruik is, sluit biologiese aktiewe verbindings in. Die O,O'-skenkings bidentate ligand sisteme wat gebruik is, is asetielasetoon (Acac), trifluooroasetielasetoon (TFA) en heksafluooroasetielasetoon (HFA), terwyl efedrien (Eph) en 8-hidroksiekinolien (8-Quin) as N,O-skenkende ligande gebruik is.

Drie ^{99m}Tc komplekse is ook gesintetiseer, insluitende fac-[^{99m}Tc(Acac)(CO)$_3$(H$_2$O)], fac-[^{99m}Tc(TFA)(CO)$_3$(H$_2$O)] en fac-[^{99m}Tc(HFA)(CO)$_3$(H$_2$O)]. Die vorming van hierdie produkte is deur middel van die omgekeerde fase 'TLC' metode bevestig. Die R$_f$ waardes vermeerder as

volg: *fac*-[^{99m}Tc(Acac)(CO)$_3$(H$_2$O)] (0.227) > *fac*-[^{99m}Tc(TFA)(CO)$_3$(H$_2$O)] (0.392) > *fac*-[^{99m}Tc(HFA)(CO)$_3$(H$_2$O)] (0.537). Dit is 'n indikasie van die oplosbaarheid van hierdie komplekse in 0.1 % trifluooroasynsuur.

Pyridien is gebruik as 'n inkomende ligand, om die metanol ligand te verplaas in die substitusie kinetika studie. Hoofstuk 4 beskryf die karakterisering van die gesintetiseerde verbindings deur middel van IR, UV/VIS, ^{1}H-KMR asook ^{13}C-KMR. *fac*-[Re(TFA)(CO)$_3$(Py)] en *fac*-[Re(HFA)(CO)$_3$(Py)] is deur middel van X-straal kristallografie gekarakteriseer. Albei komplekse kristalliseer in 'n *P*2$_1$/*c* ruimtegroep, met Re-O,O' bindings afstande van 2.135(3) Å en 2.117(3) Å, vir *fac*-[Re(TFA)(CO)$_3$(Py)] en *fac*-[Re(HFA)(CO)$_3$(Py)] onderskeidelik.

'n Patroon is waargeneem met betrekking tot die strekkingsfrekwensies (v_{co}) van die verbindings. 'n Toename in die v_{co} (invloed van die elektron ontrekkende fluoor atome) is as volg waargeneem: *fac*-[Re(Acac)(CO)$_3$(OH$_2$)] (2015 cm^{-1}, 1907 cm^{-1}, 1879 cm^{-1}) < *fac*-[Re(TFA)(CO)$_3$(OH$_2$)] (2018 cm^{-1}, 1895 cm^{-1}, 1878 cm^{-1}) < *fac*-[Re(HFA)(CO)$_3$(OH$_2$)] (2025 cm^{-1}, 1917 cm^{-1}, 1888 cm^{-1}). Die afname in elektron digtheid rondom die metal senter, veroorsaak dat die CO π-terugbinding af neem, dus verkort die Re-OH$_2$ binding. Die kinetika studie in die substitusie van die metanol ligand, het die volgende resultate opgelewer: *fac*-[Re(Acac)(CO)$_3$(CH$_3$OH)] (k_1 = 13.7(1) x 10^{-3} M^{-1}.s^{-1} > *fac*-[Re(TFA)(CO)$_3$(CH$_3$OH)] (k_1 = 0.35(3) x 10^{-3} M^{-1}.s^{-1}) > *fac*-[Re(HFA)(CO)$_3$(CH$_3$OH)] (k_1 = 0.17(3) x 10^{-3} M^{-1}.s^{-1}). Hierdie verskil in die reaksie tempo word hoofsaaklik deur die elektron ontrekkende fluoor atome, wat gebind is aan die bidentate ligande van *fac*-[Re(TFA)(CO)$_3$(CH$_3$OH)] en *fac*-[Re(HFA)(CO)$_3$(CH$_3$OH)], beinvloed. Die resultate van die aktiverings parameters is as volg: $\Delta H^{\neq}$ = 64(1) kJ mol^{-1} en $\Delta S^{\neq}$ = -65(5) J K^{-1} mol^{-1}. Die negatiewe $\Delta S^{\neq}$ waarde dui op 'n interuitruiling assosiatiewe tipe meganisme.

Die komplekse wat getoets is op slukderm kanker sel lyne is *fac*-[Re(Acac)(CO)$_3$(Py)] (IC$_{50}$ = 14.92) en *fac*-[Re(TFA)(CO)$_3$(Py)] (IC$_{50}$ = 16.13). Die sel studie was gedoen met behulp van die sogenaamde 'MTT assay protocol' en dit het nie belowende resultate opgelewer nie.

1 INTRODUCTION AND AIM

1.1 Introduction

Cancer is a deadly disease with a high morbidity and mortality rate, due to late detection and diagnosis. This disease is caused by uncontrolled multiplication of cells in the body, which result in a mass growth (see Figure 1.1), called a tumour. These cancer cells spread to other parts of the body through the bloodstream and lymphatic systems.

Normal cell division

Cell damage - no repair

Cell suicide or Apoptosis

Cancer cell division

First mutation   Second mutation   Third mutation   Uncontrolled growth
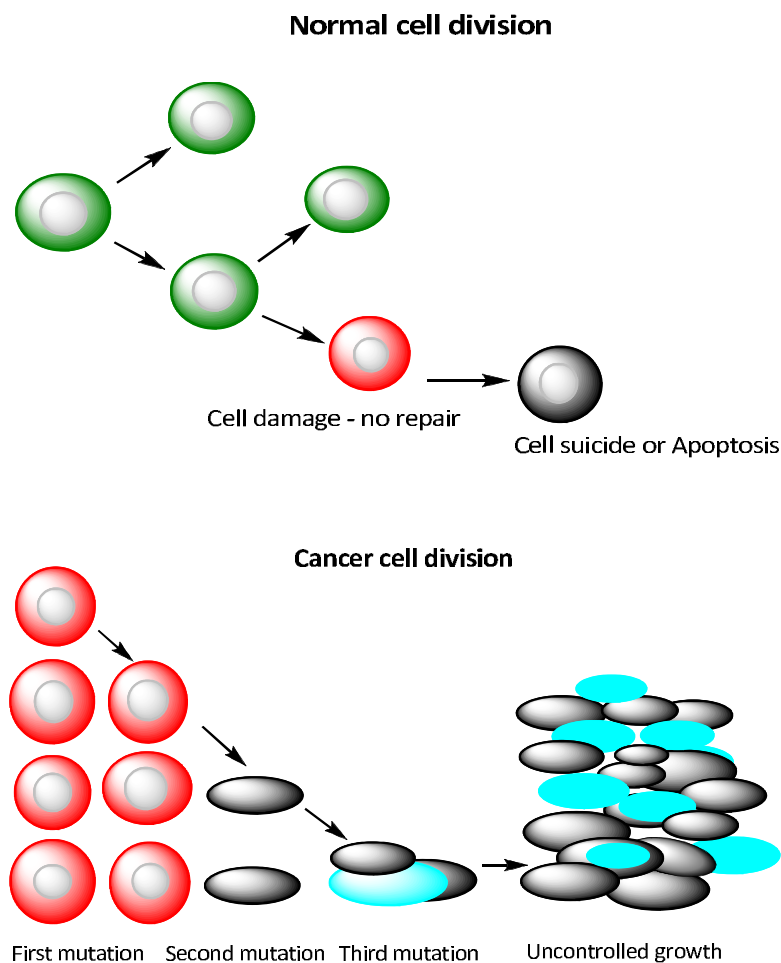
Figure 1.1: Schematic illustration of normal and abnormal cell division.

An estimated 1.6 million new cases and approximately 600 000 deaths were reported in the United States alone, in the year 2010.[1] In South-Africa, radiopharmaceutical companies, Axim Radiopharmacy and PET-Labs Pharmaceuticals, have supplied radiopharmaceuticals for diagnostic purposes for over 10 000 and 2 812 patients respectively, for the year 2010. There is a collection of a hundred different forms of cancer of which lung cancer, prostate cancer and breast cancer are labeled as the most common.

Researchers have discovered that the risk of getting cancer can be lowered by a) doing physical activities b) not smoking and c) following a good balanced diet. Cancer is difficult to treat, however prevention, early detection and surgery can terminate cancer in some cases. The most common treatment for cancer is radiation therapy and chemotherapy.[2] Since the figures of cancer cases are so alarming, researchers in chemistry and nuclear medicine are highly interested in the development of new drugs for early detection and the curing of cancer.

Nuclear medicine owes its advancement to a number of scientists, who contributed to the field with their discoveries and new developments. Nuclear medicine takes advantage of a) the nuclear properties of the radionuclide and b) the pharmacological properties of the radioactive tracer. These radiotracers were studied from the early 1920's and it involves the administration of trace amounts of radionuclides (compounds labeled with radioactivity) that are used to diagnose a wide range of diseases.

The drugs used in the diagnosis and therapy of cancers are also referred to as radiopharmaceuticals (i.e. radiotracers).[3] "Pharmaceutical" refers to organic, medicinal or natural products and most therapeutic drugs are organic or bio-organic molecules. The majority of radiopharmaceuticals are a combination of a radioactive molecule (allows external detection) and a biologically active molecule (acts as a carrier and determines localization and biodistribution). These drugs contain radionuclides and in the case of imaging cancer sites, the radionuclide is a photon emitter (gamma-γ or positron-β), while for therapy it is a particle emitter (alpha-α, beta-β or Auger/conversion e⁻)[4], (see Table 1.1 for decay modes). When using

---

[1] National Cancer Institute; http://www.cancer.gov/cancertopics/cancerlibrary/what-is-cancer, **2011**

[2] *e*CancerAnswers.net; http://ecanceranswers.net/cancer_risk_factors.php, **2011**

[3] Anderson, C. J.; Welch, M. J.; *Chem. Rev*. 99, 2219, **1999**

[4] Zuckman, S. A.; Freeman, G. M.; Troutner, D. E.; Volkert, W. A.; Holmes, R. A.; Van Derveer, D. G.; Barefield, E. K.; *Inorg. Chem*, 20, 2386, **1981**

β-particle emitters, a highly homogeneous radiation dose is produced, although their deposition is heterogeneously distributed in the cancer site. α-particles can be defined as high energy helium nuclei. These high linear energy transfer (LET) particles produce high densities of ionization along their linear tracks.[5]

Table 1.1: An illustration of the decay modes for radionuclides.[6]

Decay mode	Symbol	Radiation emitted	Decay process examples
α-decay	α	Helium nuclei	$^{226}Ra(\alpha)\ ^{222}Rn$
β-decay	β^-	Electrons	$^{174}Lu(\beta^-)\ ^{174}Hf$
	β^+	Positrons	$^{11}C(\beta^+)\ ^{11}B$
γ-decay	γ	Photons (hv)	$^{99}Tc(\gamma)\ ^{99m}Tc$
Electron capture	ε	Characteristic X-rays of the daughter nuclide	$^{118}Sn(\varepsilon)\ ^{118}In$
Proton decay	p	Protons	$^{147}Tm(p)\ ^{146}Er$

There are differences between diagnostic and therapeutic radiopharmaceuticals. Diagnostic radiopharmaceuticals are gamma-emitting or positron emitting radionuclides, which are injected into a patient to differentiate normal from abnormal anatomic (biochemical or physiological functions) structures, using imaging. Currently a greater percentage (> 80%) of all radiopharmaceuticals is used for the diagnosis of cancers. These radiotracers are mostly metal complexes with a chelator or chelator-biomolecule conjugate. The difference is that the latter is used for target specific radiopharmaceuticals, and metal complexes with a chelator are used for metal essential agents.

Therapeutic radiopharmaceuticals are administered to a patient to deliver radiation doses to body tissues internally. These drugs are targeted to specific areas of the body and they normally have short half-lives. Predominantly, therapeutic drugs are organic or bioorganic molecules with a definite composition.

There are two factors that generally distinguish the biological distribution of radiopharmaceuticals: (a) blood flow (perfusion) and (b) specific biochemical processes (such as receptor/antigen binding).[7]

---

[5] Volkert, W. A.; Hoffman, T. J.; *Chem. Rev*. 99, 2271, **1999**
[6] Lieser, K. H.; *Nuclear and Radiopharmacy,* 2nd Revised Edition, 48, **2001**

A new research area in the medical field includes radiopharmaceuticals and biomolecules as diagnostic agents. The success of the pharmaceutical industry is under pressure, since the registration of new drugs has decreased over the years.[8] Radiopharmaceuticals are administered to humans and there are numerous boundaries on the detection of radiations by the current instruments available, therefore radiopharmaceuticals should contain some important properties. The characteristics that the ideal radiopharmaceutical should have are as follows: (i) it should be inexpensive and easily available (ii) it must have a short, but effective half-life, (iii) it must have an appropriate particle emission (iv) the decay mode should either be electron capture or isomeric transition for diagnostic radiopharmaceuticals and (v) the radiopharmaceutical should have a high target to non-target activity ratio. The factors influencing the design of a new radiopharmaceutical also need to be considered before, during and after preparation. These factors include compatibility, stoichiometry and charge of the molecule, size of the molecule, protein binding, solubility, stability and biodistribution. If one is informed about these factors, it can help to predict its *in vivo* behaviour.[3]

1.2   The Start of Nuclear Medicine and Radiopharmaceuticals

As mentioned earlier, the development of nuclear medicine involves contributions from a large number of scientists and physicians. Wilhelm Conrad Roëntgen discovered X-ray photography in 1895 after he took an X-ray of his wife's hand (see Figure 1.2), showing the bones within it.[9]
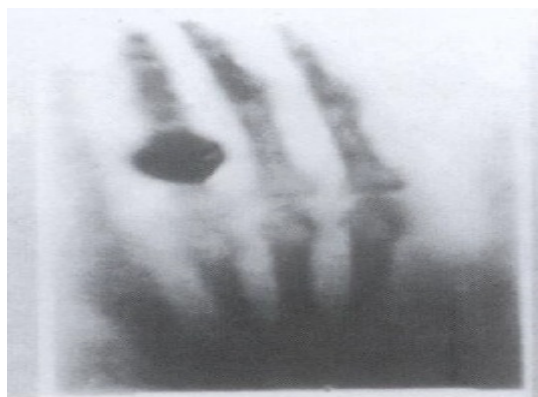
Figure 1.2: Wilhelm Conrad Roentgen's X-ray photo, depicting his wife's hand.

[7] Jurisson, S.; Berning, D.; Jia, W.; Ma, D.; *Inorg.Chem*, 93, 1137, **1993**
[8] Hambley, T. W.; *Dalton Trans.*, 4929, **2007**
[9] Morris, R. R.; *Society of Nuclear Medicine 1954-2004*, 20, **2005**

This discovery caught Antoine Henri Bequerel's attention and in 1896, the Parisian scientist discovered radioactivity. He found that unusual rays were emitted from uranium.

de Hevesy was the first person to use radioactive tracers (in 1943) and he was also involved in the first administration of radioisotopes to humans with ^{32}P (as Na_3PO_4). The first successful treatment with ^{32}P was done in 1939 to treat *polycythemia vera*, (a bone marrow disease that leads to an abnormal increase in the number of blood cells, primarily red blood cells). The invention of the first cyclotron (see Figure 1.3)[10], by Ernest O. Lawrence in 1932, follows after Hermann Blumgart injected himself with radioisotopes in 1925. Blumgart followed blood flow, by using an electroscope.
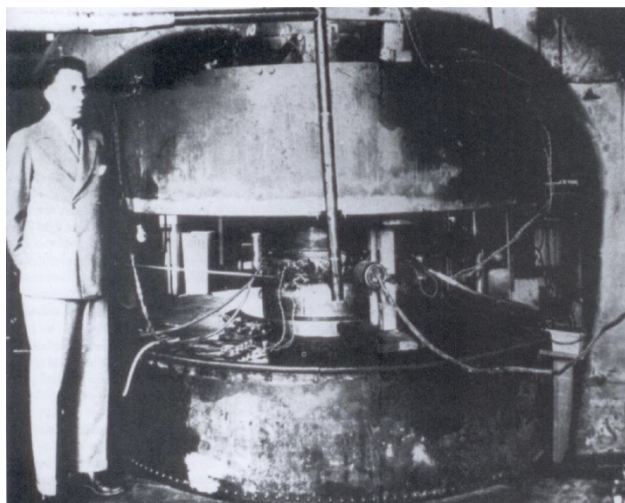
Figure 1.3: Ernest O. Lawrence next to his invention, the first cyclotron (a device that produces high-energy ions without using high voltage).

Artificial radionuclides were successfully produced in 1935 by Irene and her husband Frederic Juliot. The first clinical trial using artificial radioactivity was done at the University of California in 1937 by John H. Lawrence (Ernest Lawrence's brother) for treating a *leukemia* patient.

In 1946, Glenn Seaborg created a radioactive isotope of iodine for medical use. This radioisotope had a longer half-life ($t_{1/2}$) than that of ^{128}I (25 minutes), for studying thyroid

---

[10] Treichel, P. M.; *Kirk-Othmer Encyclopaedia of Chemical Technology* (3rd Ed.),20, John Wiley and Sons, New York, **1982**

metabolism. Seaborg than created the radioisotope ^{131}I, using the cyclotron.[8] Currently, ^{131}I is the most frequently used radioactive isotope for the treatment of thyroid cancer.

The 1950's marks the development of technology that allowed scientists and physicians to obtain images of radionuclides in the human body. This was possible after the development of the gamma camera (Anger camera- see Figure 1.4)[11] in 1950 and the development of the rectilinear scanner (by Benedict Cassen) in 1951.
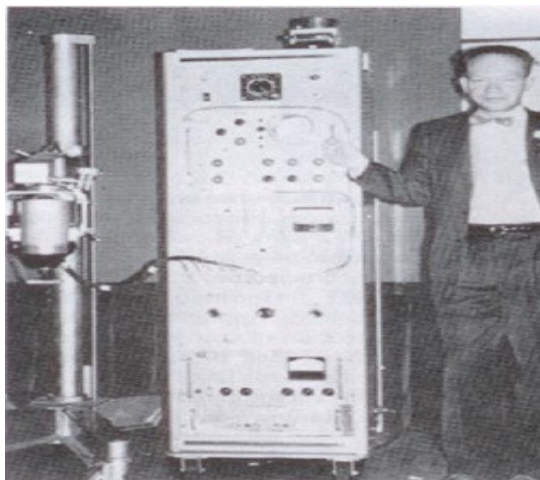
Figure 1.4: Hal Anger with the first gamma camera in 1958.

The Anger camera, which is labeled as the fore-runner of all modern nuclear medicine single photon imaging systems (gamma camera) was developed in 1958 by Hal Anger. Until the early 1960's, ^{131}I was mainly used for studying and diagnosing thyroid disorders and a variety of other radionuclides that were individually appropriate for a few specific organs. An enormous turning point in the development of nuclear medicine came in 1964 when Paul Harper and his colleagues[12] used ^{99m}Tc as an imaging agent. The advantages of using ^{99m}Tc was a) the gamma rays emitted by the radionuclide had very good imaging properties, b) it was very flexible for labeling an assortment of compounds that could be used to study virtually every organ in the human body and c) it could be produced in a moderately long-lived generator form, which allowed hospitals to have a readily available supply of the radionuclide. The 1970's marks the start of the modern era of nuclear medicine, because of the development of the mathematics

---

[11] Anger, H. O.; Scintillation camera. *Rev. Sci. Instr.* 29, 27-33, **1958**
[12] Harper, P. V.; Beck, R.; Charleston, D.; Lathrop. K. A.; *Optimization of a Scanning Method using Technetium-99m,* Nucleonics 22, 50-54, **1964**

to reconstruct tomographic images from a set of angular views around a patient. This replaced the two-dimensional representation of the three-dimensional radioactivity distributions, with three-dimensional representations.[13]

Table 1.2: A summary of the history of nuclear medicine and radiopharmaceuticals.

Year	Contribution to nuclear medicine and radiopharmaceuticals
1895	Wilhelm Conrad Roëntgen discovered X-ray after taking an X-ray of his wife's hand, showing the bones within it.
1896	The X-ray discovery caught Antoine Henri Bequerel's attention and this lead to the discovery of radioactivity.
1897	Pierre and Marie Curie progressed in the discovery of radium and polonium.
1923	George Charles de Hevesy discovered radioactive tracers, by studying the absorption and translocation of lead nitrate in plants.
1925	Herman Blumgart injected himself with radioisotopes and followed blood flow, using an electroscope.
1932	Ernest O. Lawrence invented the first cyclotron.
1935	Irene (daughter of Marie Curie) and Frederic Juliot produced the first artificial radionuclides.
1937	George Charles de Hevesy was involved in the first administration of radioisotopes (^{32}P as Na_3PO_4) in humans.
	First clinical trial using artificial radioactivity done by John H. Lawrence (Ernest Lawrence's brother), treating *leukemia*.
	Joseph G. Hamilton suggested a much wider use of radioisotope treatments and called it *nuclear medicine*.
1939	First successful treatment of *polycythemiavera* with ^{32}P.
1946	Marks the birth of nuclear medicine.
1950's	Marks the development of technology that allowed scientist to obtain images of radionuclides in the human body – development of the gamma-camera by Hal Anger.
1951	Benedict Cassen developed the rectilinear scanner.
1964	Paul Harper and his colleagues used ^{99m}Tc as an imaging agent.
1970's	Marks the start of the modern era of nuclear medicine, because of the development of Computed tomography (CT), Positron emission tomography (PET), Single photon emission computed tomography (SPECT) and Magnetic resonance imaging (MRI).

---

[13] Morris, R. R.; *Society of Nuclear Medicine 1954-2004*, 26, **2005**

1.3 Metals Used in Medicine and Radiopharmaceuticals

1.3.1 History of Metals in Medicine

The impact that metals have on medicinal chemistry has been practised for almost 5 000 years, which was performed by the ancient Romans, Greeks and Egyptians when they used copper to treat open wounds as well as in the sterilisation of water. In contrast, 3 500 years ago, gold was used in Arabia and China in various medicines, for its value, rather than its medicinal properties. About 1 500 BC, a number of iron remedies were used and around the same time, zinc was discovered to shorten the time that it takes for an open wound to heal. During the early 20th century, silver coins were placed in milk bottles to prolong the freshness of the milk. Silver ions and silver compounds are also used to kill bacteria, viruses, algae and fungi. Mercurous chloride was used as a diuretic in Renaissance era Europe, which was about the same time that the nutritional value of iron was discovered. In the early 1900's more compounds were discovered to have medicinal benefits: $K[Au(CN)_2]$ was used in the treatment of tuberculosis, various antimony compounds used for *leishmaniasis* (a parasitic disease spread by the bite of the sand-fly, which affects the skin and sometimes the mucus membrane) and the antibacterial properties of gold salts.[14]

1.3.2 Metals in Biological Systems

Iron is a vital component of haemoglobin, which indicates that certain metals play very important roles in living systems. The formation of positively charged ions, which occurs by the loss of electrons, is a common characteristic of metals. This proposes the tendency to dissolve in biological fluids and make it possible for metals to play their role in biology. This biological phenomenon is possible, because most biological molecules, such as DNA and protein are electron rich and a metal in its cationic form is electron deficient. This leads to the general tendency for ionic metals to bind to biological molecules. Metals perform a number of essential functions in the human body: the iron-containing protein, haemoglobin, transports oxygen in the body; zinc is a natural component of insulin and calcium forms a major part of human

---

[14] Orvig, C.; Abrams, M. J.; *Chem. Rev,* 99**,** 2202, **1999**

bones. Copper, zinc, iron and manganese forms part of the catalytic proteins, which play a vital role in the facilitation of chemical reactions in the body.[10]

1.3.3 Current Practice of Nuclear medicine

Nuclear medicine is used for a wide variety of diagnostic tests, as well as for therapeutic purposes. Today, more than 2 700 radionuclides have been produced, using cyclotrons, accelerators, nuclear generators and nuclear reactors.[15] These radionuclides are produced from a variety of different radiolabeled compounds; they cover all the major organ systems in the body and provide a great deal of different measures of biological functions.

Among the list (see Table 1.2)[16] of some of the most commonly used radiopharmaceuticals is the metabolic tracer, ^{18}F-Fluorodeoxyglucose ([18]FDG). Its popularity is credited to its widespread applications in cancer, heart disease and neurological disorders. [18]FDG ($t_{1/2}$ = 109.8 min) has been used in imaging since 1999 and is primarily produced in places where a cyclotron is available, locally.

Table 1.3: A selection of radionuclides used in nuclear medicine.

Nuclide	Compound	Mode of decay	Imaging	Measurement
[131]I	Sodium iodide	Beta minus	Planar	Thyroid function
[67]Ga	Gallium citrate	Electron capture	Planar	Sites of infection
[111]In	Labeled white blood cells	Electron capture	Planar	Sites of infection
[18]F	Fluorodeoxyglucose	Electron capture	PET	Glucose metabolism
[13]N	Ammonia	Electron capture	PET	Myocardial perfusion
[153]Sm	Samarium-153 EDTMP	Beta minus	Planar	Palliation of bone pain
[99m]Tc	Sestamibi	Isomeric transition	Planar	Coronary artery disease

After the bombardment of [18]O to yield [18]F (see Figure 1.5)[17], in the cyclotron, deoxyglucose is labeled with the radioactive [18]F. This involves the nucleophilic displacement of an acetylated sugar derivative followed by hydrolysis.[18] After the administration to the patient, it is taken up by cells using glucose. In the metabolism, [18]FDG is phosphorylated by hexokinase to

---

[15] Saha, G. B.; *Fundamentals of Nuclear Pharmacy*, 4th Edition, Springer, **1998**
[16] Cherry, S. R.; Sorensen, J. A.; Phelps, M. E.; *Physics in Nuclear medicine*, 3rd Edition, 5, **2003**
[17] http://www.mecsnm.net/www/documents/f18fdgproduction_d.pdf [Consulted on **1 July 2011**]
[18] Saha, G. B.; *Fundamentals of Nuclear Pharmacy*, 5th Edition, 144-145, **2004**

FDG-6-phosphate, which is not metabolized further, and stays trapped in the myocardium.[18,19] FDG experiences further metabolism and combines with glycogen and [18]FDG metabolites diffused into the blood pool. The fact that [18]FDG gets metabolized as normal sugar in the end, makes it ideal for imaging tissues (brain, heart, liver and malignant tumours) with high glucose uptake. A disadvantage when using [18]FDG is that it is very sensitive and not specific.
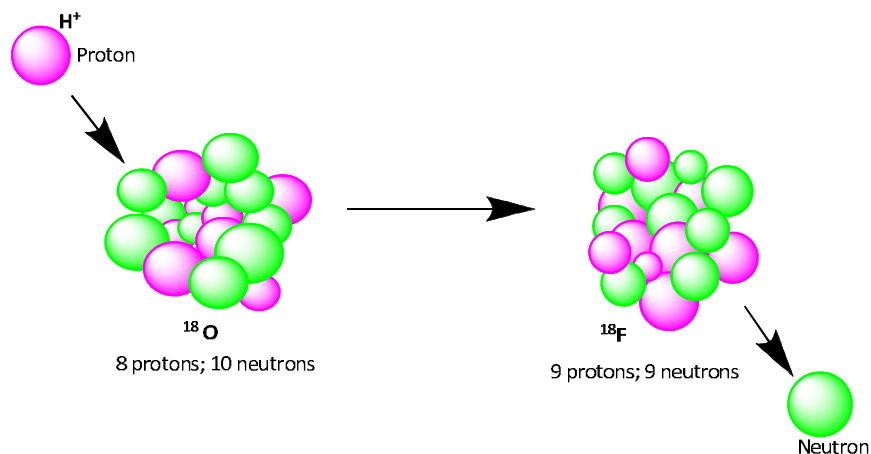
Figure 1.5: Schematic illustration of the bombardment of [18]O to yield [18]F.

1.3.4 Imaging Affected Areas

There are a number of nuclear medicine cameras capable of imaging gamma-ray-emitting radionuclides in the world. Gamma scintigraphy (radionuclides ranging from 10 min to several days) and PET are the most widely used imaging cameras in nuclear medicine. When imaging the cancer site with PET-CT, the required half-life is dependent on the time required for the radiopharmaceutical to localize in the targeted tissue.[20]

1.3.4.1 Gamma Scintigraphy

Gamma scintigraphy requires the radiopharmaceutical that is used for imaging, to emit γ-rays.[21] This would include the metal isotopes: [67]Cu, ^{67}Ga, ^{111}In and ^{99m}Tc, just to name a few. It also requires a gamma camera and for the energy of the gamma photons to fall within the range of

[19] Reivich, M.; *Positron Emission Tomography*, 131, **1985**
[20] Anderson, C. J.; Welch, M. J.; *Chem. Rev*. 99, 2220, **1999**
[21] McCarthy, T. J.; Schwarz, S. W.; Welch, M. J.; *J. Chem. Ed*., 71, 830

100-250 keV. An energy that does not fall within this range can cause too much scatter (at < 100 keV) or the gamma energies are more difficult to collimate (at > 250 keV) and in both cases insufficient images are produced.[3]

1.3.4.2 PET

PET was developed by Michel Ter-Pogossen in the 1970's and it requires a radiopharmaceutical, which is labeled with a positron-emitting radionuclide (β^+). Radionuclides typically used in PET imaging are those with short half-lives. The patient is injected with a radioactive isotope, incorporated into a biologically active molecule, which is then imaged with a PET camera. The radioisotope undergoes decay which result in the emission of two 511 keV photons which are exactly 180° apart (annihilation-effect). The emitted 511 keV photons are specifically detected in opposite directions by the scanner that is fitted with a circular array of detectors.[3] Currently in South-Africa; there are only three PET radiopharmacies (PET-Labs Pharmaceuticals, Ithemba Pharmaceuticals and NTP-Pelindaba).

1.4   Aim of this Study

At present, the most widely used nuclide in diagnostic imaging is ^{99m}Tc, with more than 7 million scans performed each year. This is due to its availability and complimentary nuclear properties ($t_{1/2}$= 6.02 hours; γ = 140 keV, 100 %).[22] Rhenium is the third row congener and 5d analogue of technetium, which contribute to the similarities in nuclear properties that they possess ie. size, shape, lipophylicity, dipole moment, charge and ionic mobility. Their similarities make it impossible for biological systems to differentiate between rhenium and technetium complexes and will therefore treat these compounds in the same manner. This enables the use of rhenium complexes to successfully replicate corresponding ^{99m}Tc complexes. Unlike technetium, rhenium is non-radioactive in its natural form, which is very advantageous, because it makes it easier and safer to work with. Intense research has been done over the last decade on these triaqua-tricarbonyl {fac-[M(CO)$_3$(H$_2$O)$_3$]$^+$, M = ^{99m}Tc, $^{186/188}$Re} complexes,

---

[22] Botha, J. M.; Roodt, A.; Kinetic and High-Pressure Mechanistic Investigation of the Aqua Substitution in the *Trans*-Aquaoxotetracyano complexes of Re(V) and Tc(V): Some Implications for Nuclear Medicine, *Metal-Based Drugs, 1,* **2008**

because of its potential use in diagnostic and therapeutic radiopharmaceuticals.[23] Complexes from this precursor, *fac*-$[M(CO)_3(H_2O)_3]^+$, are easily prepared, by substituting the three labile water molecules, with a wide range of appropriate chelating systems, containing for example, amines and carboxylic acids. Interesting to note, is the thermodynamic and kinetic properties of the water molecule on the metal complex. The low-spin d^6-electron configuration of the metal core in the *fac*-$[M(CO)_3]^+$ moiety results in stable complexes of high kinetic inertness.

The aim of this study addresses aspects of this *fac*-$[Re(CO)_3(H_2O)_3]^+$ complex, focussing on the kinetics of a range of *fac*-$[Re(CO)_3(O,O')X]^{n-1}$ [where O,O' is acetylacetone (Acac), trifuoroacetylacetone (TFA) and hexafluoroacetylacetone (HFA)] complexes]. The main objectives are achieved according to the following summary:

1.   Synthesis of the *fac*-$[Re(O-O')(CO)_3X]^{n-1}$ complexes, by alternating the O,O'- Bid donor ligand systems, with Acac, TFA and HFA, where X = H_2O, Br^- or pyridine (Py).

2.   Synthesis of the *fac*-$[Re(L-L')(CO)_3X]^{n-1}$ complex, (X = H_2O), by alternating the N,O- Bid- and O,O'- Bid donor ligand systems with biologically active compounds, such as ephedrine and 8-hydroxyl-quinoline.

3.   Synthesis of *fac*-$[^{99m}Tc(O,O')(CO)_3(H_2O)]$ complexes, by alternating the O,O'- Bid donor ligand systems, with Acac, TFA and HFA.

4.   Cell studies of selected synthesized complexes.

5.   Characterisation of the synthesized complexes with single-crystal X-ray crystallography and confirmation of results with IR, UV/VIS, ^{1}H NMR and ^{13}C NMR.

6.   To perform kinetic studies in order to determine the mechanism of the substitution of the methanol species in *fac*-$[Re(O-O')(CO)_3(CH_3OH)]$ (O,O = Acac, TFA, HFA) complexes, using Py as incoming ligands.

ooOoo

---

[23] Gmelin; *Handbook of Inorganic Chemistry*, Springer, Heidelberg, 8th ed., **1989**

volg: *fac*-[^{99m}Tc(Acac)(CO)$_3$(H$_2$O)] (0.227) > *fac*-[^{99m}Tc(TFA)(CO)$_3$(H$_2$O)] (0.392) > *fac*-[^{99m}Tc(HFA)(CO)$_3$(H$_2$O)] (0.537). Dit is 'n indikasie van die oplosbaarheid van hierdie komplekse in 0.1 % trifluooroasynsuur.

Pyridien is gebruik as 'n inkomende ligand, om die metanol ligand te verplaas in die substitusie kinetika studie. Hoofstuk 4 beskryf die karakterisering van die gesintetiseerde verbindings deur middel van IR, UV/VIS, ^{1}H-KMR asook ^{13}C-KMR. *fac*-[Re(TFA)(CO)$_3$(Py)] en *fac*-[Re(HFA)(CO)$_3$(Py)] is deur middel van X-straal kristallografie gekarakteriseer. Albei komplekse kristalliseer in 'n *P*2$_1$/*c* ruimtegroep, met Re-O,O' bindings afstande van 2.135(3) Å en 2.117(3) Å, vir *fac*-[Re(TFA)(CO)$_3$(Py)] en *fac*-[Re(HFA)(CO)$_3$(Py)] onderskeidelik.

'n Patroon is waargeneem met betrekking tot die strekkingsfrekwensies (v_{co}) van die verbindings. 'n Toename in die v_{co} (invloed van die elektron ontrekkende fluoor atome) is as volg waargeneem: *fac*-[Re(Acac)(CO)$_3$(OH$_2$)] (2015 cm^{-1}, 1907 cm^{-1}, 1879 cm^{-1}) < *fac*-[Re(TFA)(CO)$_3$(OH$_2$)] (2018 cm^{-1}, 1895 cm^{-1}, 1878 cm^{-1}) < *fac*-[Re(HFA)(CO)$_3$(OH$_2$)] (2025 cm^{-1}, 1917 cm^{-1}, 1888 cm^{-1}). Die afname in elektron digtheid rondom die metal senter, veroorsaak dat die CO π-terugbinding af neem, dus verkort die Re-OH$_2$ binding. Die kinetika studie in die substitusie van die metanol ligand, het die volgende resultate opgelewer: *fac*-[Re(Acac)(CO)$_3$(CH$_3$OH)] (k_1 = 13.7(1) x 10^{-3} M^{-1}.s^{-1} > *fac*-[Re(TFA)(CO)$_3$(CH$_3$OH)] (k_1 = 0.35(3) x 10^{-3} M^{-1}.s^{-1}) > *fac*-[Re(HFA)(CO)$_3$(CH$_3$OH)] (k_1 = 0.17(3) x 10^{-3} M^{-1}.s^{-1}). Hierdie verskil in die reaksie tempo word hoofsaaklik deur die elektron ontrekkende fluoor atome, wat gebind is aan die bidentate ligande van *fac*-[Re(TFA)(CO)$_3$(CH$_3$OH)] en *fac*-[Re(HFA)(CO)$_3$(CH$_3$OH)], beinvloed. Die resultate van die aktiverings parameters is as volg: Δ$H^{\neq}$ = 64(1) kJ mol^{-1} en Δ$S^{\neq}$ = -65(5) J K^{-1} mol^{-1}. Die negatiewe Δ$S^{\neq}$ waarde dui op 'n interuitruiling assosiatiewe tipe meganisme.

Die komplekse wat getoets is op slukderm kanker sel lyne is *fac*-[Re(Acac)(CO)$_3$(Py)] (IC$_{50}$ = 14.92) en *fac*-[Re(TFA)(CO)$_3$(Py)] (IC$_{50}$ = 16.13). Die sel studie was gedoen met behulp van die sogenaamde 'MTT assay protocol' en dit het nie belowende resultate opgelewer nie.

order: fac-[^{99m}Tc(Acac)(CO)$_3$(H$_2$O)] (0.227) > fac-[^{99m}Tc(TFA)(CO)$_3$(H$_2$O)] (0.392) > fac-[^{99m}Tc(HFA)(CO)$_3$(H$_2$O)] (0.537), indicative of their solubility in 0.1 % trifluoroacetic acid.

In the substitution kinetic study, pyridine was used as the entering ligand to substitute the methanol ligand. Chapter 4 describes the characterisation of the synthesised compounds, using IR, UV/VIS, ^{1}H-NMR as well as ^{13}C-NMR. The complexes that were characterised by X-ray crystallography are: fac-[Re(TFA)(CO)$_3$(Py)] and fac-[Re(HFA)(CO)$_3$(Py)]. Both complexes crystallised out in the $P2_1/c$ space group, with their Re-O,O' bond distances at 2.135(3) Å and 2.117(3) Å, for fac-[Re(TFA)(CO)$_3$(Py)], and 2.127 (2) Å and 2.1376 (19) Å for fac-[Re(HFA)(CO)$_3$(Py)].

A trend was observed in the IR data in terms of the stretching frequencies (v_{co}), with an increase in the v_{co} (caused by the influence of the electron withdrawing fluorine atoms) in the following order: fac-[Re(Acac)(CO)$_3$(OH$_2$)] (2015 cm^{-1}, 1907 cm^{-1}, 1879 cm^{-1}) < fac-[Re(TFA)(CO)$_3$(OH$_2$)] (2018 cm^{-1}, 1895 cm^{-1}, 1878 cm^{-1}) < fac-[Re(HFA)(CO)$_3$(OH$_2$)] (2025 cm^{-1}, 1917 cm^{-1}, 1888 cm^{-1}), indicating a decrease in the electron density surrounding the metal centre and thus a decrease in the CO π-back bonding, causing the Re-OH$_2$ bond to shorten. The kinetic rate for the substitution of the methanol ligand (at 25 °C) yielded the following results: fac-[Re(Acac)(CO)$_3$(CH$_3$OH)] (k_1 = 13.7(1) x 10^{-3} M^{-1}.s^{-1}) > fac-[Re(TFA)(CO)$_3$(CH$_3$OH)] (k_1 = 0.35(3) x 10^{-3} M^{-1}.s^{-1}) > fac-[Re(HFA)(CO)$_3$(CH$_3$OH)] (k_1 = 0.17(3) x 10^{-3} M^{-1}.s^{-1}). This difference in the kinetic rate is highly affected by the electron withdrawing fluorine atoms, attached to the coordinated bidentated ligands of fac-[Re(TFA)(CO)$_3$(CH$_3$OH)] and fac-[Re(HFA)(CO)$_3$(CH$_3$OH)]. The activation parameters obtained were as follows: $\Delta H^{\neq}$ = 64(1) kJ mol^{-1} and $\Delta S^{\neq}$ = -65(5) J K^{-1} mol^{-1}, with the negative $\Delta S^{\neq}$ value indicating towards an interchange associative type mechanism.

A cell study performed on oesophageal cancer cell lines with fac-[Re(Acac)(CO)$_3$(Py)] (IC$_{50}$ = 14.92) and fac-[Re(TFA)(CO)$_3$(Py)] (IC$_{50}$ = 16.13), using the MTT assay protocol did not yield promising results.

2   LITERATURE STUDY

2.1 Rhenium

In 1914, the existence of the undiscovered element at position 75 on the periodic table was predicted by Henry Moseley.[1] However, June 1925 marks the discovery of rhenium by an x-ray specialist with the help of Otto Berg. This metal is one of the last elements to be discovered, with its name derived from the Latin word *Rhenus* (honouring the Rhine river in Germany).

Rhenium is an expensive metal with a market value of U\$ 6 000 per kilogram (kg) as of 2009. This is due to the fact that it is rarely found in the earth's crust, with a concentration of 1 part per billion (ppb). The major sources for rhenium are parts of Europe (Russia, Kazakhstan and Ukraine) and South-American country, Chile.[2]

During roasting of molybdenite concentrates, gasses are given off, from which Rhenium is extracted. This silver-white metal is a secondary by-product of copper mining, because these molybdenite concentrates are found in porphyry ores of copper.

Table 2.1: Selective important properties of the rhenium metal.

Element category	Density (g/cm^{-3})	Melting Point (°C)	Boiling Point (°C)	Oxidation States	Crystal structure	Isotopes of rhenium	
						Non-radioactive	Radioactive
Transition metal	21.04	3180	5630	-3, -1, 0, 1, 2, 3, 4, 5, 6, 7	Hexagonal	^{185}Re (37.4 %) ^{187}Re (62.6 %)	^{186}Re ^{188}Re

Illustrated in Table 2.1 are the properties that make this metal unique. It has the second highest melting point, with only osmium, platinum and iridium exceeding its density. Rhenium is classified as a refractory metal (metals that are extraordinarily resistant to heat or wear), due to

---

[1] Weeks, W. E.; Journal of Chemical Education, **1933**
[2] http://www.rhenium.com/what.asp?menu_id=4 [Consulted on 3 March **2011**]

its high melting point, which in turn contributes to its hexagonal close packed crystallographic structure. Structures made from rhenium have good stability and rigidity, owed to its high modulus of elasticity.

The unique properties of this metal, makes it appropriate in many important applications:

> It is used in small rocket thrusters, in outer space, to position satellites;

> Radioactive rhenium is used in prevention and treatment of restenosis;

> This metal is highly effective when treating liver tumours;

> Catalyst in the petroleum industry;

> Rhenium alloys with molybdenum are used as superconductors.

2.1.1 Rhenium-186 and Rhenium-188 isotopes

Therapy of cancer is very important, if not more important than the imaging of cancers. As mentioned previously, radioactive isotopes of rhenium can be used as therapeutic radiopharmaceuticals, because of its β-irradiation. The radioactive isotopes of rhenium are rhenium-186 (^{186}Re) and rhenium-188 (^{188}Re), (see Table 2.1) and they are used in the treatment of liver cancer.

^{186}Re has numerous current and potential applications, with many still in the investigative stages. One of ^{186}Re nuclear properties that make it an appropriate choice for radiolabeling is its moderate half-life (see Table 2.1). It emits gamma radiation of 137 keV with an intensity of 21 % that enables diagnostic imaging of tissue.[3] Another advantage of ^{186}Re is that its half-life ($t_{1/2}$ = 3.7 days) complements the biological half-life of antibodies. This radioisotope is produced in a nuclear reactor by direct neutron activation of metallic rhenium, enriched with ^{185}Re.

^{188}Re has stirred up interest among researchers for a number of medical applications. The nuclear properties that are particularly attractive for radiotherapy is the half-life, β-emission and the high end-point energies (see Table 2.2). Ideal γ-rays at 155 keV are provided for imaging with an intensity of 15 %. For the production of ^{188}Re, the target is tungsten-186 (^{186}W), from which tungsten-188 (^{188}W) is produced by double neutron capture. ^{188}W undergoes beta decay, to give ^{188}Re. The separation of ^{188}Re is done in generators by chromatography,

---

[3] Welch, M. J.; Redvanly, S.; *Handbook of Radiopharmaceuticals*, 109, **2005**

extraction or by gel technology.[4] [188]Re has an average equilibrium dose rate of 1.78 g-rad/μCi-h and it is available in the carrier-free state from a generator system, making it more suitable for peptide receptor radionuclide therapy than [186]Re. This isotope also has a shelf life of many months.

Table 2.2: Properties of [186]Re and [188]Re isotopes.[5]

[186]Re isotope	[188]Re isotope
$t_{1/2}$ = 3.7 days	$t_{1/2}$ = 16.9 hours
Intermediate energy β⁻ emissions 107 MeV (71%) and 0.94 MeV (21%)	Decays by β⁻ emission with energy of 2.12 MeV (100 %)
5 mm penetration depth in tissue	11 mm penetration depth in tissue
Decays by γ-emission following β⁻ with 137 keV (21 %)	γ-emission energy 155 keV (15 %)
Suitable for small tumours	Suitable for larger tumours
Produced by the [185]Re(n; γ) reaction in a nuclear reactor	Obtained from [188]W/[188]Re radionuclide generator in high specific activity
Inevitably contaminated by non-radioactive [185]Re	Separated from [188]W by ion exchange methods, by eluting with saline solution

2.2 Technetium

Technetium (Tc) is a radioactive, crystalline transition metal and is shiny-grey in colour. This completely artificially produced metal is the lowest atomic number element, which does not have any stable isotopes. It is insoluble in hydrochloric acid, tarnishes gradually in humid air and when in powder form, it ignites. To date, 25 isotopes and 10 isomers of this partially paramagnetic element has been identified, ranging from [88]Tc to [113]Tc.[6] Selective chemical properties of technetium are tabulated in Table 2.3.

Table 2.3: Selected chemical properties of the technetium.

Element category	Density (g/cm⁻³)	Melting Point (°C)	Boiling Point (°C)	Oxidation States	Crystal structure	Most stable isotopes
Transition metal	11	2157	4265	-3, -1, 0, 1, 2, 3, 4, 5, 6, 7	Hexagonal	[95m]Tc, [96]Tc, [97]Tc, [97m]Tc, [98]Tc, ^{99}Tc, [99m]Tc

---

[4] Welch, M. J.; Redvanly, S.; *Handbook of Radiopharmaceuticals*, 703, **2005**
[5] Shuang, L.; *Chem. Soc. Rev.*, 33, 446, **2004**
[6] Welch, M. J.; Redvanly, C. S.; *Handbook of Radiopharmaceuticals*, **2003**

2.2.1 Element 43 - The missing one

Dimitri Mendeleev predicted in 1871 that the element that will occupy position 43 on the periodic table would have similar chemical properties to manganese and named it *ekamanganese*.[7] Researchers first thought that element 43 was found in platinum ores and named it *polinium*, however it turned out to be contaminated iridium. Again in 1846 and 1847, *ilmenium* and *pelopium* was respectively claimed to be the element to occupy position 43, but in both cases it was later determined to be impure niobium.[8] The next claim at element 43 (in 1877) was *davyum*, which actually turned out to be a mixture of iridium, rhodium and iron. Then again in 1896, *lucium* turned out to be yttrium. The presence of element 43 (named *Nippon*) was claimed to be in thorianite by Masataka Ogawa in 1908, but was later found to be rhenium.[9] Once again in 1925, German chemists (Noddack, Berg and Tacke) claimed to have found the 'missing element' by X-ray diffraction spectrograms. It was called *masurium*, but later experimenters could not repeat the discovery so it was dismissed as an error for many years.[10] December 1936 marks the discovery of element 43 by Carlo Perrier and Emilio Segre. They took molybdenum foil that was discarded from a cyclotron and used it to prove through comparative chemistry that molybdenum activity was definitely Z = 43. Element 43 was the first artificially made element and in 1947 it was named technetium (*technetos* - Greek word meaning artificial).

The earth's crust contains only minute amounts of technetium, due to its instability. The two ways that natural technetium occurs by is: a) the spontaneous fission of uranium in uranium ores and b) by neutron capture in molybdenum ores. The chemical properties of this metal are intermediates between rhenium and manganese.

Nuclear rods produce large amounts of ^{99}Tc each year. Neutron activation of molybdenum-98 (^{98}Mo) forms molybdenum-99 (^{99}Mo; $t_{1/2}$ = 65.94 h) and from this ^{99m}Tc ($t_{1/2}$ = 6h) is produced, which is technetium's most widely used isotope.[11]

---

[7] Jonge, F. A. A.; Technetium the Missing Element, *European Journal of Nuclear Medicine*, 23, p 336-344, **1996**
[8] Holden, N. E.; *History of the origin of the Chemical Elements and their discoverers*, **2004**
[9] Yoshihara, H. K.; *Atomic Spectroscopy (Spectrochim. Acta. Part B)*, 59, p 1305-1310, **2004**
[10] Van der Krogt, P.; *Elentymolgy and Elements Multidict,* **2009**
[11] Emsley, J.; *Nature's Building Blocks*, p 424, **2001**

2.2.2 ^{99m}Technetium and ^{99}Technetium isotopes

Radiopharmaceuticals are almost synonymous with technetium, which explains why more than 85% of diagnostic scans are done, using ^{99m}Tc. This element has no stable isotope; however it was first used as a radiopharmaceutical agent in 1964 for thyroid imaging. Back then, very little was known about technetium, except that it was an artificial radionuclide obtained from radioactive decay of ^{99}Mo, see Figure 2.1.
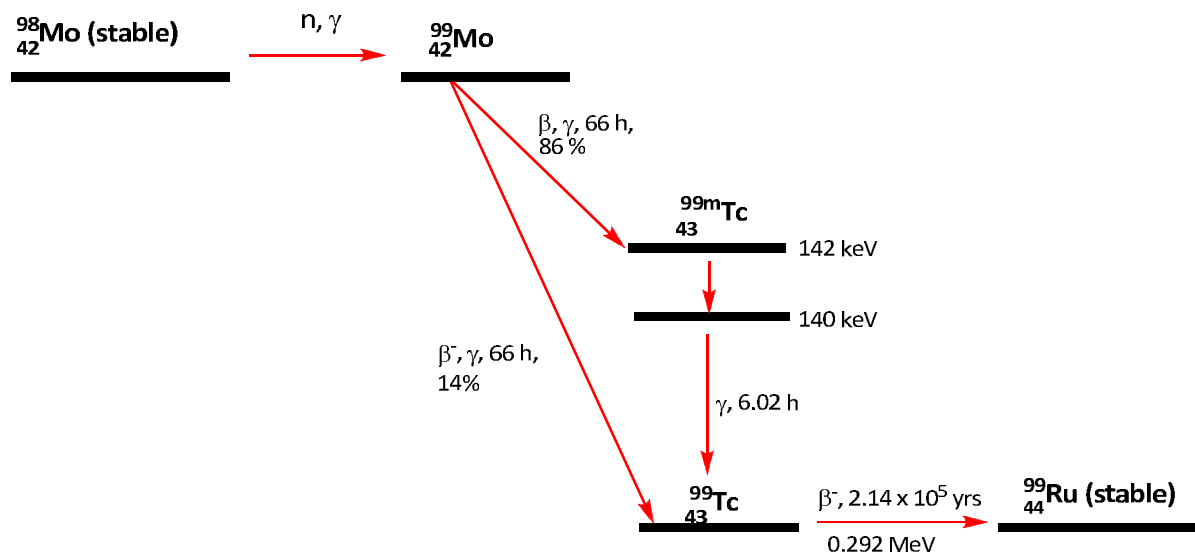
Figure 2.1: An illustration of the decay mode and production of ^{99m}Tc.

^{99m}Tc is prepared from the fission product ^{99}Mo ($t_{1/2}$ = 67 hours), in a ^{99}Mo/^{99m}Tc generator (see Figure 2.2) developed in the early 1960's in Brookhaven. The production involves the absorption of ^{99}MoO$_4$$^{2-}$ onto an alumina column by decaying ^{99}Mo. ^{99}Mo continuously decay to ^{99m}Tc, which is eluted from the column with saline, as an aqueous sodium pertechnetate (Na^{99m}TcO$_4$) solution, over a period of 7-10 days.
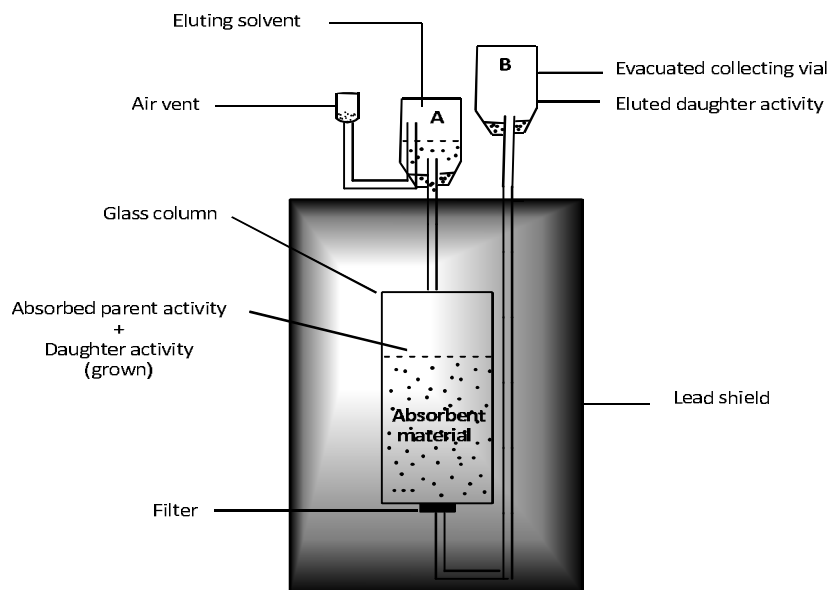
Figure 2.2: An illustration of a typical generator system, in which the daughter activity (^{99m}Tc) is grown by decay of the parent (^{99}Mo) and is chemically separated from the parent. The eluent in vial A is drawn through the column and the daughter nuclide is collected in vial B under vacuum.[12]

There are a few quality criteria that every generator should adhere to and they should be evaluated for:

➢ Elution efficiency - the percentage yield (between 80 and 100 %) obtained from the generator

➢ Radionuclidic purity of the eluate – less than 0.1 % ^{99}Mo present in eluate is still acceptable

➢ Radiochemical purity of the eluate – of its seven oxidation states, not less than 95 % should be identified as Na^{99m}TcO$_4$

➢ Chemical purity of the eluate – aluminium cations are normally present in the eluate, if the alumina bed is subjected to strong acids and its limit is 20 ppm

➢ pH of the eluate – a pH range of between 4.0 and 8.0 is permitted

The use of ^{99m}Tc is very advantageous in medical applications, because it emits γ-rays which sufficiently penetrate tissue with minimal damage.[13] It has ideal properties for imaging, because the 140 keV γ-rays that are emitted give images of high spatial resolution. The 6 hour half life of

---

[12] Baker, R. J.; *Int. J. Appl. Radiat. Isot.*, 22, p 483, **1971**
[13] Abram, U.; Alberto, R.; *J. Braz. Chem. Soc.*, 17, **2006**

[99m]Tc provides sufficient time to synthesize, prepare the dosage, administer the drug and collect useful images, yet short enough for minimal exposure to the patient.

[99]Tc has a much longer half life ($t_{1/2}$ = 66 hrs) and is a product of β-emission of [99]Mo. The ^{99}Tc is also used to isolate technetium complexes and to characterise them by the full range of spectroscopic methods, including x-ray crystallography. This isotope also has weak β-emitting properties, which means that complexes can be handled safely with proper precautions and inside conservative glassware.[14]

2.3 Aqueous chemistry of *fac*-[M(CO)₃(H₂O)₃]⁺ (M = Re, Tc)

Aqueous technetium chemistry is very difficult and ^{99m}Tc is only available in small amounts, resulting in difficult characterization of its compounds. Since rhenium is the third row congener and 5d analogue of technetium, it is safe to conclude that they will have similar properties. This conclusion initiated studies on the rhenium metal to model technetium. The low concentrations of [[99m]TcO4]⁻ solutions involve characterisation using HPLC or other chromatographic methods with γ-detection, in order to follow the chemistry. Thus far, most studies using HPLC revealed that rhenium and ^{99m}Tc products are not exactly the same but relatively similar.[15] This could be due to different reaction conditions and problems arising due to the hydrolysing and polymerising tendencies of technetium compounds in water.

Technetium has an assortment of oxidation states (see Table 2.3), which contributes to its complexes being unstable. Contrary to this, it presents a number of opportunities for chelation. Tricarbonyl complexes of rhenium and technetium were not very popular, until Alberto *et al*. introduced the synthesis of the air stable *fac*-[M(CO)₃(H₂O)₃]⁺ (M = Re, Tc) synthon, produced by reduction of M(VII) to M(I) in an aqueous medium. The synthesis of *fac*-[M(CO)₃(H₂O)₃]⁺ (M = Re, Tc) is prepared from permetallates under mild conditions in aqueous solution (see Figure 1.2).[16,17,18,19,20,21] When using the ^{99m}Tc kit, the formulation is disodium

[14] Dilworth, J. R.; Parrott, S. J.; *Chem. Soc. Rev.*, 43, 27, **1998**

[15] Sagnou, M.; Tsoukalas, C.; Triantis, C.; Raptopoulou, C. P.; Terzis, I. P.; Pirmettis, I.; Pelecanou, M.; Papadopoulos, M.; *Inorg. Chim. Acta*, 363, p 1649-1653, **2010**

[16] Alberto, R.; Schibli, R.; Waibel, R.; Abram, U.; Schubiger, A. P.; *Coord. Chem. Rev.*, 192, p 901, **1999**

[17] Alberto, R.; *J. Organomet. Chem.*, 692, p 1179, **2007**

boronocarbonate, $Na_2[H_3BCO_2]$, which provide *in situ*, the CO groups, and simultaneously reduce the technetium centre.[20] $Na_2[H_3BCO_2]$ is relatively stable in an aqueous medium, and upon adding the ^{99m}Tc-eluent with heating to 100 °C for 20 min, yields the $[^{99m}Tc(OH_2)_3(CO)_3]^+$ precursor. When preparing the $[^{188}Re(OH_2)_3(CO)_3]^+$ synthon, $H_3B.NH_3$ is used as the reducing agent, since rhenium is more difficult to reduce. This formulation is done in an acidic medium with H_3PO_4 and currently there is no instant kit available on the market.
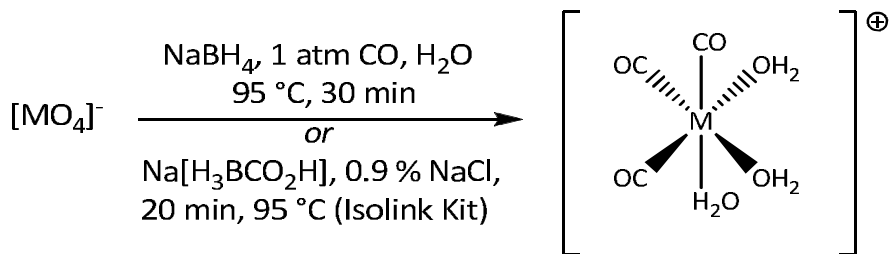
Figure 2.3: The two reaction pathways in which the *fac*-$[M(CO)_3(H_2O)_3]^+$ complex can be synthesised.

The *fac*-$[M(CO)_3(H_2O)_3]^+$ synthon is an easily accessible, highly attractive platform for the synthesis of new radiopharmaceuticals labeled with ^{99m}Tc (for diagnosis) and ^{188}Re (for therapy). This synthon have the potential of exchanging labile solvent ligands and they are very stable against hydrolysis or redox decomposition.

[18] Alberto, R.; Schibli, R.; Egli, A.; Schubiger, P. A.; Herrmann, W. A.; Artus, G.; Abram, U.; Kaden, T. A.; *J. Organomet. Chem.*, 493, p 119, **1995**

[19] Alberto, R.; Schibli, R.; Egli, A.; Schaffland, A. O.; Abram, U.; Abram, S.; Kaden, T. A.; Schubiger, P. A.; *J. Labelled Compds. Radiopharm.*, 39, p 443, **1997**

[20] Schilbli, R.; Alberto, R.; Abram, U.; Abrams, S.; Egli, A.; Schubiger, P. A.; Kaden, T. A.; *Inorg. Chem.*, 37, p 3509, **1998**

[21] Alberto, R.; Ortner, K.; Wheatly, R.; Schibli, A. P.; *J. Am. Chem. Soc.,* 123, p 3135, **2001**

2.4   The ideal radiopharmaceutical

An ideal radiopharmaceutical should possess all the characteristics listed; to provide maximum efficiency in the diagnosis of ailments and a minimum radiation dose to the patient.

2.4.1 Choosing a radionuclide with easy availability

Radiopharmaceuticals are administered to humans and this in itself creates a number of aspects that need to be considered. There are several limitations on the detection of radiation by currently available instruments; therefore radiopharmaceuticals should possess some important characteristics.

When opting for a radionuclide, the factors, properties and characteristics[22,23] to be considered are: cost and availability, half-life, particle emission, decay mode, target-to-non-target activity ratio, stability, biochemical properties, the type of radionuclide and compatibility.

2.4.2 Short-effective half-life

The half-life of a radionuclide (see Table 2.4) is defined as the time needed for half of the radiopharmaceutical to disappear from the biologic system. All radionuclides decay with their own unique half-life and it is not dependent on any physicochemical condition.   When radiopharmaceuticals are administered to humans, it disappears from the biological system through fecal, urinary excretion, perspiration or other mechanisms. The loss of radiopharmaceuticals is credited to the physical decay of the radionuclide and the biological removal of the radiopharmaceutical.

The ideal radionuclide has a half-life that is relatively short but effective. It is not longer than the time required to complete the following: a) its preparation b) transportation to its destination c) administration to the patient d) its accumulation in the target organ and e) the complete clearance of the radiopharmaceutical from non-target tissue and organs. When the target is distributed cells or tumors, radiopharmaceuticals with a longer half-life is required.[24]

---

[22] Ehrhardt, G.J.; Ketring, A.R.; Ayers, L.M.; *Appl. Radiat. Isot.*, 49, 295, **1998**
[23] Volkert, W.A.; Goeckeler, W.F.; Ehrhardt, G.J.; Ketring, A.R.; *J. Nucl. Med.*, 32, p 257, **1991**
[24] Carlsson, J.; Aronsson, E. F.; Hietala, S.; Stigbrand, T.; Tennvall, J.; *Radiotherapy & Oncology*, 66, p 107, **2003**

Table 2.4: A table containing the characteristics of radionuclides commonly used. [25], [26]

Nuclide	Physical half-life	Mode of decay	γ-ray energy (MeV)	Production method
^{3}H	12.3 yr	β^- (100)	___	^{6}Li (n,α) ^{3}H
^{11}C	20.4 min	β^+ (100)	0.511	^{10}B(d,n)^{11}C
^{13}N	10 min	β^+ (100)	0.511	^{12}C(d,n)^{13}N
^{14}C	5370 yr	β^- (100)	___	^{14}N(n,p)^{14}C
^{15}O	2 min	β^+ (100)	0.511	^{14}N(d,n)^{15}O
^{18}F	110 min	β^+ (97)	0.511	^{18}O(p,n)^{18}F
^{32}P	14.3 days	β^- (100)	___	^{32}S(n,p)^{32}P
^{51}Cr	27.7 days	EC (100)	0.320	^{50}Cr(n,γ)^{51}Cr
^{52}Fe	8.3 hr	β^+ (56)	0.165	^{55}Mn(n,4n)^{52}Fe
^{57}Co	271 days	EC (100)	0.014	^{56}Fe(d,n)^{57}Co
^{58}Co	71 days	β^+ (14.9)	0.811	^{55}Mn(α,n)^{58}Co
^{59}Fe	45 days	β^- (100)	1.099	^{58}Fe(n,γ)^{59}Fe
^{60}Co	5.2 yr	β^- (100)	1.173	^{59}Co(n,γ)^{60}Co
^{62}Zn	9.3 hr	β^+ (8)	0.420	^{63}Cu(p,2n)^{62}Zn
^{62}Cu	9.7 min	β^+ (97)	0.511	^{62}Ni(p,n)^{62}Cu
^{67}Cu	2.6 days	β^- (100)	0.185	^{67}Zn(n,p)^{67}Cu
^{67}Ga	78.2 hr	EC (100)	0.093	^{68}Zn(p,2n)^{67}Ga
^{68}Ga	68 min	β^+ (89)	0.511	^{68}Zn(p,n)^{68}Ga
^{82}Rb	75 s	β^+ (95)	0.511	^{82}Sr(EC)^{82}Rb
^{82}Sr	25.5 days	EC (100)	___	^{85}Rb(p,4n)^{82}Sr
^{89}Sr	50.6 days	β^- (100)	___	^{88}Sr(n,γ)^{89}Sr
^{90}Sr	28.5 yr	β^- (100)	___	^{235}U(n,f)^{90}Sr
^{90}Y	2.7 days	β^- (100)	___	^{89}Y(n,γ)^{90}Y
^{99}Mo	66 hr	β^- (100)	0.181	^{98}Mo(n,γ)^{99}Mo
^{99m}Tc	6 hr	IT (100)	0.140	^{99}Mo(β^-)^{99m}Tc
^{111}In	2.8 days	EC (100)	0.171	^{111}Cd(p,n)^{111}In
^{113m}In	100 min	IT (100)	0.392	^{112}Sn(n,γ)^{113}Sn
^{123}I	13.2 hr	EC (100)	0.159	^{121}Sb(α,2n)^{123}I
^{124}I	4.2 days	β^+ (23)	0.511	^{124}Te(p,n)^{124}I
^{125}I	60 days	EC (100)	0.035	^{124}Xe(n,γ)^{125}Xe
^{131}I	8 days	β^- (100)	0.284	^{130}Te(n,γ)^{131}Te
^{137}Cs	30 yr	β^- (100)	0.662	^{235}U(n,f)^{137}Cs
^{153}Sm	1.9 days	β^- (100)	70	^{152}Sm(n,γ)^{153}Sm
^{186}Re	3.8 days	β^- (92)	137	^{185}Re(n,γ)^{186}Re
^{188}Re	0.71 days	β^+ (100)	2.13	^{188}W(n,γ)^{188}Re
^{201}Tl	73 hr	EC (100)	0.167	^{203}Tl(p,3n)^{201}Pb
^{177}Lu	6.7 days	β^- (100)	0.497	^{177}Lu (n, γ)^{176}Lu

[25] Saha, G. B.; *Fundamentals of nuclear pharmacy,* 5th Edition, p 60-61, **2004**

[26] Brown, E.; Dairiki, J.; Doebler, R.E.; Shibab-Elden, A. A.; Jardine, L. J.; Tuli, J. K.; Byurn, A. B.; *Table of Isotopes,* 7th Ed., **1978**

2.4.3 Particle emission

In diagnostic radiopharmaceuticals, radionuclides that decay by α- or β-particle emission should not be used, since they cause more damage to tissue than γ rays. α-particle emitting radionuclides should never be used for *in vivo* diagnostic studies, due to high radiation exposure. β-particle emitters are mostly used in clinical studies.

> **Radionuclides emitting β-particles** - β-particles are very high energy electrons that are emitted from the nucleus and its energy is much greater than that of α-particles. If particles with high energies are emitted during radiation, sterilization of non-target tissue can occur. Depending on the amount of energy that the β-particle possesses, the tumour size for optimal curability will differ.[27,28]

> **Radionuclides emitting α-particles** - α-particle are classified as high LET radiation[29,30,31,32] and they deposit their energies over short ranges (normally between 40µm to 100µm). It is better to use α-particle emitting radionuclides where radiation is used in small cell diameters. Therefore in contrast to β-particle emitters, they are used in the treatment of smaller tumours and where their area inside the tumour is more spatially homogeneous.

> **Radionuclides emitting Auger electrons** - Emitted Auger electrons have a lower energy, when compared to α-particles and β-particles. During radioactive decay, the emitted Auger electrons leave their energy over a sub-cellular scale, which then produce highly restricted energy density in the direct vicinity of the decay area. It was shown in an experiment involving *in vivo* and *in vitro* studies that the poisonous dose of Auger-electron emitter estimates for a low LET radiation when the emitter is restricted to the cytoplasm. For a high LET α-particle radiation, the Auger electron emitters are covalently bound to the DNA in the nucleus. Therefore, when a high LET-like response is

[27] Langmuir, V. K.; Sutherland, R. M.; *Antibody ImmunoconjugatesRadiopharm.,* 1, p 195, **1988**
[28] Wheldon, T. E.; O'Donoghue, J. A.; *Int. J. Radiat. Biol,.* 58, 1, **1990**
[29] Howell, R. W.; Azure, M. T.; Narra, V. R.; Rao, D. V.; *Radiat. Res.*, 137, 352, **1994**
[30] Humm, L. J.; *Nucl. Med.*, **1990,** 31, 75
[31] Zalutsky, M. R.; Bigner, D. D.; *Act.Oncol.*, 35, 373, **1996**
[32] Black, C. D. V.; Atcher, R. W.; Baret, J.; Brichbiel, M. W.; Holton, O. D.; Hines, J. J.; Gansow, O. A.; Wenistein, J. N.; *Antibody ImmunoconjugatesRadiopharm*, 1, 43, **1988**

desired, one would encourage Auger election emitter uptake by the potential therapeutic radiopharmaceutical, which is tagged with Auger electron emitters.[33]

2.4.4 Decay by electron capture or isomeric transition

Particle emitting radionuclides are less attractive; therefore using radionuclides that decay by electron capture or isomeric transition for diagnostic purposes are more advantageous. γ-emitting particles with high energy (between 30 keV and 300 keV) is much more applicable in diagnostic studies. In the past, it was difficult to achieve a γ-ray collimation at energy above 300 keV, because the technology was not as advanced. However, nowadays collimators for 511 keV is available and it is used for SPECT imaging using [18]FDG.

2.4.5 Relatively high target-to-nontarget activity ratio

The ideal radiopharmaceutical has a high target-to-nontarget activity ratio, and it is of high importance that the radiopharmaceuticals used, be localized in the target organ. This is merely because the radiated non-target areas can interfere with the quality of the picture of the target organ.

2.5 Factors influencing radiopharmaceutical design[34]

➢ Compatibility - when integrating a radiolabel into a molecule, both its chemical properties should firstly be evaluated. The primary reason is that only specific radionuclides can be used to label certain compounds, because it is dependent on their chemical behavior.

➢ Stoichiometry – in tracer level chemistry, it is utterly important to know the amount of each component to be added, because excessively high or low concentrations of either component can affect the integrity of its preparation. The ratios of the different compounds can be obtained by equating the chemical reactions in question.

---

[33] Volkert, W. A.; Hoffman, T. J.; *Chem. Rev.*, 99, 2272, **1999**

[34] Saha, G.B.; *Fundamentals of Nuclear Pharmacy*, 4th Edition, Springer, **1998**.

➢ Charge of the molecule – this factor becomes very important when it comes to the solubility of the radiopharmaceutical, because in an aqueous solution, the greater the charge, the higher the solubility of the radiopharmaceutical. An obvious fact is that non-polar molecules will only dissolve in organic solvents and lipids.

➢ Size of a molecule – the molecular size of a radiopharmaceutical has a direct influence on its biological absorption, because larger molecules (> 60 000) will not be filtered by the glomerulus in the kidneys.

➢ Protein binding – most drugs bind to protein and albumin is the main contender in this type of binding. The factors that influence the binding of proteins are: pH, concentration of anions in plasma, the charge on the molecule and also the nature of the protein. Protein binding can affect plasma clearance, tissue distribution and organ uptake, therefore the determination of the extent of protein binding should be done.

➢ Solubility – when a radiopharmaceutical agent is administered to a patient by injection, its ionic strength and osmolality should be suitable for blood and it should be at the same pH as blood (pH = 7.4).

➢ Stability – one of the most important factors to keep in mind when designing new radiopharmaceuticals is its *in vivo* and *in vitro* stability, since *in vivo* breakdown can cause undesirable biodistribution of radioactivity. Factors that can influence the stability of radiopharmaceuticals are pH, temperature, and light.

➢ Biodistribution – one needs to do a proper evaluation regarding the biodistribution of the radiopharmaceutical. This will include the efficiency, usefulness, tissue distribution, plasma clearance, urinary - and fecal excretion. Toxic effects must also be studied, which include the extent of damage to tissues and the consequential physiologic dysfunction of organs.

2.6   Important factors in labeling

During the labeling process, several important factors need to be considered. These factors are briefly discussed below:[35]

 ➢ Efficiency of the labeling process – High product yields are not always attainable and the only time low yields are acceptable is when: a) the product is pure and intact, b) the cost involved is minimal and c) no better method is available for labeling.

 ➢ Chemical stability of the product – Stability highly depends on the bond linking the radionuclide and the compound, therefore a large stability constant is required. A compound yielding a covalent bond is comparatively stable under various physicochemical conditions.

 ➢ Denaturation or alteration – During labeling, numerous physicochemical conditions can change the structure and/or the biological properties of a labeled compound eg. proteins are denatured at high (pH > 10) and low (pH < 2) $[H]^+$ concentrations, and red blood cells denature at high temperatures (> 37 °C).

 ➢ Isotope effect – Sometimes different physical and biological properties are found when the isotopes of atoms are used, due to the difference in mass numbers, causing a change in the properties of the labeled compound.

 ➢ Carrier-free or No-carrier added state (NCA) – Packaging techniques has to be developed whereby the labeling yield is unaffected by low concentrations of the tracer in the carrier-free or NCA state, because radiopharmaceuticals tend to absorb on the inner walls of containers if they are in these states.

 ➢ Storage conditions – External factors like temperature and light can aid in decomposition of radiopharmaceuticals, therefore the conditions of storage is highly important.

 ➢ Specific activity – Specific activity is the activity per gram of labeled substance and high specific activity is required in the applications of radiolabeled compounds, although in some instances it can cause radiolysis in the labeled compound.

---

[35] Saha, G.B.; *Fundamentals of Nuclear Pharmacy*, 4th Edition, Springer, p 84, **1998**.

➢ Radiolysis – This is the phenomenon in which the radiation emitted by the radionuclide cause decomposition of the labeled compound. The radiation can break down the chemical bonds within the molecule and also produce free radicals, by decomposition of the solvent.

➢ Purification and analysis – Impurities are normally caused by fission of heavy metals, producing many product nuclides and these contaminants can be removed by separation methods. Incomplete radiation cause radiochemical and chemical impurities, which can be removed by e.g. ion exchange, solvent extraction, etc.

➢ Shelf-life – The efficiency of a labeled compound is effective when used within the shelf life period. Its efficiency highly depends on the half-life, the solvent, additives, nature of the emitted radionuclides, the labeled molecule, as well as the nature of the chemical bond between the molecule and the radionuclide.

2.7 Methods for labeling

Radiolabeling can primarily be described as the process whereby atoms or groups of atoms of a molecule are substituted by similar or different radioactive atoms or groups of atoms. There are six major radiolabeling techniques employed in the preparation of labeled compounds for medical use (see Table 2.5).

Table 2.5: General techniques used in radiolabeling.[36]

Technique	Example
Exchange of isotopes	^{14}C-; ^{35}S-; ^{3}H-labeled compounds
Introducing a foreign label	^{18}F-fluorodeoxyglucose (FDG)
	All ^{99m}Tc radiopharmaceuticals
	^{111}In-DTPA-albumin
Biosynthesis	^{57}Co-cyanocobalamin
	^{75}Se-selenomethionine
Recoil labeling	^{3}H-labeled compounds
Excitation labeling	^{123}I-labeled compounds (by ^{123}Xe-decay)
	^{77}Br-labeled compounds (by ^{77}Kr-decay)

---

[36] Saha, G. B.; *Fundamentals of nuclear pharmacy,* 5th Edition, p 87, **2004**

➤ **Reactions involving isotope exchange:** Involves the replacement of one or more atoms in a molecule by the isotope of the same element. The daughter molecule (radiolabeled molecule) and the parent molecule are exactly the same (similar biological and chemical properties), except for isotope effect.

➤ **Introducing a foreign label (Integrated approach):** Radionuclides are integrated into molecules that have recognized biological functions, which mimic the binding site of a biomolecule.

➤ **Labeling with bifunctional chelators (Biofunctional approach):** Bifunctional chelating agents are conjugated to a large molecule (eg. proteins; antibodies) on the one side and to a metal ion (eg. In or Tc) by chelation on the opposite side.

➤ **Biosynthesis:** Living organisms are grown in a cultured medium, which have a radiotracer. The tracer is integrated into the metabolites produced by the metabolic processes of the organism, and the metabolites are then chemically separated.

➤ **Recoil labeling:** During the decay process, particles are emitted which produces recoil atoms or ions (interaction of an atom with an energetic elementary particle) that can form a bond with other compounds that are present in the target material. This method is not used on a large scale because it has the following disadvantage: the high energy of the recoil atoms result in low yields thus low specific activity of the labeled compound.

➤ **Excitation labeling:** This low yield producing method involves the usage of radioactive and extremely reactive daughter ions produced in a nuclear decay process. β decay or electron capture result in the production of energetic charged ions, which are able to label a range of compounds of interest.

The most frequently used methods are illustrated in Figure 2.4, with a more in depth look at these methods (see Paragraphs 2.6.1. and 2.6.2). Radioactive labeled compounds are widely used in the medical and biochemical field. However in the medical field, compounds labeled with β-emitting radionuclides are mostly used in *in vivo* experiments and therapeutic treatments, whereas γ-emitting radionuclides have fairly broader applications. γ-emitting radionuclides are particularly useful for the imaging of different internal organs.
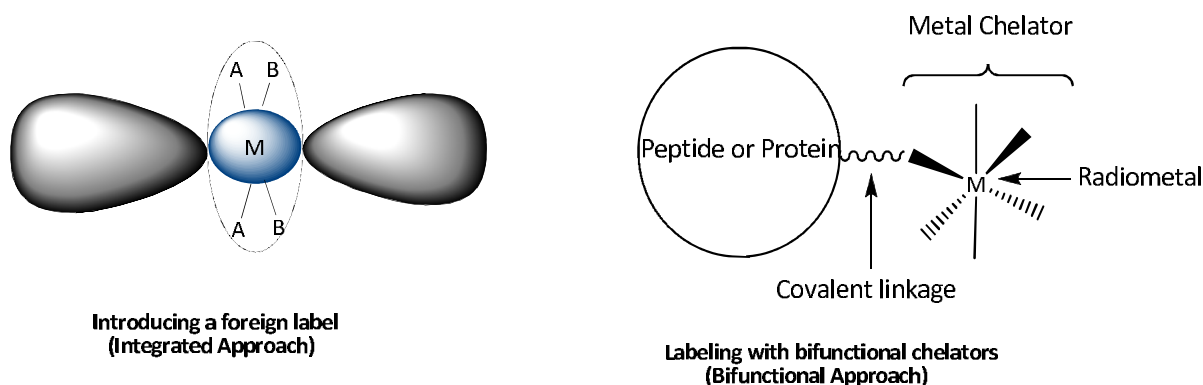
Figure 2.4: Illustration of the integrated – (left) and bifunctional approach (right) used for radiolabeling.

2.7.1 Integrated approach

The integrated approach[37] involves the replacement of a component of a high affinity receptor ligand with a foreign radionuclide chelate, by the formation of covalent or coordinate covalent bonds. The alteration of the molecule is minimal regarding its binding affinity, chemical and biological properties, conformation and size. The labeling radionuclide is not familiar to the molecule and the labeling does not occur by the exchange of one of its isotopes.

The disadvantages of using this method are:

➢ the uncertainty of the *in vivo* stability;

➢ consequently a more challenging target needs to be synthesized and

➢ the receptor binding affinity can be lost.

Most compounds that are synthesized using this method, involves chemical bond formation by chelation (more than one atom donates a pair of electrons to the foreign acceptor atom), which is normally a transition metal. Figure 2.5[38] illustrates a few structures of complexes synthesized using this approach.

---

[37] Engelbrecht, H.P.; Otto, S.; Roodt, A.; *Acta Crystallogr. Sect. C*, 199, C55, 1648
[38] Hom, R.K.; Katzenellenbogen, J.A.; *Nucl. Med. Biol.*, 24, 485, **1997**

Parent ligand   **Integrated approach**
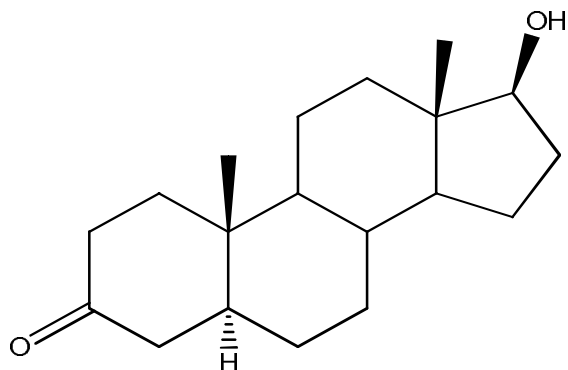
5α-Dihydrotestosterone (DHT)
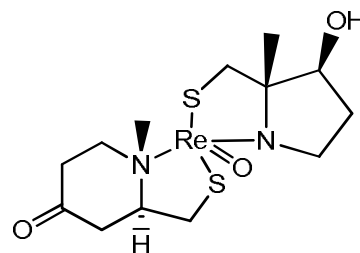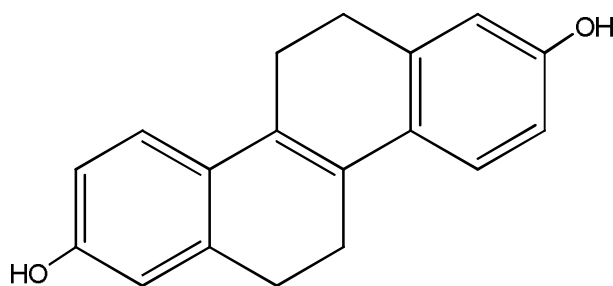
[2 + 2] N$_2$S$_2$ Complex

Non-Steroidal Estrogen
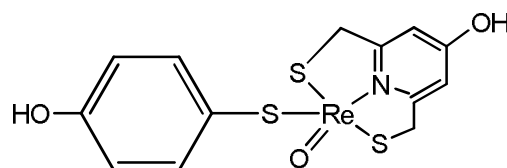
[3 + 1] NS$_3$ Complex
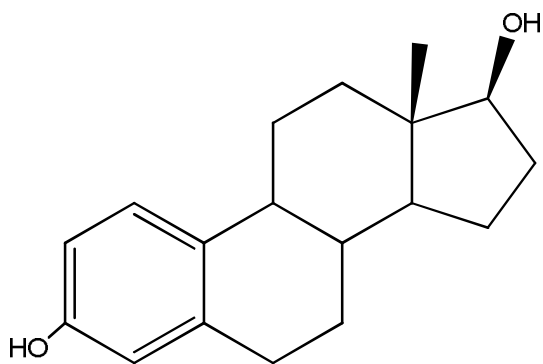
Estradiol
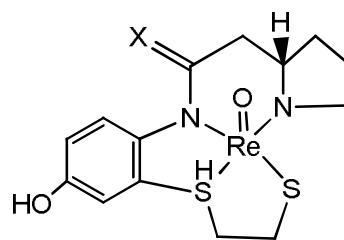
Tetradentate N$_2$S$_2$ Complex
X = O (unstable)
X = H, H (moderately stable)

Figure 2.5: Structures of integrated inorganic metal (Re or Tc) chelate systems that mimic estrogens.

A radioactive metal (Re or Tc) is incorporated into the parent ligand to form complexes that mimics estrogens. These complexes are prepared by treating the heteroatom chelate system

with $Tc(O)Cl_4^-$ or $(Ph_3P)_2Re(O)Cl_3$, in which the complex replace two of the central rings of the steroid ligand.[39]

Two more examples are given to illustrate the integrated approach. These compounds mimic epinephrine and dopamine (see Figure 2.6),[40] with a radioactive carbon and fluorine respectively incorporated in the molecule.

$[^{11}C]$ Norephedrine   6-$[^{18}F]$ Fluorodopamine
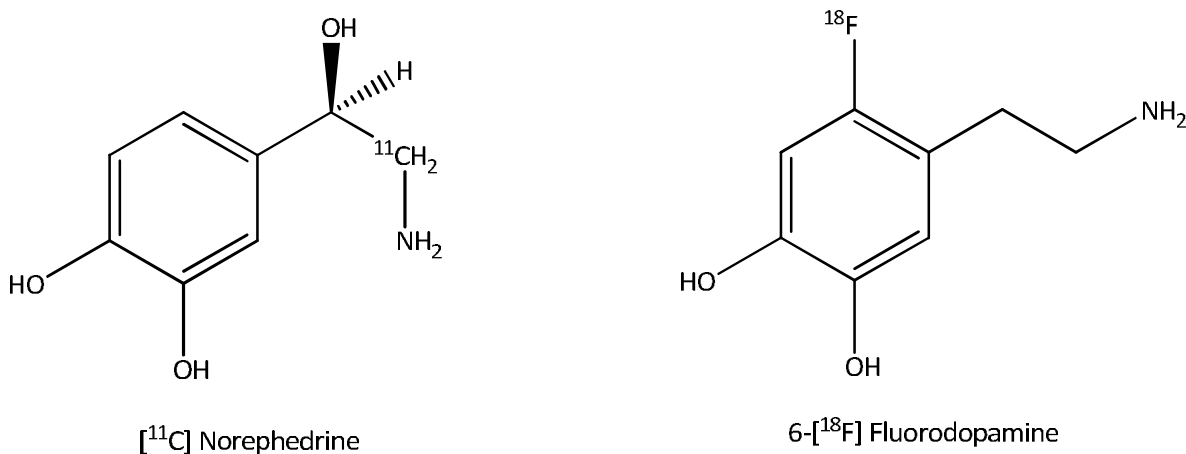
Figure 2.6: Structures of positron labeled epinephrine and dopamine compounds.

2.7.2 Bifunctional approach

The bifunctional approach[41] involves the following:

➢ the use of a biofunctional chelating agent (BFCA) for the conjugation of the receptor ligand;

➢ the chelation of the radiometal;

➢ and a linker as the pharmacokinetic modifier.

In the last 20 years, there has been a substantial amount of research in the area of BFCA design. When designing new receptor based radiopharmaceuticals, this is the most well-liked approach to use, primarily because of the likelihood of retaining the receptor binding affinity. A BFCA consists of a chelator, complexed to a radiometal and a functional group for attachment to the

---

[39] Skaddan, M. B.; Katzenellenbogen, J. A.; *Bioconj. Chem.*, 10, 119-129, **1999**
[40] Chakraborty, P.; Gildersleeve, D.; Jewett, D.; Toorongian, S.; Kilbourn, M.; Schwaiger, M.; Weiland, D*.; Nucl. Med. Biol.*, 20, 939-44, **1993**
[41] Liu, S.; Scott Edwards, D.; *Chemical Reviews*, 99, 2237, **1999**

biomolecule (eg. monoclinical antibodies, peptides and smaller organic molecules such as folic acid – see Figure 2.4). These are molecules that are specifically designed for the purpose of functionalization of biomolecules and subsequent radiometals. Schubiger *et al.* describes in his review the most common BFCA's used for radionuclides of copper, technetium and rhenium. Prerequisites of an optimal BFCA: a) it should be strong enough to coordinate to the radiometal at dilute concentrations, b). it should give a high yield with the formation of only the desired product, c). *in vivo*, it should yield a kinetically and thermodynamically stable complex with the radiometal and d). it should not influence the biological properties of the conjugate.

Linkers connect the radiometal complex to the target molecule and they are equipped with functional groups like carboxylic acids and hydroxyls, which can bind to the biomolecule (see Figure 2.7). They are compounds frequently used for modifying pharmokinetics. Linkers that can be metabolized by the biological system are sometimes used, mainly to increase the blood clearance and to reduce background activity. Until now, functional groups that form amide, thiourea, urea, Schiff base or thioether linkages with amine or thiol groups on proteins and peptides have been depicted.[42,43,44,45]
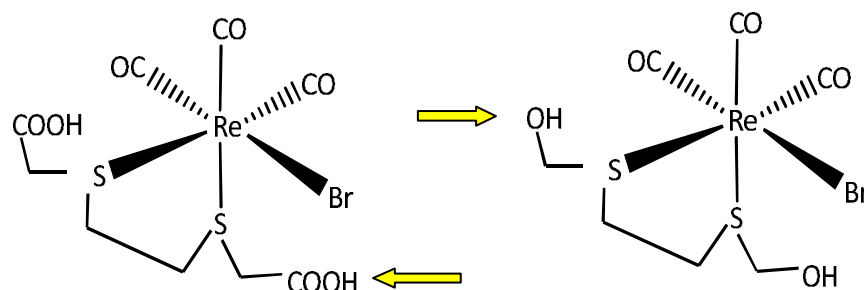
Figure 2.7: Illustration of compounds that can be used as linkers.[46]

A vast variety of mono-, bi- and tridentate ligand systems encompassing different donor atoms and groups have been developed and are still designed and optimized. A number of BFCA's has been designed specifically for the $M(CO_3)^+$ core, of which bidentate ligands have proven to be very fast coordinating entities. When compared to bidentate chelates, tridentate ligands do not

[42] Meares, C.F.; *Nucl. Med. Biol.*, 13, 311, **1986**

[43] Parker, D.; *Chem Soc. Rev.*, 19, 271, **1990**

[44] Gansow, O. A.; *Nucl. Med. Biol.*, 18, 369, **1991**

[45] Schubiger, P. A.; Alberto, R.; Smith, A.; *Bioconjugate Chem.*, 7, 165, **1996**

[46] Pietzsch, H. J.; Gupta, A.; Reisgys, M.; Drews, A.; Seifert, A.; Syhre, R.; Spies, H.; Alberto, R.; Abram, U.; Schubiger, P.A.; Johannsen, B.; *Bioconjugate Chem.***,** 11, 414-424, **2000**

show significantly increased thermodynamic stability, however, their reaction rate is much faster. Due to guaranteed results, the most investigated bioconjugated technetium and rhenium complexes are the ones using tetradentate N,S donating ligand systems.

Mixed ligand approaches (4+1, 3+1, 3+2 etc.) are well documented for Tc and Re in higher oxidation states. These mixed ligand systems can be used on different metal cores: $(MO)^{3+}$, $(MN)^{2+}$, $[M(CO)_3]^+$ or M^{3+}.
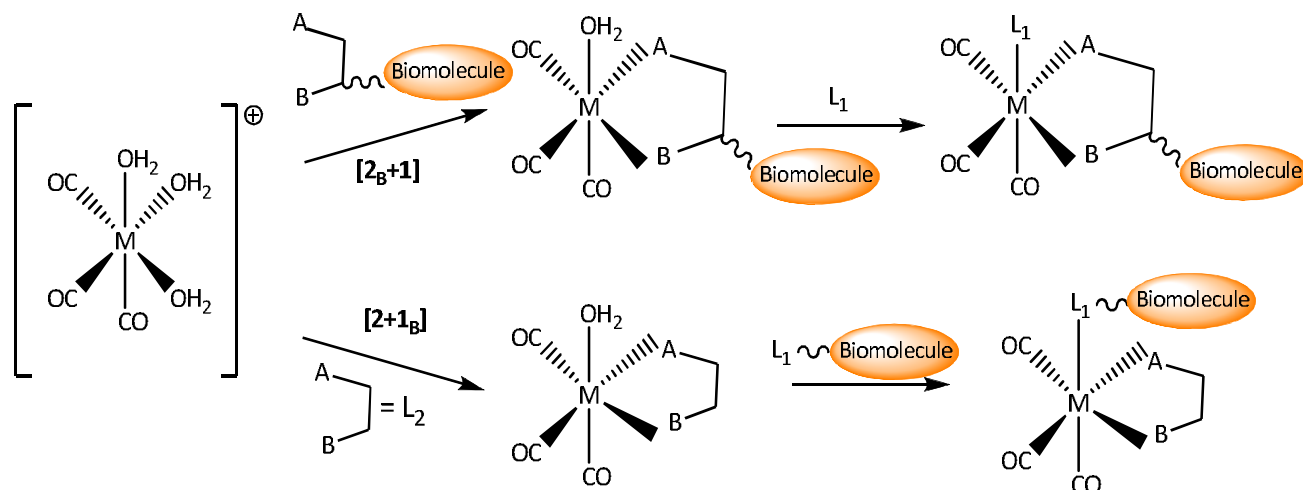
M = Tc or Re; L_1 = monodentate ligand; A,B = O, N, S, etc.

Figure 2.8: An illustration of mixed ligand approaches, using a combination of mono- and bidentate ligannd systems, coupled to biomolecules.

The $[M(CO)_3]^+$ core permits comparable potentials, since the H_2O ligands in the *fac*-triaquatricarbonyl entity are readily substituted, as mentioned earlier. The water ligand in complexes of the type $[M(H_2O)L_2)(CO)_3]$ (L_2 = bidentate ligand) is loosely bound and can be replaced by a strong monodentate ligand (L_1), forming complexes of the form $[M(L_1)(L_2)(CO)_3]$, creating the possiblity of coupling either L_1 or L_2 to biomolecules (see Figure 2.8).[47] The mixed ligand system of interest here is the 2+1 ligand system. This approach has several advantages:

➢ the functionalization of the biomolecules is minimized or simplified,

➢ the resulting complexes or bioconjugates are coordinately saturated, and

➢ further flexibility concerning the potential modification of the physicochemical properties of the radiopharmaceutical is possible.

---

[47] Mundwiler, S.; Kundig, M.; Ortner, K.; Alberto, R.; *Dalt. Trans.*, 1320-1328, **2004**

Several Re(I) and Tc(I) complexes have been prepared, using this approach, using dithiocarbamate isocyanide chelating systems[48], a N, N-dimethyldiocarbamate bidentate ligand[49] and monodentate ligands like imidazole and benzyl isocyanide.

This BFCA approach can be used to perform receptor imaging, because it contains a biologically active molecule and the physic-chemical properties of the latter can be altered. Compared to the integrated approach, the usage of the BFCA approach is more advantageous, because the receptor binding affinity can be retained. This is because the radiometal is not directly attached to the target moiety, which in turn can disturb the conformation of the target molecule.

2.8   Technetium imaging agents

When technetium was administered in the form of $[^{99m}TcO_4]^-$ for thyroid disease in 1961, new possibilities in the radiopharmaceutical field opened. The thyroid takes up iodide, and the use of the pertechnetate anion was exclusively based on the size and charge of the complex, thus expecting it to mimic iodide behavior. This marks the first of a series of technetium essential agents, giving birth to the possibility of using technetium agents in heart, brain, kidney and liver imaging, i.e. the *first generation* [Figure 2.9 (A)] agents. The *second generation* [Figure 2.9 (B)] was a series of more specific agents, whereby the targeting potential is located in the biologically active molecule (BAM), which is covalently bonded to the technetium complex. In the case of the under developed *third generation* [Figure 2.9 (A)] agents, the outer surface of the complex itself, contains the groups necessary for receptor binding.

---

[48] Gorshkov, N.I.; Schibli, R.; Schubiger, A. P.; Lumpov, A. A.; Miroslavov, A. E.; Suglobov, D. N.; *J. Organomet. Chem.*, 689, 4757, **2004**

[49] Riondato, M.; Camporese, D.; Martín, D.; Suades, J.; Alvarez-Larena, A.; Mazzi, U.; *Eur. J. Inorg. Chem.*, 4048, **2005**
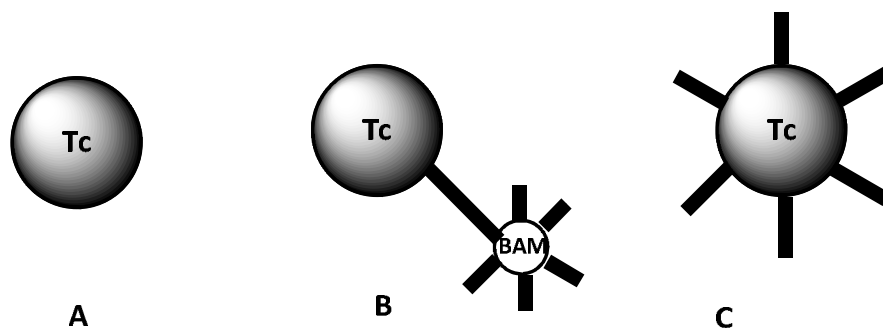
Figure 2.9: First- (A), second- (B) and third generation (C) technetium imaging agents.

2.8.1 First generation technetium imaging agents

2.8.1.1 Brain imaging

The standard of brain imaging is governed by a mechanism called the blood-brain barrier (BBB). Thus it is vitally important for all brain imaging agents to cross the BBB hence be fairly lipophylic and have an overall neutral charge. Based on the BBB principle, radiopharmaceuticals for brain imaging can be categorized in two groups: diffusible and non-diffusable. The successful commercially developed Ceretec® (see Figure 2.10)[50], a compound that uses the hexa-methylpropyleneamineoxime proligand (HMPAO hexametazime), falls in the diffusible category, since it is lipophylic and readily cross the BBB. Back in the 1980's, The University of Missouri did research on a series of neutral amine-oxime complexes, demonstrating that it could be readily prepared from $[TcO_4]^-$ after reduction with Sn^{2+} ion. This research led to the development of the Ceretec® agent, by Amersham International. When Ceretec® crosses into the brain; it is converted to a secondary complex which is hydrophilic, making it incapable of backing out of the brain.

---

[50] Leonard, J. P.; Novotnik, D. P.; Neirinckx, R. D.; *J. Nucl. Med.*, 27, 1819, **1986**
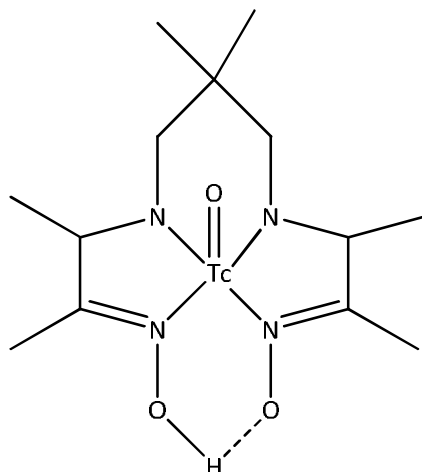
Figure 2.10: The molecular structure of Ceretec®.

Another popular brain imaging agent is ethylenecysteine diester (ECD), commercially known as Neurolite® (see Figure 2.11).[51] It is also a lipophilic complex that localize in the brain, whereby one of the ester groups are hydrolysed in an enzyme-catalyzed reaction, to form an anionic complex. This anionic complex cannot diffuse across the BBB, thus preventing the washout from the brain.
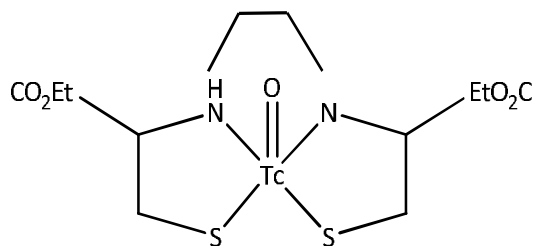
Figure 2.11: The molecular structure of Neurolite®.

2.8.1.2 Heart imaging

The initial heart imaging agent used ^{201}Tl as the radionuclide, which they thought is blood flow dependent, meaning people had to exercise for optimal uptake. They then found that during the excersice test, the normal tissues accumulate more thallium (due to high blood flow) than ischemic tissue (reduced blood flow). Further research was done, as scientist originally assumed that lipophilic positively charged complexes would collect in the heart, via the Na$^+$/K$^+$ ATPase

---

[51] Cheesman, E. H.; Blanchette, M. V.; Ganey, L. J.; Maheu, L. J.; Miller, S. J.; Watson, A. D.; *J. Nucl. Med.*, 33, 1888, **1992**

mechanism. This led to the synthesis of the cationic complex (see Figure 2.12), $[^{99m}Tc(dmpe)_2Cl_2]^+$, where dmpe = 1,2-bis(dimethylphosphino)ethane, as a perfusion agent.
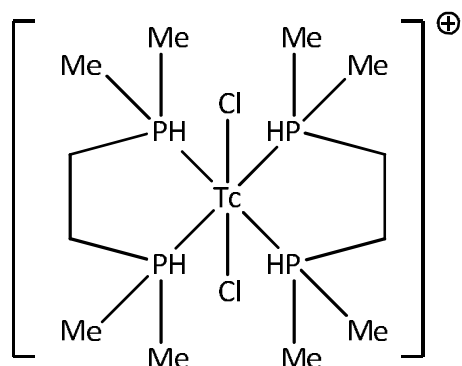
Figure 2.12: The molecular structure of $[^{99m}Tc(dmpe)_2Cl_2]^+$.

However, later it was discovered that this complex goes through *in vivo* reduction to the neutral complex $[^{99m}Tc(dmpe)_2Cl_2]$, leading to rapid washout from the heart.[52] With further research into cationic complexes as myocardial perfusion agents, the discovery of the octahedron $[^{99m}Tc(MIBI)_6]^+$, where MIBI = 2-methoxy-2-methylpropyl-isocyanide, commercially known as Cardiolite® (see Figure 2.13), surfaced.[53] This cationic complex, also known as Sestamibi, accumulates via diffusion mechanism and electrostatic binding.

---

[52] Gerson, G. C.; Deutch, E. A.; Nishyama, H.; Libson, K. G.; Adolph, R. J.; Grossman, L. W.; Sodd, V. J.; Fortman, J. L.; Vanderhagden, C. C.; Williams, C. C.; Salinger, E. L.; *Eur. J. Nucl. Med.*, 8, 371, **1983**
[53] Holman, B. L.; Jones. A. G.; Lister-James, J.; Davison, A.; Abrams, M. J.; Kirschenbaum, J. M.; Tubeth, S. S.; English, R. J.; *J. Nucl. Med.*, 25, 1350, **1984**
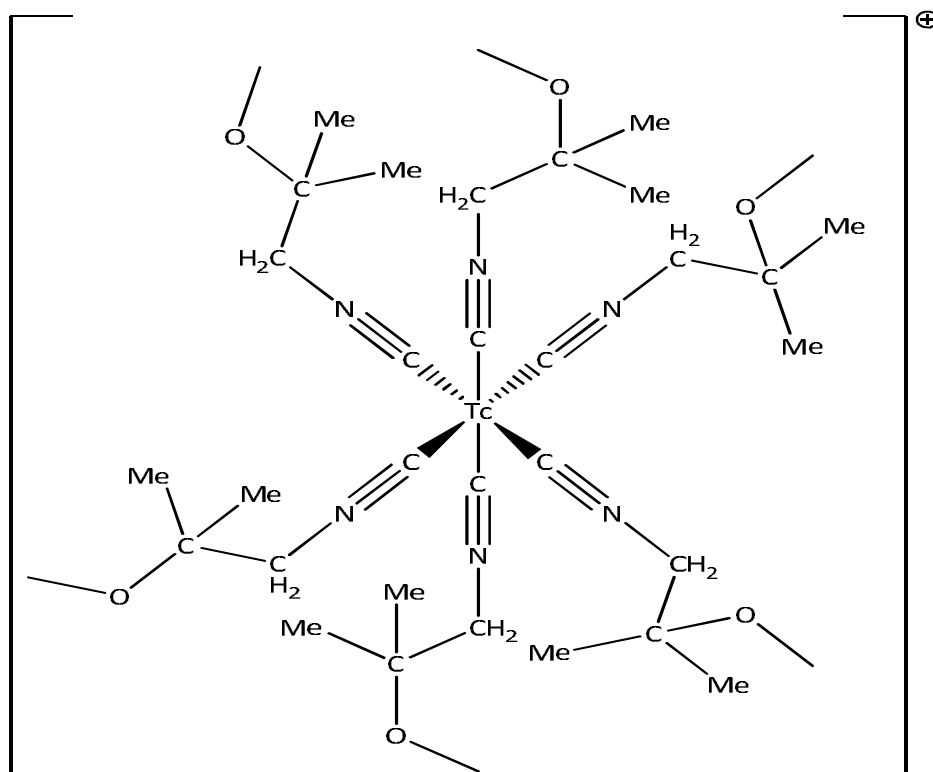
Figure 2.13: The molecular structure of [^{99m}Tc(MIBI)$_6$]$^+$.

Neutral complexes were also investigated; scientists found the first neutral myocardial perfusion agent, ^{99m}Tc-teboroxime (see Figure 2.14), commercially known as Cardiolite®.[54] The formula for this compound is [TcCl(CDO)(CDOH)$_2$BMe], where (CDOH)$_2$ = cyclohexanedione dioxime, and it accumulate in the heart *via* an unknown mechanism.
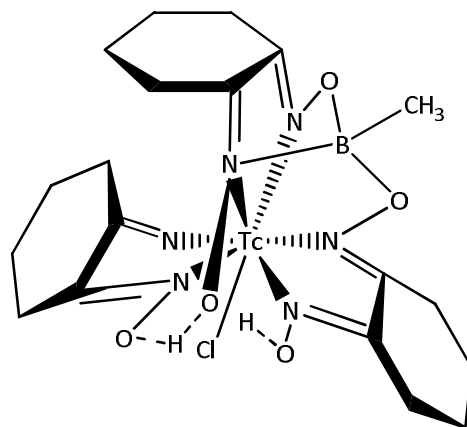
Figure 2.14: The molecular structure of Cardiolite®.

---

[54] Liner, K. E.; Malley, M. F.; Gongoutas, J. Z.; Unger, S. E.; Nunn, A. D.; *Inorg. Chem.*, 29, 2428, **1990**

$^{99m}TcN^{2+}$-core (see Figure 2.15) containing imaging agents was assessed as a myocardial imaging agent next. ^{99m}Tc-NOET, where NOET = *N*-ethoxy-*N*-ethyldithiocarbamate,[55] was the new heart imaging radiopharmaceutical and it was different from the positively charged lipophilic agents, as this compound was neutral. The development of this neutral compound confirmed that the positively charged myocardial imaging agents are not vital, but the mechanism of its accumulation in the heart is unknown.
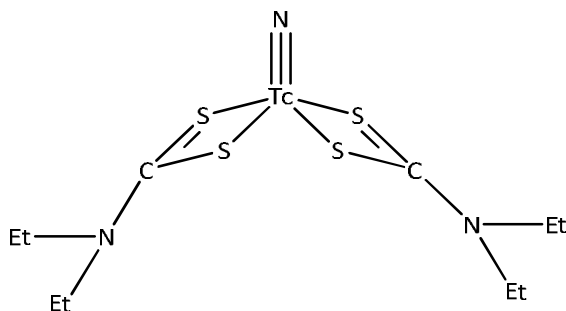
Figure 2.15: The molecular structure of ^{99m}Tc-NOET**.**

Two more positively charged myocardial imaging agents has also been introduced in recent years, ^{99m}Tc-P53, where P53 = *trans*-dioxo*bis*[*bis*(2-ethoxo*bis*(2-ethoxy-ethyl)phosphino] ethane, see Figure 2.16 A, and ^{99m}Tc-Q12, a mixed N_2O_2-donor Schiff base/phosphine cation, see Figure 2.16 B.[56] These complexes are commonly known as tetrofosmine or Myoview® and TechneCard® respectively.

---

[55] Pasqualini, R.; Duatti, A.; *J. Chem. Soc., Chem. Commun.*, 1354, **1992**

[56] Kelly, J. D.; Forster, A. M.; Higley, B.; Archer, C. M.; Booker, F. S.; Canning, L. R.; Edwards, B.; Gill, H. K.; McPartlin, M.; Noyle, K. R.; Lathan, I. A.; Pickett, R. D.; Storey, A. E.; Webbon, P. M.; *J. Nucl. Med.*, 24, 353, **1992**
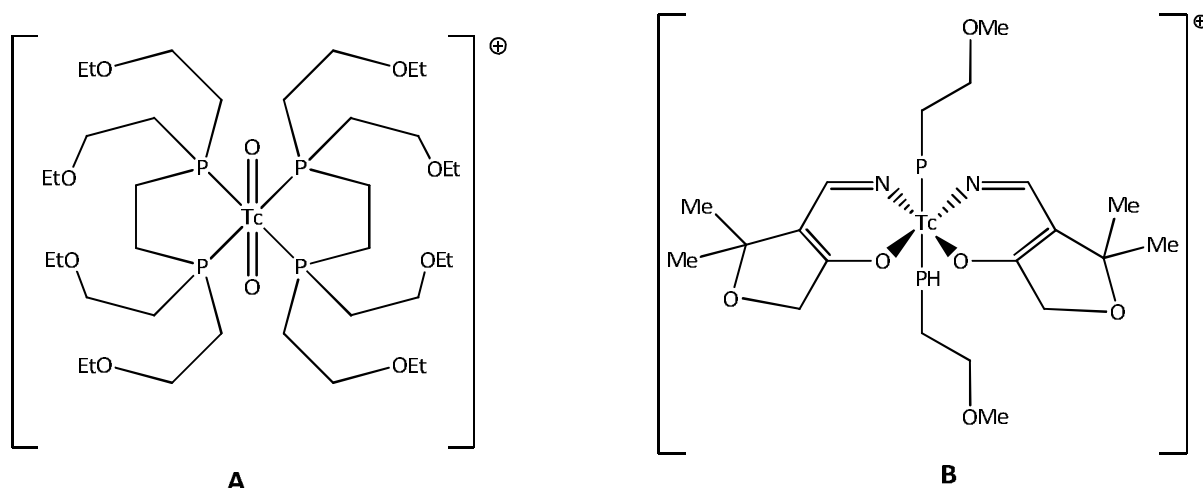
Figure 2.16: The molecular structures of Myoview® (A) and TechneCard® (B).

2.8.1.3 Liver imaging

When imaging the hepatobiliary system, Tc-sulfur colloid (made up of $^{99m}Tc_2S_7$ and colloidal sulphur) and the successful anionic ^{99m}Tc-HIDA, where HIDA = (2,6-dimethylphenylcarbamoylmethyl) iminodiacetic acid,[57] complexes are used and the latter has three endorsed analogues. These three compounds are ^{99m}Tc-Lidofenin (TechneScan®), ^{99m}Tc-Disofenin (Hepatolite®) and ^{99m}Tc-Mebrofenin (Choletec®), see Figure 2.17.

With R =

Lidoferin if $R_1 = CH_3$
Disoferin if $R_1 = $ Isopropyl
Mebroferin if $R_1 = R_3 = CH_3$; $R_2 = $ Br
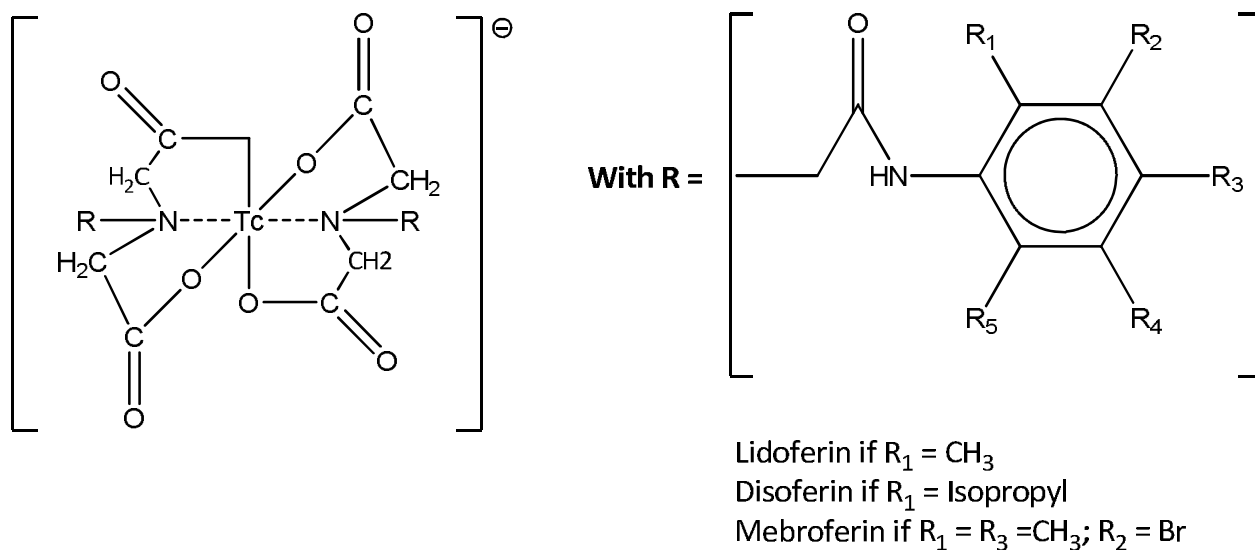
Figure 2.17: The proposed molecular structures of ^{99m}Tc-HIDA.

---

[57] Fritzberg, A. R.; Kasina, S.; Eschima, D.; Johnson, D. L;, *J. Nucl. Med.*, 27, 111, **1986**

2.8.1.4 Kidney imaging

$[^{99m}TcO(glucoheptonate)_2]^-$ is one of the first kidney imaging agents, however the precise structure of this compound is unknown, but researchers believe that it might have a five coordinate structure as illustrated in Figure 2.18.[58] It is commonly known as TechneScan® or Glucoheptate® and these are not one of the most widely used imaging agents, because of the accessibility of improved options.
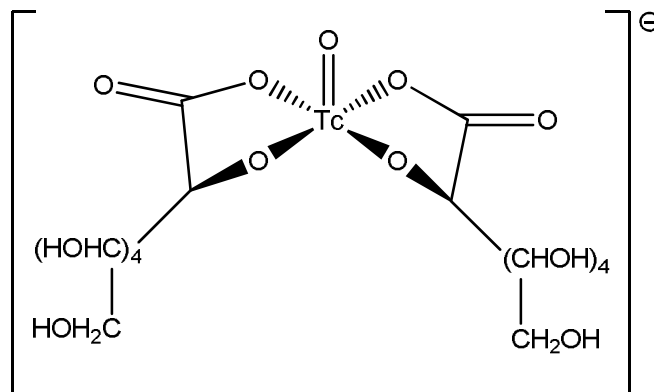
Figure 2.18: The proposed molecular structures of $[^{99m}TcO(glucoheptonate)_2]^-$.

In recent years, the most frequently used anionic kidney imaging agent $[^{99m}TcO(MAG_3)]^-$, where MAG_3 is mercaptoacetyltriglycine, was developed by Fritzberg.[59] $[^{99m}TcO(MAG_3)]^-$ is a square pyramidal complex (see Figure 2.19), containing a free carboxylic acid group, which is believed to be necessary for efficient renal excretion. This complex does not have a chiral centre, like other kidney imaging agents, therefore no complications arise from the existence of isomers. The rhenium analogue of this structure has also been determined.

---

[58] Costello, C. E.; Brodack, J. W.; Jones, A. G.; Davison, A.; Johnson, D. L.; Kasina, S.; Fritzberg, A. R.; *J. Nucl. Med.*, 24, 353, **1983**
[59] Holman, B. L.; Devous, M. D.; *J. Nucl. Med.*, 33, 1888, **1992**
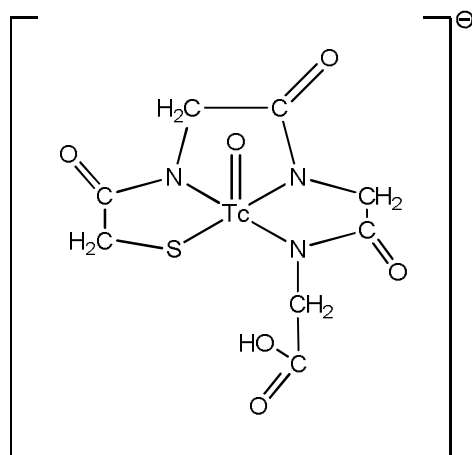
Figure 2.19: The molecular structures of [^{99m}TcO(MAG$_3$)]$^-$.

2.8.1.5 Bone imaging

Initially a series of ^{99m}Tc compounds complexed with phosphonate ligands, using pyrophosphates, was used to develop bone-imaging agents. However, later it was discovered that diphosphonates, such as methylenediphosphonate (MDP, see Figure 2.20 A) gave a much better performance.

A	B
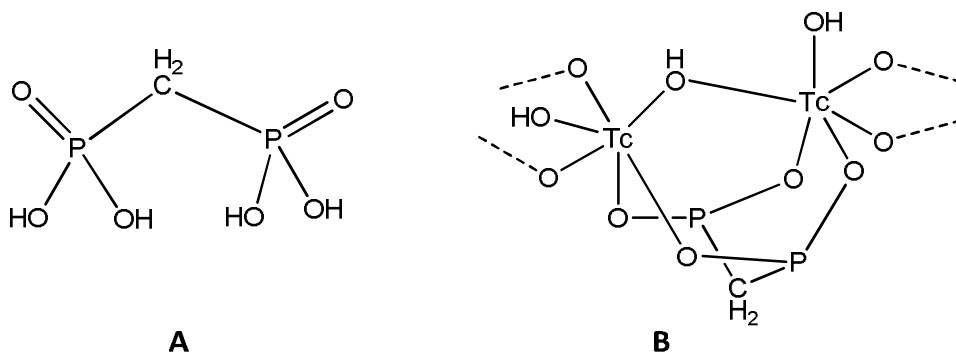
Figure 2.20: The molecular structures of MDP and the polymeric structure that forms.

It is believed that the dominant oxidation state for ^{99m}Tc/MDP is Tc(IV) and when [^{99}TcBr$_6$]$^{2-}$ is reacted with H$_4$MDP, a polymeric complex is formed as illustrated in Figure 2.20 B.

2.8.2 Second generation technetium imaging agents

2.8.2.1 Steroid receptors

Complexes of technetium targeting the steroid receptors have been an active research field, because estrogen, progesterone and androgen receptors are known to be over-expressed in breast, ovarian and prostate cancers. Katzellenbogen *et al.* has done extensive research with steroid receptor ligands using technetium as the metal core. The first technetium complexes that they reported were progestin conjugates of N_2S_2 chelates via a phenyl spacer (see Figure 2.21 A). Another approach to synthesise a complex that is overall similar to progesterone, is to incorporate the receptor binding sites directly onto the outer periphery of the Tc ligands. A structure of this calibre is illustrated in Figure 2.21 B. An illustration of an analogues complex of estradiol is apparent in Figure 2.21 C.[60]
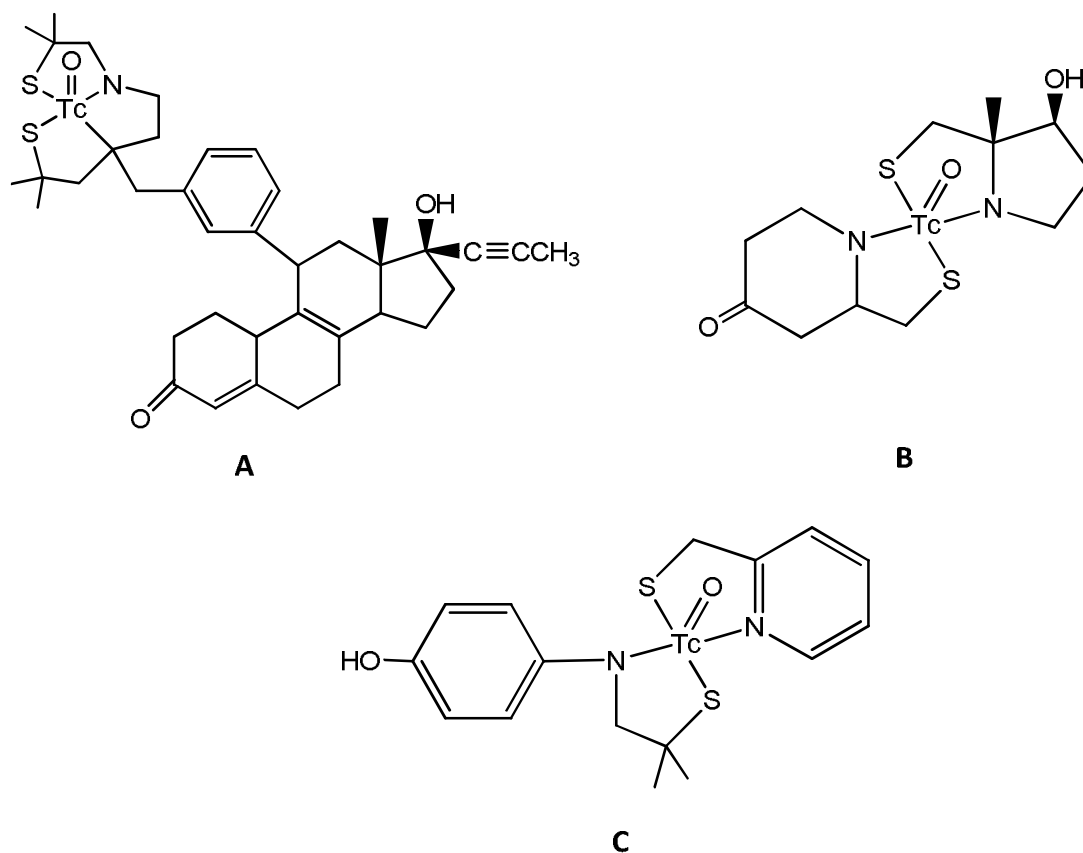
Figure 2.21: Molecular structures of progestin (A and B) and estradiol analogues (C).

[60] Chi, D. Y.; O'Neil, J. P.; Anderson, C. J.; Welch, M. J.; Katzenellenbogen, J. A.; *J. Med. Chem.*, 27, 928, **1994**

2.8.2.2 Central nervous system (CNS) receptors

There are several significant diseases and psychiatric illnesses that are related to the alterations in the densities of neurotransmitter receptor sites in the brain, eg. benzodiazepene (epilepsy), muscarinic and nicotinic (Alzheimer's disease), dopaminergic (Parkinson's disease and psychiatric conditions), serotonergic (psychiatric conditions). PET imaging was initially used in the first studies, but due to the limited availability of a cyclotron in close proximity, it was difficult to effectively follow studies. ^{123}I was used for brain receptor imaging; however, this isotope is expensive and not extensively available, like the ^{99m}Tc isotope. This led to a worldwide effort directed into producing ^{99m}Tc-CNS receptor imaging agents, using the bioconjugate approach. The potent antagonist for serotonin (5-HT) receptor sites is ketanserin (see Figure 2.22 A), which is has also been incorporated onto the Re=O core, yielding a square pyramidal complex (see Figure 2.22 B). The Re analogue has flexible side chains, containing the receptor sites.

A   **B**
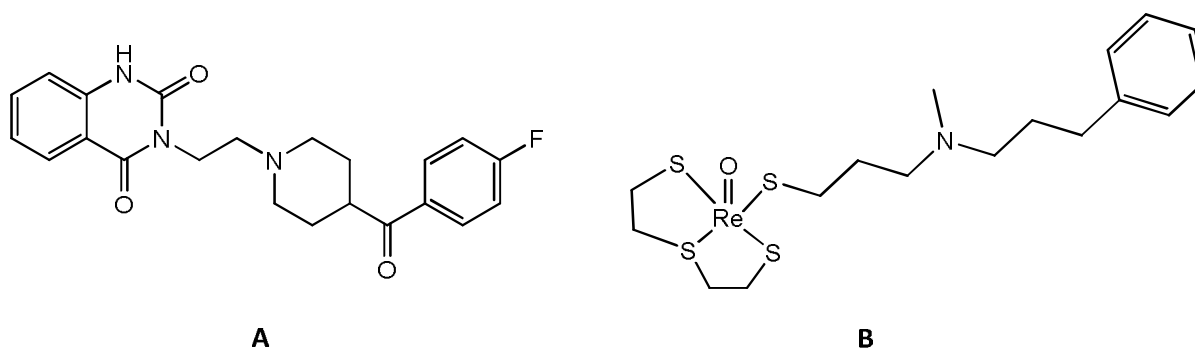
Figure 2.22: Structures of ketanserin (A) and the structure of the Rhenium analogue (B).

Compounds that have been proven to block dopamine transporter sites are cocaine, (see Figure 2.23 A) and analogues thereof. Derivatives of cocaine was linked *via* the seven membered Tc(V) oxo-core, yielding the Tc-TRODAT conjugate illustrated in Figure 2.23 B.
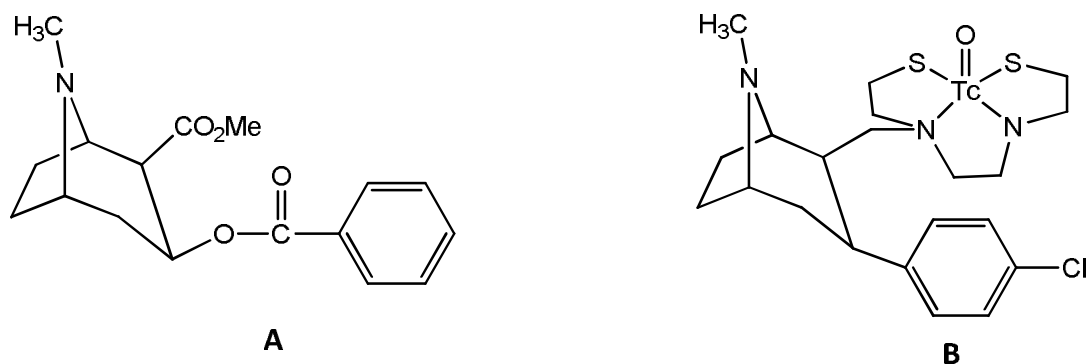
Figure 2.23: Molecular structures of cocaine (A) and Tc-TRODAT (B).

2.8.2.3 Monoclonal antibodies

Monoclonal antibodies (mAbs) are monovalent (bind to the same epitope) and they can be specifically useful in the transporting of radioisotopes to specific sites in the body. For this transporting to be optimal, the radiolabel must be able to be introduced, without any interference with binding to the receptor site. Whole antibodies are very slow with regard to distribution in the body, which in turn slows down the biodistribution kinetics for imaging. This problem was solved when scientist directed their attention into using antibody fragments, which holds on to the characteristics of the specific binding. Fragment usage lessens the likelihood of immunogenicity and unpleasant allergic reactions. When developing ^{99m}Tc labeled antibodies and their fragments, one must keep in mind that the linkage between the radionuclide and the antibody is vital. This is highly important, because the chance of premature release of the isotope exists. Several methods can be used to prevent this problem. One coordinating method involves the linkage of antibodies to the metal chelation group, which is followed by the radionuclide coordination. In this approach, one can use thiolacetone or hydrazine nicotinamide derivatives.[61] Another approach requires the initial synthesis of the radionuclide chelate, which contains an activated ester group, followed by linkage of the fragment. The illustration in Figure 2.24 shows a diamidedithiolate ligand containing a pendant tetrafluorophenyl (TFP) activated ligand.

---

[61] Hnatowich, D. J.; Mardirossan, G.; Ruscowski, M.; Fargarasi, M.; Firzi, F.; Winnard, P.; *J. Nucl. Med. Chem.*, 34, 172, **1993**
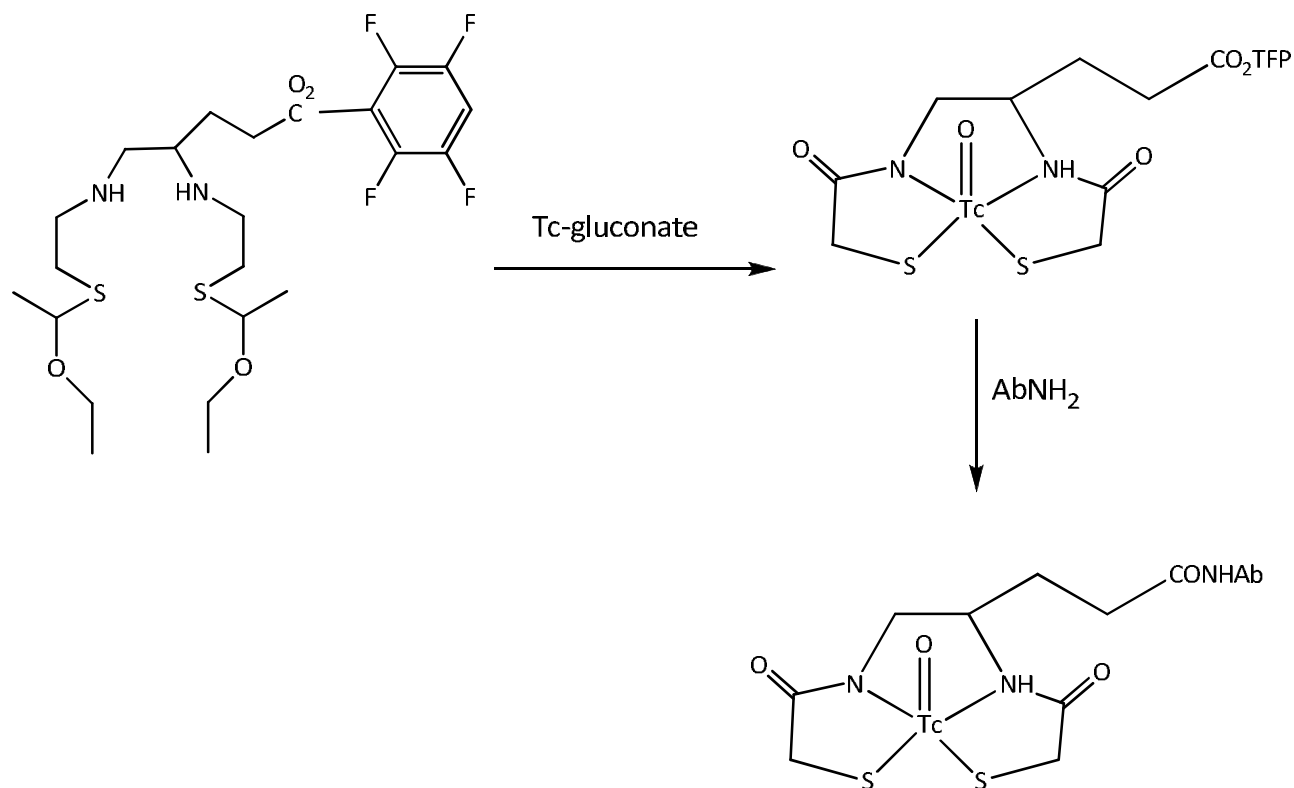
Figure 2.24: The preformed chelation of ^{99m}Tc antibody attachment.

2.8.2.4 Hypoxia imaging

In cancer patients, the chances of cells becoming hypoxic (a condition in which the whole body or a region of the body is deprived of adequate oxygen supply) in several disease states is high. A large portion of tumours can become hypoxic and in imaging these tumours, one would be at a great advantage to find suitable treatments for it. There has been a great effort from a number of scientists to link 2-nitroimidazoles to ^{99m}Tc in the aid of imaging hypoxic sites.[62] Compound A (see Figure 2.25) has presented promising results for *in vivo* hypoxic imaging, however due to its slow clearance from the tissue and lipophilic nature, it was not ideal. It's hydrophobic (Figure. 2.25 B) counterpart guaranteed better results, with faster liver clearance.

---

[62] Archer, C. M.; Edwards, B.; Powell, N. A.; *Current Directions in Radiopharmaceutical Research and Development*, ed. Mather, S. J.; Kluwer Academic Press, Netherland, p. 81, **1996**
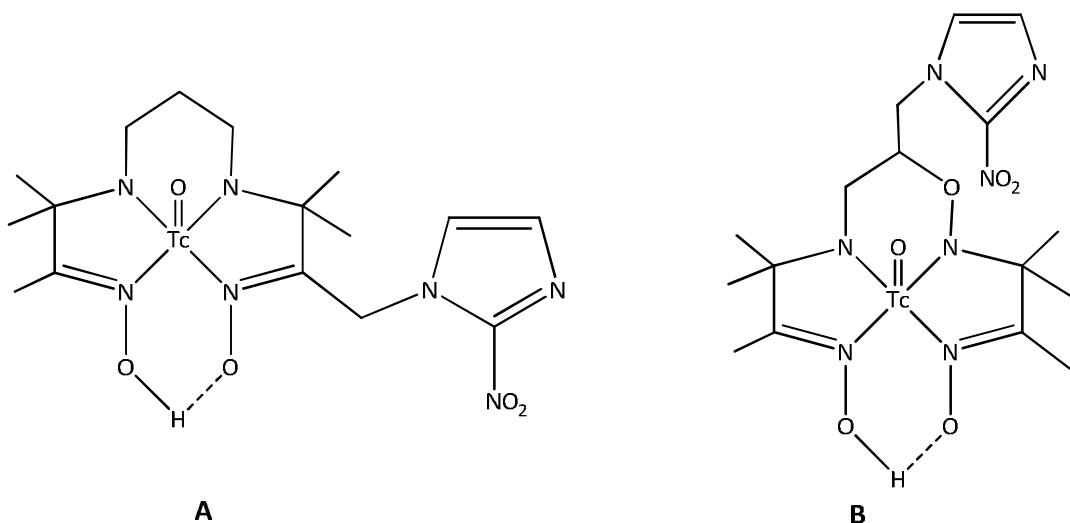
Figure 2.25: Molecular structures of the lipohilic (A) and hydrophophic conjugates.

2.9 Rhenium radiopharmaceuticals

Scientists have identified ^{186}Re and ^{188}Re as highly significant radioimmunotherapy agents. [63,64]
The ^{188}Re isotope is available in high specific activities as ^{188}ReO$_4^-$ and if it is used in this form (oxidized form) it holds a huge advantage, because the oxidized form provides an ultimate clearance route via the kidneys. The two rhenium radioactive isotopes are available in high specificity from a ^{188}W/^{188}Re generator. The availability of both isotopes offers flexibility in the design of radiolabeled agents that are comparable with: a). their *in vivo* applications and b). their pharmokinetic properties. The advantage of having both isotopes is that the ^{188}Re isotope has higher β-particle energy, with a short half-life (17 h, ensuring rapid clearance from the blood, avoiding unwanted radiation to non-target tissues), making it suitable for targeting larger tumors and the ^{186}Re isotope ($t_{1/2}$ = 3.7 days) with its medium β-particle emission is better for use with the biomolecules that do not clear quickly from the blood.

The chemistry of the $^{186/188}$Re isotopes for the use of therapeutic radiopharmaceutical in humans is under developed, because of its complex labeling chemistry. [65,66] However, there is

[63] Volkert, W. A.; Goeckeler, W. F.; Ehrhardt, G. J.; Ketring, A. R.; *J. Nucl. Med.* 32, 74, **1991**

[64] Mausner, L. F.; Srivastava, S. C.; *Med. Phys.*, 20, 503, **1993**

[65] Griffiths, G. L.; *Cancer Therapy with Radiolabeled Antibodies*; Golden, D. M.; Ed.; CRC Press: Boca Raton, FL. Chapter 5, p. 47, **1995**

[66] Zamora, P. O.; Bender, H.; Gulhke, S.; Marek, M. J.; Knapp, F. F.; Rhodes, B. A.; Biersack, H. J.; *Anticancer Res.*, 17, 1803, **1997**

an active investigation in the development of new approaches and methods to form $^{186/188}$Re-labeled biomolecules. [67, 68]

2.9.1 Studies of - and/or existing rhenium agents

2.9.1.1 Palliation of bone pain agents

Worldwide, it is not an uncommon practise to use radiation in the relief of pain, when metastases are not widely distributed through the skeletal structure. This has triggered a search in the direction of β-emitting radiopharmaceuticals. Rhenium is a β-emitting radiopharmaceutical that can be targeted to bone lesions and the existing rhenium radiopharmaceutical agents for palliation of bone pain are based diphosphonate ligands. [69]

2.9.1.2 Medullary thyroid carcinoma

For the imaging of medullary thyroid carcinoma, (a form of thyroid carcinoma, which originates from the parafollicular cells, which produce the hormone calcitonin) a Tc (V) complex coordinated with dimercaptosuccinic acid (DMSA) is used. The same complex with a rhenium metal centre has a square pyramidal structure (see Figure 2.26) and exists as a mixture of isomers in solution. These isomers are dependent on the carboxylate group orientations, with regard to the S_4 plane. The rhenium complex exhibit selective absorption in tumour tissue, analogous to that of the technetium species, thus presenting a possible therapeutic treatment for this disease.

[67] Safavy, A.; Khazaeli, M. B.; Qin, H.; Buchsbaum, D. J.; *Cancer (Suppl.)*, 80, 2354, **1997**

[68] Schubiger, P. A.; Alberto, R.; Smith, A.; *Bioconjugate Chem.* 7, 165, **1996**

[69]Volkert, W. A.; Deutsch, E. A.; *Advances in Metals in Medicine*, ed. Abrams, M. J.; Murrer, B. A.; JAI Press, USA, p. 115, **1993**
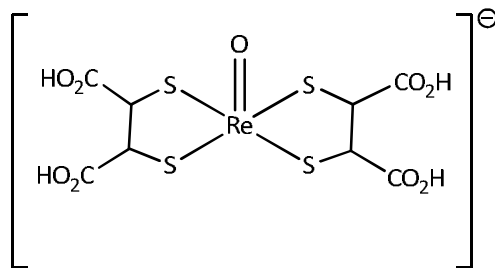
Figure 2.26: Square pyramidal Rhenium analogue with its apical oxo-groups.

2.9.1.3 Monoclonal antibodies

Monoclonal antibodies and their fragments are promising targeting agents for the therapeutic uses of radionuclides. The technetium agent (MAG$_3$) used for kidney imaging (see Paragraph 2.7.1.4) is widely used. Direct labeling methods, yielding good product formation, has been used to produce stable (*in vitro* and *in vivo*) biologically active [188]Re-labeled monoclinical antibodies.[70] It also presented rapid clearance from the blood as well as accelerated excretion in non-targeted tissue when compared to analogues ^{131}I and [88]Y. MAG$_3$ (mercaproacetyltriglycine) and MAG$_2$-GABA (mercaptoacetylglycylglycyl-γ-aminobutyric acid), N$_3$S chelators, are two regularly used biofunctional chelating agents in the labeling of proteins, peptides and mAbs. Both these chelators have a MAG$_3$ framework (see Figure 2.27 A and B), with MAG$_2$-GABA containing a spacer between the chelate (Tc/Re-N3S) and the biomolecule.
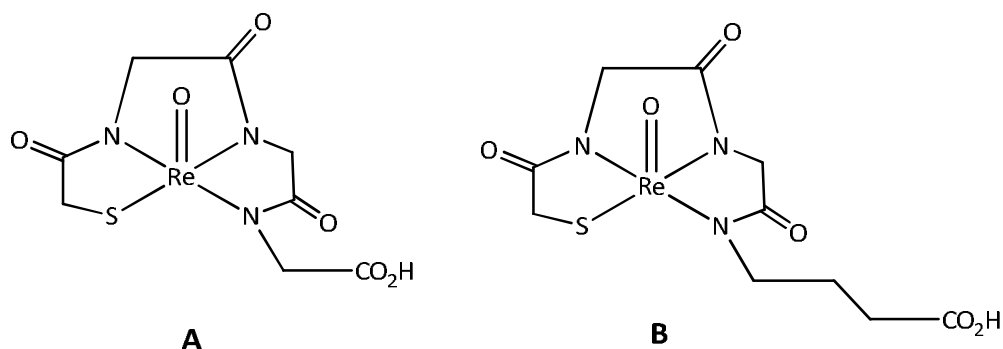
Figure 2.27: The structures of MAG$_3$ (A) and MAG$_2$-GABA (B).

---

[70] Griffiths, G.L.; *Cancer Therapy with Radiolabeled Antibodies*, 47, **1995**

2.9.1.4 Steroids and bioactive peptides

Pituitary -, malignant breast - and pancreatic tumors have numerous receptors for tetradecapeptide somatostatin (TDPS) including octreotide (the cyclic analogue of TDPS). The direct labeling method, presenting high yields, is the reduction of the disulfide bridges on octreotide, which is then reacted with ^{188}ReO$_4$/stannous/citrate.

The attachment of steroids to rhenium oxo-complexes of N$_2$S$_2$ ligand systems (see Paragraph 2.6.1) shows good uptake in steroid receptor rich target tissue, making it possible for the delivery of therapeutic radiation to the appropriate tumours. The alternative approach is to join the rhenium cyclopentadienyltricarbonyl unit, to position 17 of the estradiol derivative (see Figure 2.28).
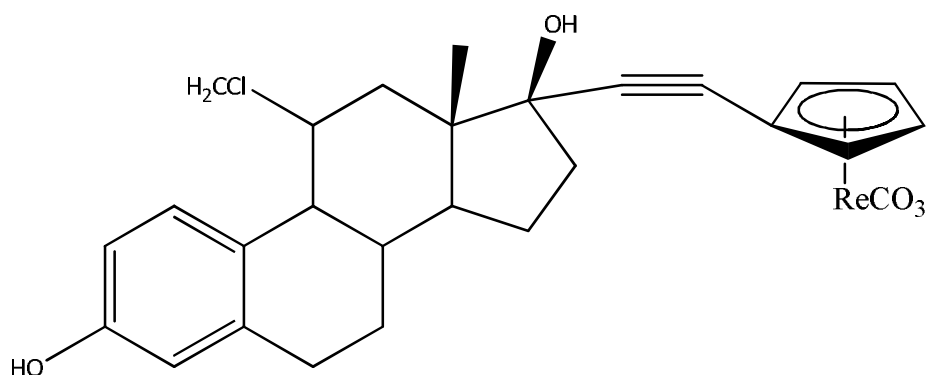
Figure 2.28: The structure of the rhenium cyclopentadienyltricarbonyl complex.

2.10 Re(I)tricarbonyl complexes with N-O and O-O' bidentate ligands

The rhenium(I)tricarbonyl complex has received a lot of attention over the years due to its use as a precursor for potential labeing of biomolecules. Rhenium coordination chemistry gained serious attention, particularly complexes containing the *fac*-$[M(CO)_3]^+$ moiety, for use in radioimmunotherapy (β-emitters, ^{186}Re and ^{188}Re). In the synthesis of most rhenium(I) tricarbonyl complexes, the starting material is $[NEt_4]_2[ReBr_3(CO)_3]$ and $[Re(CO)_3(OH_2)_3]$, due to the high stability of the *fac*-$[M(CO)_3]^+$ core in water and the replacement of the labile solvent ligands. The anionic $[NEt_4][M(CO)_3X_3]$ (M = Tc, Re; X = halides) complex is water soluble and upon substitution of the halide ligands with H_2O, the cationic *fac*-$[M(CO)_3(H_2O)_3]^+$ is formed. The *fac*-$[M(CO)_3(H_2O)_3]^+$ moiety has three coordination sites that are occupied by strong π-acceptor CO groups, while the remaining sites are coordinated by three labilized water ligands. This aqua complex is coordinated by three strongly bound CO ligands and three labilized water compounds, with a near spherical *fac*-$[M(CO)_3]^+$ core. This characteristic makes this coordinated complex ideal for reactions with appropriate ligand systems, such as tridentate or [2+1] ligand systems. An advantage of using the tricarbonyl core is that it is possible to design complexes using ligand systems with properties such as hydro/lipophilicity which can adapt to those of the biomolecules.

2.10.1 N-O Bidentate ligand systems

In a literature search, the crystal structures of twelve $[Re(CO)_3(N,O)X]$ (X=Br or H_2O) complexes were obtained, whereby three complexes had an aqua ligand in the third coordination site and the remaining complexes a coordinated bromide ligand. Alvarez *et al.*[71] prepared several new carbonyl complexes, utilizing pyridine 2-carboxaldehyde as bidentate ligand. These complexes were in turn then used as starting material for synthesizing complexes with iminopyridine ligands with a pendant ester arm. They used Alberto's procedure of starting with anionic $[ReBr_3(CO)_3]^{2-}$, and using methanol as a solvent, however it did not yield the isolation of the

---

[71] Alvarez, C.M.; Garcia-Rodriguez, R.; Miguel, D.; *Dalton Trans.*, 3546, **2007**

desired complex (see Figure 2.29), but an acetal derived from methanol, which dimerized spontaneously.[72]
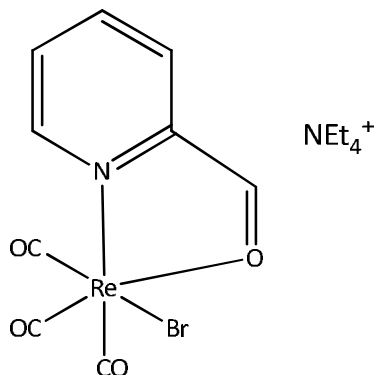
Figure 2.29: Structure of *fac*-[Bromo-tricarbonyl-(pyridine-2-carboxaldehyde-N,O)-rhenium.

Creber[73] and his co-workers synthesized several [ReBr(CO)$_3$L] complexes with metylethyldipicolinate as the bidentate ligand, alternating the R goups (with Me, Et and H, see Figure 2.30) on the ligand backbone.
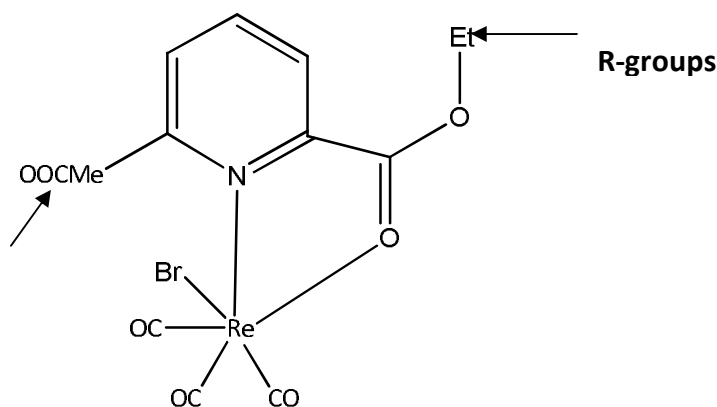
Figure 2.30: Structure of *fac*-tricarbonyl-bromo-(2-methoxycarbonyl,6-ethoxycarbonyl pyridine-N,O) rhenium(I).

Wei and Zubieta[74] synthesized the complex, *fac*-Bromotricarbonyl [2-(2-pyridyl-methyl))-2,3-dihydro-1*H*-isoindol-1-one]rhenium(I) methanol solvate (see Figure 2.31) unexpectedly, instead of the intended 2-[*N*-(2-pyridylmethyl)aminomethyl] benzoic acid as the bidentate ligand.

---

[72] Wang, W.; Spingler, B.; Alberto, R.; *Inorg. Chim. Acta.*, 355, 386, **2003**

[73] Creber, M.L.; Orrell, K.G.; Osborne, A.G.; Sil, V.; Hursthouse, M.B.; Light, M.E.; *Polyhedron*, 20, 1973, **2001**

[74] Wei, L.; Zubieta, J.; *Acta Crystallogr., Sect. C., Cryst. Struct. Commun.*, 61, m95, **2005**
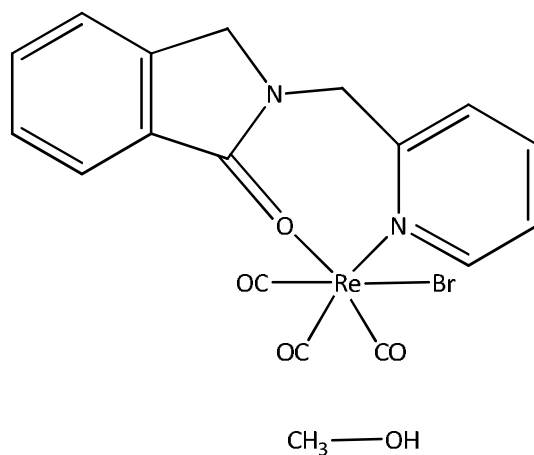
Figure 2.31: Structure of *fac*-**Bromotricarbonyl [2-(2-pyridyl-methyl))-2,3-dihydro-1***H*-**isoindol-1-one]rhenium(I) methanol solvate.**

Krinninger[75] prepared several complexes, as well as the tricarbonylrhenium(I) bromide complex, [ReBr(CO)$_3$(1-imino-1*H*-naphthalene-2-one)] (see Figure 2.32).
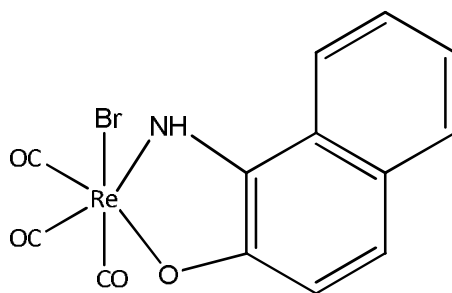
Figure 2.32: Structure of [ReBr(CO)$_3$(1-imino-1*H*-**naphthalene-2-one)].**

Wang *et al.*[76] studied the reactivity towards aromatic or aliphatic amines, which in turn will permit the direct labeling of biomomlecules with ^{99m}Tc. They synthesized the complex [ReBr(CO)$_3$(C$_5$H$_4$NCOCH$_3$)], Figure 2.33, as well as Re(I) and Tc(I) complexes containing various coordinated aldehyde and ketones.

---

[75] Krinninger, C.; Wirth, W.; Ruiz, J. C. G.; Klufers, P.; Noth, H.; Lorenz, I.P.; *Eur. J. Inorg. Chem.*, 4094, **2005**
[76] Wang, W.; Spingler, B.; Alberto, R.; *Inorg. Chim. Acta*., 355, 386, **2003**
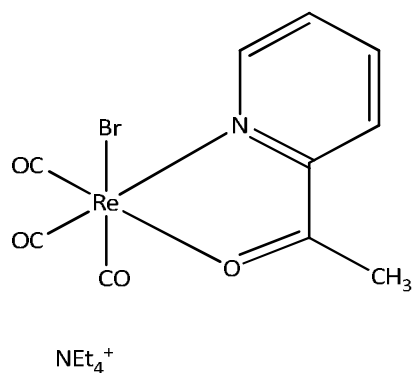
Figure 2.33: Structure of (2-Acetylpyridine)-bromo-tricarbonyl-rhenium(I).

Heard and his colleagues[77] synthesized a tricarbonylrhenium(I) bromide complex with the coordinated bidentate ligand, 2,6-bis[(4R,5R)-dimethyl-1,3-dioxon-2-yl]pyridine, see Figure 2.34. The study included the influence of different donor atoms on stereodynamics.
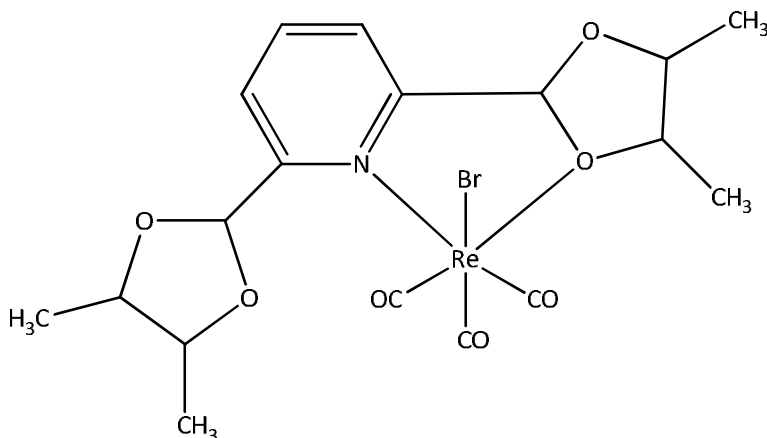
Figure 2.34: Structure of *fac*-(Bromo-tricarbonyl-(2,6-bis(dimethyl-1,3-dioxan-2-yl)pyridine)rhenium(I).

In a different study, Heart *et al.*[78] did an investigation on the structure and solution stereodynamics of tricarbonyl rhenium (I) halide complexes, yielding the complex [ReBr(CO)$_3$L], with L = 2,6-bis[(4R,6R)-4,6-dimethyl-1,3-dioxan-2-yl)pyridine], see Figure 2.35.

---

[77] Heard, P. J.; King, P. M.; Bain, A. D.; Hazendonk, P.; Tocher, D. A.; *J. Chem. Soc., Dalton Trans.*, 4495, **1999**
[78] Heard, P. J.; King, P. M.; Tocher, D. A.; *J. Chem. Soc., Dalton Trans.*, 1769, **2000**
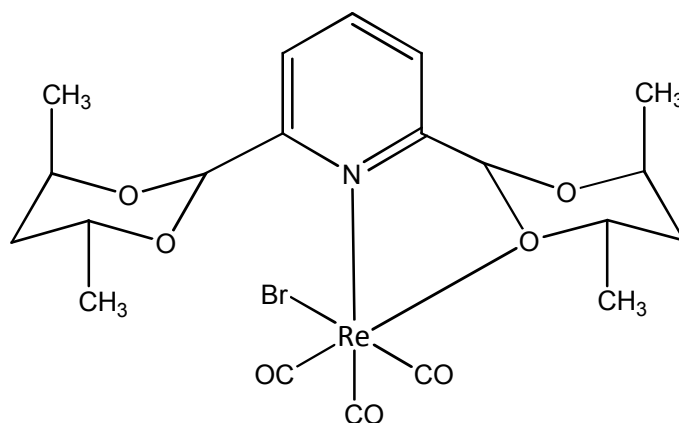
Figure 2.35: Structure of *fac*-Bromo-(2,6-bis[(4R,6R)-4,6-dimethyl-1,3-dioxan-2-yl]pyridine) tricarbonylrhenium(I).

Barbazán *et al.*[79] prepared the complex [ReBr(CO)$_3${H(Fe)L^1}] (with L^1 = acetylpyridine benzoylhydrazone), Figure 2.36, in good yield, in a study entitled 'the synthesis and characterization of ferrocenylcarbaldehyde benzoylhydrazone and its Re(I) complex.'
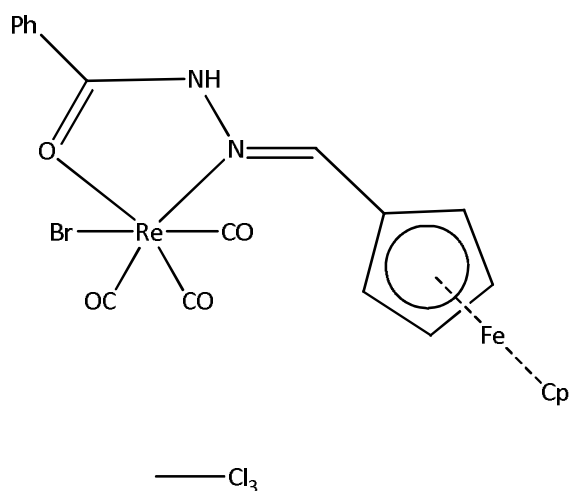
Figure 2.36: Structure of [ReBr(CO)$_3${H(Fe)L^1}].

Barbazán and his co-workers[80] prepared the complex **B** [ReBr(CO)$_3${H$_2$(Fc)L$_2$}] (with **(A)** H$_2$L$_2$ = as a hydrazone derivative of 2-hydroxybenzoic and ferrocenyl carbaldehyde), Figure 2.37, in good yield, in a study entitled the 'synthesis and characterization of several rhenium(I) complexes of 2-acetylpyridine and ferrocenyl carbaldehyde derivatives of 2-hydroxybenzoic acid hydrazide.'

[79] Barbazán, P.; Carballo, R.; Abram, U.; Pereiras-Gabián, G.; Vázquez-López, E. M.; *Polyhedron,* 25, 3343–3348, **2006**
[80] Barbazán, P.; Carballo, R.; Prieto, I.; Turnes, M.; Vázquez-López, E. M.; *J. Org. Chem.,* 694, 3102–3111, **2009**
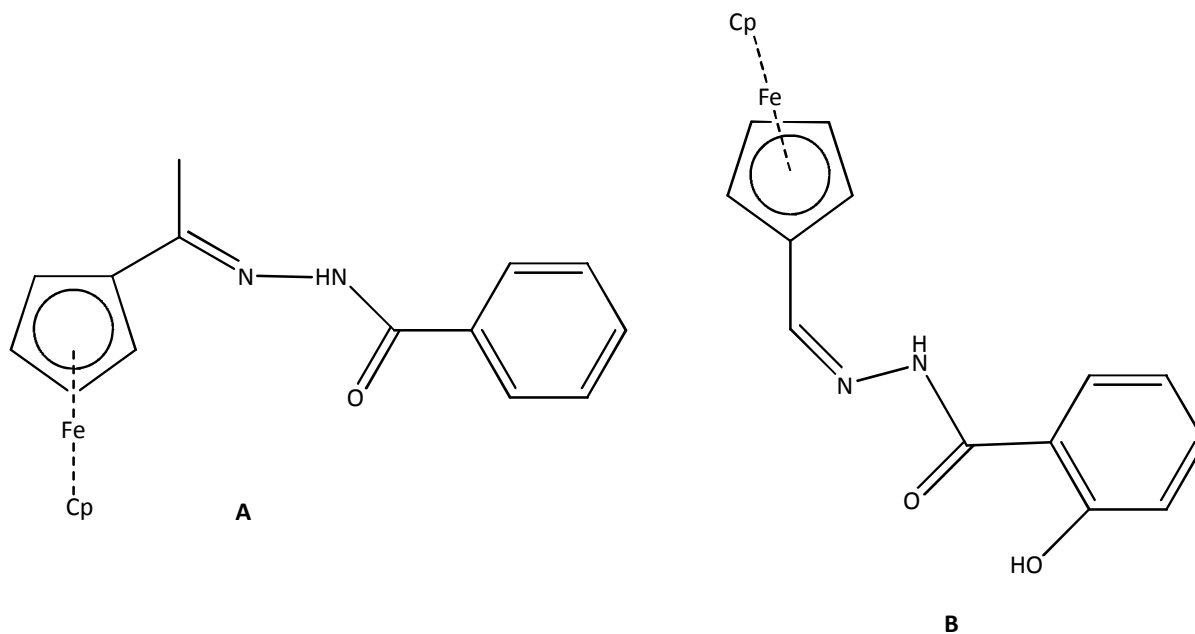
Figure 2.37: Structure of (A) H_2FcL_2 and (B) [ReBr(CO)$_3$\{H$_2$(Fc)L$_2$\}].

Two similar structures of Re(C$_{10}$H$_6$NO$_8$), see Figure 2.38, with different bond orientations were prepared by Mundwiler *et al.*[81] and Schutte *et al.*[82], utilizing the N,O bidentate ligand pyridine carboxylic acid.
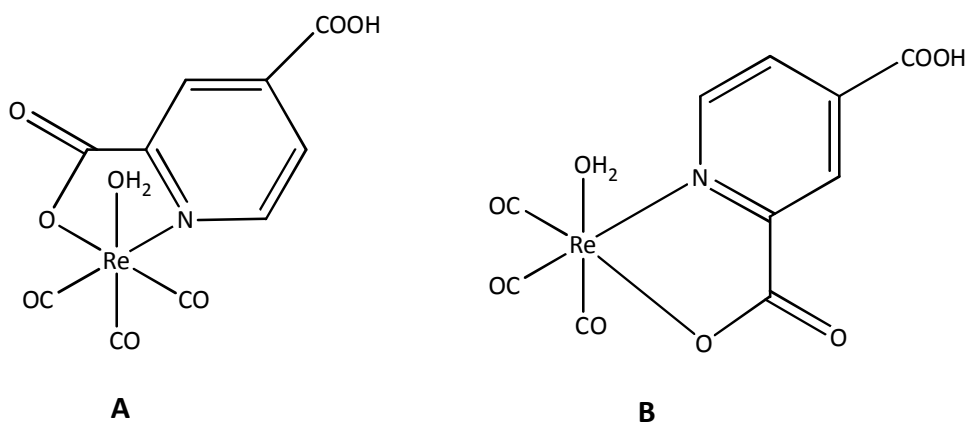
Figure 2.38: Structures of Re(C$_{10}$H$_6$NO$_8$), prepared by (A) Mundler *et al.* and (B) Schutte *et al.*

[81] Mündwiler, S.; Kündig, M.; Ortner, K.; Alberto, R.; *Dalton Trans*., 1320, **2004**
[82] Schutte, M.; Visser, H.G.; *Acta Cryst*., E64, m1226-m1227, **2008**

In an article by Li *et al.*[83] the tricarbonylrhenium(I) aqua–NOBIN Schiff-base (NOBIN = 1-amino-1'-hydroxylbinaphthyl) complex was prepared and its catalytic properties were explored (see Figure 2.39).
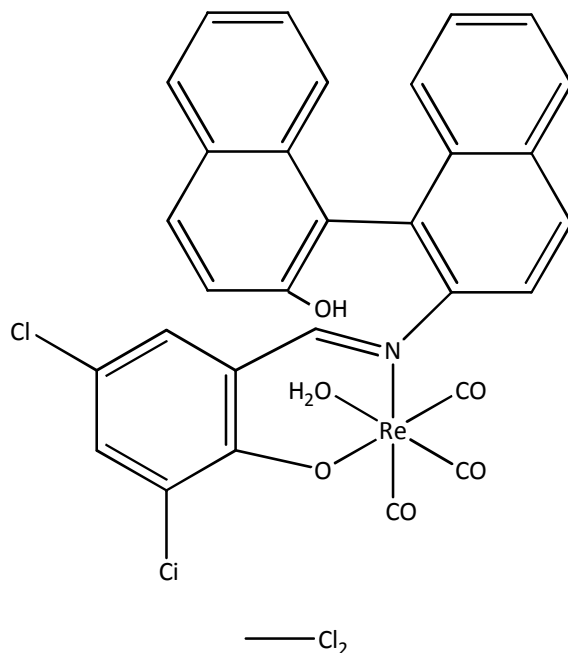
Figure 2.39: Structure of Re(I)–NOBIN Schiff base complex.

[83] Li, Z. K.; Li, Y.; Lei, L.; Che, C.; Zhou, X.; *Inorg Chem Com.*, 8, 307–309, **2005**

2.10.2 O-O' Bidentate ligand systems

In a CSD[84,85,86,87,88,89,90,91,92,93] search, ten rhenium(I)tricarbonyl crystal structures with O,O'-bidentate ligand systems were reported. Figure 2.40 (A - Bochkova *et al.*, B – Cheng *et al.*, C – Gibson *et al.*, D – Brasey *et al.*, E – Benny *et al.*, F – Shutte *et al.*, G – Shutte *et al.*, H – Shutte *et al.*, I – Sagnou *et al.*, J – Brink *et al.*) gives an illustration of all these structures.

A

B

C

D
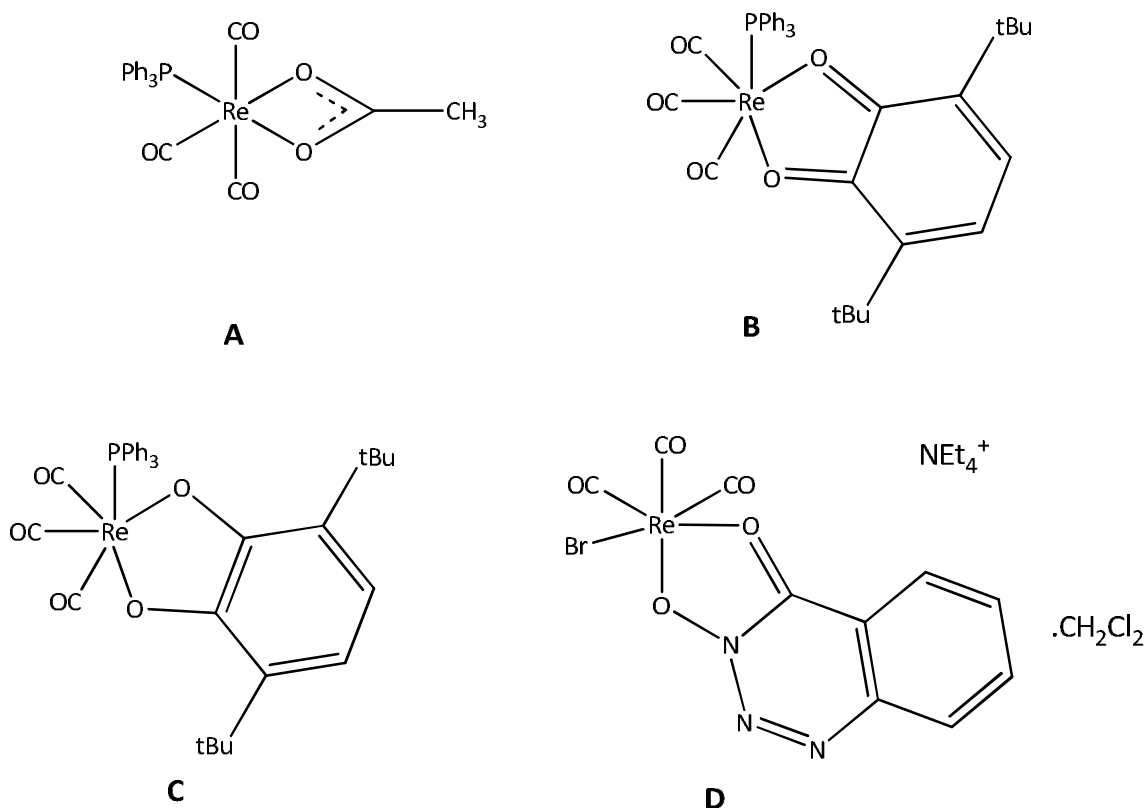
[84] Bochkova, R. I.; Zakharov, L.N.; Patrikeeva, N. V.; Shal'nova, K. G.; Abakumov, G. A.; Cherkasov, V. K.; *Koord. Khim. (Russ.)(Coord. Chem.)*, 13, 702, **1987**

[85] Cheng, C. P.; Wang, S. R.; Lin, J. C.; Wang, S. L.; *J. Organomet. Chem.*, 349, 375, **1988**

[86] Gibson, D.H.; Ding, Y.; Miller, R. L.; Sleadd, B. A.; Mashuta, M. S.; Richardson, J. F.; *Polyhedron*, 18, 1189, **1999**

[87] Brasey, T.; Buryak, A.; Scopelliti, R.; Severin, K.; *Eur. J. Inorg. Chem.*, 964, **2004**

[88] Benny, P. D.; Fugate, G. A.; Barden, A. O.; Morley, J. E.; Silva-Lopez, E.; Twamley, B.; *Inorg. Chem.*, 47, 2240, **2007**

[89] Schutte, M.; Visser, H.G.; Roodt, A.; *Acta Cryst.*, E63, m3195-m3196, **2007**

[90] Schutte, M.; Visser, H.G.; Roodt, A.; *Acta Cryst.*, E64, m1610-m1611, **2008**

[91] Schutte, M.; Visser, H.G.; Roodt, A.; *Acta Cryst.*, E66, m859-m860, **2010**

[92] Sagnou, M.; Tsoukalas, C.; Triantis, C.; Raptopoulou, C. P.; Terzis, I. P.; Pirmettis, I.; Pelecanou, M.; Papadopoulos, M.; *Inorg. Chim. Acta*, 363, 1649-1653, **2010**

[93] Brink, A.; Visser, H. G.; Roodt, A.; *Acta Cryst.*, E67, m34-m35, **2011**

E

F

G

.CH$_3$OH
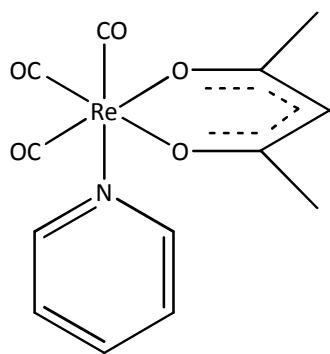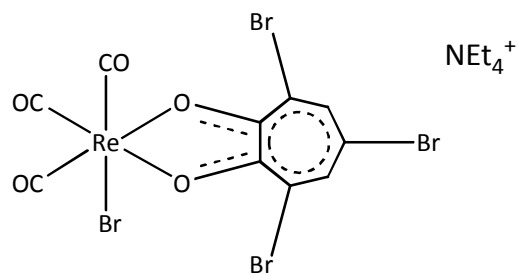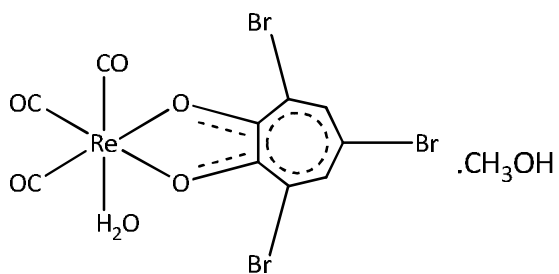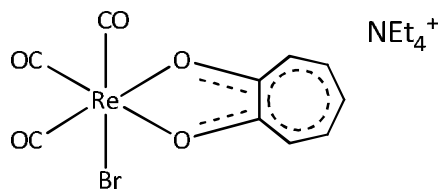
H
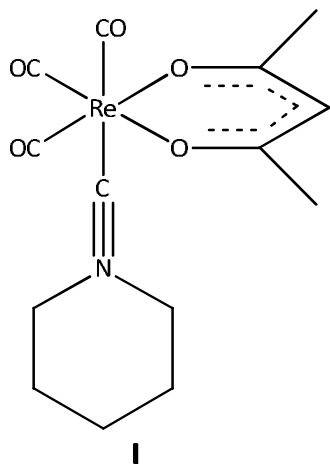
I
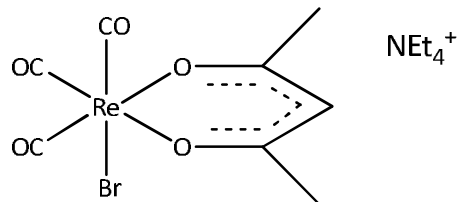
J

Figure 2.40: The structures of Re(I)tricarbonyl complexes with O,O'-donor bidentate ligands.

2.11 Kinetics of [Re(OH$_2$)$_3$(CO)$_3$]$^+$

2.11.1 Introduction

The aqua species, [M(OH$_2$)(CO)$_3$]$^+$, (M = Re, Tc), is coordinated with three labilized water ligands and three tightly bound CO ligands, that is highly attractive, especially for radiopharmaceutical design. These aqua complexes appeal to researchers, because of its highly stable tri-carbonyl core, and the potential of easily exchanging the three aqua ligands bound to it. Scientists believe and some researchers have proven that the chemistry of technetium and rhenium is similar, thus labeling of its radioactive isotopes (^{99m}Tc and [186]Re/[188]Re) will yield similar results. This means ^{99m}Tc will be mostly used for the diagnostic application and the rhenium isotopes for therapy.[94]

Chemical kinetics is mostly done to gain insight on the reactivity and mechanisms of compounds and this is what will be discussed later in the study (Chapter 6). In this section, already investigated substitution and exchange of the water ligands on the triaqua-tricarbonyl compound, will be discussed. This will give a better understanding of how fast and thorough the chemistry of the [M(OH$_2$)(CO)$_3$]$^+$, M = Re, Tc, occur. Information about the rate of water exchange can aid in complex formation reactions, which is done by using ^{17}O NMR.

2.11.2 [M(OH$_2$)(CO)$_3$]$^+$ - H$_2$O ligand exchange

Saligna *et al. p*erformed the water exchange on the [Re(OH$_2$)(CO)$_3$]$^+$ (ReAq) species for first time, in 2003.[95] The thermodynamic and kinetic data obtained, for the water exchange experiments on the rhenium complex were done, using various ligands (e.g. acetonitrile (CH$_3$CN), bromide (Br$^-$), dimethylsulfide (DMS), 1,3,5-triaza-7-phosphaadamantane (TPA) amongst others). One of the important properties of ReAq is the mean residence time of the coordinated water ligands. The rate for the water exchange process was calculated as k$_{eq}$ = 6.3 (1) x 10^{-3} s^{-1}. On the monohydroxo species, [Re(OH$_2$)$_2$(OH)(CO)$_3$], the water rate exchange constant was found to be much higher, k$_{OH}$ = 2.7 (1) s^{-1}. pH did have an influence as the basic form significantly contributed to the kinetic exchange at [H]$^+$ < 3 x 10^{-3}. At lower pH, the kinetic

---

[94] Alberto, A.; *Comp. Coord. Chem. II*, 5, 127, **2004**
[95] Salignac, B.; Grundler, P. V.; Cayemittes, S.; Frey, U.; Scopelliti, R.; Merbach, A.; *Inorg. Chem.*, 42, 3516, **2003**

studies are conducted only by ReAq. The activation parameters for the water exchange process indicate a dissociative interchange mechanism ($\Delta H^{\neq}$ = 90 (3) kJ mol^{-1}, $\Delta S^{\neq}$ = 14 (10) J K^{-1}).

All the elements in group 7 are able to form tricarbonyl-triaqua complexes and a comparison in the exchange of their water ligands can be done. By using NMR techniques, Helm introduced technetium and manganese systems.[96] The water exchange rate for complexes of the type $[M(OH_2)(CO)_3]^+$, (M = Re, Tc, Mn) differs over a large scale, with Mn reactions being the fastest followed by Tc and then Re (see Table 2.6). A decrease in the water exchange rate is observed for group 6 and 7 when going down the group; also from left to right in the periodic row, paralleled by an increase in charge. Complexes of $[Ru(H_2O)_6]^{2+}$ and $[Rh(H_2O)_6]^{3+}$ presented a similar trend, since an increase in the bond strength can result in the water exchange mechanism modifying from a I_d (interchange dissociative mechanism) to I_a (interchange associative mechanism).

Table 2.6: Mechanism and kinetic data for water exchange reactions for selected group 7 metal aqua complexes.

	$k_{ex}^{(298)}$ (s^{-1})	$\Delta H^{\neq}$ (kJ mol^{-1})	$\Delta S^{\neq}$ (J K^{-1}mol^{-1})	$\Delta V^{\neq}$ (cm^3 mol^{-1})	Mechanism	pK$_a$
$[Cr(CO)_3(H_2O)_3]$ [97]	11 x 10^4	50	+80			< 8
$[W(CO)_3(H_2O)_3]$ [97]	31	58	-22			< 4.5
$[Mn(CO)_3(H_2O)_3]^+$ [98]	23	72.5	+24.4	+7.1	I_d	9-10
$[Tc(CO)_3(H_2O)_3]^+$ [98]	0.49	78.3	+11.7	+3.8	I_d	
$[Re(CO)_3(H_2O)_3]^+$ [95]	6.3 x 10^{-3}	90.3	+14.5		I_d	7.5
$[Re(CO)_3(OH)(H_2O)_3]$ [95]	27					
$[Ru(H_2O)_6]^{2+}$	1.8 x 10^{-2}	87.8	+16.1		I_d	6-8
$[Ru(CO)_3(H_2O)_3]^{3+}$ [99]	10^{-4} – 10^{-3}					-0.14
$[Ru(CO)_3(OH)(H_2O)_3]^+$	5.3 x 10^{-2}					
$[Rh(H_2O)_6]^{3+}$	2.2 x 10^{-9}	131	+29		I_a	3.5
$[Ir(H_2O)_6]^{3+}$	1.1 x 10^{-10}	130.5	+2.1		I_a	4.45

[96] Helm, L.; *Coord. Chem. Rev.*, 252, 2346, **2008**

[97] Prinz, U.; *Ph.D Thesis.*, RWTH Aachen, Aachen, Germany, **2000**

[98] Grundler, P. V.; Helm, L.; Alberto, R.; A. E. Merbach, *Inorg. Chem.*, 45, 10378, **2006**

[99] Meier, U. C.; Scopelliti, R.; Solari, E.; A. E. Merbach, *Inorg. Chem.* 39, 3816, **2000**

2.11.3 $[M(OH_2)(CO)_3]^+$ - H_2O substitution

Chemical kinetics studies are important as highlighted in Paragraph 2.10.1. In this section the water substitution of the coordinated H_2O ligands of $[Re(CO)_3(H_2O)_3]^+$ is discussed in studies done by Grundler *et al*. and other researchers. These labile H_2O ligands are readily substituted by monodentate ligands (TPA, CH_3CN, TU, DMS and I) and can characteristically be presented with equilibrium constants K_i, (i = 1-3), as indicated below:

$$fac\text{-}[M(CO)_3(H_2O)_3]^+ + L \underset{k_{-1}}{\overset{k_1}{\rightleftharpoons}} [M(OH_2)_2(CO)_3(L)]^+ + H_2O \qquad K_1 = \frac{k_1}{k_{-1}}$$

$$fac\text{-}[M(OH_2)_2(CO)_3(L)]^+ + L \underset{k_{-2}}{\overset{k_2}{\rightleftharpoons}} [M(OH_2)(CO)_3(L)_2]^+ + H_2O \qquad K_2 = \frac{k_2}{k_{-2}}$$

$$fac\text{-}[M(OH_2)(CO)_3(L)_2]^+ + L \underset{k_{-2}}{\overset{k_2}{\rightleftharpoons}} [M(CO)_3(L)_3]^+ + H_2O \qquad K_3 = \frac{k_3}{k_{-3}}$$
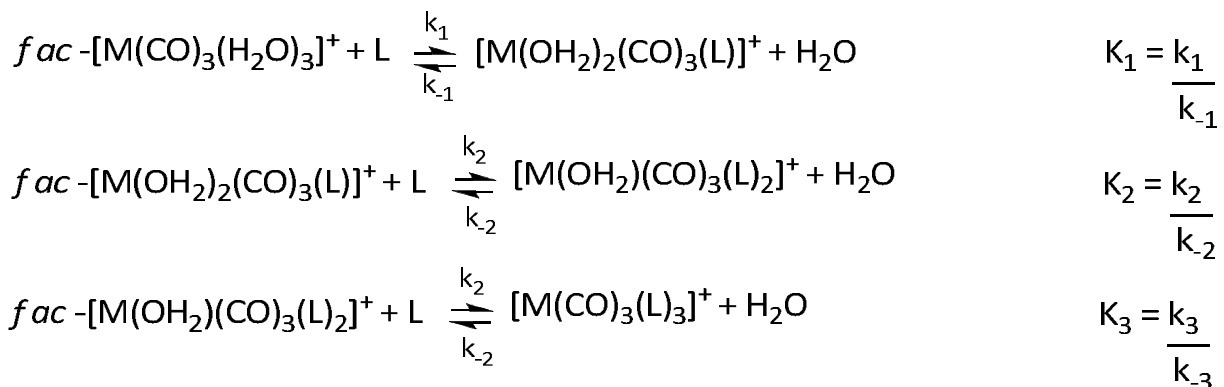
To further validate his water exchange research findings, Helm *et al*. studied the water substitution of $[M(OH_2)_3(CO)_3]^+$ complexes (M = Tc, Mn, Re) with DMS and acetonitrile, which is listed in Table 2.7 Their findings confirmed their water exchange results and the mechanisms were found to be, I_d. All three complexes are less stable with CH_3CN than DMS, with a higher affinity for S-binding DMS than the N-binding CH_3CN.

Table 2.7: Kinetic and thermodynamic parameters for water substitution on fac-[M(OH$_2$)$_3$(CO)$_3$]$^+$ complexes.[100]

	K_1^{298} (M^{-1})	$k_{f,1}^{298}$ (M^{-1} s^{-1})	$k_i{}'$ (s^{-1})	$\Delta H_{f,1}^{\ddagger}$ (kJ mol^{-1})	$\Delta S_{f,1}^{\ddagger}$ (kJ mol^{-1})	$\Delta V_{f,1}^{\ddagger}$ (cm^3 mol^{-1})
			fac-[Mn(CO)$_3$(OH$_2$)$_3$]$^+$			
CH$_3$CN	4.5	1.75	29	83.9	+41.3	+4.2
DMS	25.2	5.34	89	71.2	+8.1	11.3
H$_2$O			23	72.5	+24.4	+7.1
			fac-[Tc(CO)$_3$(OH$_2$)$_3$]$^+$			
CH$_3$CN	2.9	0.0399	0.665	77.8	-10	
DMS	14.9	0.0608	1.01	70.6	-31.1	
H$_2$O			0.490	78.3	+11.7	+3.8
			fac-[Re(CO)$_3$(OH$_2$)$_3$]$^+$			
CH$_3$CN	4.8	0.00076	0.013	98.6	+26.6	
DMS	8.3	0.00118	0.02			
H$_2$O			0.0054	90.3	+14.5	
Py	237	0.00106	0.0177			+5.4

In Table 2.8 a broad range of equilibrium and kinetic constants for the aqua substitution reactions of *fac*-[Re(CO)$_3$(OH$_2$)$_3$]$^+$, with various ligands systems, are summarized.

Table 2.8: Kinetic constants for complex formation of various ligands at 25 °C.

	N-bonded[100]		S-bonded[100]			Anionic[95]	
	CH$_3$CN	Pyz	DMS	THT	TU	Br$^-$	CF$_3$COO$^-$
k_1 x 10^3 (M^{-1} s^{-1})	0.76	1.06	1.18	1.28	2.49	1.6	0.81
k_{-1} x 10^5 (s^{-1})	16	0.45	14.2	3.05	1.6	230	99
$k_{-1}{}'$ x 10^5 (s^{-1})^a	12.7	17.7	20	3.05	1.6	230	99
K_1 (M^{-1})	4.8	237	8.3	41	160	0.7	0.82

^{a} Water exchange rate k_{ex} = 6.3 x 10^{-3} s^{-1}

(Pyz = Pyrazine, THT = Tetrahydrothiophene, TU = Thiourea)

Grundler *et al.* found that the substitution rates were slightly dependent on the nature of the ligand (i.e. the softer ligands, S-bonded, coordinates more rapid to the rhenium metal centre, than the O- and N-bonded ligands).

Interesting to note in the formation of *fac*-[Re(CO)$_3$(OH$_2$)$_3$]$^+$, is the increase in the rate constant for the reverse reaction (k_{-1}), Br$^-$ (k_{-1} = 230 x 10^5 s^{-1}) >>> pyz (k_{-1} = 0.45 x 10^5 s^{-1}). This is due to

---

[100] Grundler, P. V.; Salignac, B.; Cayemittes, S.; Alberto, R.; Merbach, A. E.; *Inorg. Chem.*, 43, 865, **2004**

the difference in their nucleofugal abilities of these species, Br$^-$ and pyz, with pK$_a$ values of -4.7 and 0.6 respectively.

The water exchange rate, k$_{ex}$, is almost equivalent to the interchange rate constants (k$_i^{'}$), indicating that the rate of the complex formation might be limited by the mechanism which breaks the Re-H$_2$O bond. I_d mechanisms are the mechanisms where the leaving group has the greatest influence and the I_a mechanisms are those with the highest sensitivity to the nature of the incoming groups. Activation volumes ($\Delta V^{\neq}$) help to fully differentiate between the two mechanisms, because negative $\Delta V^{\neq}$ indicates I_a mechanisms and $\Delta V^{\neq}$ I_d mechanisms. Negative $\Delta V^{\neq}$ and positive $\Delta V^{\neq}$ values were found for S-bonded and N-bonded ligands respectively.[98,100] The mechanism changes from I_d with harder ligands (e.g. Pyz) to I_a for softer ligands, such as DMS and THT, which are better nucleophiles.

The water substitution on *fac*-[Re(CO)$_3$(OH$_2$)(L,L')]$^{n+}$ (L,L' = N-O, N-N', O-O' bidentate ligands, n = -1, 0, +1) has been studied under the supervision of Prof. A. Roodt and Prof. H. G. Visser.[101,102,103] This initiative brought about a further understanding of the axial water substitution in the *fac*-[Re(CO)$_3$(OH$_2$)(L,L')]$^{n+}$ complex. The other two aqua binding reactive sites were blocked off by bidentate ligands. The neutral and monoanionic, incoming monodentate ligands that was used in this study, ranged from halides to pyridines, also including S and P donor groups (see Table 2.9). This substitution of the axial water ligand was studied under pseudo first order conditions.

[101] Kemp, G.; *Ph. D. Thesis*, University of Johannesburg, Johannesburg, South-Africa, **2006**
[102] Schutte, M.; *MSc. Dissertation*, University of the Free State, Bloemfontein, South-Africa, **2008**
[103] Schutte, M.; Kemp, G.; Visser, H. G.; Roodt, A.; *Inorg. Chem.*, manuscript accepted, **2011**

Table 2.9: Kinetic constants and activation parameters for different certain rhenium complexes, using neutral and monoanionic ligands at 25 °C.[103]

	k_1 x 10^3 (M^{-1} s^{-1})	k_{-1} x 10^3 (s^{-1})	K_1 (M^{-1})	$\Delta H_1^{\neq}$ (kJ mol^{-1})	$\Delta S_1^{\neq}$ (kJ mol^{-1})	$\Delta G_1^{\neq}$ (kJ mol^{-1})
			fac-[Re(Phen)(CO)$_3$(H$_2$O)]$^+$			
Br$^-$	50(3)	0.59(3)	84(7)			
I$^-$	53(1)	0.7(1)	76(11)	70(1)	-35(3)	80(2)
Py	0.064(3)	0.0058(4)	11(1)			
m-MePy	0.012(1)	0.005(2)	2.4(9)			
p-MePy	0.014(1)	0.0035(1)	4.0(3)			
PTA	7.9(1)	0.11(1)	70(1)			
Metu	13.7(1)	0.011(1)	1245(122)	80(1)	-9(3)	82(2)
			fac-[Re(Pico)(CO)$_3$(H$_2$O)]			
Br$^-$	11.8(1)	0.8(1)	15(2)			
I$^-$	14(1)	0.64(1)	22(2)	77(1)	-19(3)	82(2)
Py	1.6(1)	0.0084(1)	190(10)	84(1)	-16(4)	89(2)
m-MePy	0.11(1)	0.011(1)	10(1)			
p-MePy	1.39(1)	0.066(1)	21.0(4)			
PTA	5(1)	0.004(1)	1.3(4)			
Metu	25.8(2)	0.006(1)	4300(1)	57(1)	-85(3)	
			fac-[Re(TropBr$_3$)(CO)$_3$(H$_2$O)]			
Br$^-$	70.6(4)	4(1)	18(4)	63(6)	-54(19)	79(6)
Py	20.3(7)	1.6(2)	13(2)	53(5)	-102(17)	83(6)
DMAP	34.5(7)	0.26(2)	133(11)	69(4)	-42(12)	82(5)
			fac-[Re(Flav)(CO)$_3$(H$_2$O)]			
Br$^-$	7.2(3) x 10^3	3.17(9) x 10^3	2.5(2)	52(5)	-52(15)	68(6)
Py	1.38(8) x 10^3	0.3(1)	4.6(1) x 10^3	54(6)	-60(21)	72(6)
DMAP	5.1(2) x 10^3	0.16(4)	3.2(8) x 10^3	84(4)	51(14)	69(5)

Metu = **methyl-thiourea; DMAP** = **4-dimethylaminopyridine; m-MePy** = **m-methylpyridine;**

p-Mepy = p-methylpyridine

The group found that there was a good agreement with the kinetic and thermodynamic values with the different rhenium compounds. They also noted that there is a change in the stability constants (K_1) of all the *fac*-[Re(CO)$_3$(X)(L,L')]$^{n+}$ complexes: N,N'-Bid, halides is approximately equal to PTA ligands; N,O-Bid, halides < py and in O,O'-Bid, halides <<< Py.

In N,N'-Bid complexes, the formation constants (k_1) were found to be 300 to 400 times faster for halides, than the rates obtained for the neutral pyridine ligands. The N,N' containing metal complexes have a large affinity for the halides, indicative of I_a mechanisms.

In N,O-Bid complexes, the reactions with Br$^-$ as the entering ligand, the reaction is 5-7 times faster at 298 K, than with the neutral ligands as the entering entity. The k_1 value for the

rhenium complexes containing DMAP has an I_a activated mechanism, with a pK_a value of 9.8, higher than that of imadazole (6.99), pyridine (5.25) and pyrazole (2.49).[104]

In O,O-Bid containing complexes, Schutte found that the k_1 value for the reaction between *fac*-[Re(CO)$_3$(Flav)(MeOH)] and DMAP is more than 100 times faster than that of *fac*-[Re(CO)$_3$(TropBr$_3$)(MeOH)]. The reason given for this was that it is due to the electron withdrawing effects, which the bromide substituents situated on the TropBr$_3$ ligand have on the complex.

The researchers then concluded that the N,N' positively charged complexes have slower coordinated methanol substitution rates, and the O,O'-Bid type ligands activates the metal centre more than the N,O-Bid type ligands.

When designing new possible radiopharmaceuticals one should consider, based on this study, that the use of bidentate ligands in a [2+1] mixed ligand approach, may affect the labile site as well as the reactivity of the one site.

ooOoo

---

[104] Perrin, D. D.; *Dissociation Constants of Organic Bases in Aqueous Solution*; Butterworths: London, **1965**; Supplement, **1972**

3 THEORY OF IR, ^{1}H- AND ^{13}C NMR, UV/VIS, X-RAY DIFFRACTION AND CHEMICAL KINETICS

3.1 Introduction

All the Re(I) tricarbonyl complexes synthesized in this study was characterized using infrared spectroscopy (IR), ^{1}H- and ^{13}C nuclear magnetic resonance (NMR) spectroscopy as well as ultraviolet-visible (UV/Vis) spectroscopy. A brief theory overview of these characterization techniques will be discussed in this chapter. Two of the synthesized complexes were completely characterized by means of X-ray diffractometry (see Chapter 5). X-ray crystallography is a powerful technique used in characterization of complexes in their solid state.

The importance of these characterization techniques is vital, because it helps identify all reagents and products (i.e. starting material, intermediate - and final products).

3.2 Spectroscopic techniques

3.2.1 Infrared spectroscopy

Infrared Spectroscopy is a very important, quick and cost effective analytical tool used by scientists in the quantitative identification of compounds and functional groups. Most organic and inorganic compounds containing covalent bonds, except homonuclear compounds (H_2, N_2, and Cl_2) absorb infrared radiation. Bonds that have a dipole moment which changes as a function of time are capable of absorbing infrared radiation. In order for energy to be

transferred, bonds must possess an electrical dipole that changes at the same frequency as the entering radiation. It is then only that the changing electrical dipole of the bond couples with the electromagnetic field of the incoming radiation. All molecular compounds besides chiral compounds in its crystalline state have a unique spectrum. Even when the same type of bond or functional group is present in two different compounds, the frequency will be chemically different, because the two bonds experience different environments.[1] This technique is primarily the absorption measurement of the different IR frequencies of a sample, located in the course of an IR beam.

The infrared area in the electromagnetic spectrum extends from 14 000 cm^{-1} to 10 cm^{-1}, whereas the mid-infrared area (4000 cm^{-1} to 400 cm^{-1}) is the most important for chemical analysis. The infrared region extending from 400 cm^{-1} to 10 cm^{-1} is mainly used for the analysis of inorganic compounds containing heavy metals. It is impossible to use infrared spectroscopy as the only characterization technique to identify unknown compounds; however this method is very effective in identifying functional groups with single bonds (eg. C-H), double bonds (e.g. C=O) and triple bonds (e.g. C≡C).

A conversion of infrared radiation to molecular vibration energy occurs upon IR radiation absorbed by molecules.[2] When the radiation energy is equal to the vibrational frequency of the molecule, absorption will take place and a change in the amplitude of the molecular vibration is observed.

IR radiation energy has the ability to excite vibrational and rotational transitions; however the energy is not sufficient to induce electronic transitions. For every vibrational state, splitting of the peaks occur with change in rotational energy. With compounds in the liquid or solid state, this rotation is often hindered or prevented, causing the effects of these small energy differences to be undetected. Thus IR spectra originate in transitions between two vibrational levels of the molecule in the electronic ground state and are normally observed as the absorbed spectra.[3] Two types of molecular vibrations can occur, this is stretching and bending. It is

[1] Coates, J.; *Encyclopedia of Analytical Chemistry*; Interpretation of infrared Spectra, A Practical Approach, 10815, **2000**

[2] Nakamoto, K.; *Infrared Spectra of Inorganic and Coordination Compounds*, 2nd Ed., New York: John Wiley & Sons Inc., **1970**

[3] Skoog, D. A.; West, D. M.; Holler, F. J.; Crouch, S. R.; *Fundamentals of Analytical Chemistry*, 8th Ed.; 507, **2004**

important to take note that bond lengths and bond angles that are presented in literature are only an average measure of position, since no bond is rigid.

Carbonyl groups are permanently polarized because of the difference in electronegativity between the carbon and oxygen atoms. Thus the vibrational stretching of the carbon-oxygen bond affects the dipole moment. This is primarily the reason for the use of the carbonyl groups as a complex characterization tool. Carbonyl stretching has a distinct absorption peak on IR spectra.[4] Stretching and bending frequencies of carbonyls are generally in the range of 2360 to 1080 cm^{-1}, whereas stretching frequencies of metal complexes (M-CO) have a range from 2000 to 1700 cm^{-1}.[2] CO is a strong π-acceptor ligand therefore it is an outstanding ligand for the stabilization of an electron-rich low-valent metal cores. The absolute amount of electron density that the metal experiences hugely depends on the electron density donation from the ligand. An increase in the electron density on the metal centre causes an increase in the π-backbonding to the CO group, thus the strength of the metal carbonyl bond depends on the extent of back donation from the filled *d* orbitals of the metal.

The ligands which are *trans* to a carbonyl group largely effect the CO π-backbonding to the metal. Therefore if the *trans* ligand is of a σ-donating species than the strength of the M-CO bond will increase, because of metal to CO π-backbonding, as illustrated in Figure 3.1.
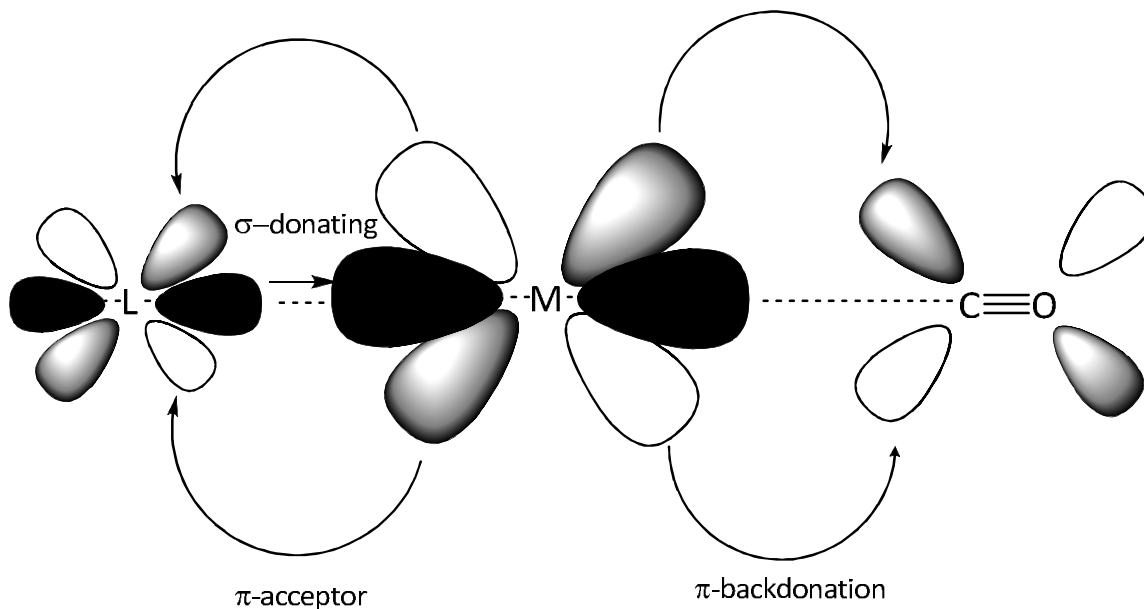
Figure 3.1: Strong σ-donor ligands tend to increase the metal-carbonyl bond strength, because of the CO π-backbonding.

---

[4] Stuart, B.; *Modern Infrared Spectroscopy*; Editor: Ando, D.J., England: John Wiley & Sons, Ltd., **1996**

3.2.2 Ultraviolet-visible spectroscopy

Ultraviolet-visible spectroscopy (UV/Vis) is a highly helpful technique based on the absorbance of energy in the transition between electronic states. In the electromagnetic spectrum, the UV/Vis wavelength ranges between 200 and 400 nm for ultraviolet and between 400 and 800 for the visible area. This technique can be used to: a) determine the content of a substance and b) in the identification of functional groups.

UV/VIS spectroscopy is based on the absorption of energy, whereby upon absorption, atoms or molecules pass from a lower energy (ground state) to a higher energy (excited state). The main types of electronic transitions which can be considered in UV/VIS spectroscopy are: transitions involving single (σ) bonding -, double or triple (π) bonding- and non-bonding (*n*, lone pair electrons) orbitals.

Upon absorption of energy by molecules, its valence electrons are excited from its highest occupied molecular orbital (HOMO) to the lowest molecular orbital (LUMO), see Figure 3.2.[5] The wavelength, at which molecules absorb energy, is dependent on how tight the valence electrons are bound to the atom. With compounds containing double - or triple bonds, electrons are loosely bound; therefore excitation is easy, yielding useful absorption peaks.
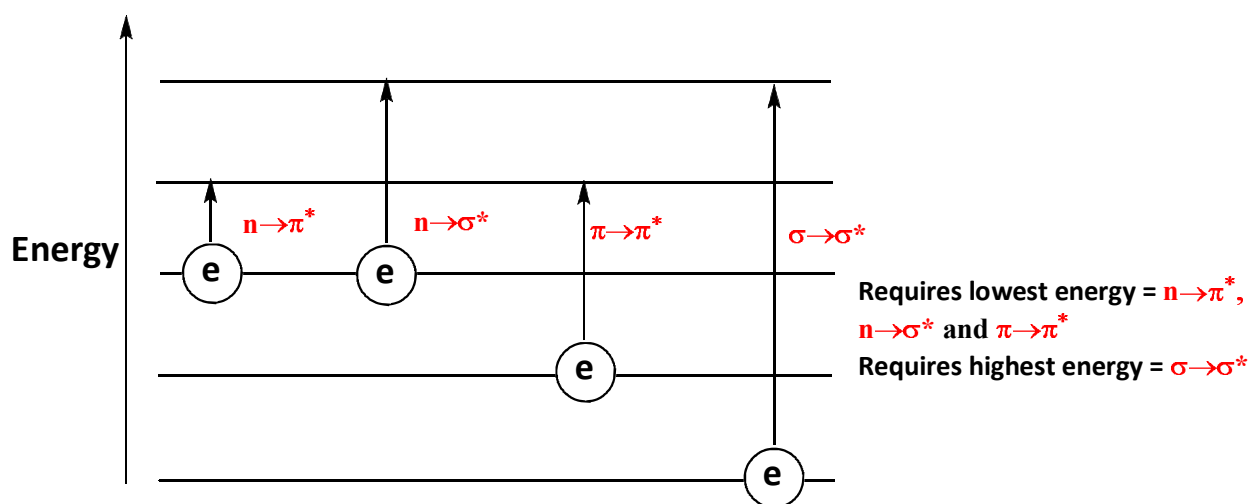
Figure 3.2: The electronic transitions of π-, σ- and n electrons, from LUMO (π* = nonbonding and σ* = bonding) to HOMO (π = bonding, σ = bonding and n = bonding).

[5] Pavia, D. L.; Lampman, G. M.; Kriz, G.S.; *Introduction to Spectroscopy*, 3rd Ed.; Thomson Learning Inc., New York, **2001**

3.2.2 Nuclear Magnetic Resonance spectroscopy

Since the discovery of nuclear resonance spectroscopy (NMR) in 1946, a dramatic change evolved in the characterization of chemical compounds. It is a powerful analytical tool, because it gives detailed information of chemical structures. One can obtain accurate structural information of unknown compounds in a relatively short amount of time, requiring less than a milligram of a sample. NMR has a widespread use, in different fields such as chemistry, physics and also in living biological material for medical diagnosis (magnetic resonance imaging, MRI).

NMR utilizes the magnetic properties of the nucleus of an atom to provide chemical information about the atom. The magnetic nucleus has an intrinsic angular momentum, known as the spin of the nucleus. Particles such as protons, electrons and neutrons spin around their own axes, whereas in atoms like carbon-12, oxygen-16 and sulphur-32, the spins are paired (i.e. the nucleus contain no overall spin). This implies that these atoms (^{12}C, ^{16}O and ^{32}S) cannot be used in NMR studies; however atoms with a nucleus that has an overall spin (e.g. ^1H, ^{13}C, ^{15}N, ^{19}F, ^{29}Si and ^{31}P) can be utilized. The overall spin (*I*), also known as the spin quantum number is important and can have one of the following values:

$$I = 0, 1/2, 1, 3/2, 2....$$

For a nucleus to be observed by NMR, the spin must have a non-zero value. Compounds such as ^1H, ^{13}C, ^{15}N, ^{19}F, ^{29}Si and ^{31}P have a spin number of ½ and nuclei with a spin greater than ½ generally give broad NMR lines.[6] In order to determine *I*, Table 3.1 can be used.

Table 3.1: A table to aid in the determination of the overall spin of a nucleus.

Atomic mass	Atomic number	Spin quantum number (*I*)
uneven	even or uneven	1/2, 3/2, 5/2....
even	even	0
Even	uneven	1, 2, 3....

When a magnetic nucleus is placed in a magnetic field, it can have a few orientations e.g. a nucleus with a spin of *I* will have a possible 2*I* + 1 orientation. Generally the orientations are equal in energy, unless a magnetic field is applied, which will split the energy levels. Each level

---

[6] Hore, P. J.; *Nuclear Magnetic Resonance*; New York: Oxford University Press, Inc.; **1995**

is given a quantum number (m) e.g. a hydrogen nucleus only have two permitted orientations. These are a clockwise spin (+ ½) with a magnetic moment aligned with the magnetic field or an anti-clockwise spin (− ½) with a magnetic moment pointing opposite the magnetic field, see Figure 3.3.
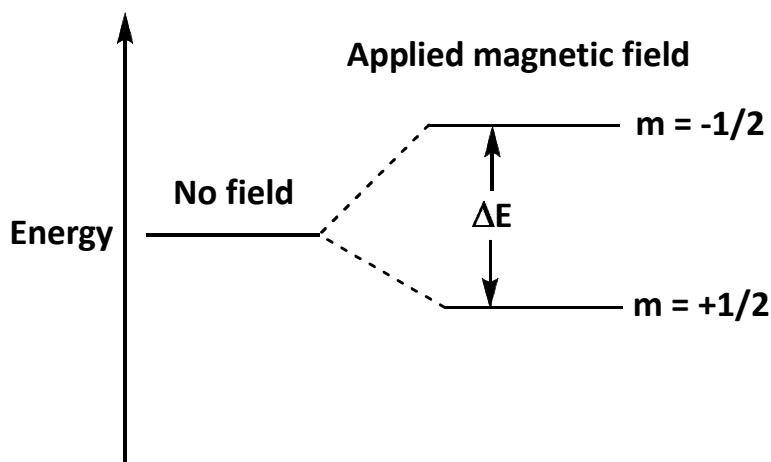
Figure 3.3: Energy levels of a hydrogen nucleus in a magnetic field.

The spin state +½ have the lowest energy because of its alignment with the magnetic field and the spin state −½ has the highest energy, due to its magnetic moment opposing the external magnetic field.   The two different energy states are separated by an energy difference, ΔE. This is dependent on the nuclear magnetic moment size and on the magnetic field strength. When determining the value of ΔE, an electromagnetic radiation frequency (v) is applied to the nucleus, which flips it (180 °) from a lower energy level to a higher energy level (the resonance condition ΔE = hv, must be satisfied). This phenomenon is called NMR spectroscopy.[5]

The nucleus experiences a magnetic field which is unequal to the applied magnetic field. This is due to negatively charged electrons moving in spherical orbitals (s-orbitals) about the nucleus and generating a local magnetic field perpendicular to the applied magnetic field, as shown in Figure 3.4. This causes the nucleus to not experience the applied magnetic field, but rather an effective magnetic field which resonates at a lower Larmor frequency (v), which is the applied field modified by the environment of the nucleus (e.g. electron density, proximity of the nuclei, etc.).[7] This interaction is known as nuclear shielding (chemical shift, δ) and varies with different

---

[7] Friebolin, H.; *Basic One- and Two-Dimensional NMR Spectroscopy*, 2nd Ed., VCH Publishers, New York, **1993**

nuclei. When a molecule contains electrons in its non-spherical orbitals (*p*- and *d*- orbitals), a relatively large magnetic field is produced in the nucleus, compared to the spherical *s* orbitals. The last *s* orbitals produce a low field shift, called deshielding, where non-spherical orbitals produce a high field shift, shielding. The main factors that can influence chemical shift are the inductive effect and the anisotropic effect. With the inductive effect, when the electron density of a nucleus is high, the induced field is stronger, due to the electrons and the opposite is also true, when the electron density decreases, the induced field is weaker. Deshielding and shielding occurs due to electron withdrawing groups (lower field resonance) and electron donating groups (higher field resonance) respectively. The anisotropic effect is a phenomenon that when a local magnetic field is generated by the delocalization of π-electrons in a molecule, it causes the protons to resonate at a higher or lower chemical shift, effectively causing shielding and deshielding respectively.
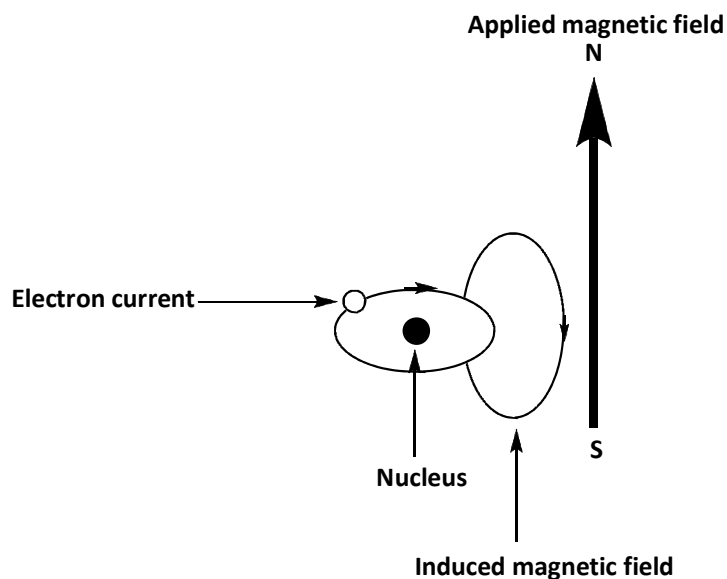
Figure 3.4: A schematic illustration of nuclear shielding

Protons can be affected by the magnetic field of a nearby proton, resulting in magnetic interactions between nuclei called spin-spin coupling. In spin-spin coupling, the resonance frequency of the first proton is split by the presence of the second proton and the difference between the peaks of the split frequency is indicated by the coupling constant, *J*. The coupling constant is a measurement of how strongly nuclei are affected by the spin states of its neighboring atoms.[6]

In NMR spectroscopy, the values of the chemical shift and the spin-spin coupling can provide important information on the position, environment and forces which are experienced by the atoms in different chemical species.

^{13}C-NMR is analogous to ^{1}H-NMR and is used in many industrial applications such as quantification of drug purity and also in the determination of the composition of polymers.[8] It allows the identification of carbon atoms in a molecule and it only detects the ^{13}C isotope, which has a natural abundance of 1.1 %. As explained earlier, ^{12}C isotope cannot be detected by NMR, since it has a netto spin state of zero.

There are a few contrasts between ^{13}C- and ^{1}H NMR:

➢ The intensities of a signal is not proportional to the number of equivalent ^{13}C atoms, but is highly dependent on the number of surrounding spins.

➢ Chemical shift in ^{13}C-NMR follows the exact same principles as in ^{1}H-NMR, however the range of chemical shifts is much larger (typically ranging from 0 to 220 ppm).

➢ In proton NMR, there is coupling between protons, however with ^{13}C-NMR, one can ignore coupling between carbons, because of the low natural abundance of ^{13}C.

➢ Proton NMR shows multiplets for each proton position, however in a typical carbon NMR spectrum, single peaks for each chemically non-equivalent carbon atom are observed.

➢ The chemical shift reference standard for ^{13}C is the carbon atoms in tetramethylsilane (TMS), with a chemical shift of 0 ppm.

There are also several complications pertaining ^{13}C-NMR:

➢ ^{13}C-NMR is far less sensitive to carbon, than ^{1}H-NMR is to hydrogen, due to the fact that the major isotope is ^{12}C ($I = 0$) and the latter is magnetically inactive.

➢ There are large J coupling constants present between carbon and hydrogen, which requires a proton decoupling (removal of signal splitting caused by carbon hydrogen interaction).

---

[8] http://en.wikipedia.org/wiki/Carbon-13_NMR [Consulted on **10 April 2012**]

3.3 Theoretical aspects of X-ray crystallography

3.3.1 Introduction

Mineralogy (the study of natural occurring compounds) contributed to the scientific field of crystallography, with the first experimental investigation been done in 1669. Crystals have always been fascinating to humans, with the term crystal derived from the Greek word *krystallos.*

3.3.2 X-ray diffraction

X-rays was not very well explored, until 1912 when a German physicist, Max von Laue, first predicted that crystals would exhibit diffraction qualities when bombarded with X-ray beams. When observing X-ray diffraction of X-ray beams, scientists believed that X-rays were a form of electromagnetic radiation.[9] In 1922 the photon model was confirmed by the study of scattering of X-rays from electrons, which resolved all remaining doubt about the nature of X-rays.[10]

Prior to the discovery of X-rays, scientists measured the angles between crystal faces and made their assumptions on that, regarding the arrangements of atoms in a crystal. The discovery of X-rays by C. W. Röentgen in 1885 made it possible to observe a crystal on the inside and obtain complete information on the structure and the size of the unit cell. When tools like X-ray crystallography and NMR did not exist, chemists assigned the correct structures from indirect data and logical thinking. They used certain properties (e.g. reactivity of molecules, number of isomers, empirical formulas, etc.) to do this. What makes X-ray crystallography useful in the exploration of crystals is the fact that X-rays are electromagnetic radiation with wavelengths in the region of 2×10^{-2} Å to 100 Å. This wavelength is comparable with the size of atoms. The reason why the use of X-rays are advantageous is a) it has smaller wavelengths than visible light and therefore can penetrate matter easily b) it can be used to observe numerous objects, because it has a suitable wavelength (0.01 to 10 nm) and c) it is relatively useful for mapping internal structures and organs. X-ray crystallography is an analytical tool which measures the

---

[9] Friedrich, W.; Knipping, P.; von Laue, M.; *Interferenz-Erscheinungenbie Rontgenstrahlen*, 202, **1912**
[10] Compton, A.; *Physical Review*, 21, 483, **1923**

variation in intensity with direction, in terms of the scattering of monochromatic radiation. It gives scientist an idea on microscopic levels of the arrangement of atoms in a unit cell, within a crystal. The atomic positions, bonds, angles etc. can be derived from the electronegativity inside the crystal, producing a three dimensional picture when X-rays are scattered from the electrons of atoms.[11] The scattered electromagnetic radiation can constructively or deconstructively add, depending on the direction of the diffracted beam and the atomic positions.[12]

To simplify a crystal structure, each atom is represented by a single point, resulting in a regular array of points. The array of identical points, which are equivalent to each other by translation, is called a lattice. A unit cell is the characteristic position of the crystal, from which the entire part of the crystal can be reproduced.[13] The lattice is made up from numerous unit cells (consists of three sides *a, b, c*, and three angles *α, β, γ*). Crystal symmetry can be divided into seven crystal systems and there are 230 space groups (describes the symmetry of a unit cell). The space groups are described in *The International Tables for Crystallography*.[14] To describe the directions and planes in a crystal lattice, Miller indices (*h, k, l*) are used.

Diffraction patterns are produced by X-rays that are radiated on the electrons in a crystal, yielding the conversion to density maps. To obtain a three dimensional image, the crystal is rotated, with a detector producing two dimensional electron density maps for each angle of rotation. Within a single crystal, a large number of molecules are arranged in the same orientation. This increases the signal to a more measurable level. Reflections are the pattern of spots produced by an X-ray that is imitated from consistently spaced planes and correspond to three properties of the crystal structure:

➢ The pattern has a specific geometry and is related to the lattice and unit cell geometry of the crystal structure.

➢ The pattern has symmetry and is related to the symmetry of the unit cell of the crystal structure.

---

[11] Clegg, W.;*Crystal Structure Determination*, New York: Oxford University Press, Inc., **1998**
[12] Ladd, M. F. C.; Palmer, R. A.; Structure determination by X-ray Chrystallography, New York: Plenum Press, **1977**
[13] Sharpe, D. W. A.; *The Penguin Dictionary of Chemistry*, 3rd Ed., London: Penguin Books Ltd., **2003**
[14] *International Tables for Crystallography*, A, 5th Ed., Kluwer Academic Publishers, **2002**

> ➢ The pattern has a variation of intensities and it reveals information about the position of atoms in the unit cell.[11]

3.3.3 Bragg's Law

W. L. Bragg assumed that when a monochromatic X-ray beam is diffracted by a crystal, it acts like it is reflected by atomic mirror planes within the crystal. When the incident beam has a definite value, reflection occurs. This is highly dependent on the wavelength and the lattice constants of the crystal. Sometimes it can occur that a portion of an X-ray beam may not be reflected at a certain crystal plane. The X-ray beam can however pass through and be subjected to a comparable process at another level, which is deeper into the crystal. Within a specific plane, it is known that all X-ray beams that are reflected off it remain in phase after reflection. It is also obvious that two X-rays that are reflected from neighbouring planes will be out of phase following reflection, due to the fact that they have travelled different path lengths. Thus Bragg's law is used to correct this difference in phases that exist.[15]

The definition of Bragg's law (see Figure 3.5) for the reflection of rays reflected by two adjacent planes is:

$$2d \sin\theta = n\lambda$$
...... **Eq. 3.1**

where n is an integer, λ is the wavelength, *d* is the distance between the two successive parallel crystal planes and θ is the angle of incidence and reflection of the reflected X-ray beam.
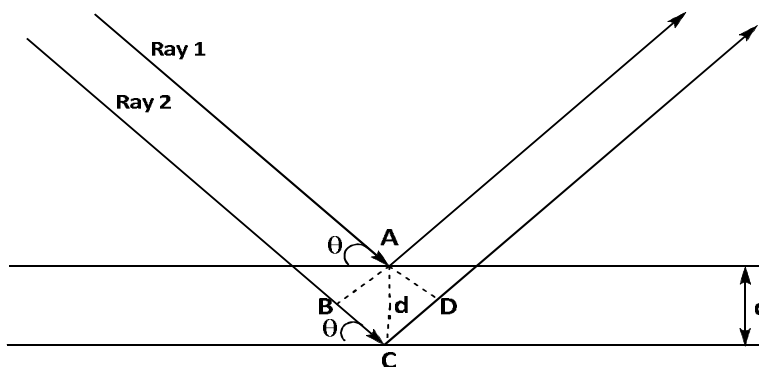
Figure 3.5: X-ray diffraction as proposed by Bragg.

---

[15] Hammond, C.; *The Basics of Crystallography and Diffraction*, 2nd Ed., New York:Oxford University Press, Inc., **2001**

Where:

$$BC + CD = 2d \sin\theta$$

..... **Eq. 3.2**

It is clear from the equation that Bragg's law forms the base of all methods for obtaining unit cell geometry from the measured geometry of the diffraction pattern.

3.3.4 Structure factor

In a unit cell, all atom positions have to be expressed and in X-ray crystallography they are given the *h*, *k*, *l* coordinates. Each coordinate is also assigned a number between 0 and 1, with the cell edges expressed as vectors (*a, b, c*). If all of this is defined, an atom's position can be articulated as:

$$r = hx + ky + lz$$

...... **Eq. 3.3**

The structure factor, F_{hkl}, can be utilized to obtain a value, which will correspond to the intensity and capability of X-rays for the diffraction from a specific plane. It expresses the combined scattering of all atoms (*j*) in a unit cell, which is relative to a single electron. Thus the resultant equation for the unit cell is:[12]

$$F_{hkl} = \sum_{j=1}^{N} f_j \exp\left[i2\pi\left(hx_j + ky_j + lz_j\right)\right]$$

...... **Eq. 3.4**

where f_j is equal to the scattering factor of each atom (N).

This equation indicates that the structure factor's magnitude depends only on the relative disposition of the N atoms in the unit cell as well as on their atomic scattering factor. Equation 3.3 represents a wavelet with f_j as the amplitude and the phase $\emptyset_j = 2\pi\left(hx_j + ky_j + lz_j\right)$, which expresses the path length for each scattered wavelet.[16]

---

[16] Azároff, L. V.; *Elements of X-ray Crystallography*, New York: McGraw-Hill, Inc., **1968**

Equation 3.4 can now also be expressed as follows:

$$F_{hkl} = \sum_{j=1}^{N} f_j \left[\cos 2\pi \left(hx_j + ky_j + lz_j \right) + i\sin 2\pi \left(hx_j + ky_j + lz_j \right) \right]$$

...... **Eq. 3.5**

The energy of the cosine wave is directly proportional to the square of the amplitude of the wave. It is now expressed in X-ray diffraction, in terms of the intensity of the scattered wave from the unit. I_o(hkl) can represent IFhklI^2, where subscript *o* signifies an experimentally observed quantity and IFhklI^2 is often called the ideal intensity, therefore:

$$I_o(hkl) \propto \left| F_o(hkl) \right|^2$$

...... **Eq. 3.6**

Eq. 3.6 serves as the platform for X-ray structure analysis. This allows the experimental quantities of I_o(hkl) to be directly related to the structure through IFhklI. Atoms with high atomic numbers have a higher concentration of electrons than do atoms of low atomic numbers. Electron density (ρ) is basically the concentration of electrons and its distribution around the atom and it is measured in electrons per cubic angstroms (é. Å^{-3}). Generally, since electron density is a function of position, it can be specified at a point X, Y, Z which is given as ρ (X, Y, Z). The structure factor can now be given in terms of electron density as expressed in Equation 3.7:

$$F_{hkl} = \int \rho(x, y, z) \exp \left[i2\pi \left(hx_n + ky_n + iz_n \right) \right] dV$$

...... **Eq. 3.7**

3.3.5 The "Phase problem"

When determining a crystal structure, it is not done directly from the observed intensity data. Generally the modulus, IFhklI, can be obtained from the intensity data directly using Equation 3.6, however the determination of the phase $\varnothing_{hkl}$ corresponding to IFhklI cannot be measured directly in order to determine a crystal structure. To determine the structure, both the phase and the amplitude must be known. To overcome this inability a number of means can be used.

This inability of determining the phase is termed the "Phase problem". There are two possible approaches that can be used, i.e. the Patterson function and the direct method.

3.3.5.1 Direct method

The direct method is useful in the determination of the phase information for light atom containing structures. This method deals with the determination of the reflection phases from measured X-ray intensities, using mathematical formulae. The Patterson function is useful in determining phases for molecules which contain only one atom or a small number of atoms with significantly more electrons.[12]

3.3.5.2 Patterson function

The Patterson function or Patterson map is similar to a map of electron density with positive electron density peaks in various positions and is expressed by Equation 3.8. *V* represents the volume of the unit cell.

$$P\ (u,\ v,\ w) = V^{-1} \sum \sum \sum (F_{hkl})^2 \exp[-2\pi i\ (h_u + k_v + l_w)] \qquad \text{...... Eq. 3.8}$$

These peaks positions are not the atom positions in the structure; however they are a function of vectors between pairs of atoms within the structure. This indicate that the Patterson Function exclusively produce information on where the atoms are situated relative to each other and not relative to the unit cell origin. [17]

3.3.6 Least Squares Refinement

A calculated diffraction pattern can be made following the fact that the obtained structure is the correct one. The least square refinement also serves as a 'tool' in the comparison of the calculated diffraction pattern and the observed pattern. With this method it is also possible to compare and calculate degree of resemblance between the calculated and observed pattern. One then compare the structure factor (F_c) to the experimental data (F_0) and it is expressed in terms of *residual index* or *R-factor*.[17]

---

[17] Stout, G. H.; Jensen, L. H.; *X-ray Structure Determination: A Practical Guide*, The Macmillan Company, London, **1968**

$$R = \frac{\sum \left| \left| F_o \right| - \left| F_c \right| \right|}{\sum \left| F_o \right|}$$

...... **Eq. 3.9**

An R-factor below 1 (specifically between 0.02 and 0.07) is an indication of a complete and correct structure, which was determined from good experimental data. When one wants to obtain an even better refinement, it can be obtained from the incorporation of weighing factor for each reflection, *w*. This is a reliability factor of the different measured data and this new residual factor is used for determining crystal structures.

3.4 Chemical kinetics

3.4.1 Introduction

Chemical kinetics is important because it is mainly used for:

➢ the sole purpose to gain insight into the mechanism of chemical changes,

➢ to learn more about the characteristics of a chemical reaction,

➢ to investigate the transition of a system as it adjust to another state and

➢ to determine the time it takes for these transitions to occur.

There are numerous factors that can play a significant role and can influence the rate constant and reaction mechanism of a reaction. These are as follows:

➢ temperature

➢ concentration

➢ light sensitivity

➢ pressure

➢ homogeneity

Therefore if the reaction is kept constant in temperature exposure, pressure and volume, the rate constants are just defined as the rate of change in time of any products and reactants.

All molecules have unique absorption spectra and by using a UV/VIS, one can study kinetic measurements, however it is almost impossible to study fast reactions. A solution will absorb a certain measure of an incident beam with an intensity of I_o and then emit a transmitted

intensity beam, I_{trs}. This is the Beer-Lambert law, which expresses the relationship between the concentrations (*c*) of a single absorbing compound and the intensity of the incident monochromatic light and the transmitted intensity.[18]

$$Log_{10} \frac{I_o}{I_{trs}} = \varepsilon Cl = A$$

...... **Eq. 3.10**

where *l* = path length, ε = extinction coefficient and A absorbance. Deduced from this equation is that the absorbance is a linear function of concentration and the total absorbance of a sample is the sum total of the individual absorbencies of each solution, thus:

$$A = \sum \varepsilon Cl$$

..... **Eq. 3.11**

3.4.2 Reaction rates and rate order

When determining the rate of a reaction, one can simply define the study as the investigation of the concentration as a function of time. This is usually done in an isothermal system, with one or more concentrations that are measured as a function of time. In the following reaction:

$$a[A] + b[B] \xrightarrow{k_1} c[C] + d[D]$$
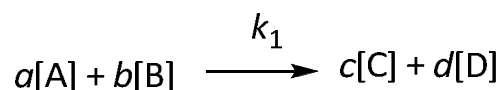
the rate can be expressed as a derivative since the rate consistently changes with time.

$$Rate = \frac{-d[A]}{dt} = \frac{-d[B]}{dt} = \frac{d[C]}{dt} = \frac{d[D]}{dt} = k\,[A]^a[B]^b$$

...... **Eq. 3.12**

whereby *t* represents the time, [A], [B], [C] and [D] the concentrations of the different species, *a* is the order of the reaction with respect to compound A, *b* is the order of the reaction with respect to compound B, *k* is the rate constant and the sum of *a* and *b* is the overall rate of the reaction. The negative sign symbolizes the disappearance of the reactants and the formation of another product is symbolized by a positive sign. When referring to Equation 3.12, k, *a* and *b*

---

[18] Atkins, P.W.; *Physical Chemistry*, Oxford University Press, **1994**

are not dependent on the concentration and the time. For a specific reaction, k is unique, however it can differ with difference in temperature and the type of solvent involved.

The order of a reaction can vary, if the concentrations of one or both of the reactants are altered and it is simply the exponent of the particular component in question. *Pseudo* first order conditions are used to overcome the problem arising from the difficulty in determining the reaction rate, when the concentrations of the reactants are changed. *Pseudo* first order conditions simply entails the change in concentration of one of reactants, while the other is kept constant. So when we look at the reaction:

$$a[A] + b[B] \xrightarrow{k_1} c[C] + d[D]$$
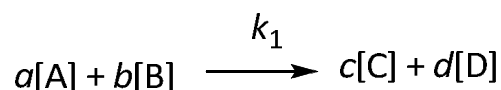
the concentration of B will be altered to be much larger than that of A (i. e. [B]>>>[A]), now from Equation 3.12 the rate is simply as follows:

$$Rate = k_{obs}[A]^a \hspace{4cm} \text{...... Eq. 3.13}$$

which gives rise to Equation 3.14.

$$k_{obs} = k[B]^b \hspace{4cm} \text{...... Eq. 3.14}$$

From Equation 3.14, the rate constant can now be determined, by altering the concentration of B and k_{obs} is simply the observed *pseudo* first order rate constant.

When determining the rate law for a second order reaction, a = b = 1 and it is expressed as follows:

$$a[A] + b[B] \underset{k_2}{\overset{k_1}{\rightleftarrows}} c[C] + d[D] \hspace{3cm} \text{...... Eq. 3.15}$$

From Equation 3.15, the rate law can be defined as:

$$Rate = k_1[A][B] + k_2[A] \hspace{3cm} \text{...... Eq. 3.16}$$

Under *pseudo* first order conditions, the rate is now expressed as:

$$k_{obs} = k_1[B] + k_2$$

.... **Eq. 3.15**

This equation is also applicable in equilibrium reactions, with k_1 and k_2 representing the forward reverse reactions respectively. The equilibrium constant for an equilibrium reaction is now expressed as:

$$K_{eq} = \frac{k_1}{k_2}$$

...... **Eq. 3.16**

When integrating Equation 3.10, between t = 0 and t, Equation 3.17 follows:

$$\ln \frac{[C]_t}{[C]_0} = k_{obs} \quad \text{or} \quad [C]_t = [C]_0\, e^{k_{obs}t}$$

...... **Eq. 3.17**

$[C]_0$ = concentration change at t = 0 and $[C]_t$ = concentration change at t.

The Beer-Lambert law relates the absorption of light to the concentration of a solution, by the substitution of Equation 3.11 into Equation 3.17, yielding:

$$A_t = A_\infty (A_\infty - A_0)\, e^{k_{obs}t}$$

...... **Eq. 3.18**

A_t = the absorbance after time t

A_∞ = the absorbance at time infinite (the time when the reaction is complete)

For the first order reaction, the absorbance against time data can be fit into a least-square equation, for the calculation of the observed rate constant (k_{obs}) and Equation 3.18 is used in the kinetic studies to evaluate k_{obs}.

3.4.3 Half-life of a reaction

Reaction half lives are important, because it gives the time required for the reaction concentration to decay to 50 % of its initial amount. In a first order reaction (A $\rightarrow$ B, t = $t_{1/2}$ when [A] = ½ [A]$_0$), by substituting t = $t_{1/2}$ and [A] = ½ [A]$_0$ into [A] = [A]$_0 e^{-k_1 t}$ the half life can be calculated, which yields:

$$\frac{1}{2}[A]_0 = [A]_0 \, e^{-k_1 t1/2} \quad \text{or} \quad t_{1/2} = \frac{\ln 2}{k_1} = \frac{0.693}{k_1}$$

...... **Eq. 3.19**

Half-life calculation in chemical kinetics is advantageous in that when the concentration decrease exponentially; the reaction will consume equal fractions of [A] in consecutive periods of time ($t_{1/2}$). The half-live involving reactions with different reaction orders can also be identified, as indicated in Table 3.2.

Table 3.2: The equations for the calculation of half-life, with respect to the different reaction orders.

Reaction order	Half-live ($t_{1/2}$)
0	$\dfrac{\frac{1}{2}[A]_0}{k_0}$
1	$\dfrac{\ln 2}{k_1}$
2	$\dfrac{1}{k_2[A]_0}$
3	$\dfrac{3}{2\,k_3[A]_0^2}$

ooOoo

4 SYNTHESIS OF COMPOUNDS

4.1 Introduction

Modern medicine demands advanced and more sophisticated methods for the accurate diagnosis of diseases, therefore there is a massive worldwide research effort into developing and improving imaging and therapeutic radiopharmaceutical agents. As previously mentioned, the ^{99m}Tc nuclear isotope is used for medical imaging, due to its almost perfect nuclear properties of a 6 h half-life and γ-ray emission of 141 keV. The 'lanthanide contraction' makes sure that the complexes of two elements are similar in terms of their physical properties (size, lipophylicity etc. - see Paragraph 1.4). Rhenium is the third row congener of technetium, making it impossible for biological systems to distinguish between their complexes.[1]

Several studies involving the Tc and Re tricarbonyl core was done thus far, however the kinetic studies of complexes involving the substitution of different ligands on the rhenium tricarbonyl core is still under explored.[2]

Quite a few radiopharmaceuticals, bearing a Tc(V) or Re(V) core, with donating N-, S-, O-, and P ligand system variations have already been synthesised. Research involving the *fac*-[Re(CO)$_3$]$^+$ core is currently very popular and a literature research reveal that only a few compounds of the form *fac*-[Re(CO)$_3$(L,L')X], with X = Br, H$_2$O and Py and L,L' = N, O or O,O' bidentate ligand systems, has been synthesised. Thus leading us in the direction of exploring the ability of the *fac*-[Re(CO)$_3$]$^+$ core to interact with O,O' bidentate ligands and to establish its kinetic behaviour towards substitution of its axial monodentate ligands.

As indicated in Figure 4.1, the O,O' donor bidentate ligands acetylacetone (Acac), trifluoro-acetylacetone (TFA) and hexafluoro-acetylacetone (HFA) were chosen, while ephedrine (EPH) and 8-hydroxyl-quinoline (8-Quin) have been chosen as N,O donor bidentate

[1] Dilworth, J. R., Parrott, S. J., *Chem. Soc. Rev.*, 27, 43, **1998**

[2] Salignac, B., Grundler, P.V., Cayemittes, S., Frey, U., Scopelliti, R., Merbach, A.E., *Inorg. Chem.*, 42, 3516, **2003**

ligands. Pyridine (Py) was selected as entering ligand in the kinetic study. This chapter deals with the synthesis and spectroscopic characterisation of these complexes.

Acetylacetone - Acac   **Trifluoroacetylacetone - TFA**   **Hexafluoroacetylacetone - HFA**

8-Hydroxyquinoline - 8-Quin   **Ephedrine - EPH**
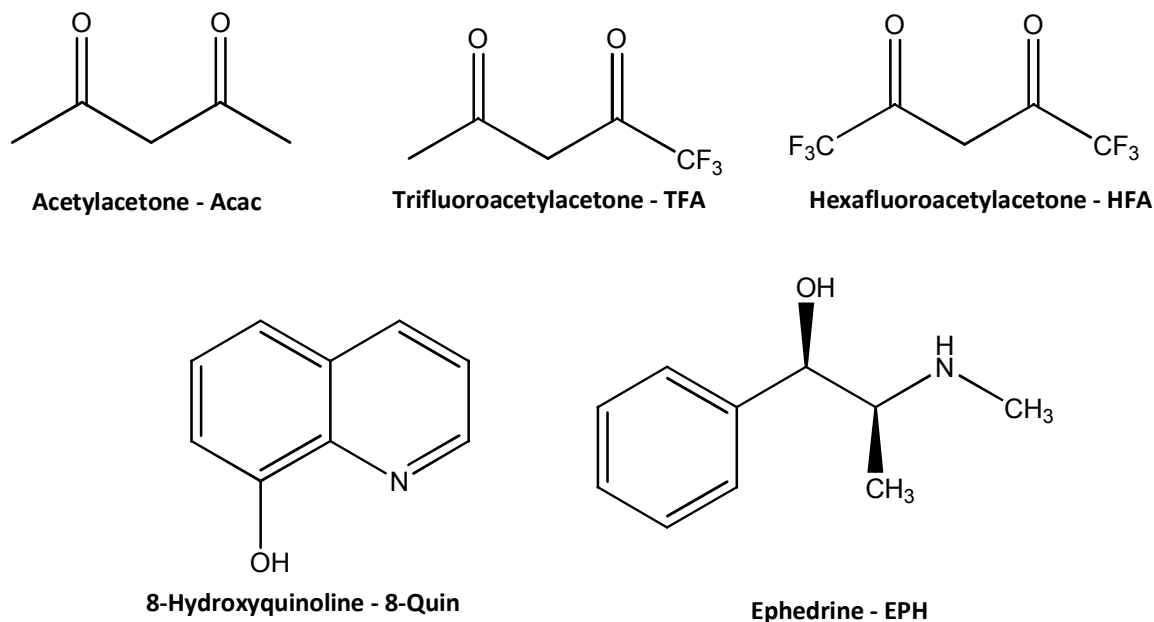
Figure 4.1: A representation of the bidentate ligands used in the synthesis of rhenium and technetium-99m compounds.

4.2 Apparatus and Chemicals

Chemicals used in this study for synthetic and characterisation purposes were reagent grade and if stated otherwise, purchased from Sigma-Aldrich, South-Africa. Reagents were used as received, without further altering or purification. All organic solvents were purchased from SAARCHEM (South-Africa) and were of analytical grade; however they were dried and distilled prior to use. The bidentate ligands are protonated during synthesis, using HNO_3 to adjust the pH of the reaction mixture. All the experiments were done under aerobic conditions, using double distilled water and methanol. Technetium pertechnetate was supplied by Axim radiopharmacy, eluted from a Technetium generator, with a radioactivity measurement of 250 mCi. The TLC C-18 reverse phase plates were purchased from Merck, South-Africa.

All the infrared spectra of the complexes were recorded using a temperature cell regulated (accurate within 0.3°C) Bruker Tensor 27 Standard System spectrophotometer with a laser

range of 4000 – 370 cm^{-1}, coupled to a computer. Solid samples were analyzed in the form of potassium bromide (KBr) pellets and all data were recorded at room temperature.

UV/visible measurements were performed on a Cary 50 Conc UV/VIS spectrophotometer equipped with a Julabo F-12 temperature cell regulator (accurate to 0.1°C).

All ^{1}H and ^{13}C NMR spectra were obtained in C_3D_6O and CD_3OD on a Bruker 600 MHz nuclear magnetic resonance spectrometer. Chemical shifts are reported relative to TMS using the C_3D_6O (^{1}H = 2.05 ppm) and CD_3OD (^{1}H = 3.31 ppm and ^{13}C = 49.05 ppm) peak.

For thin layer chromatography (TLC) of the ^{99m}Tc complexes, a Bioscan AR-2000, equipped with a Win Scan V3 program was used. A trifluoroacetic acid (0.1 %) and water mixture was used as the mobile phase. The front was measured as 200 mm and all solutions are plotted at 1 mm.

4.3   Radioactive isotope handling

In order to use rhenium (therapeutic) and technetium (diagnostic) in nuclear medicine, the availability of unstable, radioactive forms of certain metals are essential. Thus when handling radioactivity, a special facility is required for shielding from emitted radiation and also to prevent contamination of the environment by the radioactive materials released during handling and processing.[3] In this study, all experimental procedures, involving ^{99m}Tc was done at an equipped, registered facility (i.e. Petlabs Pharmaceuticals).

Since rhenium posses the qualities of a possible therapeutic agent, (^{186}Re and ^{188}Re are both unstable), its natural abundant form, ^{186}Re is used in basic research and development. ^{186}Re is found in a mixture of two isotopes, ^{185}Re (37.4 %) and ^{187}Re (62.6 %, $t_{1/2}$ = 6.6 x 10^{10} yrs), where the latter isotope is a weak β-emitter (β = 2.62 keV).[4] ^{188}Re has a long half-life and emits soft β-rays, thus no special handling methods are necessary.

^{99m}Tc is recognized as the workhorse of the nuclear medicine world, because of its nuclear benefits, chemical characters and easy availability from the ^{99m}Mo/^{99m}Tc generator. It emits low energy γ-rays, 0.143 MeV with a specific activity of 5.3 x 10^7 Ci/g.

---

[3] International Atomic Energy Agency, Radioisotope handling facilities and automation of radioisotope production, IAEA-TECDOC-1430, **2004**
[4] Riley, G. H.; *J. Sci. Instrum.*; 44, 769, **1967**

All [99mTc] isotopes were handled behind a thick lead shield tower. Disposable gloves, safety glasses and protective overcoats were used at all times. Radioactive waste both liquid and solid was disposed of in special equipped containers.

4.4 Experimental procedures

The preparation of the rhenium starting synthon was performed under a nitrogen atmosphere (Schlenk conditions).

4.4.1 Preparation of starting material

4.4.1.1 Synthesis of $[NEt_4]_2[ReBr_3(CO)_3]$ – (ReAA)

This synthesis was performed under strict nitrogen atmosphere (Schlenk conditions) and all apparatus must be flame dried.

$$Re_2(CO)_{10} + Br_2 \longrightarrow 2\ ReBr(CO)_5$$
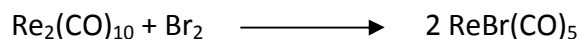
$Re_2(CO)_{10}$ (5.06 g; 7.75 mmol) was dissolved in 150 ml of dry hexane and Br_2 (0.240 ml; 9.32 mmol) was added, drop wise. A white precipitate immediately formed upon adding bromine. The reaction mixture was then stirred for 24 hrs, until the orange/red colour disappeared. The mixture was filtered and dried under vacuum over night. (Yield = 5.50 g; 87 %)

IR (KBr, cm^{-1}): υ_{CO} = 2154, 2033, 1963

$$ReBr(CO)_5 + 2\ (NEt_4)Br \xrightarrow{N_2;\ diglyme} [NEt_4]_2[ReBr_3(CO)_3] + 2\ CO$$
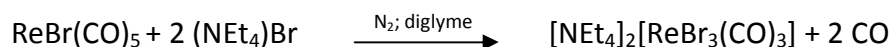
After grinding $(NEt_4)Br$ (5.60 g; 0.027 mol) into a fine powder, it was dried under vacuum overnight. 2,5,8 trioxanone diglyme (150 ml) was added to $(NEt_4)Br$ under a dry nitrogen atmosphere and heated to 80 ˚C for 1 hr. $[Re(CO)_5Br]$ (5.50 g; 0.014 mol) was added to the reaction mixture as a solid and stirred at 120 ˚C for 24 hrs. The reaction mixture was cooled down and filtered. The product was washed with cold diglyme and cold ether, followed by washing it twice with cold ethanol. The ethanol dissolves the excess $(NEt_4)Br$. The product, white to light yellow in color, was left to dry under vacuum. (Yield = 9.50 g; 88 %)

IR (KBr, cm^{-1}): υ_{CO} = 1999, 1868

Elemental analysis: calculated: C: 29.62%, H: 5.23%, N: 3.64%; found: C: 29.59%, H: 5.19%, N: 3.65%.

4.4.2 Synthesis of rhenium complexes

4.4.2.1 Synthesis of *fac*-[Re(Acac)(CO)$_3$Br][NEt$_4$]

To ReAA (300 mg; 0.389 mmol) dissolved in methanol (5 ml), AgNO$_3$ (132 mg; 0.778 mmol) was added as a solid and stirred at 70 °C for 24 hours. The precipitate, AgBr, was filtered off and weighed (146 mg). Acetylacetone (0.039 g; 0.389 mmol) dissolved in methanol (5 ml) was slowly added and the mixture was stirred at 70 °C for a further 24 hrs. Upon the evaporation of the solvent, a light yellow product precipitated out of the reaction mixture after a few days. (Yield = 0.151 g; 86 %)

IR (KBr, cm^{-1}): ν_{CO} = 2006, 1868

UV/VIS: 265 nm

^{1}H NMR (600 MHz, Methanol-*d$_4$*): δ = 1.28 (d of d of d, *J* = 7.3, 4.6, 1.8 Hz, 12H, NEt$_4$); 2.01 (s, 6H); 2.49 (q, *J* = 7.2 Hz, 8H, NEt$_4$); 5.64 (s, 1H)

^{13}C NMR (600 MHz, Methanol-*d$_4$*): δ = 6.16 (NEt$_4$); 27.59; 51.92; 104.70; 190.37; 194.74

4.4.2.2 Synthesis of *fac*-[Re(Acac)(CO)$_3$(OH$_2$)]

ReAA (500 mg; 0.648 mmol) was stirred in 10 ml of water at pH 2.2 for 20 minutes until dissolved. AgNO$_3$ (330 mg; 1.945 mmol) was added to the solution and stirred for 24 hours at room temperature. The precipitate, AgBr, was filtered off and weighed (365 mg). Acetylacetone (0.0650 g; 0.649 mmol) was added to the filtrate and stirred for 36 hours at room temperature. The solution had a colorless to light yellow color with a light yellow precipitate. The product was filtered off, dried and weighed. (Yield = 0.236 g; 93 %)

IR (KBr, cm^{-1}): ν_{CO} = 3443 (H$_2$O), 2015, 1907, 1879

UV/VIS: 266 nm

^{1}H NMR (600 MHz, Acetone-d$_6$): δ = 1.95 (s, 3H); 1.97 (s, 3H); 2.84 (s, 2H); 5.60 (s, 1H)

^{13}C NMR (600 MHz, Acetone-d$_6$): δ = 27.48; 27.50; 102.66; 189.06; 189.11; 198.57; 198.97

4.4.2.3 Synthesis of *fac*-[Re(Acac)(CO)$_3$(Py)]

ReAA (500 mg; 0.648 mmol) was dissolved in 10 ml of water at pH 2.2. AgNO$_3$ (330 mg; 1.945 mmol) was added to the solution and stirred for 24 hours at room temperature. The precipitate, AgBr, was filtered off and weighed (365 mg). Acetylacetone (0.0650 g; 0.648 mmol) was added to the filtrate and stirred for 48 hrs at room temperature. The light yellow solution was filtered and pyridine (0.0510 g; 0.648 mmol) was added to the filtrate. The product was a yellow precipitate, which formed after stirring the solution for 10 min at room temperature. It was filtered off and weighed. (Yield = 0.253 g; 86 %)

IR (KBr, cm^{-1}): v_{CO} = 2017, 1906

UV/VIS: 255 nm

^{1}H NMR (600 MHz, Acetone-d$_6$): δ = 1.93 (s, 6H); 5.45 (s, 1H); 7.67 (q of d, *J* = 7.7, 5.2, 1.4 Hz, 2H); 8.18 (t of t, *J* = 7.6, 1.5 Hz, 1 H); 8.61 (d of d, 2H)

^{13}C NMR (600 MHz, Acetone-d$_6$): δ = 26.67; 52.19; 101.94; 126.02; 139.54; 151.51; 151.76; 188.40

4.4.2.4 Synthesis of *fac*-[Re(TFA)(CO)$_3$Br][NEt$_4$]

ReAA (300 mg; 0.389 mmol) was dissolved in methanol (5 ml) and AgNO$_3$ (132 mg; 0.778 mmol) was added as a solid and stirred at 70 °C for 24 hours. The precipitate, AgBr, was filtered off and weighed (146 mg). Trifluoroacetylacetone (0.060 g; 0.389 mmol) dissolved in methanol (5 ml) was slowly added and the mixture was stirred at 70 °C for a further 24 hrs. The product crystallised out as a bright yellow solid upon evaporation of the solvent. (Yield = 0.243 g; 98 %)

IR (KBr, cm^{-1}): v_{CO} = 2012, 1872

UV/VIS: 266 nm

^{1}H NMR (600 MHz, Methanol-d$_4$): δ = 1.27 (m, 12H, NEt$_4$); 2.20 (s, 3H); 2.58 (q, *J* = 7.2 Hz, 8H, NEt$_4$); 6.05 (s, 1H)

^{13}C NMR (600 MHz, Methanol-d$_4$): δ = 7.56 (NEt$_4$); 28.81; 53.21; 98.68; 119.02; 169.06; 169.28; 197.28; 198.63

4.4.2.5 Synthesis of *fac*-[Re(TFA)(CO)$_3$(OH$_2$)]

ReAA (500 mg; 0.648 mmol) was stirred in 10 ml of water at pH 2.2 for 30 minutes until dissolved. AgNO$_3$ (330 mg; 1.945 mmol) was added to the solution and stirred for 24 hours at room temperature. The precipitate, AgBr, was filtered off and weighed (365 mg). Trifluoroacetylacetone (0.1 g; 0.649 mmol) was added to the solution and stirred for 36 hours at room temperature. A yellow solution formed and after a few days a yellow product precipitated out at 5 °C. (Yield = 0.231g; 80 %)

IR (KBr, cm^{-1}): v_{CO} = 3425 (H$_2$O), 2018, 1895, 1878

UV/VIS: 262 nm

^{1}H NMR (600 MHz, Acetone-d$_6$): δ = 1.38 (s, 3H); 2.84 (s, 2H); 5.90 (s, 1H)

^{13}C NMR (600 MHz, Acetone-d$_6$): δ = 24.70; 52.04; 100.24; 120.21; 175.30; 197.27; 197.77

4.4.2.6 Synthesis of *fac*-[Re(TFA)(CO)$_3$(Py)]

ReAA (500 mg; 0.648 mmol) was dissolved in 10 ml water (pH 2.2) and stirred for 30 min. To this solution, AgNO$_3$ (330 mg; 1.945 mmol) was added and stirred for 24 hours at room temperature. The precipitate, AgBr, was filtered off and weighed (365 mg). Trifluoroacetylacetone (0.1 g; 0.649 mmol) was added to the filtrate and stirred for 48 hrs. To the yellow solution, pyridine (0.0512 g; 0.648 mmol) was added and stirred for 10 min at room temperature. A bright yellow precipitate formed which was filtered off and recrystallized in acetone (3 ml). Yellow cuboid crystals, suitable for single crystal X-ray diffractometry were obtained. (Yield = 0.292 g; 90 %)

IR (KBr, cm^{-1}): v_{CO} = 2030, 1930, 1888

UV/VIS: 260 nm

^{1}H NMR (600 MHz, Acetone-d$_6$): δ = 2.21 (s, 3H); 5.94 (s, 1H); 7.70 (q of d, *J* = 7.6, 5.0, 1.4 Hz, 2H); 8.18 (t of t, *J* = 7.6, 1.5, 1H); 8.60 (d of d, *J* = 6.4, 1.5 Hz, 2H)

^{13}C NMR (600 MHz, Acetone-d$_6$): δ = 28.22, 97.66; 126.42; 140.07; 151.58; 155.58; 167.24; 197.70

4.4.2.7 Synthesis of *fac*-[Re(HFA)(CO)$_3$(Br)][NEt$_4$]

Hexafluoroacetylacetone (0.134 g; 0.648 mmol) dissolved in methanol (5 ml), was added to a solution of ReAA (500 mg; 0.648 mmol) in 5 ml methanol. The reaction mixture was stirred at 60 °C for 18 hrs. A bright orange product crystallised out of the reaction mixture after a few days. (Yield = 0.319 g; 71 %)

IR (KBr, cm^{-1}): v_{CO} = 2018, 1903

UV/VIS: 270 nm

^{1}H NMR (600 MHz, Acetone-d$_6$): δ = 1.40 (m, 12H, NEt$_4$); 2.81 (q, *J* = 7.3 Hz, 8H, NEt$_4$); 6.14 (s, 1H)

^{13}C NMR (600 MHz, Acetone-d$_6$): δ = 7.54 (NEt$_4$); 53.21; 94.08; 133.30; 133.82; 166.87; 179.45; 186.69

4.4.2.8 Synthesis of *fac*-[Re(HFA)(CO)$_3$(OH$_2$)]

ReAA (500 mg; 0.648 mmol) was stirred in water (10 ml) at pH 2.2 for 20 minutes until dissolved. AgNO$_3$ (330 mg; 1.945 mmol) was added to the solution and stirred for 24 hours at room temperature. The precipitate, AgBr, was filtered off and weighed (365 mg). Hexafluoroacetylacetone (0.135 g; 0.648 mmol) was added to the solution and stirred for 48 hours at room temperature. The solution turned orange and orange crystals, not suitable for X-ray crystallography formed after a few days. (Yield: 0.274 g; 85 %)

IR (KBr, cm^{-1}): v_{CO} = 3449 (H$_2$O), 2025, 1917, 1888

UV/VIS: 260 nm

^{1}H NMR (600 MHz, Acetone-d$_6$): δ = 2.82 (s, 2H); 5.01 (s, 1H)

^{13}C NMR (600 MHz, Acetone-d$_6$): δ = 52.09; 95.70; 116.59; 118.48; 174.04; 193.03; 193.24

4.4.2.9 Synthesis of *fac*-[Re(HFA)(CO)₃(Py)]

ReAA (500 mg; 0.648 mmol) was dissolved in 10 ml of water at pH 2.2 for 30 minutes. To this solution, AgNO₃ (330 mg; 1.945 mmol) was added and stirred for 24 hours at room temperature. The precipitate, AgBr, was filtered off and weighed (365 mg). Hexafluoroacetylacetone (0.134 g; 0.648 mmol) was added to the filtrate and stirred for 48 hrs at room temperature. The orange solution was filtered and pyridine (0.0513 g; 0.648 mmol) was added to the filtrate. The product was an orange precipitate, which formed after stirring the solution for 10 min at room temperature. The precipitate was filtered, dried and recrystallized in acetone (3 ml) to form orange needle-like crystals. These were suitable for single X-ray diffractometry. (Yield = 0.271 g; 75 %)

IR (KBr, cm^{-1}): v_{CO} = 2036, 1939, 1873

UV/VIS: 265 nm

^{1}H NMR (600 MHz, Acetone-d₆): δ = 6.33 (s, 1H); 7.77 (m, 2H); 8.17 (t of t, *J* = 7.6, 1.5 Hz, 1H); 8.60 (d of d, *J* = 6.4, 1.5 Hz, 2H)

^{13}C NMR (600 MHz, Acetone-d₆): δ = 93.32; 126.44; 126.88; 140.02; 140.88; 151.52; 152.71; 174.95, 193.50

4.4.2.10 Synthesis of *fac*-[Re(8-Quin)(CO)₃(Br)][NEt₄]

ReAA (100 mg; 0.130 mmol) was dissolved in methanol (3 ml) and AgNO₃ (44 mg; 0.259 mmol) was added as a solid. The mixture was stirred at 70 °C for 24 hours and the precipitate, AgBr, was filtered off and weighed (48.70 mg). 8-Hydroxyquinoline (0.0188 g; 0.130 mmol) was added to the solution as a solid and the mixture was stirred at 70 °C for a further 24 hrs. The product precipitated out of the solution as a yellow solid (Yield = 0.0343 g; 94 %).

IR (KBr, cm^{-1}): v_{CO} = 2021, 1881

UV/VIS: 267 nm

^{1}H NMR (600 MHz, Methanol-d₄): δ = 1.31 (ddd, *J* = 7.3, 3.7, 1.9 Hz, 12H); 2.36 (q, *J* = 7.3 Hz, 8H); 7.06 (dd, *J* = 7.8, 0.6 Hz, 1H); 7.22 (dd, *J* = 18.6, 7.8 Hz, 1H); 7.57 − 7.45 (m, 3H), 7.61 (dd, *J* = 8.4, 4.8 Hz, 1H); 7.86 − 7.78 (m, 3H); 8.10 (ddd, *J* = 15.0, 5.1, 1.3 Hz, 1H); 8.52 (dd, *J* = 8.4, 1.2 Hz, 1H)

13C NMR (600 MHz, Methanol-d4): δ = 6.19 (NEt$_4$); 113.14; 121.81; 122.12; 129.23; 137.95; 148.12; 149.52; 149.63; 166.60; 195.63; 197.39; 197.47

4.4.2.11 Synthesis of *fac*-[Re(8-Quin)(CO)$_3$(OH$_2$)]

ReAA (500 mg; 0.648 mmol) was stirred in 10 ml of water at pH 2.2 for 20 minutes until dissolved. AgNO$_3$ (330 mg; 1.945 mmol) was added to the solution and stirred for 24 hours at room temperature. The precipitate, AgBr, was filtered off and weighed (365 mg). 8-hydroxyquinoline (0.0941 g; 0.648 mmol) was added to the filtrate and stirred for 36 hours at room temperature. The solution was yellow in color with a yellow precipitate. The product was filtered off, dried and weighed. (Yield = 0.240 g; 85 %)

IR (KBr, cm^{-1}): v_{CO} = 3062 (H$_2$O), 2024, 1883

UV/VIS: 265 nm

1H NMR (600 MHz, Acetone-d6): δ = 2.84 (s, 2H); 7.05 (d, *J* = 8.1 Hz, 1H); 7.21 − 7.15 (m, 1H); 8.14 (d of d, *J* = 12.7, 6.1 Hz, 1H); 8.51 (d, *J* = 8.4 Hz, 1H); 9.03 (d, *J* = 4.2 Hz, 1H); 9.10 (d, *J* = 4.0 Hz, 1H)

13C NMR (600 MHz, Acetone-d6): δ = 111.28; 122.08; 122.54; 128.82; 130.44; 138.57; 149.15; 152.05; 164.02, 198.5

4.4.2.12 Synthesis of *fac*-[Re(Eph)(CO)$_3$(Br)][NEt$_4$]

To ReAA (100 mg; 0.130 mmol) dissolved in methanol (3 ml), AgNO$_3$ (44 mg; 0.259 mmol) was added as a solid and the mixture was stirred at 70 °C for 24 hours. The precipitate, AgBr, was filtered off and weighed (48.70 mg). Ephedrine (0.0214 g; 0.130 mmol) was added to the solution as a solid and the mixture was stirred at 70 °C for a further 24 hrs. The product precipitated out as a white solid upon evaporation of the solvent (Yield = 0.0649 g; 78 %).

IR (KBr, cm^{-1}): v_{CO} = 2003, 1886

UV/VIS: 276 nm

1H NMR (600 MHz, Methanol-d4): δ = 1.07 (d, *J* = 6.8 Hz, 12H); 1.27 (s, 3H); 2.80 (s, 8H); 2.93 (s, 3H); 3.22 (q, *J* = 7.3 Hz, 1H); 4.52 (d, *J* = 11.6 Hz, 2H); 7.32 (t, *J* = 6.6 Hz, 3H); 7.42 (dt, *J* = 15.4, 7.6 Hz, 4H)

^{13}C NMR (600 MHz, Methanol-d_4): δ = 7.57 (NEt$_4$); 9.89; 31.56; 53.22; 53.24; 61.42; 70.93; 71.06; 71.75; 80.53; 126.95; 128.88; 129.50; 141.42; 200.57

4.4.2.13 Synthesis of *fac*-[Re(Eph)(CO)$_3$(OH$_2$)]

ReAA (100 mg; 0.130 mmol) was dissolved in 5 ml water (pH 2.2) and stirred for 30 min. To this solution, AgNO$_3$ (66 mg; 0.390 mmol) was added and stirred for 24 hours at room temperature. The precipitate (AgBr) was filtered off and weighed (220 mg). Ephedrine (0.0214 g; 0.130 mmol) was added to the filtrate and stirred for 48 hrs. A white precipitate formed which was dried and weighed. (Yield = 0.0536 g; 92 %)

IR (KBr, cm^{-1}): v_{CO} = 3596(H$_2$O), 2013, 1858

UV/VIS: 280 nm

^{1}H NMR (600 MHz, Methanol-d_4): δ = 1.27 (s, 3H); 2.74 (s, 3H); 3.49 (m, 1H); 4.60 (d, 1H); 7.31 (d; *J* = 6.8 Hz, 3H); 7.40 (m, 4H)

^{13}C NMR (600 MHz, Methanol-d_4): δ = 10.32; 29.37; 52.32; 63.78; 79.89; 113.99; 130.34; 134.93; 164.44; 184.01; 200.54; 201.34

4.4.3 Synthesis of technetium complexes

4.4.3.1 Synthesis of *fac*-[^{99m}Tc(Acac)(CO)$_3$(OH$_2$)]

Sodiumboranocarbonate (4.1 mg; 0.050 mmol), disodium tetraborate decahydrate (7.1 mg; 0.019 mmol), disodium tatrate dibasic dihydrate (7.3 mg; 0.032 mmol) and ^{99m}Technetium pertechnetate, 1 ml, (eluate from ^{99}Mo/^{99m}Tc generator) was added in a vial, flushed with N$_2$, and heated for 30 min at 85 $^{\circ}$C. In a separate vial flushed with N$_2$, acetylacetone (1 mg; 0.01 mmol) was added. *fac*-[^{99m}Tc(CO)$_3$(OH$_2$)]$^+$ (1 ml) was added to the ligand and heated for a further 30 min at 85 $^{\circ}$C. (Yield = 97 %)

4.4.3.2 Synthesis of *fac*-[^{99m}Tc(TFA)(CO)$_3$(OH$_2$)]

To N$_2$ flushed vial, sodium boranocarbonate (4.0 mg; 0.049 mmol), disodium tetraborate decahydrate (7.3 mg; 0.019 mmol), disodium tatrate dibasic dihydrate (7.2 mg; 0.031 mmol) and ^{99m}Technetium pertechnetate (eluate from ^{99}Mo/^{99m}Tc generator) was added and heated

for 30 min at 85 °C. In a separate N_2 flushed vial, containing trifluoroacetylacetone (1.54 mg; 0.01 mmol), *fac*-[^{99m}Tc(CO)$_3$(OH$_2$)]$^+$ (1 ml) was added and heated for a further 30 min at 85 °C, with a 93 % yield of the ligand coordinated complex.

4.4.3.3 Synthesis of *fac*-[^{99m}Tc(HFA)(CO)$_3$(OH$_2$)]

Sodiumboranocarbonate (4.2 mg; 0.051 mmol), disodium tetraborate decahydrate (7.2 mg; 0.019 mmol) and disodium tatrate dibasic dihydrate (7.1 mg; 0.031 mmol) was added to a flushed vial with N_2. 1 ml of ^{99m}Technetium pertechnetate (eluate from ^{99}Mo/^{99m}Tc generator) was then added to the vial and heated at 85 °C for 30 min. In an additional vial flushed with N_2, hexafluoroacetylacetone (2.07 mg; 0.01 mmol), *fac*-[^{99m}Tc(CO)$_3$(OH$_2$)]$^+$ (1 ml) was added and heated for 30 min at 85 °C, 98 % yield of the product was formed.

4.5 Results and discussion

This chapter reports 13 *fac*-[Re(CO)$_3$]$^+$ type and 3 *fac*-[Tc(CO)$_3$]$^+$ complexes. All the complexes in this study were prepared with relative ease and high yield was obtained. When the *fac*-[Re(L-L')(CO)$_3$Br]$^-$ complexes were prepared from the method described by Schutte[5], the ligand did not coordinate to the metal (in the preparation of *fac*-[Re(Acac)(CO)$_3$(Br)][NEt$_4$] and *fac*-[Re(TFA)(CO)$_3$(Br)][NEt$_4$]), thus yielding the starting material (ReAA). Two equivalents of the AgNO$_3$, as described by Kemp[6], were then added to strip the bromide ligands from the metal, replacing them with coordinated solvent (MeOH) ligands. Upon the addition of the ligands (Acac and TFA), the desired products were obtained.

During the synthesis of the *fac*-[Re(L,L'-Bid)(CO)$_3$(OH$_2$)] (L,L'-Bid = Acac, TFA, HFA, 8-Quin, EPH) complexes, particular care had to be taken to guarantee that the tri-aqua species are formed prior to addition of the bidentate ligands. The pH of the aqueous solutions were closely observed thus ensuring the protonated form of the bidentate ligands, especially that of EPH and 8-Quin. All the compounds containing an aqua coordinated ligand in the axial position were synthesized by the addition of three equivalents of AgNO$_3$. The AgBr precipitate obtained from

---

[5] Schutte, M.; *MSc. Dissertation*, University of The Free State, Bloemfontein, South-Africa, p 79, **2008**
[6] Kemp, G.; *Ph. D. Thesis*, University of Johannesburg, Johannesburg, South-Africa, p 56, **2006**

the addition of the silver salt was dried and weighed with every synthesis to ensure the replacement (with H_2O) of all three coordinated Br^- ligands. When Kemp[7] synthesized the *fac*-[Re(L-L')(CO)$_3$(OH$_2$)] complexes, he found that by stirring the solution (with added AgNO$_3$ in slight excess) for 24 hours at room temperature, all three bromide ligands are removed. When synthesizing the *fac*-[Re(L,L'-Bid)(CO)$_3$(OH$_2$)] complexes, it is vital to adjust the pH of the solution to 2.2, thus avoiding the formation of dimers (polymeric species).[8]

The *fac*-[Re(L-L')(CO)$_3$(Py)] (L,L'-Bid = Acac, TFA, HFA) complexes were very easily synthesized, this was done by the addition of one equivalent pyridine solution. The aqua in the axial position is replaced relatively quick, forming a precipitate (the product), almost immediately after pyridine addition.

The stretching frequencies of all the synthesized complexes are tabulated in Table 4.1, with similar complexes prepared by Kemp[7], Schutte[8], Brasey[9] *et al* and Mundwiler[10] *et al*. Infrared spectroscopy is not an effective tool when solely utilized for characterization; however this is a useful tool to get an indication of the density that the metal centre experience. One needs to keep in mind that the bending stretching frequencies require much less energy than the corresponding stretching frequencies. The symmetric stretching of the CO bond is found at a lower frequency than the asymmetric CO stretching frequency, because it requires more energy.

The two step reaction procedure for the synthesis of *fac*-[^{99m}Tc(CO)$_3$(H$_2$O)$_3$]$^+$ and *fac*-[^{99m}Tc(O,O')(CO)$_3$(H$_2$O)$_3$] (O,O'-donor Bid = Acac, TFA and HFA) was relatively easy. The reference front (R$_f$) values of the different compounds were determined, in order to establish the formation of a new product. R$_f$ values give an indication of the polarity of a substance or compound, with respect to a certain solvent. The formation of the *fac*-[^{99m}Tc(CO)$_3$(H$_2$O)$_3$]$^+$ (R$_f$ = 0.310) synthon, the *fac*-[^{99m}Tc(O,O')(CO)$_3$(H$_2$O)$_3$] complexes and the presence of the non-bonded [^{99m}TcO$_4$]$^-$ (R$_f$ = 0.304) was established using reverse phase TLC, see Figure 4.2. A line extrapolated through the TLC graphs; give an indication of the difference in the R$_f$ values of the synthesized compounds. The R$_f$ values of the synthesized complexes are 0.227 (*fac*-[^{99m}Tc(Acac)(CO)$_3$(H$_2$O)]), 0.392 (*fac*-[^{99m}Tc(TFA)(CO)$_3$(H$_2$O)]) and 0.537

[7] Kemp, G.; *Ph. D. Thesis*, University of Johannesburg, Johannesburg, South-Africa, p 59, **2006**
[8] Helm, L.; *Coord. Chem. Rev.*, doi:10.1016/j.ccr.2008.01.009, **2008**

(*fac*-[^{99m}Tc(HFA)(CO)$_3$(H$_2$O)]).   The   *fac*-[^{99m}Tc(CO)$_3$(H$_2$O)$_3$]$^+$ synthon   and   the *fac*-[^{99m}Tc(O,O')(CO)$_3$(H$_2$O)] complexes forms relatively quick (after 30 min of heating).
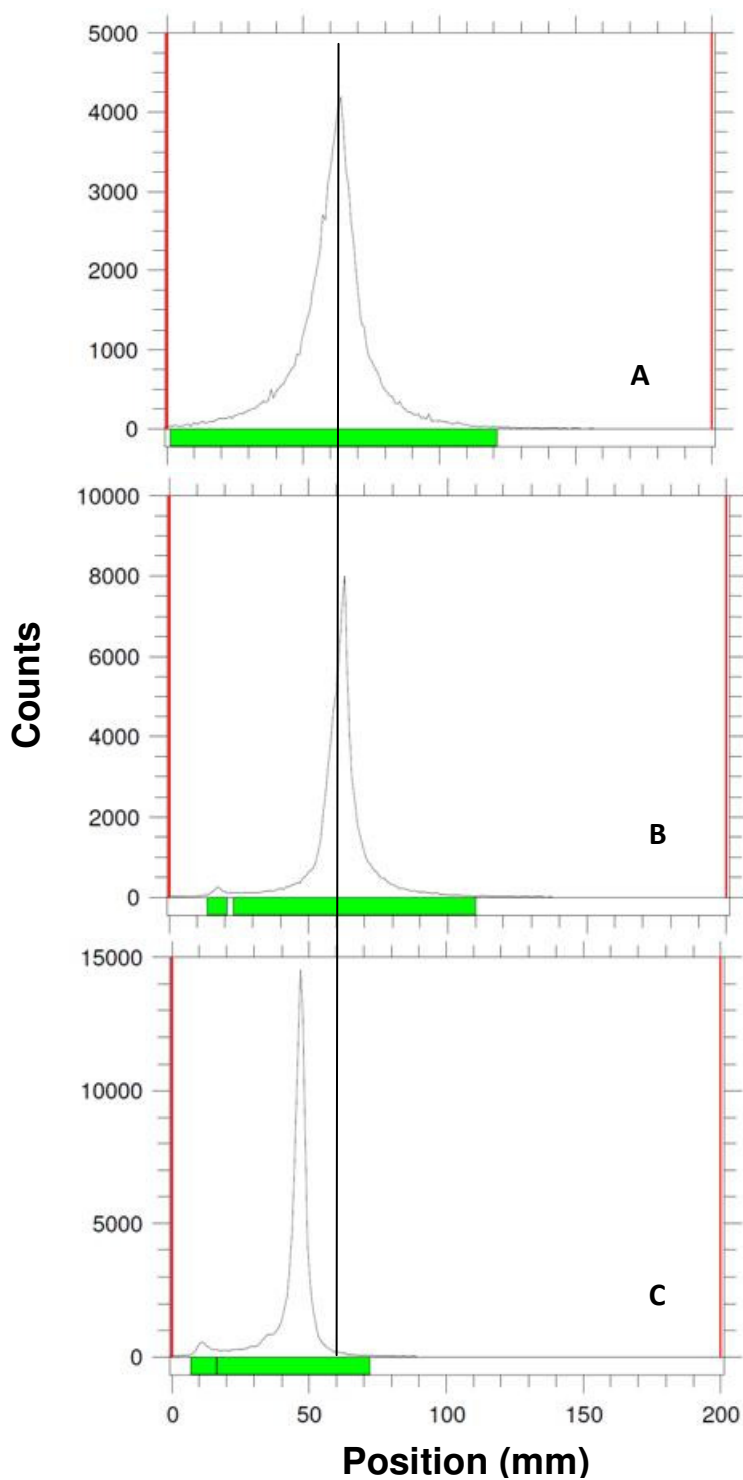
Figure 4.2: An illustration of the TLC results on reverse phase C-18 plates, showing the non-bonded (A) ^{99m}TcO$_4^-$, the **(B) [^{99m}Tc(CO)$_3$(H$_2$O)$_3$]$^+$ and the (C) [^{99m}Tc(CO)$_3$(Acac)(OH$_2$)] complex, with different R$_f$ values (MP = 0.1 % trifluoroacetic acid).**

Since different R_f values were obtained with respect to each compound, it is safe to conclude that the polarity for each complex increases as follows: *fac*-[^{99m}Tc(Acac)(CO)$_3$(H$_2$O)], > *fac*-[^{99m}Tc(TFA)(CO)$_3$(H$_2$O)] > *fac*-[^{99m}Tc(HFA)(CO)$_3$(H$_2$O)]. If normal phase silica TLC plates were used, the results would have been inverted. The electron withdrawing fluorine atoms present in the solvent structure (0.1 % trifluoroacetic acid), makes it highly polar, thus more polar compounds (on reversed C-18 TLC plates) will have higher R_f values. The reaction, involving the addition of the ligands, is highly pH dependant, therefore care should be taken to ensure a pH = 4, prior to the addition of the ligand. TLC is a relatively good analytical tool to establish the formation of a new product; however, the use of high performance liquid chromatography (HPLC) would have been a more accurate method. The desired products formed in yields above 90 %, with the presence of the starting synthons under 3 %.

Observations of v_{CO} in synthesized *fac*-[Re(O,O')(CO)$_3$X]^n compounds:

➢ In the *fac*-[Re(O,O')(CO)$_3$X]$^{n-1}$ compounds (O,O' = Acac, TFA, HFA and X = H$_2$O, Br$^-$, Py), the carbonyl stretching frequencies are highly influenced by the electron withdrawing fluoride atoms on the bidentate ligands (TFA and HFA) decreasing the electron density on the metal centre and the π-bonding from the CO ligands, thus increasing the v_{CO}. The *fac*-[Re(Acac)(CO)$_3$Br][NEt$_4$] complex has a much lower v_{CO}, indicating that it is a better electron donor than its fluoride containing counterparts.

➢ The neutral compounds *fac*-[Re(O,O')(CO)$_3$X], X = Py and H$_2$O, follow the same trend with the increase in fluoride ions on the ligand back bone i.e. increase in the v_{CO}, with increase in electron withdrawing fluoride atoms.

➢ When comparing the v_{CO} of the *fac*-[Re(Acac)(CO)$_3$X] compounds containing the neutal ligands (X = H$_2$O and Py) in the axial position an increase is observed, due to the electron withdrawing abilities of the monodentate ligands.

➢ The v_{CO} of the *fac*-[Re(Acac)(CO)$_3$Py] and the *fac*-[Re(Acac)(CO)$_3$Br] compounds synthesized in this study are comparable with that reported by Benny *et al.*[9] and Brink *et al.*[10]

[9] Benny, P.D.; Fugate, G. A.; Barden, A. O.; Morley, J. E.; Silva-Lopez, E.; Twamley, B.; *Inorg. Chem.*, 47, 2240, **2007**

Table 4.1: Carbonyl stretching frequencies of *fac*-[Re(L,L'-Bid)(CO)₃(X)]ⁿ complexes, with L,L'-Bid = O,O' and N,O bidentate ligands and X = Br⁻, H₂O and pyridine.

Complex	Carbonyl stretching frequencies $v_{(CO)}$ (cm⁻¹)			Reference
[Et₄N]₂[Re(CO)₃Br]	1999	1902	1859	
O-O' Bidentate Ligands with a coordinated bromide ion in the axial position				
[Re(Acac)(CO)₃Br][NEt₄]	2006		1868	a
[Re(TFA)(CO)₃Br][NEt₄]	2012		1872	a
[Re(HFA)(CO)₃Br] [NEt₄]	2018	1903		a
[Re(TropBr₃)(CO)₃Br][NEt₄]	2008	1900	1876	c
[Re(Flav)(CO)₃Br][NEt₄]	1999		1863	c
[Re(C₇H₄N₃O₂)(CO)₃(Br)]⁻	2007		1855	d
O-O' Bidentate Ligands with a coordinated water molecule in the axial position				
[Re(Acac)(CO)₃(OH₂)]	2015	1907	1879	a
[Re(TFA)(CO)₃(OH₂)]	2018	1895	1878	a
[Re(HFA)(CO)₃(OH₂)]	2025	1917	1888	a
[Re(TropBr₃)(CO)₃(OH₂)]	2024		1886	c
[Re(Flav)(CO)₃(OH₂)]	2013		1885	c
[Re(C₇H₄N₃O₂)(CO)₃(OH₂)]	2026	1882		d
O-O' Bidentate Ligands with a coordinated pyridine molecule in the axial position				
[Re(Acac)(CO)₃(Py)]	2017	1906		a
[Re(TFA)(CO)₃(Py)]	2030	1930	1888	a
[Re(HFA)(CO)₃(Py)]	2036	1939	1873	a
[Re(TropBr₃)(CO)₃(Py)]	2015	1904	1869	c
[Re(Flav)(CO)₃(Py)]	2012	1897	1860	c
N-O Bidentate Ligands with a coordinated bromide ion in the axial position				
[Re(8-Hydroxy-q)(CO)₃Br][NEt₄]	2021		1882	a
[Re(Eph)(CO)₃(OH₂)Br][NEt₄]	2003		1886	a
[Re(2,4-PicoH)(CO)₃Br][NEt₄]	2021		1893	c
[Re(2,4-QuinH)(CO)₃Br][NEt₄]	2020	1904	1870	c
N-O Bidentate Ligands with a coordinated water molecule in the axial position				
[Re(8-Hydroxy-q)(CO)₃(OH₂)]	2024		1883	a
[Re(Eph)(CO)₃(OH₂)]	2013		1858	a
[Re(Pico)(CO)₃(OH₂)]	2022	1908	1874	b
[Re(Quin)(CO)₃(OH₂)]	2018	1920	1880	b
[Re(2,4-PicoH)(CO)₃(OH₂)]	2035	1919		c
[Re(2,4-QuinH)(CO)₃(OH₂)]	2034	1936	1886	c
[Re(Imc)(CO)₃(OH₂)]	2039	1936		e

[a] This study, [b] Synthesized by G. Kemp[11], [c] Synthesized by M. Schutte[12], [d] Synthesized by Brasey *et al*.[13], [e] Synthesized by Mundwiler *et al*[14].

[(**TropBr₃**) = tribromotropolonato; (**Flav**) = anion of 3-hydroxyflavone;
(**Pico**) = 2-pyridinecarboxylato; (**2,4-PicoH**) = 2,4-pyridinedicarboxylato;
(**Imc**) = 4-imidazole carboxylato; (**C₇H₄N₃O₂**) = enolate of 1,2 3-benzotriazine-4(*3H*)-one;
(**Quin**) = 2-quinolinecarboxylato; (**2,4-QuinH**) = 2,4-quinolinedicarboxylato]

[10] Brink, A.; Visser, H. G.; Roodt, A.; *Acta Cryst*., E67, m34-m35, **2011**

[11] Kemp, G.; *Ph. D. Thesis*, University of Johannesburg, Johannesburg, South-Africa, **2006**

[12] Schutte, M.; *MSc. Dissertation*, University of The Free State, Bloemfontein, South-Africa, **2008**

[13] Brasey, T.; Buryak, A.; Severin, K.; *Eur. J. Inorg. Chem*., 964, **2004**

[14] Mundwiler, S.; Kündig, M.; Ortner, K.; Alberto, R.; *Dalton Trans*., 1320, **2004**

4.5 Conclusion

One can conclude that the v_{CO} stretching frequencies are highly influenced by the nucleophilic monodentate ligands in the axial positions. The more nucleophilic the monodentate ligand on the axial position in the *fac*-[Re(O,O')(CO)$_3$X]^n compounds is, the lower the C=O stretching frequencies will be and the reverse is also true for less nucleophilic ligands. The electron donating abilities of the coordinated monodentate ligands used in this study is as follows: Br$^-$ > Py (pK$_a$ = 7.2) > H$_2$O. This is apparent in the v_{CO} of the synthesized compounds.

An increase in the density on the metal centre causes an increase in the electron back-donation from the metal to the anti-bonding orbital on the carbon atom. This results in the strengthening of the Re-CO bond and a weakening in the C=O bond, causing a decrease in the carbonyl stretching frequency (v_{CO}).

NMR (^{1}H and ^{13}C) spectroscopy confirms the products obtained are the intended ones. The UV/VIS results are comparable with that found by Benny *et al.*[7] Most of the compounds synthesized are stable in air for a few weeks, except for the *fac*-[Re(O,O')(CO)$_3$H$_2$O] complexes. Storage under a nitrogen atmosphere guarantees stability for months.

The formation of the ^{99m}Tc compounds are easily established using TLC; however a more accurate method to use would be HPLC. Scientist assume that the chemical behavior of rhenium and technetium would be similar, a comparison can be done, whereby the *fac*-[Re(L,L'-Bid)(CO)$_3$X]$^{n-1}$ complex and its analogous ^{99m}Tc complex can be co-injected into the HPLC, to compare their retention times. One would expect the analogous compounds of technetium and rhenium to have the same retention times and this would be a method of establishing if this assumption is true.

ooOoo

5 CRYSTALLOGRAPHY STUDY OF RHENIUM COMPLEXES

_____

5.1 Introduction

Over the years, many crystal structures of the rhenium(I) tricarbonyl complexes has been reported. M. Schutte published two rhenium(I)[1,2] complexes during the 2008/2009 period and reported that in 2008, only four rhenium(I) complexes, containing O,O' donor bidentate ligands has been published. Since then nine complexes[1,2,3,4,5,6,7,8,9,10] of the form fac-[Re(O-O')(CO)$_3$X], (O-O' = bidentate ligands and X being halides, monodentate ligands etc.) has been reported. In this chapter, two new crystal structures of the form, fac-[Re(O-O')(CO)$_3$X], is introduced. The crystallographic data of both the neutral complexes, fac-[Re(TFA)(CO)$_3$Py] and fac-[Re(HFA)(CO)$_3$Py] are listed in Table 5.1.[11] A schematic representation of the synthetic procedure, in the preparation of these complexes is illustrated in (Figure 5.1).

[1] Schutte, M.; Visser, H.G.; Steyl, G.; *Acta Cryst*., E63, m3195, **2007**

[2] Schutte, M.; Visser, H.G.; Roodt, A.; *Acta Cryst*., E64, m1610-m1611, **2008**

[3] Bochkova, R.I.; Zakharov, L.N.; Patrikeeva, N.V.; Shal'nova, K.G.; Abakumov, G.A.; Cherkasov, V.K.; *Koord. Khim. (Russ.)(Coord. Chem.)*, 13, 702, **1987**

[4] Cheng, C.P.; Wang, S.R.; Lin, J.C.; Wang, S.L.; *J. Organomet. Chem*., 349, 375, **1988**

[5] Gibson, D.H.; Ding, Y.; Miller, R.L.; Sleadd, B.A.; Mashuta, M.S.; Richardson, J.F.; *Polyhedron*, 18, 1189, **1999**

[6] Brasey, T.; Buryak, A.; Scopelliti, R.; Severin, K.; *Eur. J. Inorg. Chem*., 964, **2004**

[7] Benny, P. D.; Fugate, G. A.; Barden, A. O.; Morley, J. E.; Silva-Lopez, E.; Twamley, B.; *Inorg. Chem*., 47, 2240, **2007**

[8] Schutte, M.; Visser, H.G.; Roodt, A.; *Acta Cryst*., E66, m859-m860, **2010**

[9] Sagnou, M.; Tsoukalas, C.; Triantis, C.; Raptopoulou, C. P.; Terzis, I. P.; Pirmettis, I.; Pelecanou, M.; Papadopoulos, M.; *Inorg. Chim. Acta*, 363, 1649-1653, **2010**

[10] Brink, A.; Visser, H. G.; Roodt, A.; *Acta Cryst*., E67, m34-m35, **2011**

[11] Visser, H.G.; Roodt, A.; Volmink, A.; Kemp, G.; *Acta Cryst*., E67, m1631, **2011**
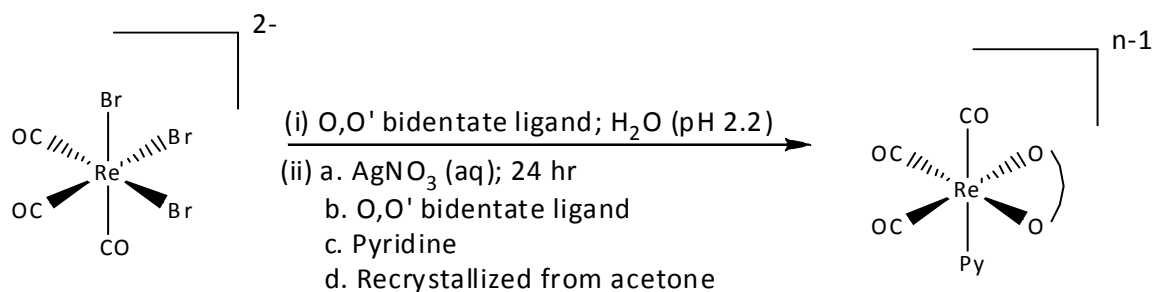
(i) Trifluoro acetylacetonate; n = 1
(ii) Hexafluoro acetylacetonate: n = 1

Figure 5.1: A schematic representation of the synthetic procedure.

5.2 Experimental

The intensity data for the structure determinations were collected on a Bruker X8 Apex II 4K diffractometer, using graphite monochromated Mo-Kα radiation (with wavelength λ = 0.71073 Å) and with ω- and φ-scans at a temperature of 100 K. All cell refinements were done using SAINT-Plus[12] and data reduction with SAINT-Plus and XPREP[2]. To correct the absorption effects, the multi-scan technique and software package SADABS[13] was used. Both the crystal structures were solved by direct method package SIR-97[14] and refined with the aid of WinGX[15], integrating SHELXL-97.[16] All the graphical representation of the crystal structures were obtained with the program DIAMOND[17]. Unless it is stated otherwise, all structures are shown with thermal ellipsoid drawn at 50% probability level. All non-hydrogen atoms were refined anisotropically, while the methyl and aromatic hydrogen atoms were placed in geometrically idealized positions (C-H = 0.95 – 0.98 Å) and constrained to ride on their parent atoms (Uiso(H) = 1.5Ueq(C) and 1.2Ueq(C)). A summary of the general crystal data and refinement parameters are given in Table 5.1 for both the rhenium(I) complexes.

---

[12] Bruker; *SAINT-Plus*, Version 7.12 (including XPREP), Bruker AXS Inc., Madison, Wisconsin, USA, **2004**

[13] Bruker; *SADABS*, Version 2004/1, Bruker AXS Inc., Madison, Wisconsin, USA, **1998**

[14] Altomare, A.; Burla, M.C.; Camalli, M.; Cascarano, G.L.; Giacovazzo, C.; Guagliardi, A.; Moliterni, A.G.G.; Polidori, G.; Spagna, R.; J. *Appl. Cryst.*, 32, 837, **1999**

[15] Farrugia, L.J.; *J. Appl. Cryst.*, 32, 837, **1999**

[16] Sheldrick, G.M.; *SHELXL97*, *Program for the refinement of crystal structures*, University of Göttingen, Germany, **1997**

[17] Brandenburg, K.; Putz, H.; *DIAMOND*, Release 3.0e, *Crystal Impact GbR*, Bonn, Germany, **2006**

Table 5.1: X-ray crystallographic data of *fac*-[Re(TFA)(CO)$_3$Py][2] **and** *fac*-[Re(HFA)(CO)$_3$Py].

Crystallographic data	*fac*-[Re(TFA)(CO)$_3$Py]	*fac*-[Re(HFA)(CO$_3$)Py]
Empirical formula	C$_{13}$H$_9$F$_3$NO$_5$Re	C$_{13}$H$_9$F$_6$NO$_5$Re
Formula weight (g.mol^{-1})	502.41	559.99
Temperature (K)	293 (2)	293 (2)
Crystal system	Monoclinic	Monoclinic
Space group	$P2_1/c$	$P2_1/c$
a (Å)	15.561(5)	15.897 (5)
b (Å)	6.982 (5)	6.857 (5)
c (Å)	14.082 (5)	14.725 (5)
α (°)	90.000 (5)	90.000 (5)
β (°)	103.27 (5)	99.369 (5)
γ (°)	90.000 (5)	90.000 (5)
Volume(Å^3)	1 489.11 (9)	1 583.70 (14)
Z	4	4
ρ_{calc} (g.cm^{-3})	2.241 g.cm^{-3}	2.346 g.cm^{-3}
Crystal color	Yellow	Yellow
Crystal morphology	Cuboid	Needles
Crystal size (mm^3)	0.15 X 0.10 X 0.03	0.36 X 0.03 X 0.02
μ (mm^{-1})	8.22	7.77
F(000)	944	1 052
θ range (˚)	2.69 – 28.00	2.60 – 28.35
Index ranges	- 20 ≤ h ≤ 20	- 21 ≤ h ≤ 19
	- 9 ≤ k ≤ 9	- 9 ≤ k ≤ 7
	- 18 ≤ l ≤ 16	- 12 ≤ l ≤ 19
Reflections collected	17 351	21 329
Unique reflections	3 603	3 948
Reflections with I > 2σ(I)	3 104	3 492
R_{int}	0.0397	0.0328
Completeness to theta (%)	100	99.80
Data/ restraints/ parameters	3 603/0/209	3 948/0/235
GooF	1.059	1.043
R[I > 2σ(I)]	R_1 = 0.0251	R_1 = 0.0190
	wR_2 = 0.0565	wR_2 = 0.0367
R (all data)	R_1 = 0.0323	R_1 = 0.0245
	wR_2 = 0.0593	wR_2 = 0.0387
ρ_{min} and ρ_{max} (e. Å^{-3})	1.427 and -1.088	1.075 and -0.800

5.3 Crystal structure of *fac*-[Re(TFA)(CO)₃(Py)]

5.3.1 Introduction

fac-[Re(TFA)(CO)₃(Py)], **(1)**, was prepared according to the procedure reported in Paragraph 4.3.2.6. Yellow crystals (0.15 X 0.10 X 0.03 mm^3) suitable for X-ray diffraction were obtained. A tabulated summary of the general crystal data is specified in Table 5.1. The molecular structure of **(1)** is represented in Figure 5.2 along with the atom numbering.
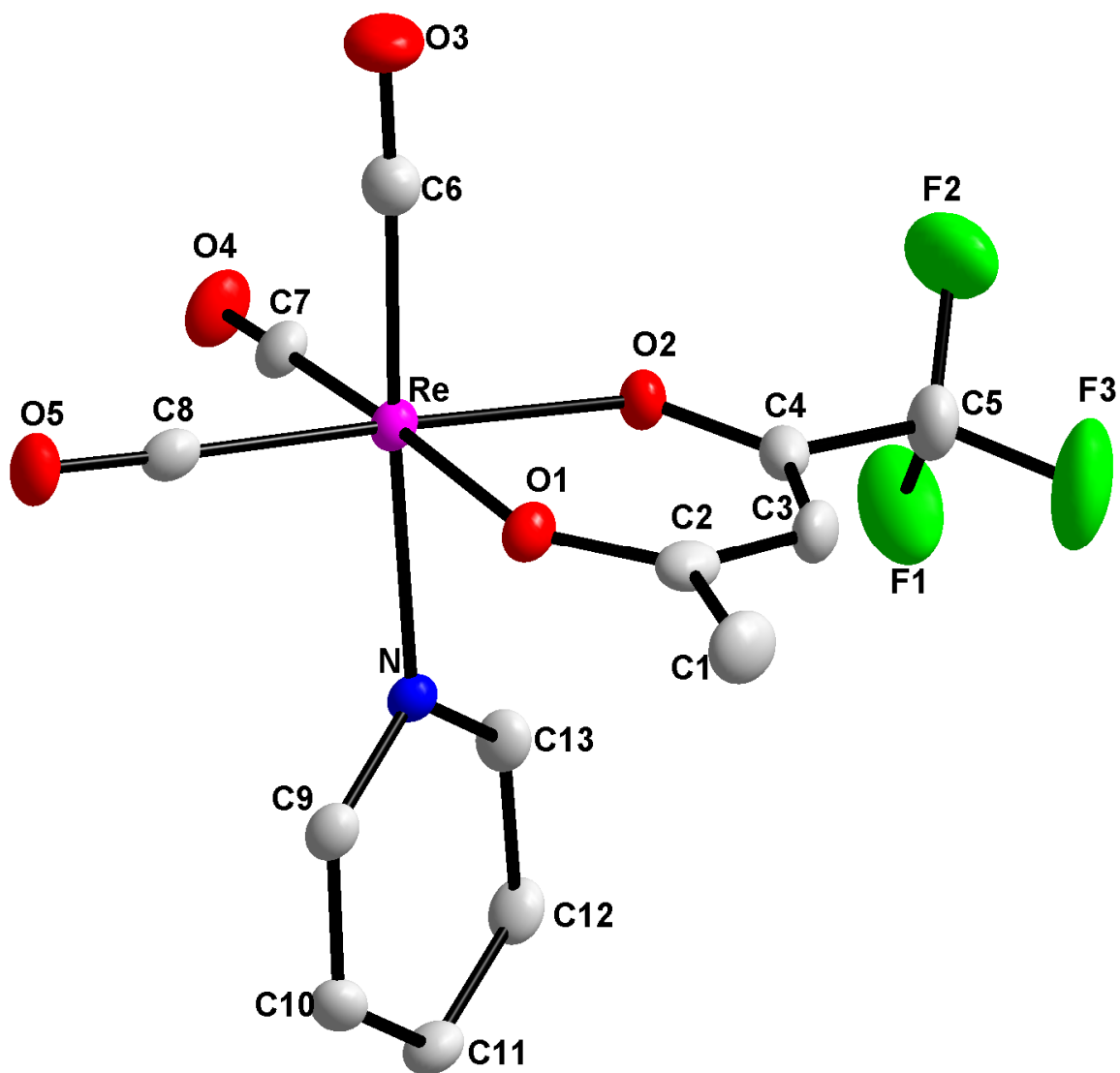
Figure 5.2: The molecular structure of *fac*-[Re(TFA)(CO)₃(Py)] showing the atom numbering system. H atoms have been omitted for clarity.

The packing fashion in the unit cell can be seen in Figure 5.3 and the positional and thermal parameters are given in Table A.1 of the Appendix. A summary of selected bond lengths and bond angles are given in Table 5.2 and Table 5.3 respectively.
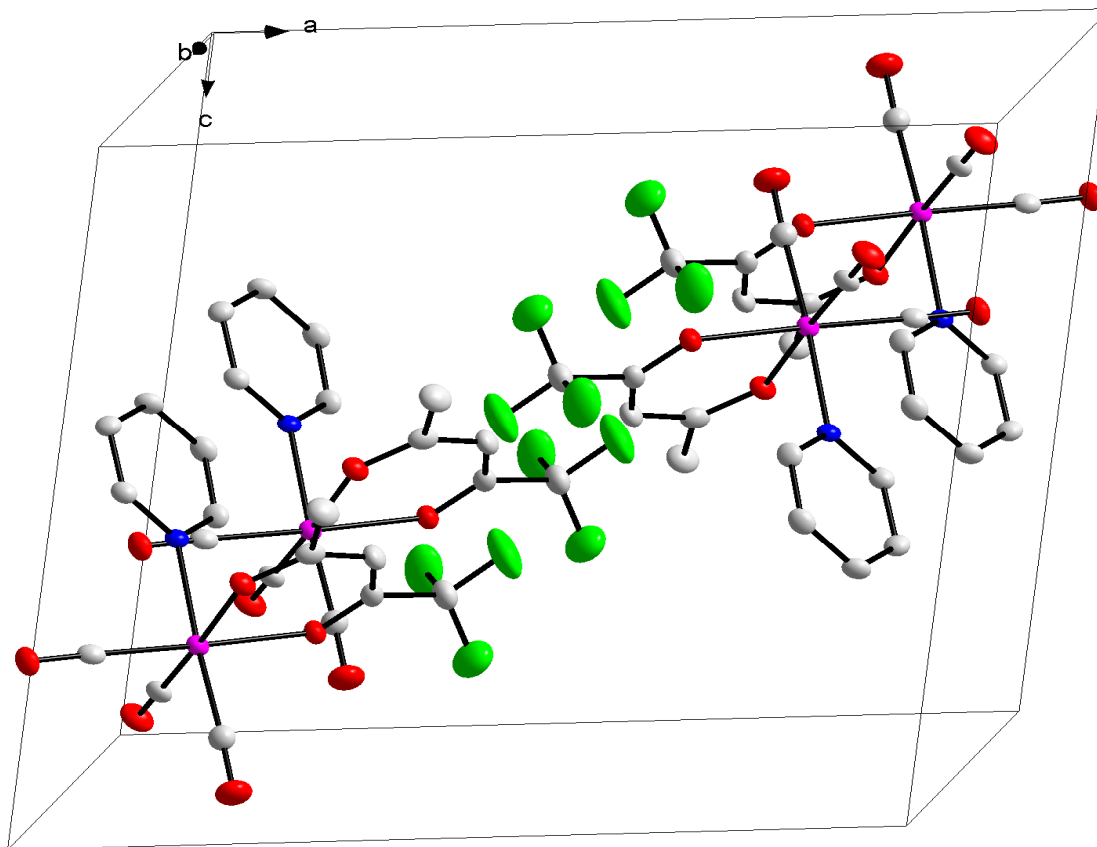
Figure 5.3: An illustration of the molecular packing in the unit cell. H atoms have been omitted for clarity.

Table 5.2: A selection of bond lenghts of *fac*-[Re(TFA)(CO)₃Py].

Selected bond distances (Å)			
Re-O1	2.135(3)	C5-F2	1.353(6)
Re-O2	2.117(3)	C5-F3	1.317(5)
Re-C6	1.932(5)	C4-C5	1.514(6)
Re-C7	1.906(4)	C1-C2	1.513(6)
Re-C8	1.906(4)	C3-C4	1.369(6)
Re-N	2.202(3)	C2-C3	1.409(6)
C4-O2	1.269(5)	N-C9	1.347(5)
C5-F1	1.298(6)	N-C13	1.360(5)

Table 5.3: Selection of bond angles of *fac*-[Re(TFA)(CO)₃Py].

Selected bond angles (°)			
O1-Re-O2	84.99(11)	**O1-Re-N**	82.72(11)
C7-Re-O2	92.70(14)	**O2-Re-N**	83.67(12)
C8-Re-O1	94.59(14)	**C4-O2-Re**	126.7(3)
C7-Re-C8	87.55(17)	**C2-O1-Re**	129.3(3)
C6-Re-C8	87.88(18)	**C7-Re-N**	91.68(15)
C6-Re-C7	90.32(18)	**C8-Re-N**	94.55(15)
C6-Re-O1	95.20(15)	**O2-C4-C3**	129.2(4)
C6-Re-O2	93.89(15)	**O1-C2-C3**	125.0(4)
C2-C3-C4	124.6(4)	**O2-C4-C5**	129.2(4)
C9-N-Re	121.9(3)	**O1-C2-C1**	125.0(4)

5.3.2 Results and discussion

Complex **(1)** consists of a Re (I) metal centre, which is bonded to three facial carbonyl ligands, a trifluoroacetylacetone bidentate ligand in the equatorial plane (the plane containing the bidentate ligand and the two CO molecules) and a pyridine ligand in the axial position. The Re (I) molecules are diagonally packed in a head-to-head manner, along the *ab* plane (see Figure 5.3).
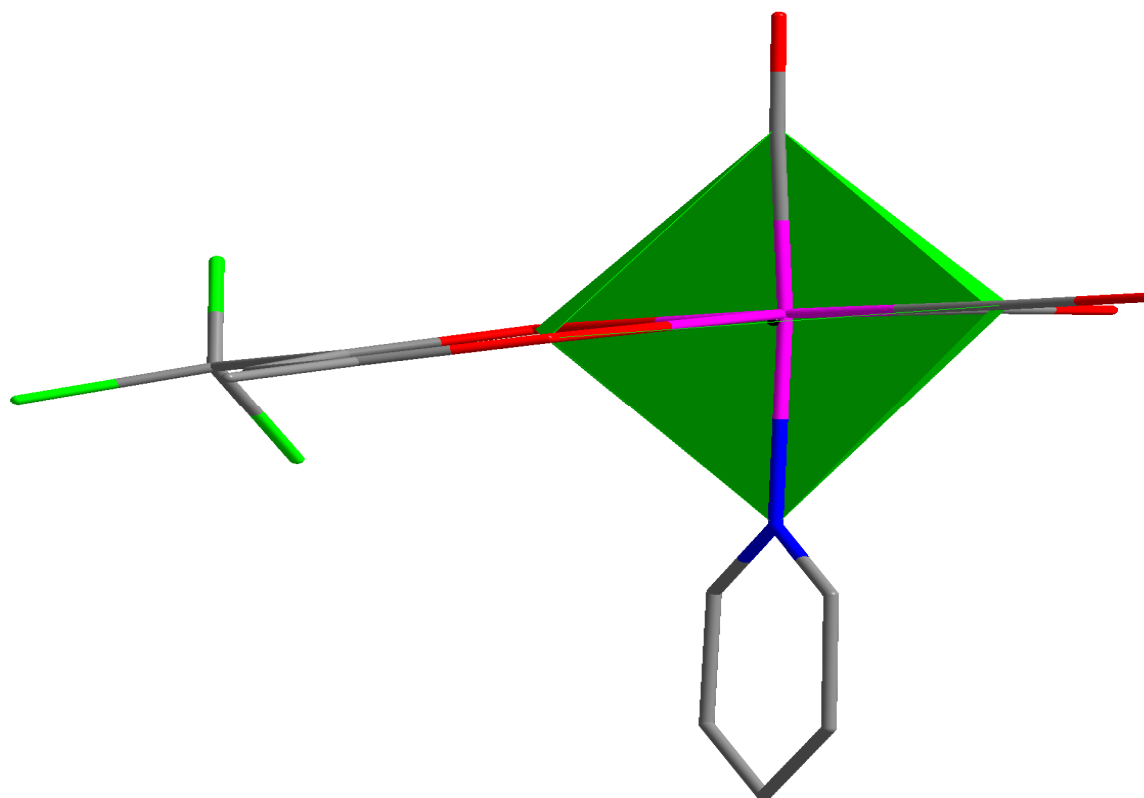
Figure 5.4: An illustration of the distortion in the octahedral complex.

This distorted octahedral (see Figure 5.4) complex crystallizes in the monoclinic space group, P2$_1$/*c*. This distortion can be seen in the slight deviations from 90 ° in the bond angles of O1-Re-N (82.72(11) °) and O2-Re-N (83.67(12) °); they are also the furthest outliers. The Re-N bond distance of 2.202(3) Å is in the range for bonds of this type.[7]

An interesting observation is that the electron withdrawing fluorine molecules (on C5) on the ligand backbone, does not significantly influence the bond distances in the molecule (especially the distance of the CO molecules *trans* to C5), when compared to that of the acetylacetone (Acac) ligand in this position. This insignificance is also seen when comparing the bond lengths of C4-C5 (1.514(6) Å) and C1-C2 (1.513(6) Å), which does not indicate a considerable difference. The C2-C3-C4 angle in the coordinated trifluoroacetylacetone ligand is 124.6(4) °, which deviates significantly from the expected angle of 120 °. In Figure 5.5, it is clear that O2 on the bidentate ligand, is out of the horizontal plane constructed through the atoms situated in the equatorial positions.
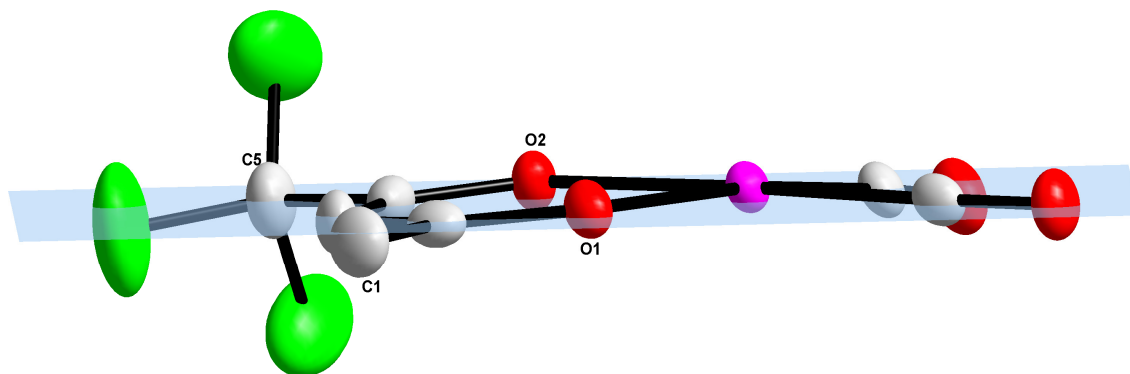
Figure 5.5: Selected part of the complex, illustrating the out-of-plane O2 and C1 atoms and the in-plane C5 atom.

The complex has comparable Re-CO bonds, the Re-C6 distance is (1.932(5) Å), the Re-C7 and Re-C8 distances are similar, (1.906(4) Å) and all these bond distances are considered normal. The Re-O1 and Re-O2 distances of 2.117(3) Å and 2.135(3) Å respectively compares well with similar structures and the trifluoroacetylacetone ligand show a minimally constrained bite angle (O1-Re-O2; 84.99(11) °). Re-O2 is slightly longer, due to the electron withdrawing properties of the fluorine molecules on C5, elongating this bond distance.

Intermolecular C-H…F hydrogen bonding is observed in the complex. This serves as a form of stabilization in the crystal. Figure 5.6 gives an illustration of the hydrogen contacts and the contact distances and angles are given in Table 5.4.
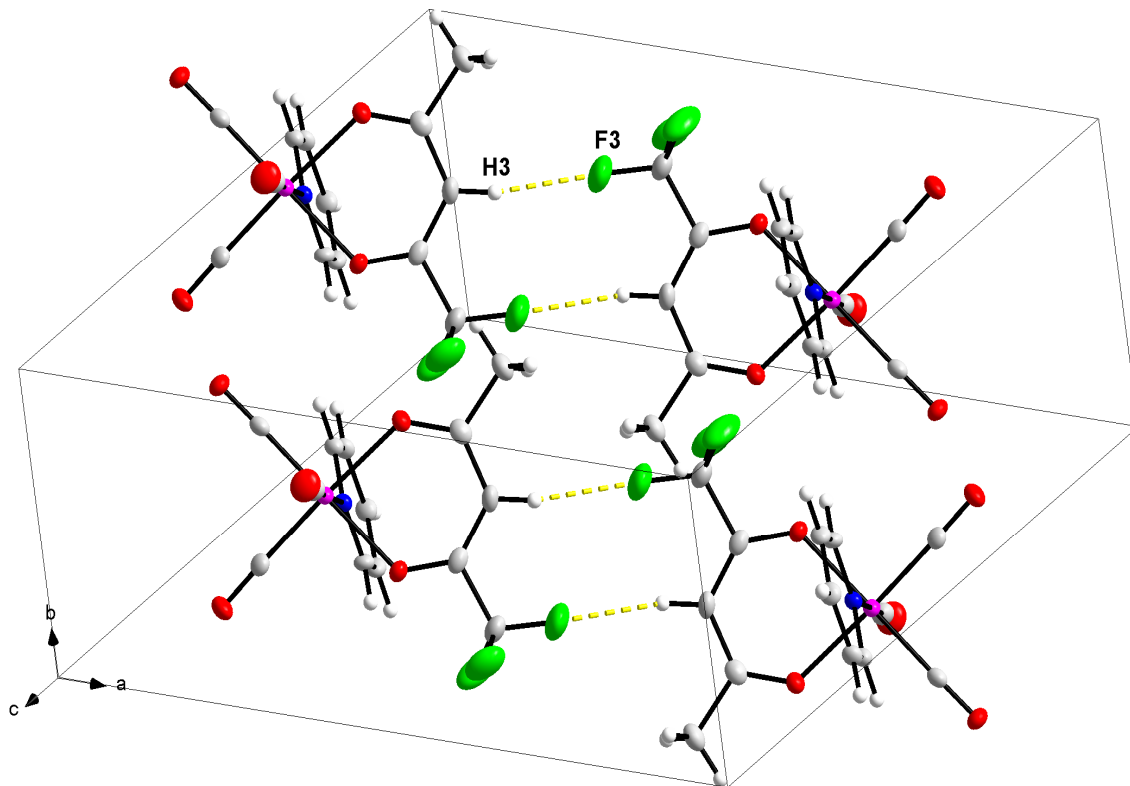
Figure 5.6: Intermolecular C-H…F interactions in *fac*-[Re(TFA)(CO)$_3$(Py)].

The diagonal packing of layers in the structure is further stabilized by C-H…O intermolecular interactions, which are illustrated in Figure 5.6. The contact distances and angles are given in Table 5.4.
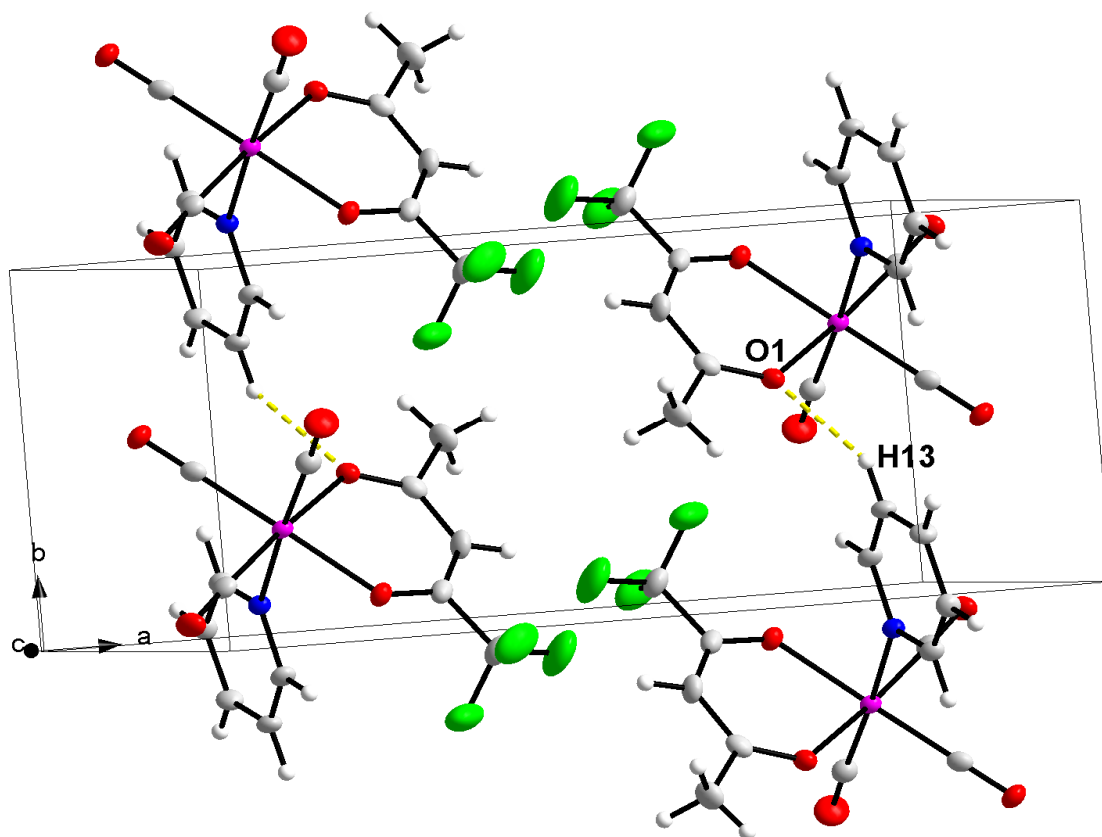
Figure 5.7: Intermolecular C-H...O interactions in *fac*-[Re(TFA)(CO)₃(Py)].

Table 5.4: Hydrogen bond geometry and distances in *fac*-[Re(TFA)(CO)₃(Py)] (Å, °).

D-H...A	d (D-H)	d (H...A)	d (D...A)	D-H...A Angle
C3-H3...F3[a]	0.93	2.55	3.407(6)	153
C13-H13...O1[b]	0.93	2.58	3.360(5)	142

Symmetry codes: (a) −*x* + 1, -*y* + 1, -*z*; (b) *x*, *y* + 1, *z*.

5.4 Crystal structure of *fac*-[Re(HFA)(CO)₃(Py)]

5.4.1 Introduction

Yellow needle-like crystals (0.36 X 0.03 X 0.02 mm^3) of the title compound were synthesized as described in Paragraph 4.3.2.9. The *fac*-[Re(HFA)(CO)₃(Py)], **(2)**, complex crystallized in a monoclinic space group with four molecules per unit cell. The structure and numbering scheme of **(2)** is illustrated in Figure 5.7, while a selection of important bond distances and angles are reported in Table 5.5 and Table 5.6 respectively.
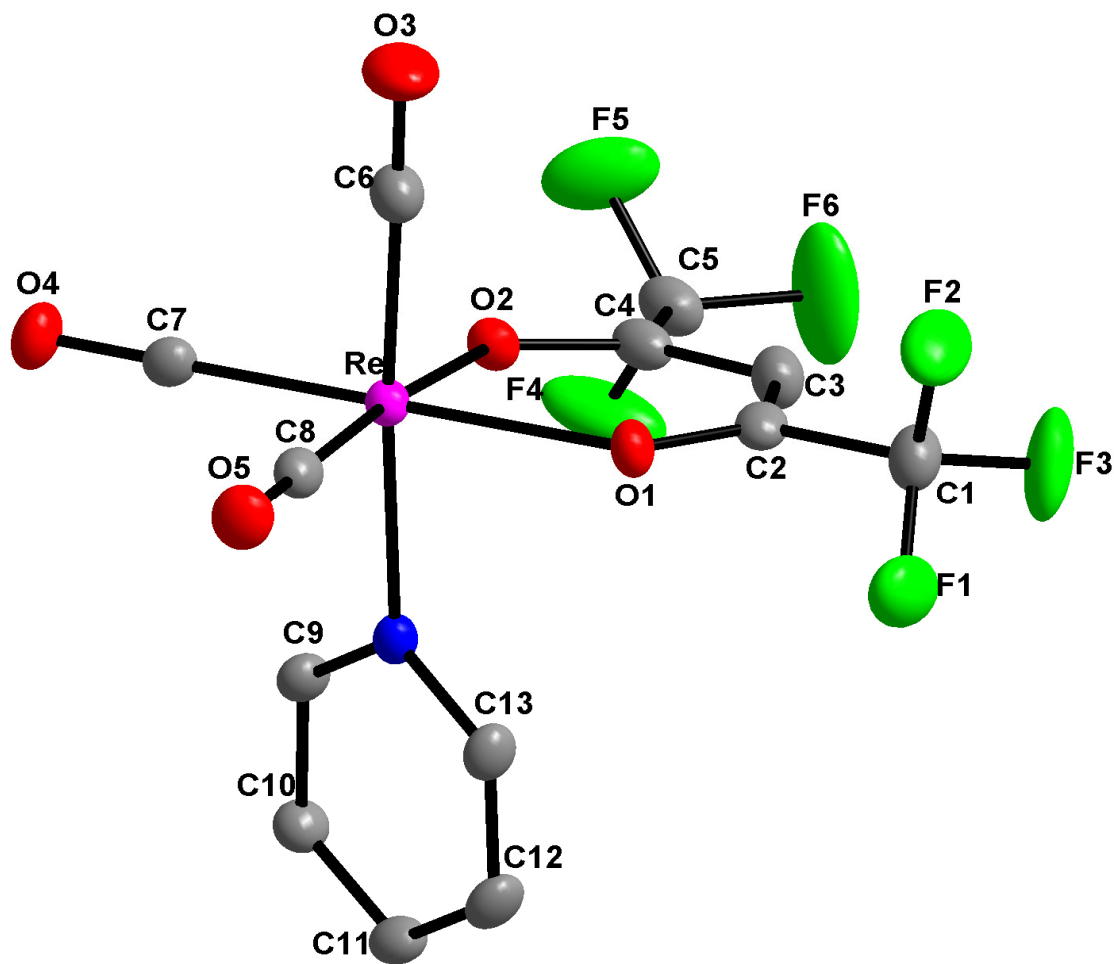
Figure 5.8: Illustration of the molecular structure of *fac*-[Re(HFA)(CO)₃(Py)] showing the atom numbering scheme. H atoms have been omitted for clarity.

The packing of molecules in the unit cell is illustrated in Figure 5.8 and the positional and thermal parameters are given in Table B.1 of the Appendix.
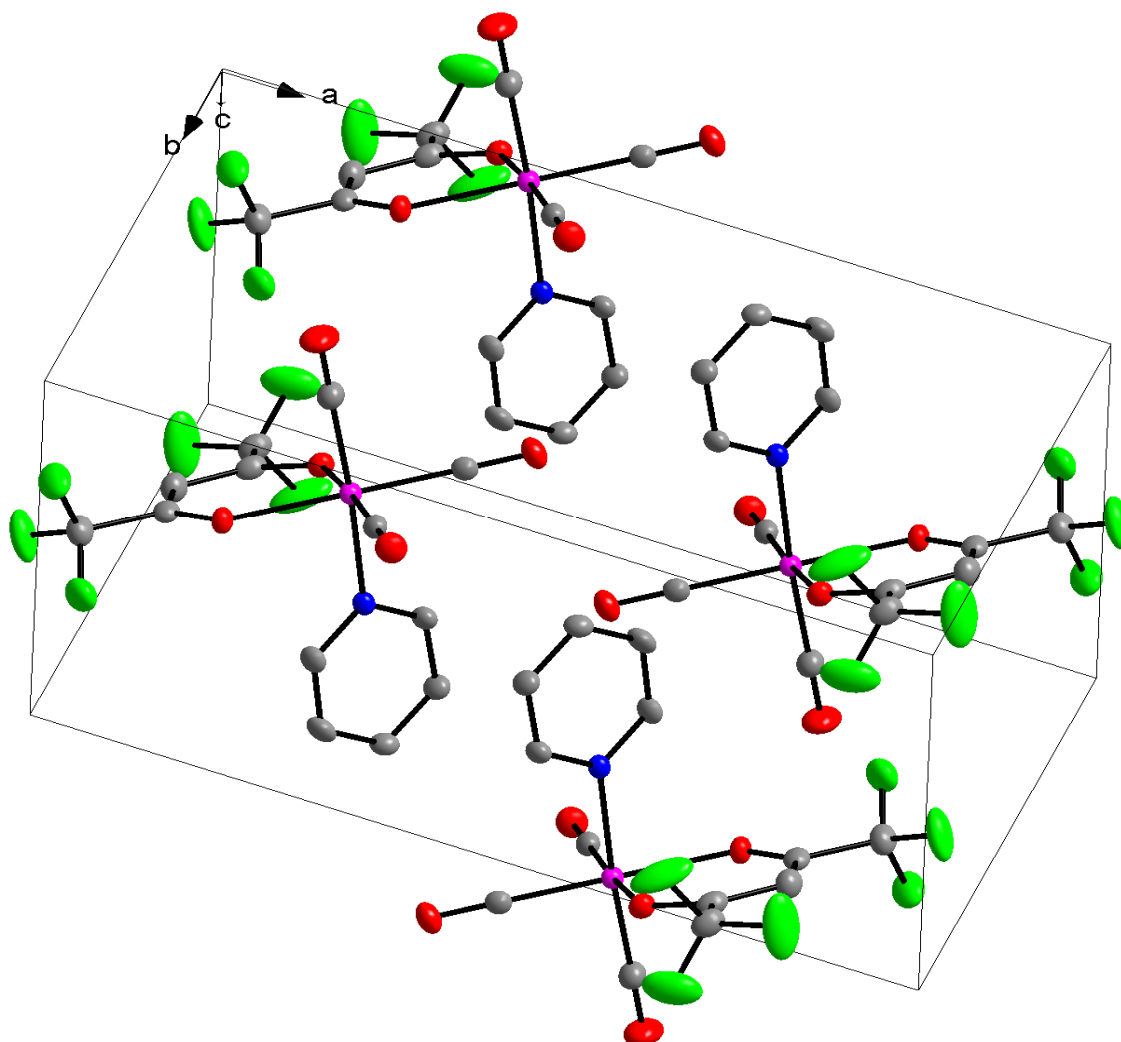
Figure 5.9: An illustration of the diagonal packing of the molecules in the unit cell.

Table 5.5: A selection of bond lenghts of *fac*-[Re(HFA)CO)$_3$Py].

Selected bond distances (Å)			
Re-O1	2.127(2)	**C5-F2**	1.326(4)
Re-O2	2.1376(19)	**C5-F3**	1.322(3)
Re-C6	1.937(3)	**C1-F4**	1.309(4)
Re-C7	1.895(3)	**C1-F5**	1.321(4)
Re-N	2.203(2)	**C1-F6**	1.307(4)
C4-O2	1.261(3)	**C4-C5**	1.535(4)
C5-F1	1.331(4)	**C1-C2**	1.529(4)

Table 5.6: A selection of bond angles of *fac*-[Re(HFA)CO)₃Py].

Selected bond angles (°)			
O1-Re-O2	84.56(8)	O1-Re-N	82.48(8)
C7-Re-O2	93.63(10)	O2-Re-N	84.62(8)
C8-Re-O1	94.62(10)	C4-O2-Re	128.08(19)
C7-Re-C8	87.17(12)	C2-O1-Re	127.52(19)
C6-Re-C8	88.52(13)	C7-Re-N	92.72(11)
C6-Re-C7	89.37(13)	C8-Re-N	95.11(11)
C6-Re-O1	95.33(11)	C2-C3-C4	122.0(3)
C6-Re-O2	91.73(11)	C9-N-Re	120.74(19)

5.4.2 Results and discussion

The molecular structure of **(2)** consists of a Re(I) metal centre which is bonded to three facial carbonyl molecules, a bidentate hexafluoroacetylacetone ligand in the equatorial plane and a pyridine ligand in the axial position. In the unit cell, the Re(I) molecules are diagonally packed in a head-to-head fashion, along the *ab* plane.
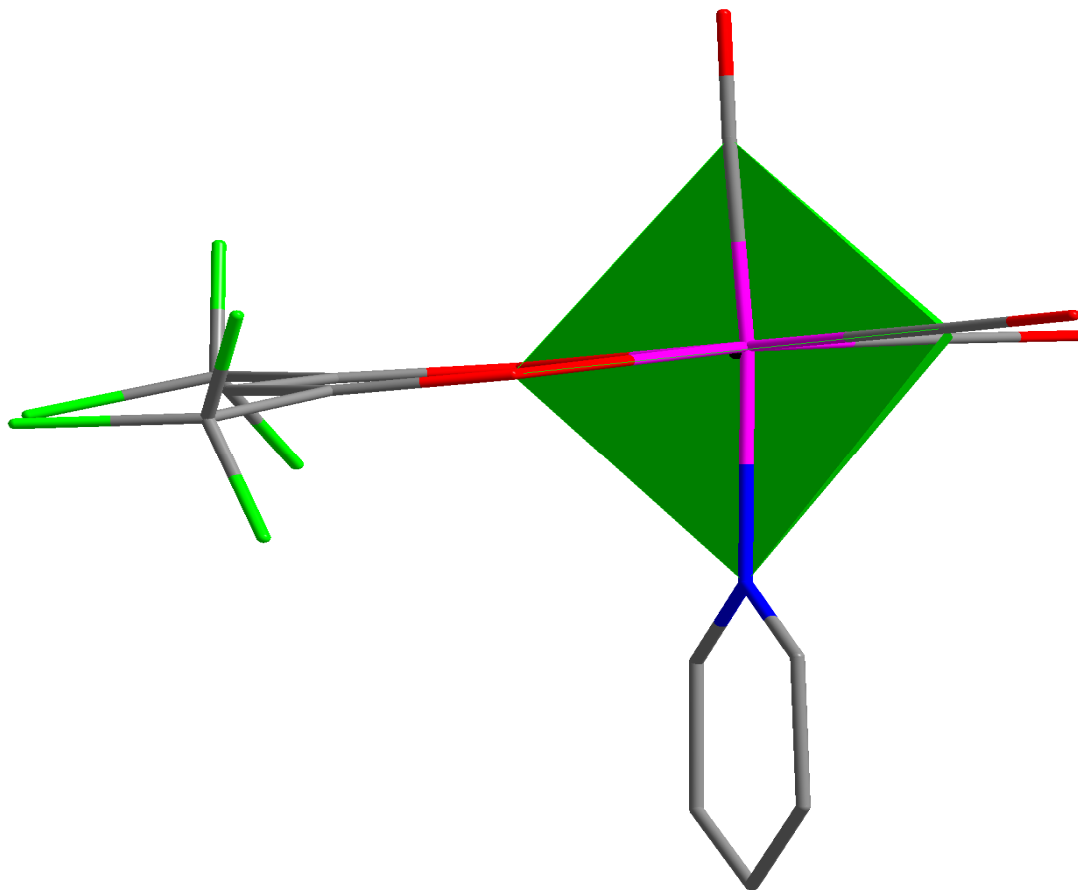
Figure 5.10: Illustrating the distortion in the octahedral complex of *fac*-[Re(HFA)CO)₃Py].

This distorted octahedral (see Figure 5.10), neutral Re(I) complex crystallizes in the monoclinic space group, P2$_1$/*c*. The distortion in the complex is apparent in the bond angles of O1-Re-N (82.48(8) °) and O2-Re-N (84.62(8) °), which significantly deviate from 90 °. Also indicating the distortion in the octahedron is the deviation from 180 ° in the C6-Re-N (175.89(10) °) bond angle. The Re-N bond length of 2.203(2) Å is in the range for bonds of this type and is considered normal.[7]
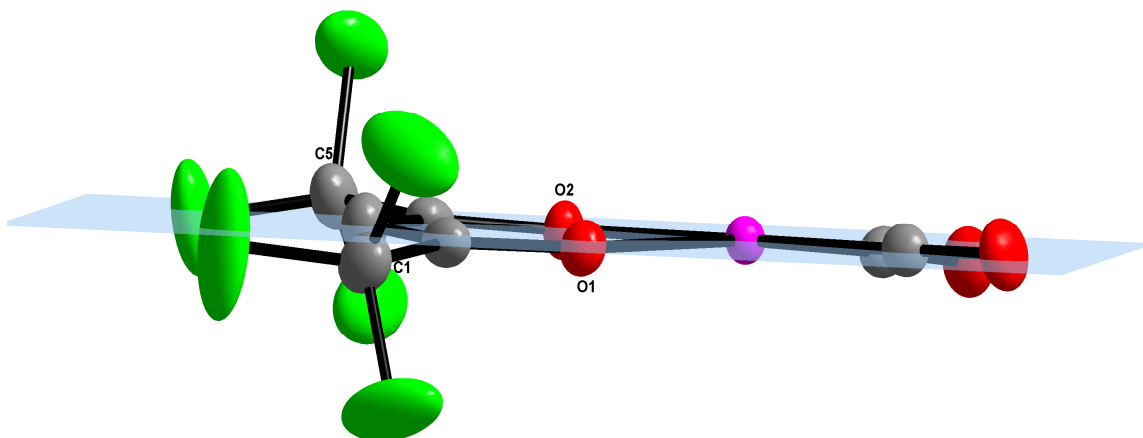
Figure 5.11: Selected part of the molecule, illustrating the in-plane O2 atom and the out-of plane C1 and C5 atoms.

In Par. 5.3.2, it was discussed that there was no significant difference in the bond distances of *fac*-[Re(Acac)(CO)$_3$Py] and **(1)**, but a significant difference in their bond angles surrounding C5 is apparent. Figure 5.11 illustrates the out-of-plane bending of C1 and C5, when a horizontal plane is constructed through the atoms situated in the equatorial position. This out-of plane bending has a significant influence on the bond angles in **(2)**. In **(2)**, the bond angles in question (O1-C2-C3 and O2-C4-C3) are significantly larger than the same angles of *fac*-[Re(Acac)(CO)$_3$Py]. In this complex it is apparent that the fluorine molecules on C1 and C5 influence the angles of O1-C2-C3 (129.0(3) °) and O2-C4-C3 (128.6(3) °), causing them to increase. In the *fac*-[Re(Acac)(CO)$_3$Py] complex, the following angles; O1-C2-C3 and O2-C4-C3 are 126.0(3) ° and 125.3(3) ° respectively. Also discussed in Par. 5.3.2 is the significant difference in the bond distances of C2-C3 and C3-C4. In complex **(2)**, the bond lengths of C2-C3 and C3-C4 are 1.395(4) Å and 1.394(4) Å respectively, indicating no significant difference between the two.

The bond lengths of C7-O4 and C8-O5 are exactly the same in **(2)**, 1.157(3) Å, which is expected, since the ligand is completely symmetrical. Again, when compared to the

fac-[Re(Acac)(CO)$_3$Py] complex, not a significant difference in the bond lengths of the CO molecules are observed, which was expected since the ligand contains six electron withdrawing fluorine atoms on its backbone. One would also expect that the bond lengths of C1-C2 (1.529(4) Å) and C4-C5 (1.534(4) Å) to be significantly longer than that of *fac*-[Re(Acac)(CO)$_3$Py], however just a slight increase in these bond lengths are observed. The C2-C3-C4 angle in the hexafluoroacetylacetone ligand is 122.0(3) °, which deviates from the expected angle of 120 °.

Complex **(2)** has comparable Re-CO bonds, and the bond distances of Re-C6 (1.937(5) Å), Re-C7 (1.895(3) Å) and Re-C8 (1.896(3) Å) are considered normal. The Re-O1 and Re-O2 distances of 2.127(3) Å and 2.138(3) Å respectively, compares well with similar structures, and the coordinated hexafluoroacetylacetone ligand show a minimally constrained bite angle (O1-Re-O2; 84.56(8) °).
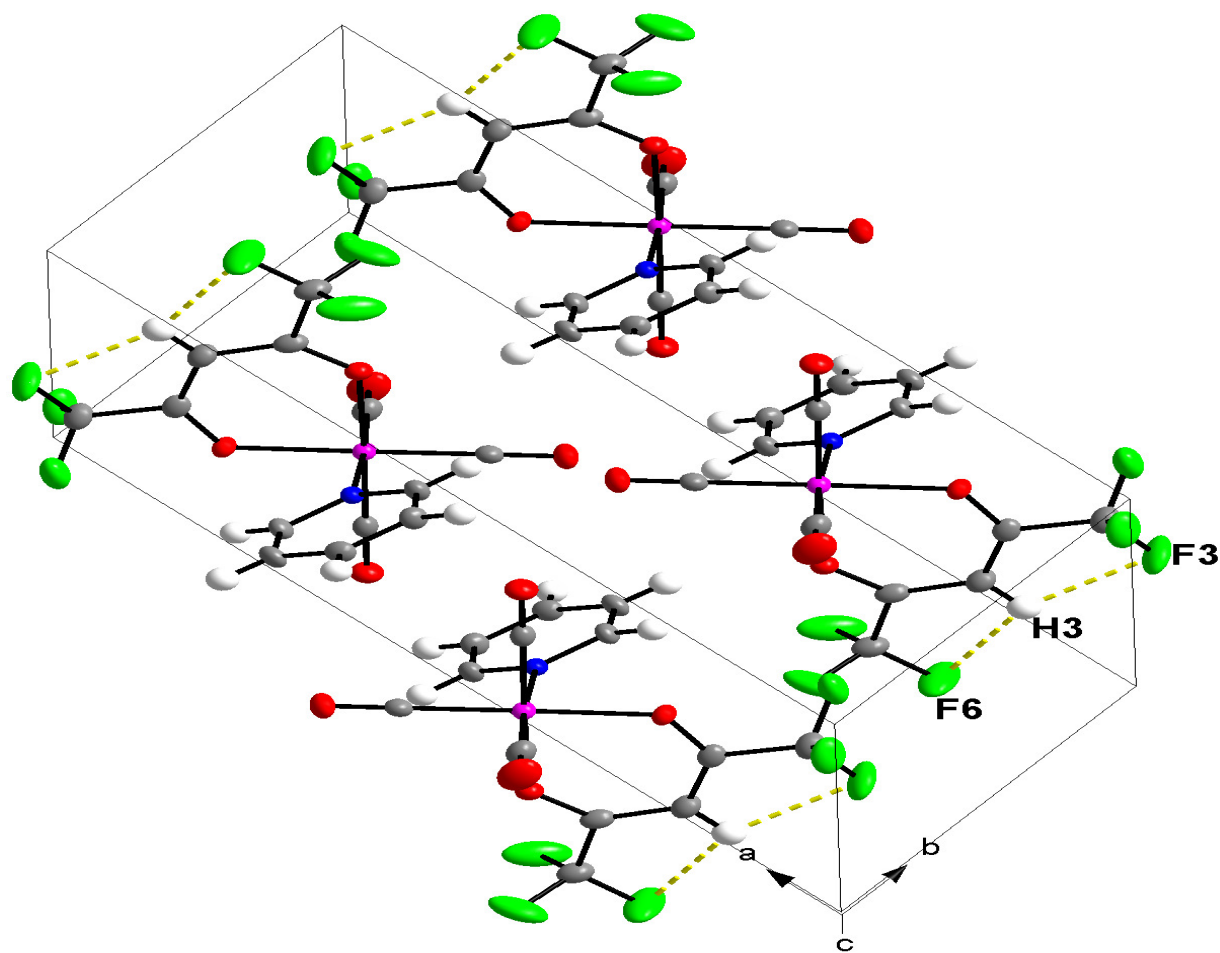
Figure 5.12: Intramolecular C-H...F interactions in *fac*-[Re(HFA)(CO)$_3$(Py)].

Intramolecular C-H…F hydrogen bonding is observed in this complex, which helps to stabilize the molecule. In Figure 5.12 an illustration of the hydrogen contacts is given and the contact distances and angles are given in Table 5.7.

The diagonal packing of layers in the structure is further stabilized by C-H…O intermolecular interactions, which are illustrated in Figure 5.13. Intramolecular C-H…O interactions are also apparent in the molecule, as seen below. The contact distances and angles are given in Table 5.7.
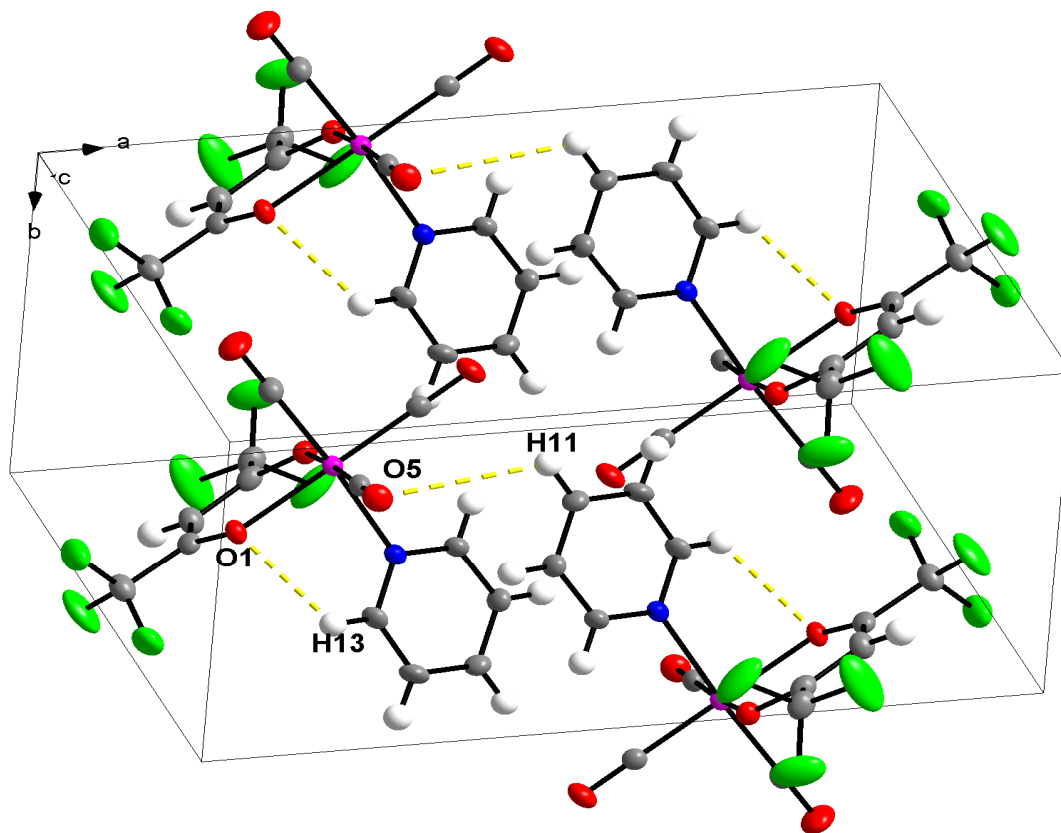
Figure 5.13: Inter- and intramolecular C-H…O interactions in *fac*-[Re(HFA)(CO)₃(Py)].

Table 5.7: Hydrogen bond geometry and distances in *fac*-[Re(HFA)(CO)₃(Py)] (Å, °).

D-H…A	d (D-H)	d (H…A)	d (D…A)	D-H…A Angle
C3-H3…F3[a]	0.93	2.37	2.725(5)	102
C3-H3…F6[a]	0.93	2.39	2.737(5)	102
C13-H13…O1[a]	0.93	2.49	2.996(4)	114
C11-H11…O5[b]	0.93	2.55	3.196(4)	127

Symmetry codes: (a) *x,y,z*; (b) *x, -y + 3/2, z-1/2*.

5.5 Discussion

Figure 5.14 illustrate the labeling system of the complexes used in this discussion and Table 5.8 gives an illustration of the bond distances of the complexes synthesized in this study, which will be compared to that of *fac*-[Re(Acac)(CO)$_3$Py].
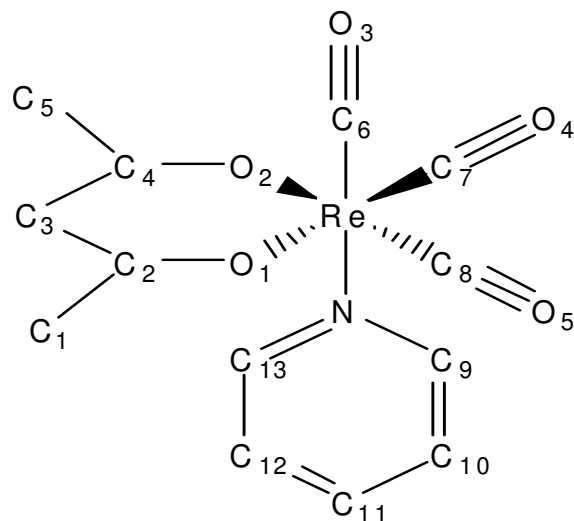
Figure 5.14: Labeling system of complexes, hydrogen atoms have been omitted for clarity.

Table 5.8: A comparison of selected bond distances of the synthesized compounds, with a similar compound.

Compounds	*fac*-[Re(Acac)(CO)$_3$Py]	*fac*-[Re(TFA)(CO)$_3$Py]	*fac*-[Re(HFA)(CO)$_3$Py]
	Bond lengths (Å)		
Re-O1	2.1189(19)	2.135(3)	2.127(3)
Re-O2	2.1226(19)	2.117(3)	2.138(3)
Re-C6	1.926(3)	1.932(5)	1.937(5)
Re-C7	1.896(3)	1.906(4)	1.895(3)
Re-C8	1.903(3)	1.906(4)	1.896(3)
Re-N	2.209(2)	2.202(3)	2.203(2)
O1-C2	1.276(4)	1.263(5)	1.260(3)
O2-C4	1.274(4)	1.269(5)	1.261(3)
C1-C2	1.506(4)	1.513(6)	1.529(4)
C4-C5	1.508(4)	1.514(6)	1.534(4)
C2-C3	1.392(4)	1.409(6)	1.395(4)
C3-C4	1.404(4)	1.369(6)	1.394(4)
C7-O4	1.166(4)	1.143(5)	1.157(3)
C8-O5	1.156(4)	1.150(5)	1.157(3)

In this study, it was expected that the bond distances in the complexes [**(1)** and **(2)**] would be significantly influenced, due to the highly electron withdrawing fluorine atoms on the ligand back bone. However, it was found that they are not considerably influenced, because the bond

lengths of Re-O1 and Re-O2 are within the same range (2.1189(19) Å to 2.138(3) Å). What is conspicuous is that the Re-C6 bond distances increases slightly, with the increase of fluorine atoms in the ligand back bone. With regards to the bond lengths of Re-C7 and Re-C8, one would have expected these bond lengths to differ completely, due to the *trans* influence of the fluorine atoms on these bonds. Yet, these bond distances are within the same range, ranging between 1.895(3) Å and 1.906(4) Å. The bond lengths of Re-N in these complexes are also slightly similar (ranging between 2.202(3) Å and 2.209(2) Å). The bond distances of O1-C2 (1.276(4) Å > 1.263(5) Å > 1.260(3) Å) and O2-C4 (1.274(4) Å > 1.269(5) Å > 1.261(3) Å), decreases with the increase in fluorine atoms on the ligand, which is the opposite effect of what is expected. Also obvious is a slight increase in the bond lengths of C1-C2 and C4-C5 (*fac*-[Re(Acac)(CO)₃Py] < **(1)** < **(2)**). It was expected that the bond lengths (C1-C2 and C4-C5) of **(1)** should be different (C4-C5 > C1-C2), due to the fluorine atoms on C5, which is not the case in this instance. The bond lengths of C2-C3 and C3-C4 are approximately similar, for complexes *fac*-[Re(Acac)(CO)₃Py] and **(2)**, with a slight difference between them in each individual complex. In **(1)** there is a significant difference in the bond lengths of C2-C3 (1.409(6) Å) and C3-C4 (1.369(6) Å).

Table 5.9: A comparison of selected bond angles of synthesized compounds, with a similar compound, *fac*-[Re(Acac)(CO)₃Py].

Compounds	*fac*-[Re(Acac)(CO)₃Py]	*fac*-[Re(TFA)(CO)₃Py]	*fac*-Re(HFA)(CO)₃Py]
Angles (°)			
O2-Re-O1	85.07(8)	84.99(11)	84.56(8)
O1-Re-C6	95.29(10)	95.20(15)	95.33(11)
O1-Re-C7	177.72(10)	174.14(14)	175.00(10)
O1-Re-C8	92.76(10)	94.59(14)	94.62(10)
O2-Re-C6	95.62(11)	93.89(15)	91.73(11)
O2-Re-C7	94.55(10)	92.70(14)	93.63(10)
O2-Re-C8	174.08(10)	178.20(14)	179.17(9)
C6-Re-N	177.88(10)	176.91(15)	175.89(10)
C7-Re-N	91.62(11)	91.68(15)	92.72(11)
O1-Re-N	83.33(8)	82.72(11)	82.48(8)
O2-Re-N	82.67(8)	83.67(12)	84.62(8)
C2-C3-C4	125.7(3)	124.6(4)	122.0(3)
O2-C4-C3	125.3(3)	129.2(4)	128.6(3)
O1-C2-C3	126.0(3)	125.0(4)	129.0(3)
O2-C4-C5	115.5(3)	111.3(4)	112.2(3)
O1-C2-C1	113.9(3)	116.3(4)	112.7(3)

Table 5.9 contains selected bond angles of the synthesized complexes [**(1)** and **(2)**], which is then compared to the bond angles from *fac*-[Re(Acac)(CO)$_3$Py]. The O2-Re-O1 angle in the complexes, decrease (*fac*-[Re(Acac)(CO)$_3$Py] > **(1)** > **(2)**) with increase in the number of fluorine atoms on the ligand backbone. There is also a significant decrease (*fac*-[Re(Acac)(CO)$_3$Py] > **(1)** > **(2)**) in the O2-Re-C6 angle as the fluorine atoms increase on the ligand. The O1-Re-N angle also shows a slight decrease in its angle, as the electron density on the metal centre decrease, and the opposite is true for the O2-Re-N angle. A conspicuous detail in the C2-C3-C4 angle is that it is more constrained when the fluorine atoms on the ligand increase, causing the O2-C4-C3 and the O1-C2-C3 angles to increase, especially in the case of complex **(2)**. Previously it was mentioned that the fluorine atoms does not have a significant influence on the bond distances, however, now it is clear that it has an influence on the bond angles, especially those on the ligand backbone. In the [*fac*-Re(Acac)(CO)$_3$Py] complex, the angles on either side of the ligand, angles O1-C2-C3 and O2-C4-C3 are, 126.0(3) ° and 125.3(3) ° respectively. In the case of complex **(2)**, these two angles, O1-C2-C3 and O2-C4-C3 are 129.0(3) ° and 128.6(3) ° respectively. Complex **(2)** and [*fac*-Re(Acac)(CO)$_3$Py] are completely symmetrical when constructing a plane along their *a*-axes. Thus the angles for [*fac*-Re(Acac)(CO)$_3$Py] (O1-C2-C3 = 126.0(3) °; O2-C4-C3 = 125(3) °) and **(2)** (O1-C2-C3 = 129.0(3) °; 128.6(3) °) fall within the same range. When one observe these angles (O1-C2-C3 = 125.0(4) °; O2-C4-C3 = 129.2(4) °) in complex **(1)**, they correspond with that of [*fac*-Re(Acac)(CO)$_3$Py] and **(2).**

As mentioned in Paragraph 5.1, nine compounds with O,O' donor bidentate ligands, has been collected thus far. Benny *et al.*,[7] Sagnou *et al.*[9] and Brink *et al.*[10] synthesized Re(I) tricarbonyl compounds with acetylacetone as O,O' donor bidentate ligand, alternating the compounds coordinating on the third coordination site. Brasey *et al.*[6] synthesized a Re(I) tricarbonyl compound with 3-hydroxy-1,2,3-benzotriazine-4(3H)-one as O,O'- donor bidentate ligand. Bidentate tribromotropolone complexes were synthesized by Schutte *et al.*,[1,2] with alternating bromine and aqua atoms occupying the third coordination site. Schutte and her co-workers also synthesized a complex using tropolone as bidentate ligand.[8] Schutte synthesized a compound in her MSc. Thesis, which had 3-hydroxyflavone present as the

O-O'- donor bidentate ligand, with a methanol atom occupying the third coordination spot. $Re(CO)_4(PPh_3)(CH_3)$ and acetic acid was used by Gibson *et al.*,[5] to synthesize the bidentate acetate complex, $[Re(OCOCH3)(CO)3(PPh3)]$. Bochkova *et al.*[3] and Cheng *et al.*[4] recorded the remaining two polymorphic structures. 3,5-di-*t*-butyl-1,2-benzosemiquinone is the O,O'- donor bidentate ligand and triphenylphosphine occupies the third coordination site.
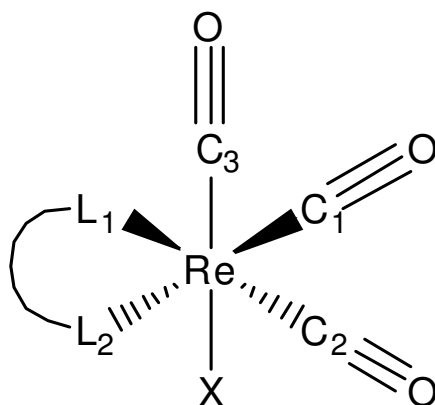
Figure 5.15: An illustration of the labeling of atoms in the rhenium core.

A selection of bond lengths are summarized in Table 5.10 for comparison purposes and labeled according to Figure 5.15. From Table 5.10 it is apparent that the Re-L_1 and Re-L_2 bond distances for O,O'- donor bidentate ligands are fairly similar for all complexes. The axial Re-C3 bond distances are similar for all complexes, ranging between 1.861(7) Å and 1.963(6) Å. The Re-C1 (1.892(4) Å to 1.934(3) Å) and Re-C2 (1.889(4) Å to 1.911(1) Å) bond distances also fall within the same ranges. The Re-X distances can be grouped into five parts: Re-Br = 2.627(3) Å to 2.654(2) Å; Re-P = 2.493(9) Å to 2.495(9) Å; Re-N = 2.202(3) to 2.209(2); Re-O = 2.170(5) Å to 2.204(4) Å and Re-C = 2.094(6) Å. What is also clear is that the Re-CH_3OH bond distance fall within the same range as the Re-N bond lengths. There are therefore five distinctive Re-X bond length ranges thus far, Br⁻ > PPh_3 > Py > CH_3OH and H_2O > CN, with all *trans* to a CO in the apical position.

Table 5.10: Illustration of the bond lengths of different rhenium complexes, with O,O' bidentate ligands.

Compounds	Re-L$_1$ (Å)	Re-L$_2$ (Å)	Re-C$_1$ (Å)	Re-C$_2$ (Å)	Re-C$_3$ (Å)	Re-X (Å)
fac-[Re(TFA)(CO)$_3$Py]	2.135(3)	2.117(3)	1.906(4)	1.906(4)	1.932(5)	2.202(3)
fac-[Re(HFA)(CO)$_3$Py]	2.127(3)	2.138(3)	1.895(3)	1.896(3)	1.937(5)	2.203(2)
fac-[Re(Acac)(CO)$_3$Py]	2.1189(19)	2.1226(19)	1.896(3)	1.903(3)	1.926(3)	2.209(2)
fac-[Re(Acac)(CO)$_3$(Isc)[a]]	2.145(4)	2.138(4)	1.910(6)	1.906(6)	1.963(6)	2.094(6)
fac-[NEt$_4$][Re(TropBr$_3$)[b](CO)$_3$Br]	2.141(2)	2.132(2)	1.894(3)	1.898(3)	1.897(3)	2.627(3)
fac-[NEt$_4$][Re(Acac)(CO)$_3$Br]	2.1265(19)	2.1248(18)	1.899(3)	1.909(3)	1.895(3)	2.6448(3)
fac-[NEt$_4$][Re(Trop)[c](CO)$_3$Br]	2.126(3)	2.135(3)	1.906(5)	1.903(5)	1.861(7)	2.6334(9)
fac-[NEt$_4$][Re(C$_7$O$_2$N$_3$H$_4$)(CO)$_3$Br].CH$_2$Cl$_2$	2.168(1)	2.163(9)	1.896(2)	1.911(1)	1.883(1)	2.654(2)
fac-[Re(TropBr$_3$)[b](CO)$_3$H$_2$O].CH$_3$OH	2.146(4)	2.123(5)	1.899(7)	1.897(6)	1.882(7)	2.170(5)
fac-[Re(Flav)[d](CO)$_3$(CH$_3$OH)].CH$_3$OH[18]	2.147(3)	2.141(3)	1.906(5)	1.905(5)	1.894(5)	2.204(4)
fac-[Re(C$_{14}$H$_{20}$O$_2$)(CO)$_3$PPh$_3$]	2.125(2)	2.158(1)	1.934(3)	1.896(1)	1.891(1)	2.493(9)
fac-[Re(OCOCH$_3$)(CO)$_3$PPh$_3$]	2.182(2)	2.210(3)	1.892(4)	1.889(4)	1.957(4)	2.495(9)

a: Isocyanide; b: tribromotropolonate; c: tropolone; d: 3-Hydroxyflavone

5.6 Conclusion

In this chapter a range of relevant complexes consisting of *fac*-[Re(TFA)(CO)$_3$Py] and *fac*-[Re(HFA)(CO)$_3$Py] have been successfully synthesized and characterized by means of IR, NMR (^{1}H and ^{13}C) and X-ray crystallography. It was also determined that the bond angles, instead of the bond distances in the synthesized complexes were significantly affected by the electron withdrawing fluorine atoms on the ligand back bone. The reactions in these systems are 'clean' processes and the reactants and products are well-defined.

ooOoo

---

[18] Schutte, M.; *MSc. Dissertation*, University of the Free State, **2008**

6 KINETIC INVESTIGATION OF RHENIUM (I) COMPLEXES

6.1 Introduction

Kinetic investigations give an indication of the rate at which chemical reactions take place, which in turn makes it possible to observe a change in reaction rate, by alternating certain factors (ie. temperature, concentration, pressure etc.). With chemical kinetics one can also achieve the possibility of specifying the intimate mechanism that the reaction in question follows.[1] This is important in the development and characterization of potential radiopharmaceuticals, because it will highlight factors such as *in vivo* stability, biodistribution (i.e. the rate at which the compound is absorbed into the blood stream) and the clearance of the radiopharmaceutical from the body.[2]

The aim involves the proposal of the mechanism for the substitution of the coordinated axial methanol ligand (equatorial plane contains the O,O'-donor bidentate ligand and two CO molecules – see Chapter 5) in the *fac*-[Re(CO)$_3$(O,O'-Bid)(X)], O,O'-Bid = Acac, TFA, HFA and X = CH$_3$OH, complex (see Figure 6.1) with the neutral pyridine (Py) ligand. This investigation is performed under *pseudo* first-order conditions at various temperatures.
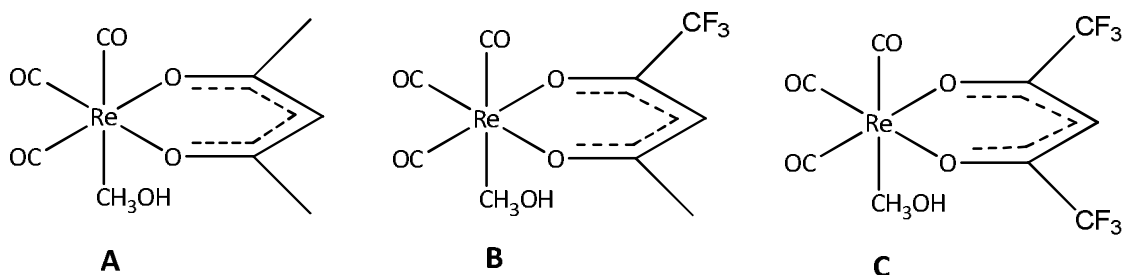
Figure 6.1: A schematic illustration of the three complexes, (A) *fac*-[Re(Acac)(CO)$_3$(CH$_3$OH)]; (B) *fac*-[Re(TFA)(CO)$_3$(CH$_3$OH)] and (C) *fac*-[Re(HFA)(CO)$_3$(CH$_3$OH)], used in the substitution of the axial coordinated ligand.

---

[1] Connors, K. A.; *Chemical Kinetics: The Study of Reaction Rates Solution*; VCH Publishers, New York, **1990**
[2] Capellos, C.; Bielski, B. H. J.; *Kinetic Systems*, Wiley-Interscience, New York, **1972**

One needs to evaluate the stability and the reaction mechanisms of complexed radionuclides (^{99m}Tc, ^{186,188}Re), in order to characterize and know the factors that may influence biodistribution.[3] The kinetic studies of Re(I) and Tc(I) tricarbonyl complexes are still very under explored, as discussed in Paragraph 2.11. This study and others performed by Schutte[4], Kemp[5], Salignac[6] and Helm[7] gives an insight into the substitution reactions of Re(I) tricarbonyl complexes.

Schutte[4] investigated the methanol substitution of the tricarbonyl rhenium complex, *fac*-[Re(Flav)(CO)$_3$(CH$_3$OH)] (with Flav = hydroxyflavonate), with DMAP and found it to occur 150 times faster than that of *fac*-[Re(CO)$_3$(TropBr$_3$)(MeOH)] (TropBr$_3$ = tribromotropolonate). In the methanol substitution reactions with Py for the complexes, *fac*-[Re(CO)$_3$(TropBr$_3$)(MeOH)] and *fac*-[Re(CO)(Flav)(MeOH)], Schutte[8] found that the latter reaction occurs approximately 70 times faster than that of   *fac*-[Re(CO)$_3$(TropBr$_3$)(MeOH)] and Py. She concluded that O,O'-Bid type donor ligands activate the metal centre more than N,O-Bid type ligands.

Kemp[5,8] investigated the substitution rates of *fac*-[Re(L,L'-Bid)$_3$(CO)$_3$(MeOH)]$^+$ complexes, with L,L' = N,N- and N,O- donor bidentate ligands, by substitution of the coordinated axial methanol ligand, with various incoming ligands. In a combined effort with Schutte[8] they established that there is a significant increase of electron density on the metal centre, promoting an increase in the rate of all the entering ligands studied for O,O'-Bid ligands, compared to the N,O- and N,N'-Bid ligands. A total increase in the kinetic rate of at least 20 000 was seen in the rate constants of the L,L'- Bid ligands (N,N' > N,O > O,O'). The activation parameters calculated from this investigation pointed towards a dissociative interchange (I_d) type mechanism for neutral complexes containing N,O- and O,O'-Bid donor ligand systems.

A detailed discussion is given in Paragraph 2.11 about the work done by Salignac[6] and Helm[7]. They investigated the aqua substitution of *fac*-[Re(OH$_2$)$_3$(CO)$_3$]$^+$ with anionic monodentate ligands, N- and S-bonded ligands. The activation parameters was indicative of a mechanism change (I_d to I_a), with hard to soft ligands respectively. Data from this water exchange

[3] Roodt, A.; Abou-Hamdan, A.; Engelbrecht, H. P.; Merbach, A. E.; Advances in *Inorg. Chem*., 49, 59, **2000**
[4] Schutte, M.; *MSc. Dissertation*, University of the Free State, Bloemfontein, South-Africa, **2008**
[5] Kemp, G.; Ph. D Thesis, University of Johannesburg, Johannesburg, South-Africa, **2006**
[6] Salignac, B.; Grundler, P. V.; Cayemittes, S.; Frey, U.; Scopelliti, R.; Merbach, A. E.; *Inorg. Chem*., 42, 3516, **2003**
[7] Helm, L.; *Coord. Chem. Rev*. 252, 2346, **2008**
[8] Schutte, M.; Kemp, G.; Visser, H. G.; Roodt, A.; *Inorg. Chem*., **2011**

investigation of *fac*-[Re(CO)$_3$(OH$_2$)$_3$]$^+$ (k_{ex} = 6.3(1) x 10^{-3} s^{-1}) and [Re(CO)$_3$(OH)(OH$_2$)$_2$] (k_{OH} = 27(1) s^{-1}), indicated a dissociative interchange type mechanism ($\Delta H^{\neq}$ = 90(3) kJ mol^{-1}; $\Delta S^{\neq}$ = 14(10) J K mol^{-1}).

6.2 Experimental

6.2.1 Procedure

All chemicals and reagents were of analytical grade. The kinetic measurements were performed on a Varian Cary 50 Conc UV-VIS spectrophotometer, equipped with a Julabo F-12 temperature cell regulator (accurate within 0.1 °C) in a 1 cm quartz cuvette. The kinetic experiments were done under *pseudo* first-order conditions and Scientist Micromath, Version 2.01[9] was used to fit the data to selected functions. The solid lines in the figures represent computer least squares fits of data, while the experimental values are represented as individual points, denoted by selected symbols.

6.2.2 Data treatment

When integrating and incorporating the well known Beer-Lambert law into the first order exponential, ln [C]$_t$/[C]$_o$ = k_{obs}t, with **[C]$_t$/[C]$_o$ = (A$_\infty$-A$_t$)/(A$_\infty$-A$_o$)**, the equation that follows is:

$$\mathbf{A_t = A_\infty - (A_\infty - A_0)e^{k_{obs}t}}$$

…… **Eq. 6.1**

where A$_{obs}$ = observed absorbance, A$_\infty$ = final absorbance, A$_0$ = initial absorbance, k_{obs} = pseudo first-order rate constant. This equation is used for the evaluation of the absorbance change *vs* time data obtained.

The pseudo first-order rate constant k_{obs}, is calculated from a least-squares fit of the absorbance *vs* time kinetic data. This equation was used in all the kinetic reactions performed in this study, (Appendix C).

The activation parameters were calculated to substantiate the type of mechanism for the substitution reactions. Generally octahedral coordinated complexes follow dissociative interchange type mechanisms (*I$_d$*) and a representation of the mechanism for the substitution reactions investigated in this study is given in Paragraph 6.3. To determine the values of the

---

[9] MicroMath Scientist for Windows, Version 2.01, Copyright © 1986 – 1995, MicorMath, Inc.

standard activation enthalpy ($\Delta H^{\neq}$) and the standard activation entropy change ($\Delta S^{\neq}$), the logarithmic form of the Eyring equations (Eq. 6.2) were used.

$$\ln\left(\frac{k}{T}\right) = \ln\left(\frac{k_B}{h}\right) - \frac{\Delta H^{\neq}}{RT} + \frac{\Delta S^{\neq}}{R}$$

…… **Eq. 6.2**

Where k_B = Boltzmann constant and h = Planck's constant. $\Delta H^{\neq}$ and $\Delta S^{\neq}$ can now be determined by plotting ln (k/T) *vs* (1/T), from which a straight line with a slope (-$\Delta H^{\neq}$/R) and an intercept [ln(k_B/h) + $\Delta S^{\neq}$/R) is obtained.

6.3 Results

The axial methanol substitution of the neutral complexes of the form, *fac*-[Re(O,O')(CO)$_3$(CH$_3$OH)], **(A)**, were investigated, where **(A)** = *fac*-[Re(Acac)(CO)$_3$(CH$_3$OH)] **(1)**, *fac*-[Re(TFA)(CO)$_3$(CH$_3$OH)] **(2)** and *fac*-[Re(HFA)(CO)$_3$(CH$_3$OH)] **(3)**. The pKa values of the coordinated bidentate ligands are pK$_a$ = 8.95[10], 6.40[11], and 4.30[12] for Acac, TFA and HFA respectively, which is a reflection of their electron donating abilities (nucleophility). All three complexes have stable chelate ligand systems and they were selected to investigate the influence which the electron withdrawing fluorine atoms could have on the kinetic rate.

The entering monodentate ligand selected for the methanol substitution was the neutral Py ligand, in order to compare to previous work done by Schutte *et al.*[8]

The synthesis and the characterisation of the starting reagents and substituted products, *fac*-[Re(L,L'-Bid)(CO)$_3$(X)] (L,L'-Bid = Acac, TFA, HFA), X = CH$_3$OH, Py) were reported in Paragraph 4.3.2. The two substituted products, *fac*-[Re(TFA)(CO)$_3$(Py)] and *fac*-[Re(HFA)(CO)$_3$(Py)] were also characterised by X-ray diffraction, see Chapter 5. Solutions of the compounds were scanned with UV/Vis over several days, in order to ensure stability. For consistency, fresh solutions (complex and ligand concentrates) were prepared every day, prior to conducting the kinetic studies.

---

[10] http://research.chem.psu.edu/brpgroup/pKa_compilation.pdf **[Consulted on 4 June 2012]**

[11] Cotton, F. A.; *Interscience Publishers*, John Wiley and Sons Inc., 7, **1966**

[12] http://www.chemicaldictionary.org/dic/H/Hexafluoroacetylacetone_479.html **[Consulted on 4 June 2012]**

All the kinetic experiments were performed: a) under *pseudo* first order conditions (entering ligand is in excess of at least 10 times that of the metal complex) and b) in methanol solution. The UV/VIS spectra of the formed reaction solution compared very well to that of the synthesized *fac*-[Re(O,O')(CO)$_3$(Py)], O,O' = Acac, TFA and HFA, complexes reported in Paragraph 4.4.2. Since *pseudo* first order conditions is based on the following principle, [L] >>> *fac*-[Re(O,O')(CO)$_3$(X)] with L = Py and X = CH$_3$OH, one would expect to observe one reaction, which was the case in this kinetic study. The rate at which the reactions took place also increased, with an increase in the entering ligand concentration. The general mechanism predicted for the reaction between *fac*-[Re(O,O')(CO)$_3$(CH$_3$OH)] and Py is as follows:

Scheme 6.1: Schematic representation of the proposed mechanism for the methanol substitution of *fac*-[Re(O,O')(CO)$_3$(CH$_3$OH)].

$$[Re(O,O')(CO)_3(CH_3OH)] + Py \; \underset{k_{-1}}{\overset{K_1, \, k_1}{\rightleftharpoons}} \; [Re(O,O')(CO)_3(Py)] + CH_3OH$$
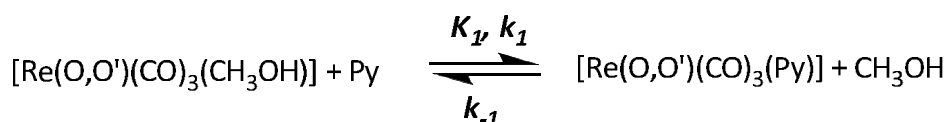
O,O' = Acac, TFA, HFA

The rate of the reaction is now denoted as:

Rate = k$_1$[Re(Bid)][L] – k$_{-1}$[Re(Bid)(L)]   ...... **Eq. 6.3**

with the forward reaction rate constant represented as k_1 and the reverse reaction rate constant as k_{-1}. [Re(Bid)] is [Re(Bid)(CO)$_3$(CH$_3$OH)] and [Re(Bid)(L)] is the final substituted product, [Re(O,O')(CO)$_3$(Py)]. Under pseudo first-order conditions with [L] >>> [Re(Bid)(L)], Eq. 6.3 yields:

k$_{obs}$ = k$_1$[L] + k$_{-1}$ ...... **Eq. 6.4**

with k_{obs} representing the observed rate constant. The rate constant can be determined at different [L] ([L] >>> [Re(Bid)]). The equation that follows is applicable for equilibrium reactions and the equilibrium constant is given as:

$$K_1 = \frac{k_1}{k_{-1}}$$

...... **Eq. 6.5**

When extrapolating a graph of k_{obs} vs [L] a straight line is obtained with an intercept of k_{-1} and a slope of k_1.

In order to determine the equilibrium constant, K_1, Eq. 6.5 was used. The equilibrium constant, for one reaction per metal complex, was alternatively obtained by a non-linear least-squares fit to Eq. 6.6, based on the UV/Vis data to confirm that the kinetically (Eq. 6.5) and the thermodymically (Eq. 6.6) determined equilibrium constants are the same.

$A_{obs} = (A_M + A_{ML}K_1[L])/(1 + K_1[L])$ ...... **Eq. 6.6**

A_M and A_{ML} represents the observed absorbance of *fac*-[Re(O,O')(CO)$_3$(CH$_3$OH)], O,O' = Acac, TFA and HFA) and *fac*-[Re(O,O')(CO)$_3$(Py)]. A_{obs} is the observed absorbance and [L] is the concentration of the entering ligand.

6.3.1 The reaction between *fac*-[Re(O,O')(CO)$_3$(CH$_3$OH)] and Py in methanol

The synthetic procedure for the preparation of *fac*-[Re(O,O')(CO)$_3$(CH$_3$OH)], with O,O' = Acac, TFA and HFA, is described in Chapter 4. A preliminary study was performed to establish the stability of *fac*-[Re(Acac)(CO)$_3$(CH$_3$OH)], *fac*-[Re(TFA)(CO)$_3$(CH$_3$OH)] and *fac*-[Re(HFA)(CO)$_3$(CH$_3$OH)] in methanol and it revealed relative stability for up to several days. The reaction between *fac*-[Re(Acac)(CO)$_3$(CH$_3$OH)] and Py was studied at various temperatures (14.9 °C, 25.1 °C, 35.0 °C, and 45.0 °C) and methanol substitution with Py for *fac*-[Re(TFA)(CO)$_3$(CH$_3$OH)] and *fac*-[Re(HFA)(CO)$_3$(CH$_3$OH)] were studied at 25.1 °C. The standard enthalphy change of activation ($\Delta H^{\neq}$) and the standard entropy change of activation ($\Delta S^{\neq}$) for the reaction between *fac*-[Re(Acac)(CO)$_3$(CH$_3$OH)] and Py were obtained from the Eyring equation.

6.3.1.1 The reaction between *fac*-[Re(Acac)(CO)$_3$(CH$_3$OH)] and Py in methanol

Figure 6.2 illustrates a typical spectrum for the methanol substitution reaction between *fac*-[Re(Acac)(CO)$_3$(CH$_3$OH)] and Py in methanol. The k_{obs} *vs* [Py] data was obtained at 14.9 °C, 25.1 °C, 35.0 °C and 45.0 °C, and fitted to Eq. 6.4 and the calculated rate constants are presented in Table 6.1. The calculated negative $\Delta S^{\neq}$ value indicates towards an associative type activated mechanism. The UV/Vis spectra obtained from the formation of the final product is identical to the one obtained from the synthesized *fac*-[Re(Acac)(CO)$_3$(Py)] complex in Paragraph 4.4.2.3.

Figure 6.2: A characteristic UV/VIS spectrum for the methanol substitution reaction of *fac*-[Re(Acac)(CO)$_3$(CH$_3$OH)] with Py at 25.1 °C; [Re complex] = 1 x 10^{-4} M, [Py] = 0.05 M, Δt = 2 min.
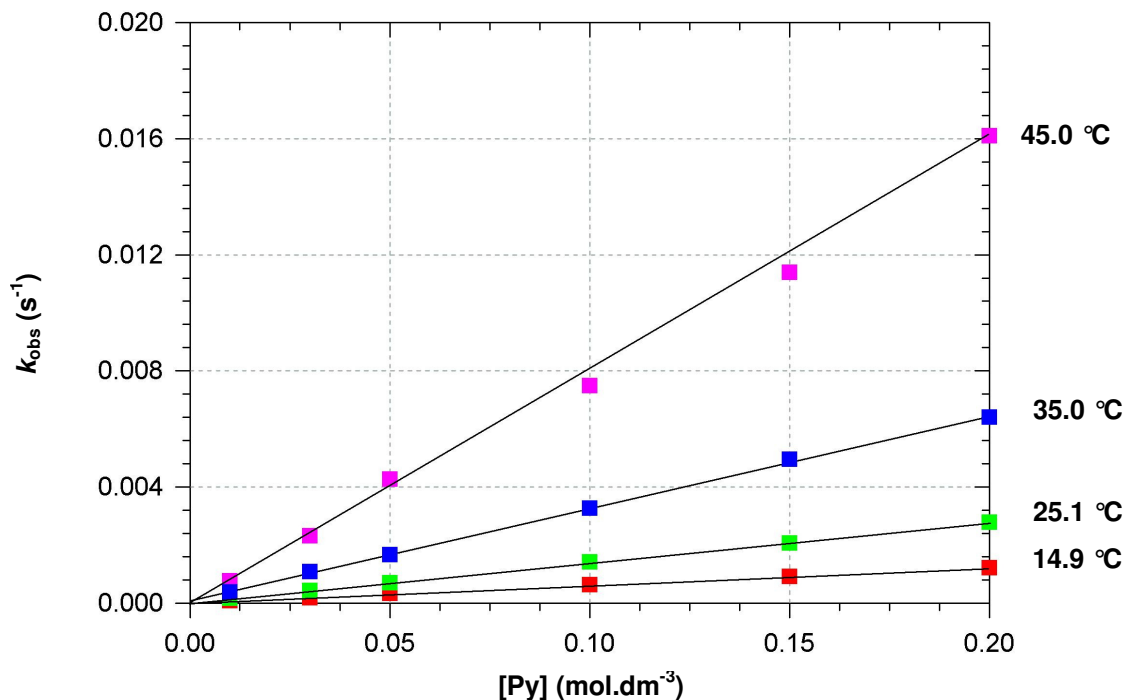
Figure 6.3: Plot of k_{obs} *vs* [Py] for the reaction between *fac*-[Re(Acac)(CO)$_3$(CH$_3$OH)] and Py at various temperatures; [Re complex] = 1 x 10^{-4} M, (λ = 340 nm) and [Py] = 0.01 – 0.2 M, (Appendix C, Table C.1.1).

Table 6.1: The kinetic data of the rate constants for the reaction between *fac*-[Re(Acac)(CO)$_3$(CH$_3$OH] and Py at different temperatures; [Re complex] = 1 x 10^{-4} M and [Py] = 0.01 – 0.2 M.

Constants	14.9 °C	25.1 °C	35.0 °C	45.0 °C
(10^3) k_1 (M^{-1}.s^{-1})	6.04(8)	13.7(1)	32.1(1)	74.1(3)
(10^3) k_{-1} (s^{-1})	0.016(6)	0.03(2)	0.075(9)	0.20(4)
K_1 (M^{-1})	378(142)	457(305)	428(51)	371(74)
K_1 (M^{-1})^a		145(25)		
$\Delta H^{\neq}_{(k1)}$ (kJ mol^{-1})		64(1)		
$\Delta S^{\neq}_{(k1)}$ (J K^{-1} mol^{-1})		-65(5)		

^{a} **Thermodynamically determined**

The activation parameters of the reaction between *fac*-[Re(Acac)(CO)$_3$(CH$_3$OH)] and Py were determined by fitting the data to Eq. 6.2 (see Figure 6.3). The standard enthalpy change of activation ($\Delta H^{\neq}_{k1}$) was calculated as 64(1) kJ mol^{-1} and the standard entropy change of activation ($\Delta S^{\neq}_{k1}$) was calculated as -65(5) J K^{-1} mol^{-1}.
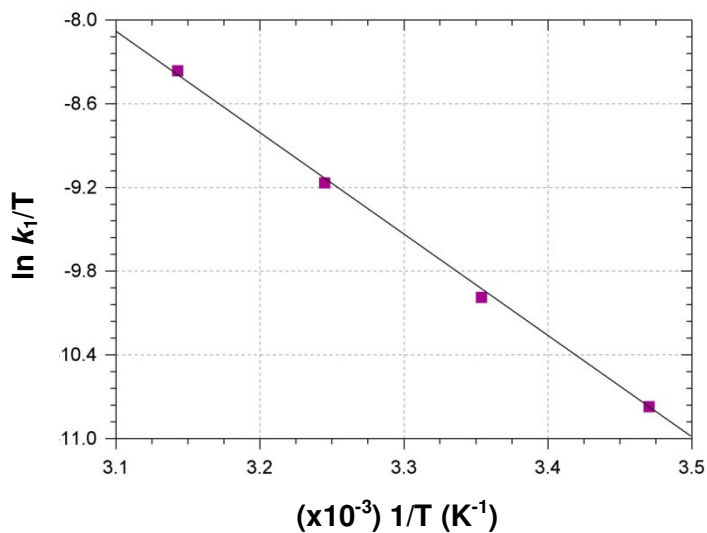
Figure 6.4: The Eyring plot of ln(k_1/T) *vs* 1/T for the reaction between *fac*-[Re(Acac)(CO)$_3$(CH$_3$OH)] and Py in methanol (Appendix C, Table C.1.2).

Figure 6.5: Thermodynamic determination of the stability constant (K_1), for the coordinated methanol substitution reaction of *fac*-[Re(Acac)(CO)$_3$(CH$_3$OH)] by Py from the UV/VIS spectral change vs [Py] at 300 nm; [Re complex] = 1 x 10^{-4} M, 25.1 °C, in methanol.

6.3.1.2 The reaction between *fac*-[Re(TFA)(CO)₃(CH₃OH)] and Py in methanol

In Figure 6.6 the characteristic spectrum of the methanol substitution, for the reaction between *fac*-[Re(TFA)(CO)₃(CH₃OH)] and Py in methanol at 25.1 °C, is given. The k_{obs} vs [Py] data obtained at 25.1 °C was fitted to Eq. 6.4, (see Table 6.3 for the calculated rate constants).

Once more there is a similarity between the UV/Vis spectra obtained from the formation of the final product and the product obtained from the synthesized *fac*-[Re(TFA)(CO)₃(Py)] complex in Paragraph 4.4.2.6. The substitution of the coordinated methanol ligand (at 25.1 °C) in the *fac*-[Re(TFA)(CO)₃(Py)] complex does not occur as rapid, as for the similar Acac complex
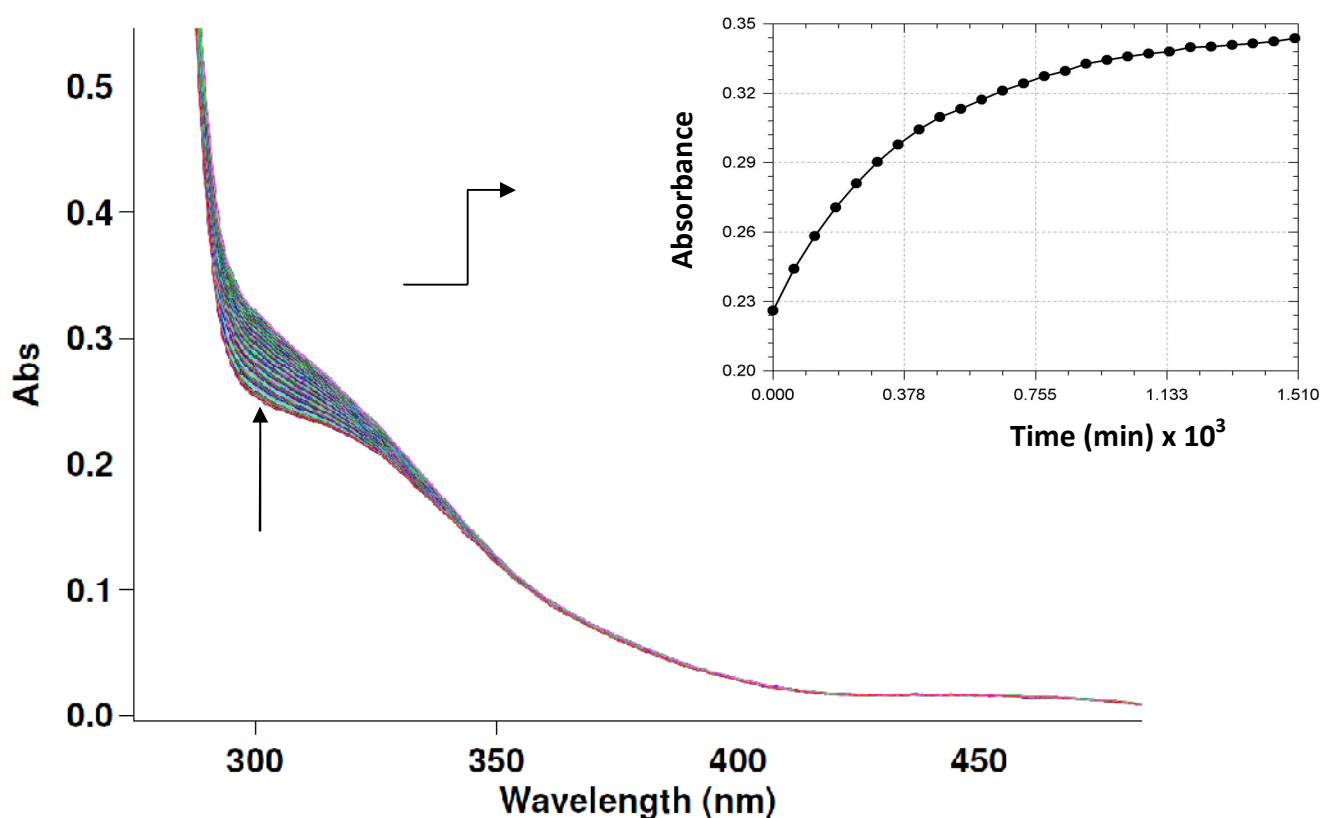
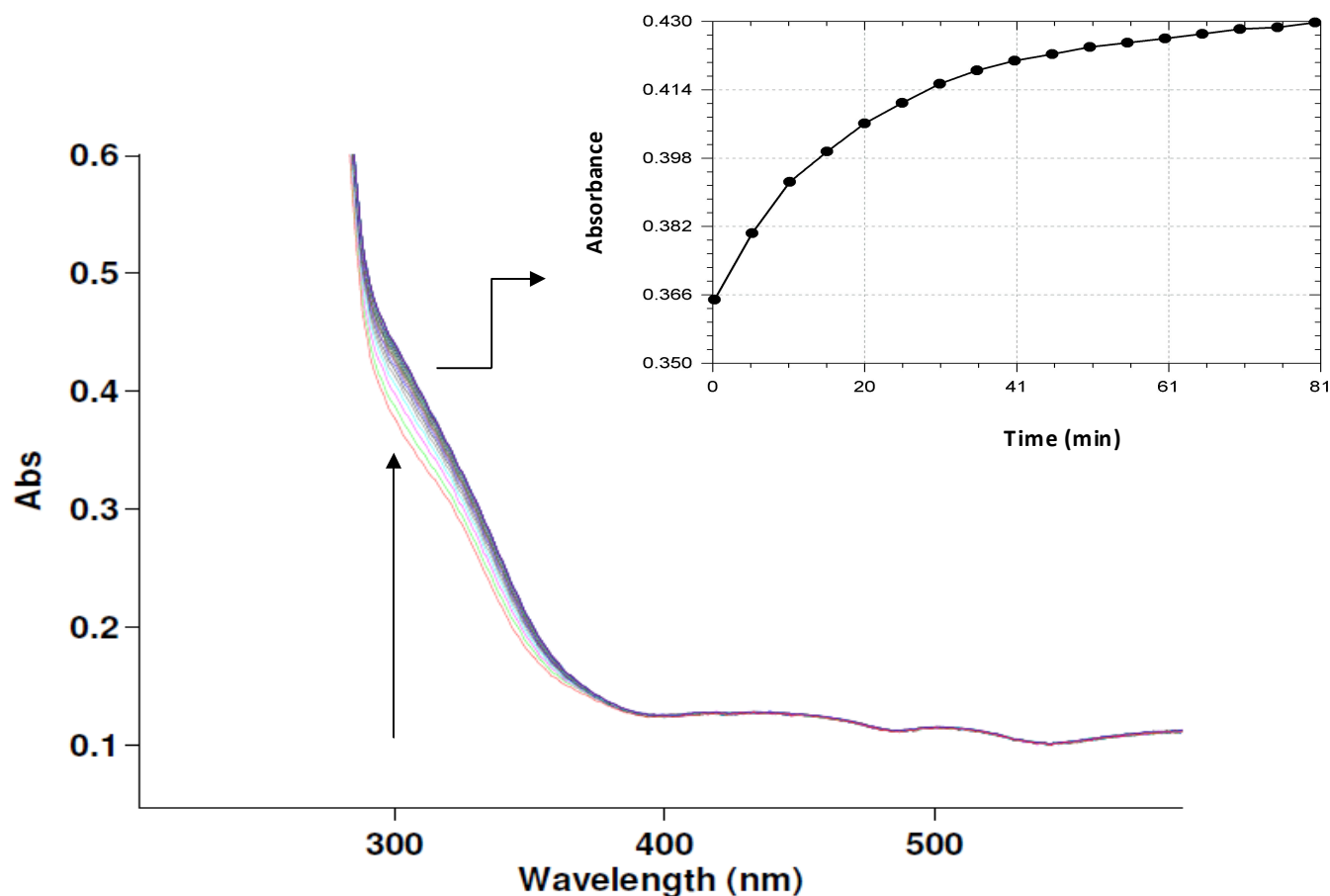**Figure 6.6: A typical UV/VIS spectrum for the methanol substitution reaction of *fac*-[Re(TFA)(CO)₃(CH₃OH)] with Py at 25.1 °C; [Re complex] = 1 x 10⁻⁴ M, [Py] = 0.05 M, Δt = 30 min.**
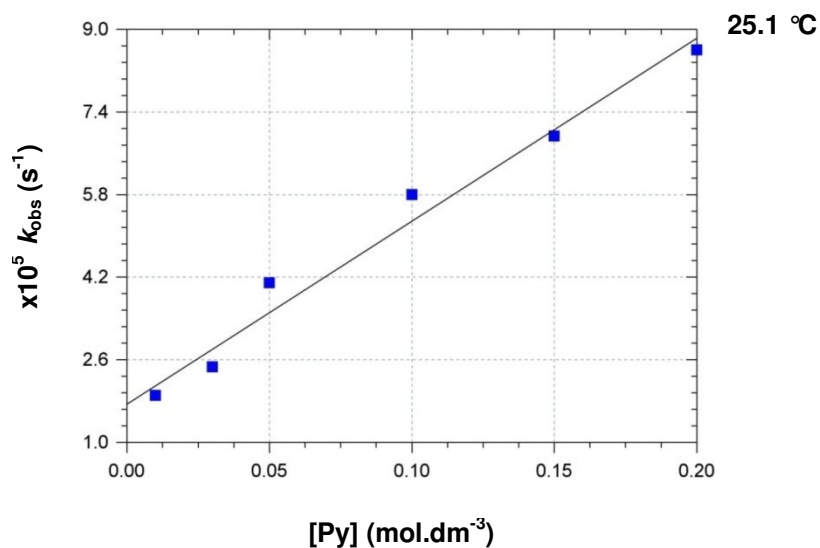
Figure 6.7: Plot of k_{obs} vs [Py] for the reaction between fac-[Re(TFA)(CO)$_3$(CH$_3$OH)] and Py at 25.1 °C; [Re complex] = 1 x 10^{-4} M, (λ = 300 nm) and [Py] = 0.01 – 0.2 M, (Appendix C, Table C.2).
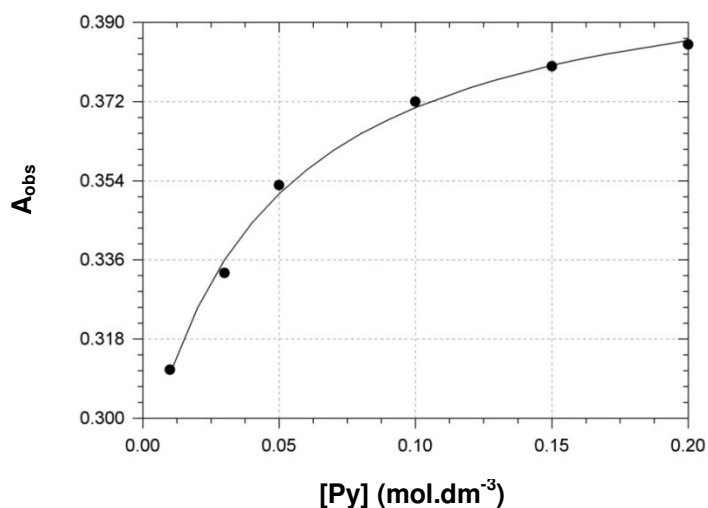
Figure 6.8: Thermodynamic determination of the stability constant (K_1), for the coordinated methanol substitution reaction of fac-[Re(TFA)(CO)$_3$(CH$_3$OH)] by Py from the UV/VIS spectral change vs [Py]; [Re complex] = 1 x 10^{-4} M, 25.1 °C, in methanol.

Table 6.2: The kinetic data of the rate constants for the reaction between fac-[Re(TFA)(CO)$_3$(CH$_3$OH)] and Py at 25.1 °C; [Re complex] = 1 x 10^{-4} M and [Py] = 0.01 – 0.2 M.

Constants	25.1 °C
(10^3) k_1 (M^{-1}.s^{-1})	0.35(3)
(10^3) k_{-1} (s^{-1})	0.018(4)
K_1 (M^{-1})	19(5)
K_1 (M^{-1})[a]	21(4)

[a] Thermodynamically determined

6.3.1.3 The reaction between *fac*-[Re(HFA)(CO)₃(CH₃OH)] and Py in methanol

Figure 6.9 is representative of a typical spectrum of the methanol substitution for the reaction between *fac*-[Re(HFA)(CO)₃(CH₃OH)] and Py in methanol at 25.1 °C. The mechanism of the methanol substitution reaction is confirmed by comparing the final UV/VIS spectrum of the reaction solution to that obtained from the synthesized *fac*-[Re(HFA)(CO)₃(Py)] complex, in Paragraph 4.4.2.9. The k_{obs} *vs* [Py] data obtained at 25.1 °C were fitted to Eq. 6.4. The values of the rate constants obtained from the fits described above are presented in Table 6.5. The k_{obs} values obtained from these fits were plotted against [Py] as indicated in Figure 6.10. This methanol substitution reaction (*fac*-[Re(HFA)(CO)₃(CH₃OH)] is very slow.
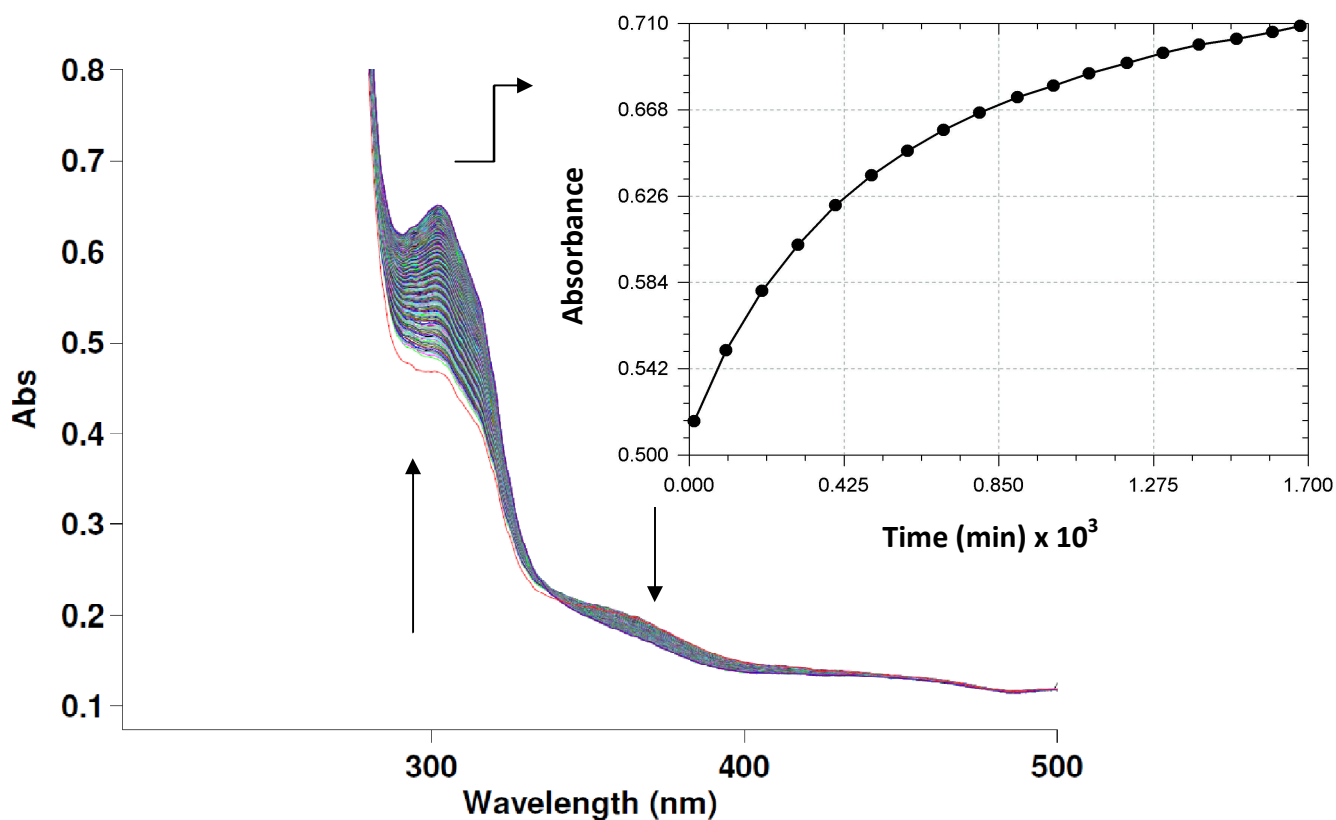
Figure 6.9: A characteristic UV/VIS spectrum for the methanol substitution reaction of *fac*-[Re(HFA)(CO)₃(H₂O)] with Py at 25.1 °C; [Re complex] = 1 x 10⁻⁴ M, [Py] = 0.05 M, Δt = 40 min.
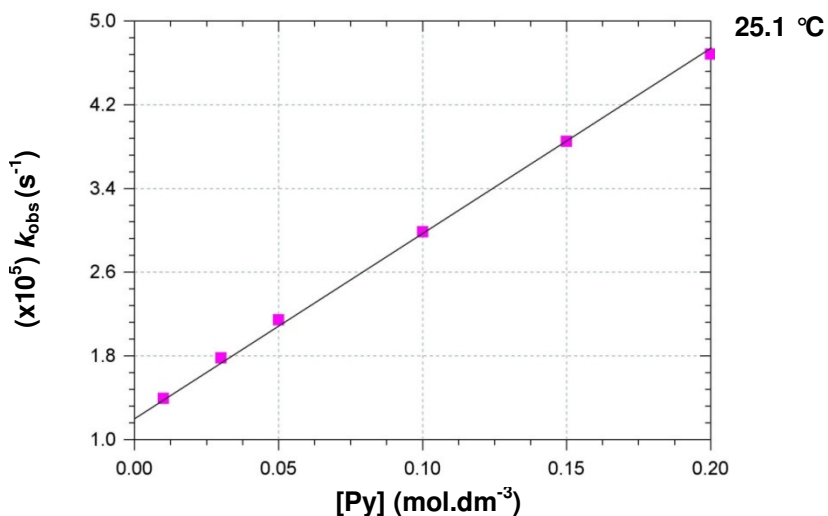
25.1 °C

Figure 6.10: Plot of k_{obs} *vs* [Py] for the reaction between *fac*-[Re(HFA)(CO)$_3$(CH$_3$OH)] and Py at 25.1 °C; [Re complex] = 1 x 10^{-4} M, (λ = 300 nm) and [Py] = 0.01 – 0.2 M, (Appendix C, Table C.3).
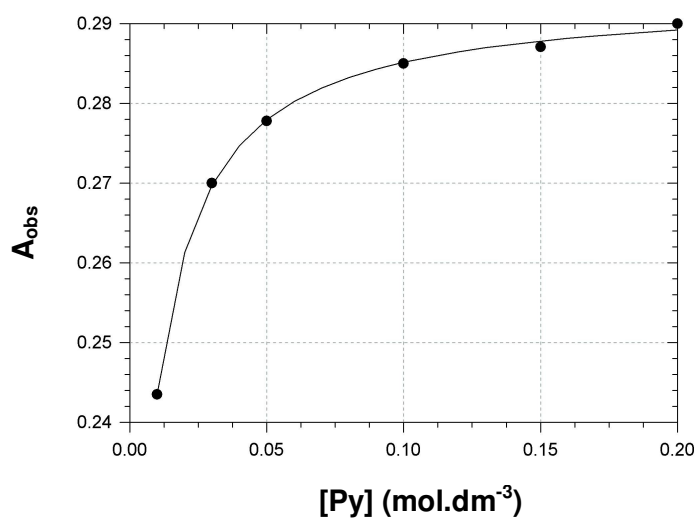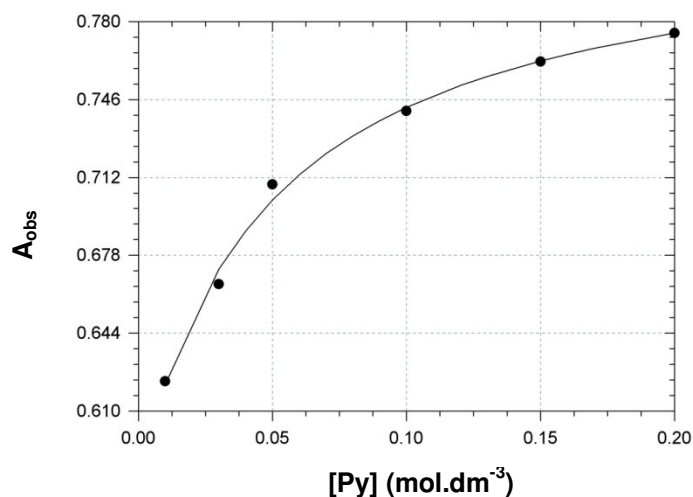

Figure 6.11: Thermodynamic determination of the stability constant (K_1), for the coordinated methanol substitution reaction of *fac*-[Re(HFA)(CO)$_3$(CH$_3$OH)] by Py from the UV/VIS spectral change vs [Py]; [Re complex] = 1 x 10^{-4} M, 25.1 °C, in methanol.

Table 6.3: The kinetic data of the rate constants for the reaction between *fac*-[Re(HFA)(CO)$_3$(CH$_3$OH)] and Py at 25.1 °C; [Re complex] = 1 x 10^{-4} M and [Py] = 0.01 – 0.2 M.

Constants	25.1 °C
(10^3) k_1 (M^{-1}.s^{-1})	0.17(3)
(10^3) k_{-1} (s^{-1})	0.013(4)
K_1 (M^{-1})	13(5)
K_1 (M^{-1})[a]	20(5)

[a] Thermodynamically determined

6.4 Discussion

The three neutral Re(I) tricarbonyl complexes that were selected in this study contains O,O'-donor bidentate ligands, with fluorine atoms (three - TFA and six - HFA) attached to the ligand backbone of two of these complexes. This kinetic study primarily focuses on the influence that the electron withdrawing fluorine atoms (attached to the ligand backbone) have on the rate of methanol substitution, with a neutral Py entering ligand. The electron withdrawing fluorine atoms on the coordinated ligands of fac-[Re(TFA)(CO)$_3$(CH$_3$OH)] and fac-[Re(HFA)(CO)$_3$(CH$_3$OH)] decreases the electron density on the metal centre, causing it to withdraw electron density from the coordinated methanol ligand. An increase in the bond strength of the methanol to the Re(I) together with a decrease in the second order substitution rate constant is indicative of a dissociative activated mechanism, as is expected for octahedral complexes. This point towards a lengthening of the Re-CH$_3$OH bond in the following order: fac-[Re(Acac)(CO)$_3$(CH$_3$OH)] > fac-[Re(TFA)(CO)$_3$(CH$_3$OH)] > fac-[Re(HFA)(CO)$_3$(CH$_3$OH)], i.e. longer Re-CH$_3$OH bonds, faster methanol substitution. The v_{CO} data (Table 6.4) for the different methanol complexes follows a similar trend as the k_1 values obtained. The v_{CO} stretching frequencies increase with increase in the number of fluorine atoms on the ligand backbone. Lower v_{CO} stretching frequencies are indicative of stronger C=O bonds, because of the decrease in the electron density surrounding the metal, thus decreasing the CO back bonding.

The rates, at which these reactions take place is compared in a summarized table, see Table 6.4. The slopes of the graphs in Figure 6.12 also illustrate the difference in the rates of these reactions. The value of the second order rate constant, k_1, obtained for the reaction between fac-[Re(Acac)(CO)$_3$(CH$_3$OH)] and Py is 39 times faster than that of fac-[Re(TFA)(CO)$_3$(CH$_3$OH)] (k_1 = 0.35(3) x 10^{-3} M^{-1}.s^{-1}) and 80 times faster than fac-[Re(HFA)(CO)$_3$(CH$_3$OH)] (k_1 = 0.17(3) x 10^{-3} M^{-1}.s^{-1}).

The negative value of $\Delta S^{\neq}$ (-65(5) J K^{-1} mol^{-1}) generally indicate towards associative type mechanisms; however this should be further investigated since it is not enough information to definitely conclude the mechanism type. High pressure studies need to be conducted in future to further investigate the current findings. Although we obtained a negative $\Delta S^{\neq}$ value, all other factors point towards a dissociative type mechanism. As already mentioned, octahedral

substitution reactions generally follow dissociative type (*D*) mechanisms and the electron withdrawing effects of the fluorine atoms also contribute to the methanol substitution reaction to indicate towards *D* mechanism. Schutte[4] and Kemp[5] also observed negative $\Delta S^{\neq}$ values in their methanol substitution kinetic investigations, using different entering ligands (Py, Br⁻, I⁻, etc.), however they also stated that further studies needs to be done before concluding that the substitution reactions follows an associated type mechanism.

There is a reasonable agreement between the stability constants (K_1) determined kinetically and those determined thermodynamically. In Table 6.4, it is apparent that the K_1 determined for complexes in this study are within range with those determined by Schutte.
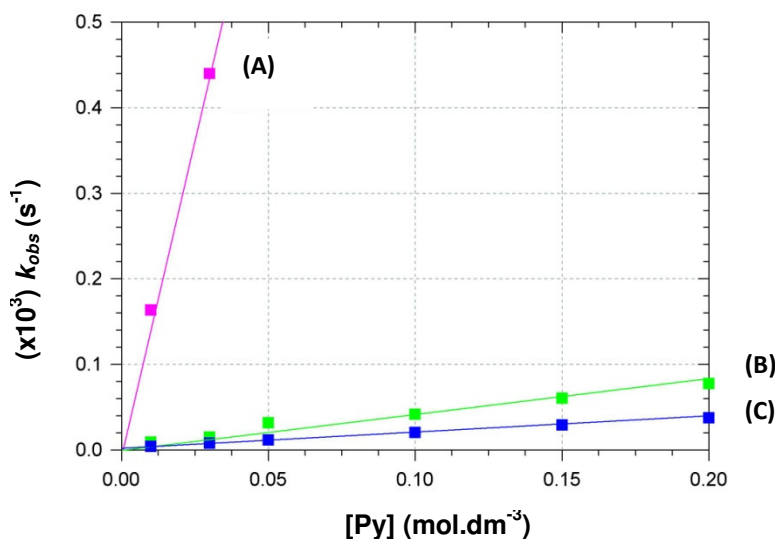
Figure 6.12: An illustration of the difference in the rate constants of the reactions between (A) *fac*-[Re(Acac)(CO)₃(CH₃OH)], (B) *fac*-[Re(TFA)(CO)₃(CH₃OH)] and (C) *fac*-[Re(HFA)(CO)₃(CH₃OH)]; [Re] = 1 x 10⁻⁴ M, and Py at 25.1 °C.

Table 6.4: The rate constants of the methanol substitution reaction between the different *fac*-[Re(O,O')(CO)₃(CH₃OH)] complexes and Py at 25.1 °C, with comparison to other rate constants under similar conditions.

Compounds	(10³) k_1 (M⁻¹.s⁻¹)	(10³) k_{-1} (s⁻¹)	K_1 (M⁻¹)	IR data (v_{CO})
fac-[Re(Acac)(CO)₃(CH₃OH)]	13.7(1)	0.03(2)	457(305)	2015, 1907, 1879
fac-[Re(TFA)(CO)₃(CH₃OH)]	0.35(3)	0.018(4)	19(5)	2018, 1895, 1878
fac-[Re(HFA)(CO)₃(CH₃OH)]	0.17(3)	0.013(4)	13(5)	2025, 1917, 1888
fac-[Re(TropBr₃)(CO)₃(CH₃OH)][a]	20.3(7)	1.6(2)	12(2)	2024, 1886
fac-[Re(Flav)(CO)₃(CH₃OH)][b]	1.38(8) x 10³	0.3(1)	4.6(1) x10³	2015, 1893

[a] TropBr₃ = Tribromotropolonate; [b] Flav = Hydroxyflavonate

General observations:

➢ The rate constants, k_1, for the methanol substitution with Py (for complexes containing O,O'-donor bidentate ligands), obtained in this study are within the same range as those found for similar compounds, under the same reaction conditions (25.0 °C). This is apparent in the k_1 value found by Schutte[8] for *fac*-[Re(TropBr$_3$)(CO)$_3$(CH$_3$OH)] (k_1 = 20.3(7) x 10^{-3} M^{-1}.s^{-1}) and *fac*-[Re(Acac)(CO)$_3$(CH$_3$OH)] (k_1 = 13.7(1) x 10^{-3} M^{-1}.s^{-1}), determined in this study.

➢ The solvent substitution in the compounds containing the electron withdrawing fluorine atoms (*fac*-[Re(TFA)(CO)$_3$(CH$_3$OH)] and *fac*-[Re(HFA)(CO)$_3$(CH$_3$OH)]) is much slower than in the *fac*-[Re(TropBr$_3$)(CO)$_3$(CH$_3$OH)] compound. This is not what one would have expected since the stretching frequencies (v_{CO}) of *fac*-[Re(HFA)(CO)$_3$(CH$_3$OH)] and *fac*-[Re(TropBr$_3$)(CO)$_3$(CH$_3$OH)] are similar and the coordinated ligands (HFA and TropBr$_3$) possess the same pK$_a$ values (pK$_a$ = 4.30)[13]. One should collect X-ray crystallographic data of these two metal complexes, (*fac*-[Re(HFA)(CO)$_3$(CH$_3$OH)] and *fac*-[Re(TropBr$_3$)(CO)$_3$(CH$_3$OH)]) to compare their Re-CH$_3$OH bond lengths, this might explain the difference in their k$_1$ values.

➢ When the number of fluorine atoms on the ligand back bone is halved, the k_1 value doubles. The fluorine atoms activate the metal centre to such an extent that the rate of substitution is almost quadrupled when the coordinated ligand contains no fluorine atoms on its back bone.

➢ As with previous studies by Schutte[4] and Kemp[5], negative ΔS$^≠$ values (associative type mechanisms) were found, thus indicating that more studies should be conducted to definitely establish the mechanism for methanol substitution reaction of Re(I) complexes.

ooOoo

---

[13] Bentley, R.; Thiessen, C. P.; Biosynthesis of Tropolones in Penicilium stipitatum, *Journal of Biological Chemistry*, **1962**

7 *IN VITRO* CANCER SCREENING OF SELECTED COMPOUNDS

7.1 Introduction

For the assaying of the toxicity of the selected compounds, (*fac*-[Re(Acac)(CO)₃Py] and *fac*-[Re(TFA)(CO)₃Py]), in an *in vitro* cell culture experiment, 3-(4,5-dimethylthiazol-2-yl]-2,5-diphenyltetrazoliumbromide (MTT) assay protocol was used. These compounds were tested on oesophageal cancer cell lines.

The MTT assay protocol is a type of colorimetric assay used to measure the activity of enzymes to reduce MTT to formazan dyes, yielding a purple colour. It can be applied in the assessment of the viability (cell counting) and proliferation of cells. The reason for its usefulness in the determination of cytotoxicity of potential medicinal agents and toxic material is the fact that these agents would either stimulate or inhibit cell viability and growth.[1]
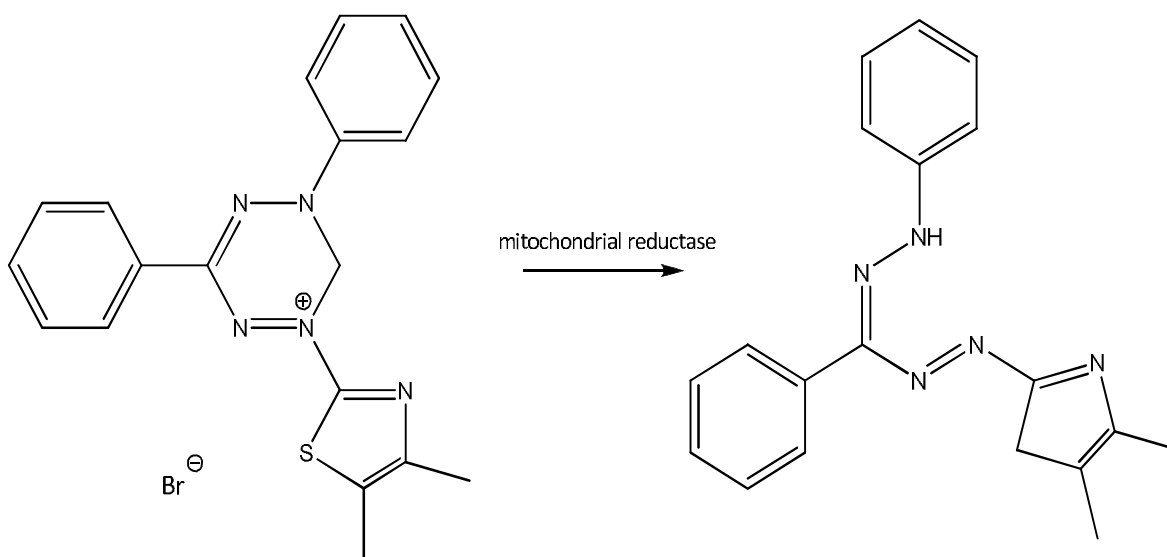
Figure 7.1: The metabolic conversion of MTT to a formazan salt.

---

[1] Mosmann, T.; *Journal of Immunological Methods*, 65, 55-63, **1983**

The general principle of MTT assay protocol is based on the addition of MTT solution to the cell cultures in microplates, followed by a 4 hour incubation period. The MTT is converted into a coloured, water-insoluble formazan salt by the metabolic activity (see Figure 7.1) of viable cells.[2] The insoluble formazan is dissolved by adding a solvent (normally dimethyl sulfoxide) and quantified by an ELISA plate reader at 550-600 nm.

7.2 Experimental

The oesophageal cancer cell lines were obtained from The University of Cape-Town (UCT), whereby cells were cultured as usual prior to subjection to a "treatment". Normally the cells are carefully transferred to a 96-well plate for treatment. After the treatment process, the MTT assay is used to check for cell survival, viability or proliferation. It is known that MTT can be metabolized by all living cells; therefore this assay can be used with all cell types. The procedure entails the removal of the medium from the cells, followed by rinsing with trypsin and trypsinize. The trypsin is then quenched and the cells are spun down. The cells are re-suspended in a fresh medium followed by a cell count determination (optimum count is 1 500 cells per 90 µL). In triplicate, 90 µL of the cell suspension is transferred into a microplate. Blank wells contained complete medium without cells. Cells are allowed to settle by incubation for 24 hours at 37 °C. The compounds were prepared at concentrations ranging from 1×10^{-4} µM to 1 000 µM. The compounds (10 µL) were added to the cells and incubated for 48 hours at 37 °C. MTT reagent (Roche diagnostic) was then added to the wells and incubated for a further 4 hours at 37 °C. Solubilisation solution (100 µL) was then added to the wells followed by a further incubation for 16 hours at 37 °C. The plates were then quantified at 595 nm.

---
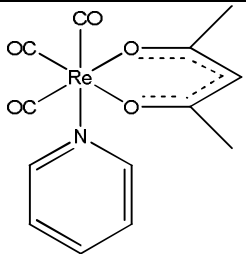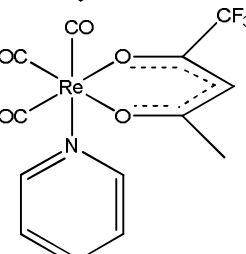
[2] Cory, A. H.; Owen, T. C.; Barltrop, J. A; Cory, J. G; *Cancer Communications*, 3, 7, 207-212, **1991**

7.3   Results and discussion

According to the Food and drug administration (FDA), the IC_{50} value represents the concentration of a drug that is required for 50 % inhibition, *in vitro*. The IC_{50} value of two compounds was determined using oesophageal cancer cell lines, with an incubation period of approximately 6 days.

Table 7.1: IC_{50} values offor a selection of compounds on oesophageal cancer cell lines.

Compound	Chemical structure	IC_{50} value (µM)
fac-[Re(Acac)(CO)$_3$Py]		14.92
fac-[Re(TFA)(CO)$_3$Py]		16.13

IC50 14.92
95% CI 0.001065 to
208959
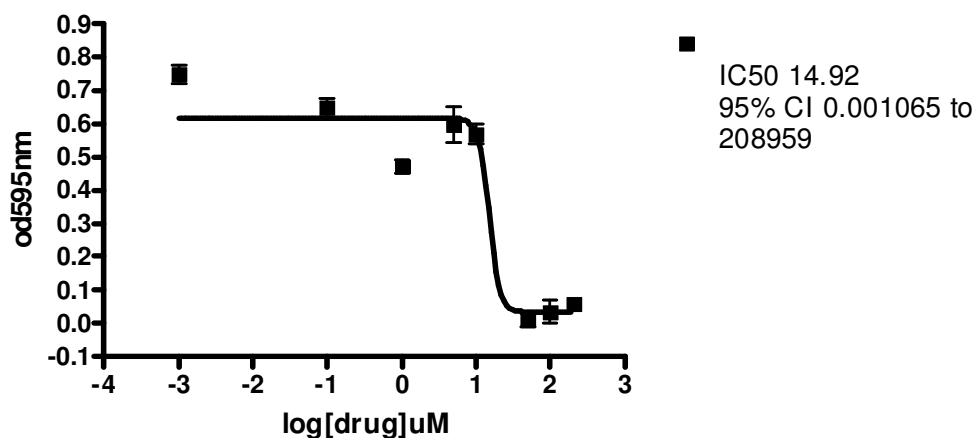
Figure 7.2: Graphical illustration of the determination of the IC_{50} value of *fac*-[Re(Acac)(CO)$_3$Py].
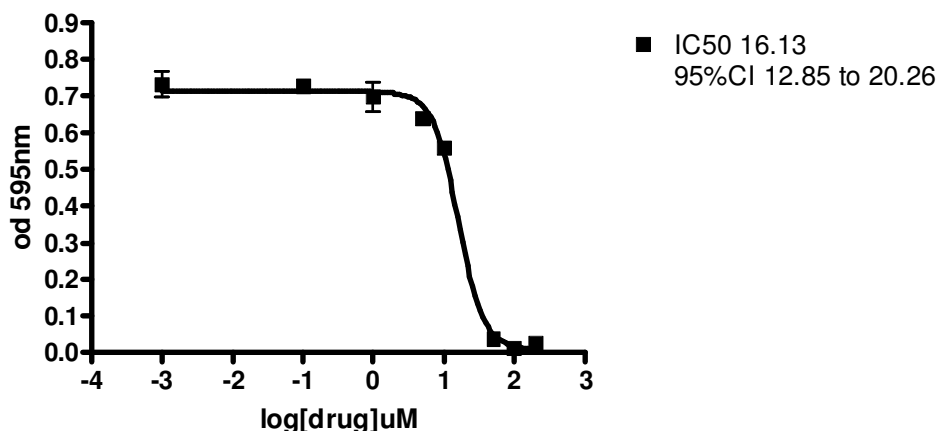
Figure 7.3: Graphical illustration of the determination of the IC$_{50}$ value of *fac*-[Re(TFA)(CO)$_3$Py].

These experiments were done in triplicate and the results are reported in Table 7.1. Generally, IC$_{50}$ values can be classified as follows: high (IC$_{50}$ < 1 μM); moderate (1μM < IC$_{50}$ < 10 μM) and low (IC$_{50}$ > 10 μM). The compounds tested in this study, did not show any reactivity towards inhibition, with IC$_{50}$ values of 14.92 and 16.13 (see Figures 7.2 and 7.3) for *fac*-[Re(Acac)(CO)$_3$Py] and *fac*-[Re(TFA)(CO)$_3$Py] respectively.

7.4   Conclusion

From the results it is apparent that none of the two compounds show any significant toxicity (IC$_{50}$ value of < 1 μM) to the selected cell line. There are however other possibilities for exploring the toxicity of these compounds. This can be done by linking the radioactive nuclide to *fac*-[Re(Acac)(CO)$_3$Py] and *fac*-[Re(TFA)(CO)$_3$Py] *via* a linker on the backbone, to essentially use them as potential imaging agents or radiotherapeutics.

There has not been much success in the clinical assessments of rhenium compounds as potential radiopharmaceuticals, however scientists still believe that rhenium can be used in the application of therapeutic agents.[3,4]

ooOoo

---

[3] Dwyer, R. M.; Havelin, R.; Morris, J. C.; O'Flathata, C.; Miller, B.; Liu, Z.; Foley, M.; Barrett, H. H.; Murphy, M.; Barry, F. P.; O'Brien, T.; Kerin, M. J.; *Cancer Res.*, 71, Supl. 1; Abstract 5392, **2011**

[4] Zahnd, C.; Kawe, M.; Stumpp, M. T.; Deasquale, C.; Tomskvic, R.; Nagy-Davidescu, G.; Dreier, B. Schibli, R.; Binz, H.K.; Waibel, R; Plückthun, A.; *Cancer Res*. 70, 1595-1605, **2010**

8 CRYTICAL EVALUTION

8.1 Introduction

The aim of this study was to gain additional information on the characteristics (coordinative and chemical behaviour) of rhenium complexes, fac-[Re(CO)$_3$(L,L')X]$^{n-1}$ (with L,L' = O,O'-Bid or N,O-Bid, X = H$_2$O, Br$^-$ and Py, n = 0, +1). Since rhenium tricarbonyl complexes are explored as a platform in the development of radiopharmaceuticals (therapeutic and/or diagnostic radiopharmaceuticals), biologically active bidentate ligands were also coordinated to it which was one of the aims of this study. The synthesis of three complexes of the form fac-[^{99m}Tc(CO)$_3$(O,O')H$_2$O] (with O,O' = Acac, TFA, HFA) was one of the objectives. An investigation into the mechanistic pathway of fac-[Re(CO)$_3$(O,O')CH$_3$OH] (with O,O' = Acac, TFA, HFA), which involves the substitution of the methanol ligand with monodentate ligand, pyridine, was one of the main objectives. The kinetic investigations yielded more insight on the equilibrium and stability constants of these complexes, thus clarifying the stability of these compounds. By means of the MTT assay protocol, cell studies were performed on selected synthesized compounds synthesized, to investigate their toxicity on oesophageal cancer cell lines.

8.2 Evaluation

8.2.1 Synthesis and crystallographic work

A large portion of the initial objectives of this study has been met. The synthesis and characterisation of two new O,O' bidentate ligand containing complexes, fac-[Re(TFA)(CO)$_3$(Py)] and fac-[Re(HFA)(CO)$_3$(Py)], by means of X-ray crystallography, ^{1}H- and ^{13}C NMR, UV/VIS and IR, have been added to this under explored research field. The crystal structures of these two complexes yielded some unexpected results: the electron withdrawing fluoride atoms did not

have a significant influence on the bond lengths within these complexes (in their solid state); however a significant difference in the bond angles was noticed. The isolated products of the rhenium tricarbonyl species containing the β-diketones (Acac, TFA and HFA), with a monodentate methanol ligand in the axial position aided in the verification of the substitution mechanism. Very little work has been done on the substitution kinetics of rhenium tricarbonyl compounds and should be expanded in future. The stretching frequencies (v_{CO}) of the rhenium complexes yielded very interesting results. The v_{CO} of the complexes increased with increase in the number of fluoride atoms on the ligand backbone: *fac*-[Re(HFA)(CO)$_3$(X)]^n > *fac*-[Re(TFA)(CO)$_3$(X)]^n > *fac*-[Re(Acac)(CO)$_3$(X)]^n, with X = Br$^-$, Py, H$_2$O. The electron withdrawing fluoride atoms decrease the electron density surrounding the rhenium metal core, thus decreasing the CO back-bonding. The monodentate ligands on the axial position also have an influence on the v_{CO} of the complexes. They were found to increase in the following order: X = Py > H$_2$O > Br$^-$.

The formation of *fac*-[^{99m}Tc(Acac)(CO)$_3$(H$_2$O)], *fac*-[^{99m}Tc(TFA)(CO)$_3$(H$_2$O)] and *fac*-[^{99m}Tc(HFA)(CO)$_3$(H$_2$O)] was successfully established by means of reverse phase TLC. It would be advantageous to attempt to isolate these complexes for characterisation with X-ray crystallography, as this would give more insight into its structural orientation.

8.2.2 Substitution kinetics

The reactivity of a selection of complexes was evaluated by means of kinetic studies, which formed an integral part of this study. A kinetic study of the methanol substitution by pyridine as the entering ligand were successfully investigated on *fac*-[Re(Acac)(CO)$_3$(CH$_3$OH)], *fac*-[Re(TFA)(CO)$_3$(CH$_3$OH)] and *fac*-[Re(HFA)(CO)$_3$(CH$_3$OH)]. Interesting results were found, with regards to the effect of the fluorine atoms (attached to the coordinated ligands of *fac*-[Re(TFA)(CO)$_3$(CH$_3$OH)] and *fac*-[Re(HFA)(CO)$_3$(CH$_3$OH)]) on the rate of the substitution reactions. Their (fluorine atoms) influence yielded the following results, with respect to the k_1, k_1 = *fac*-[Re(Acac)(CO)$_3$(H$_2$O)] > *fac*-[Re(TFA)(CO)$_3$(H$_2$O)] > *fac*-[Re(HFA)(CO)$_3$(H$_2$O)]. This is directly indicative of the Re-CH$_3$OH bond strength, resulting from the electron density that surrounds the metal centre. Upon the determination of the activation parameters, a negative $\Delta S^{\neq}$ value was obtained, indicative of an activated associative type mechanism, however this is

not applicable to the kinetic substitution reactions investigated in this study. This finding needs further investigation in future, since the methanol substitution reactions of the octahedron Re(I) complex are dissociative type mechanisms. The influence that the fluorine atoms attached to the coordinated ligand have on the methanol substitution can be further investigated by using various other entering ligands (e.g. halides and other neutral compounds).

8.2.3 Cell study

The toxicity effects of selected coordinated compounds, *fac*-[Re(Acac)(CO)$_3$(Py)] and *fac*-[Re(TFA)(CO)$_3$(Py)], were tested on oesophageal cancer cell lines, using the MTT assay protocol. The results were not promising, because no significant influences on the cancer cells were observed, however, this should not reduce interest to explore rhenium tricarbonyl complexes as possible radiopharmaceuticals.

8.3 Future work

Coordinating a wide range of biologically active bidentate ligands (N,O-, O,O'-, N,N'-, S,S'- donor bidentate ligand systems) to the Re-tricarbonyl core should be a major objective in future. This would include the use of compounds like dopamine, ephedrine, epinephrine and catechol. An interesting scope for future would be to synthesize and characterise more Re(I) complexes that contain S,S'- donor bidentate ligands. One could also explore the possibility of synthesising and isolating compounds of the form [Re(CO)$_3$(OH$_2$)$_2$L] (L = different monodentate ligands), as this would provide a very interesting range for future studies.

Another aim for future research would be to synthesize *fac*-[^{99m}Tc(L,L')(CO)$_3$(H$_2$O)] (with L,L' = O,O'-, N,O- and N,N'-donor Bid) complexes and characterise it by means of HPLC. Isolation of these complexes, using X-ray crystallography as a characterisation method should be an objective, since this will be a method to confirm the assumption that rhenium and technetium have similar chemical tendencies.

Further investigations regarding the methanol substitution kinetics of *fac*-[Re(O,O')(CO)$_3$(CH$_3$OH)] (O,O' = Acac, TFA and HFA) complexes should be done, using various entering ligands, such as Br$^-$ and other neutral complexes, to establish the affect of the

fluorine atoms on the kinetic rate constants. High pressure kinetic studies can increase the knowledge on the mechanism of methanol substitution reactions. In an attempt to confirm the reverse reaction rates (k_{-1}) and the stability constants (K_1) obtained in this study, one could do a study of solvolysis of the substitution products.

More cell studies should be conducted on the remaining Re(I) compounds synthesized in this study, especially on the *fac*-[Re(Eph)(CO)$_3$(H$_2$O)] complex, since it contains a biologically active (ephedrine) coordinated ligand.

<p style="text-align:center">ooOoo</p>

APPENDIX A

Table A.1: Atomic coordinates (x 10^4) and equivalent isotropic displacement parameters (Å^2 x 10^3) for *fac*-[Re(TFA)(CO)$_3$Py]. U(eq) is defined as one third of the trace of the orthogonalized U^{ij} tensor.

	x	y	z	U(eq)
C(1)	3568(3)	60(7)	-476(3)	29(1)
C(2)	3352(3)	1319(6)	313(3)	21(1)
C(3)	3897(3)	2909(6)	641(3)	23(1)
C(4)	3793(3)	4120(6)	1371(3)	21(1)
C(5)	4426(3)	5780(7)	1659(4)	29(1)
C(6)	2715(3)	553(6)	2774(3)	22(1)
C(7)	1608(3)	3619(6)	2583(3)	19(1)
C(8)	1142(3)	508(6)	1529(3)	18(1)
C(9)	959(3)	3368(6)	-305(3)	18(1)
C(10)	567(3)	4488(6)	-1089(3)	19(1)
C(11)	777(3)	6403(6)	-1093(3)	21(1)
C(12)	1372(3)	7145(5)	-285(3)	21(1)
C(13)	1734(3)	5963(6)	479(3)	19(1)
O(1)	2693(2)	826(4)	638(2)	19(1)
O(2)	3214(2)	4095(4)	1875(2)	19(1)
O(3)	3032(2)	-437(5)	3404(2)	36(1)
O(4)	1301(2)	4540(4)	3090(2)	27(1)
O(5)	548(2)	-508(4)	1444(2)	24(1)
F(1)	3971(3)	7446(4)	1556(3)	62(1)
F(2)	4843(2)	5667(5)	2568(2)	59(1)
F(3)	5014(2)	5958(6)	1124(3)	68(1)
Re	2133(1)	2186(1)	1712(1)	15(1)
N	1538(2)	4066(5)	481(2)	15(1)

Table A.2: Anisotropic displacement parameters ($Å^2$ x 10^3) for *fac*-[Re(TFA)(CO)₃Py].

	U^{11}	U^{22}	U^{33}	U^{23}	U^{13}	U^{12}
C(1)	32(3)	29(2)	29(2)	-2(2)	15(2)	5(2)
C(2)	23(2)	20(2)	19(2)	4(2)	4(2)	8(2)
C(3)	17(2)	31(2)	24(2)	2(2)	10(2)	-2(2)
C(4)	17(2)	22(2)	24(2)	7(2)	3(2)	-1(2)
C(5)	26(3)	31(2)	33(3)	-1(2)	11(2)	-10(2)
C(6)	22(2)	20(2)	25(2)	-1(2)	5(2)	-2(2)
C(7)	22(2)	17(2)	20(2)	3(2)	7(2)	-3(2)
C(8)	24(2)	15(2)	15(2)	-1(2)	7(2)	2(2)
C(9)	22(2)	15(2)	17(2)	-2(2)	7(2)	-2(2)
C(10)	20(2)	21(2)	15(2)	-2(2)	4(2)	1(2)
C(11)	26(2)	17(2)	20(2)	4(2)	7(2)	2(2)
C(12)	25(2)	11(2)	27(2)	-1(2)	11(2)	-1(2)
C(13)	21(2)	14(2)	22(2)	-5(2)	6(2)	-3(2)
O(1)	23(2)	16(1)	21(2)	-1(1)	9(1)	1(1)
O(2)	17(2)	20(1)	21(2)	-2(1)	6(1)	-5(1)
O(3)	39(2)	35(2)	30(2)	12(2)	0(2)	2(2)
O(4)	36(2)	22(2)	30(2)	-5(1)	20(2)	0(1)
O(5)	22(2)	20(2)	31(2)	-3(1)	9(1)	-7(1)
F(1)	50(2)	28(2)	104(3)	4(2)	11(2)	-9(2)
F(2)	59(2)	57(2)	50(2)	-1(2)	-9(2)	-25(2)
F(3)	60(2)	70(2)	88(3)	-19(2)	45(2)	-34(2)
N	18(2)	15(2)	12(2)	-1(1)	5(1)	0(1)
Re	17(1)	12(1)	16(1)	-1(1)	6(1)	-2(1)

Table A.3:   Bond distances (Å) for *fac*-[Re(TFA)(CO)₃Py].

Bond	Distance (Å)	Bond	Distance (Å)
C(2)-O(1)	1.263(5)	C(8)-O(5)	1.150(5)
C(2)-C(3)	1.409(6)	C(8)-Re	1.906(4)
C(2)-C(1)	1.513(6)	C(13)-N	1.360(5)
C(3)-C(4)	1.369(6)	C(12)-C(13)	1.370(6)
C(3)-H(3)	0.9300	C(13)-H(13)	0.9300
C(4)-O(2)	1.269(5)	C(11)-C(12)	1.392(6)
C(4)-C(5)	1.514(6)	C(12)-H(12)	0.9300
C(1)-H(1A)	0.9600	C(10)-C(11)	1.377(6)
C(1)-H(1B)	0.9600	C(11)-H(11)	0.9300
C(1)-H(1C)	0.9600	C(9)-C(10)	1.376(6)
C(5)-F(2)	1.298(6)	C(10)-H(10)	0.9300
C(5)-F(3)	1.317(5)	C(9)-N	1.347(5)
C(5)-F(1)	1.353(6)	C(9)-H(9)	0.9300
C(6)-O(3)	1.144(5)	N-Re	2.202(3)
C(6)-Re	1.932(5)	O(1)-Re	2.135(3)
C(7)-O(4)	1.143(5)	O(2)-Re	2.117(3)
C(7)-Re	1.906(4)		

Table A.4:   Bond angles (°) for *fac*-[Re(TFA)(CO)₃Py].

Bond angle	Angle (°)	Bond angle	Angle (°)
O(1)-C(2)-C(3)	125.0(4)	C(10)-C(11)-C(12)	118.2(4)
O(1)-C(2)-C(1)	116.3(4)	C(10)-C(11)-H(11)	120.9
C(3)-C(2)-C(1)	118.7(4)	C(12)-C(11)-H(11)	120.9
C(4)-C(3)-C(2)	124.6(4)	C(9)-C(10)-C(11)	119.6(4)

C(4)-C(3)-H(3)	117.7	C(9)-C(10)-H(10)	120.2
C(2)-C(3)-H(3)	117.7	C(11)-C(10)-H(10)	120.2
O(2)-C(4)-C(3)	129.2(4)	N-C(9)-C(10)	122.9(4)
O(2)-C(4)-C(5)	111.3(4)	N-C(9)-H(9)	118.6
C(3)-C(4)-C(5)	119.5(4)	C(10)-C(9)-H(9)	118.6
C(2)-C(1)-H(1A)	109.5	C(9)-N-C(13)	117.3(3)
C(2)-C(1)-H(1B)	109.5	C(9)-N-Re	120.8(3)
H(1A)-C(1)-H(1B)	109.5	C(13)-N-Re	121.9(3)
C(2)-C(1)-H(1C)	109.5	C(2)-O(1)-Re	129.3(3)
H(1A)-C(1)-H(1C)	109.5	C(4)-O(2)-Re	126.7(3)
H(1B)-C(1)-H(1C)	109.5	C(7)-Re-C(8)	87.55(17)
F(2)-C(5)-F(3)	108.3(4)	C(7)-Re-C(6)	90.32(18)
F(2)-C(5)-F(1)	106.8(4)	C(8)-Re-C(6)	87.88(18)
F(3)-C(5)-F(1)	105.9(4)	C(7)-Re-O(2)	92.70(14)
F(2)-C(5)-C(4)	111.4(4)	C(8)-Re-O(2)	178.20(14)
F(3)-C(5)-C(4)	114.4(4)	C(6)-Re-O(2)	93.89(15)
F(1)-C(5)-C(4)	109.7(4)	C(7)-Re-O(1)	174.14(14)
O(3)-C(6)-Re	177.7(4)	C(8)-Re-O(1)	94.59(14)
O(4)-C(7)-Re	177.4(3)	C(6)-Re-O(1)	95.20(15)
O(5)-C(8)-Re	178.3(4)	O(2)-Re-O(1)	84.99(11)
N-C(13)-C(12)	122.5(4)	C(7)-Re-N	91.68(15)
N-C(13)-H(13)	118.8	C(8)-Re-N	94.55(15)
C(12)-C(13)-H(13)	118.8	C(6)-Re-N	176.91(15)
C(13)-C(12)-C(11)	119.6(4)	O(2)-Re-N	83.67(12)
C(13)-C(12)-H(12)	120.2	O(1)-Re-N	82.72(11)
C(11)-C(12)-H(12)	120.2		

Table A.5: Hydrogen coordinates (x 10^4) and isotropic displacement parameters (Å^2 x 10^3) for *fac*-[Re(TFA)(CO)$_3$Py].

	x	y	z	U(eq)
H(2)	4360	3153	341	28
H(4A)	3044	-147	-978	43
H(4B)	3791	-1148	-199	43
H(4C)	4006	677	-751	43
H(21)	2129	6478	1015	23
H(22)	1524	8436	-264	25
H(23)	527	7180	-1621	25
H(24)	164	3954	-1613	22
H(25)	819	2072	-318	21

Table A.6: Hydrogen bonds for *fac*-[Re(TFA)(CO)$_3$Py] [Å and °].

D-H...A	d(D-H)	d(H...A)	d(D...A)	<(DHA)
C(13)-H(13)...F(1)	0.93	2.87	3.614(6)	137.7
C(3)-H(3)...F(3) [a]	0.93	2.55	3.407(6)	152.9
C(1)-H(1A)...O(12) [b]	0.93	2.76	3.651(6)	154.6
C(1)-H(1B)...F(2) [c]	0.93	2.61	3.330(6)	131.6
C(12)-H(12)...O(1) [d]	0.93	2.58	3.360(5)	142.0

Symmetry transformations used to generate equivalent atoms:

a. -x+1,-y+1,-z   b. x,-y+1/2,z-1/2   c. x,y-1,z   d. x,y+1,z

APPENDIX B

Table B.1: Atomic coordinates (x 10^4) and equivalent isotropic displacement parameters (Å^2 x 10^3) for *fac*-[Re(HFA)(CO)₃Py]. U(eq) is defined as one third of the trace of the orthogonalized U^{ij} tensor.

	x	y	z	U(eq)
C(1)	8550(2)	-36(5)	-504(2)	28(1)
C(2)	8350(2)	1264(4)	282(2)	22(1)
C(3)	8921(2)	2747(5)	605(2)	26(1)
C(4)	8751(2)	4090(4)	1263(2)	21(1)
C(5)	9413(2)	5659(5)	1597(2)	28(1)
C(6)	7594(2)	741(5)	2567(2)	26(1)
C(7)	6487(2)	3749(4)	2352(2)	20(1)
C(8)	6107(2)	536(4)	1419(2)	19(1)
C(9)	5972(2)	3322(4)	-363(2)	21(1)
C(10)	5604(2)	4405(4)	-1118(2)	22(1)
C(11)	5802(2)	6352(4)	-1162(2)	22(1)
C(12)	6364(2)	7155(4)	-440(2)	24(1)
C(13)	6699(2)	6000(4)	296(2)	21(1)
O(1)	7651(1)	829(3)	531(1)	20(1)
O(2)	8101(1)	4218(3)	1647(1)	20(1)
O(3)	7903(2)	-125(4)	3197(2)	44(1)
O(4)	6135(1)	4650(3)	2838(1)	27(1)
O(5)	5536(1)	-528(3)	1360(1)	27(1)
F(1)	9052(1)	7410(3)	1605(2)	44(1)
F(2)	9785(1)	5298(3)	2454(1)	43(1)
F(3)	10015(1)	5795(4)	1079(2)	54(1)
F(4)	7971(2)	194(4)	-1237(1)	60(1)
F(5)	8524(2)	-1903(3)	-289(1)	56(1)
F(6)	9302(2)	287(4)	-724(2)	76(1)

Re	7045(1)	2280(1)	1535(1)	16(1)
N	6512(1)	4088(3)	343(2)	16(1)

Table B.2: Anisotropic displacement parameters ($Å^2$ x 10^3) for *fac*-[Re(HFA)(CO)$_3$Py].

	U^{11}	U^{22}	U^{33}	U^{23}	U^{13}	U^{12}
C(1)	25(2)	36(2)	23(2)	-1(1)	5(1)	6(1)
C(2)	23(2)	29(2)	16(2)	1(1)	4(1)	6(1)
C(3)	21(2)	33(2)	25(2)	- 1(1)	6(1)	-3(1)
C(4)	20(2)	26(2)	16(1)	5(1)	-1(1)	-2(1)
C(5)	25(2)	36(2)	24(2)	1(1)	5(1)	-7(1)
C(6)	22(2)	31(2)	26(2)	2(1)	3(1)	-2(1)
C(7)	18(1)	22(2)	20(2)	1(1)	-1(1)	-3(1)
C(8)	21(2)	18(1)	17(1)	-2(1)	4(1)	1(1)
C(9)	22(2)	16(1)	23(2)	0(1)	2(1)	-2(1)
C(10)	22(2)	24(2)	19(2)	-1(1)	-1(1)	-2(1)
C(11)	25(2)	22(2)	18(2)	4(1)	4(1)	1(1)
C(12)	31(2)	15(1)	28(2)	-1(1)	7(1)	- 4(1)
C(13)	24(2)	17(2)	22(2)	-5(1)	4(1)	-5(1)
O(1)	19(1)	21(1)	21(1)	-3(1)	4(1)	1(1)
O(2)	15(1)	25(1)	20(1)	-3(1)	4(1)	-4(1)
O(3)	39(2)	53(2)	37(2)	22(1)	0(1)	5(1)
O(4)	30(1)	29(1)	26(1)	-7(1)	10(1)	0(1)
O(5)	28(1)	26(1)	30(1)	-3(1)	8(1)	-10(1)
F(1)	39(1)	32(1)	57(1)	0(1)	-4(1)	-12(1)
F(2)	39(1)	55(1)	29(1)	6(1)	-11(1)	-16(1)
F(3)	43(1)	77(2)	49(1)	-18(1)	26(1)	-36(1)
F(4)	74(2)	83(2)	19(1)	-8(1)	-7(1)	45(1)
F(5)	101(2)	33(1)	36(1)	-7(1)	19(1)	17(1)

F(6)	51(2)	101(2)	101(2)	-60(2)	49(1)	-28(1)
N	16(1)	16(1)	17(1)	-3(1)	4(1)	-2(1)
Re	15(1)	17(1)	15(1)	-1(1)	3(1)	-1(1)

Table B.3: Bond distances (Å) for *fac*-[Re(HFA)(CO)₃Py].

Bond	Distance (Å)	Bond	Distance (Å)
C(2)-O(1)	1.261(3)	C(8)-O(5)	1.157(3)
C(2)-C(3)	1.394(4)	C(8)-Re	1.896(3)
C(2)-C(1)	1.535(4)	C(13)-N	1.348(4)
C(3)-C(4)	1.395(4)	C(12)-C(13)	1.377(4)
C(3)-H(3)	0.9300	C(13)-H(13)	0.9300
C(4)-O(2)	1.260(3)	C(11)-C(12)	1.386(4)
C(4)-C(5)	1.529(4)	C(12)-H(12)	0.9300
C(1)-F(4)	1.309(4)	C(10)-C(11)	1.376(4)
C(1)-F(5)	1.321(4)	C(11)-H(11)	0.9300
C(1)-F(6)	1.307(4)	C(9)-C(10)	1.384(4)
C(5)-F(1)	1.331(4)	C(10)-H(10)	0.9300
C(5)-F(2)	1.326(4)	C(9)-N	1.344(4)
C(5)-F(3)	1.322(3)	C(9)-H(9)	0.9300
C(6)-O(3)	1.143(4)	N-Re	2.203(2)
C(6)-Re	1.937(3)	O(1)-Re	2.1376(19)
C(7)-O(4)	1.157(3)	O(2)-Re	2.127(2)
C(7)-Re	1.895(3)		

Table B.4: Bond angles (°) for *fac*-[Re(HFA)(CO)₃Py].

Bond angle	Angle (°)	Bond angle	Angle (°)
O(1)-C(2)-C(3)	129.0(3)	C(10)-C(11)-C(12)	118.3(3)
O(1)-C(2)-C(1)	112.5(3)	C(10)-C(11)-H(11)	120.9
C(3)-C(2)-C(1)	118.5(3)	C(12)-C(11)-H(11)	120.9
C(4)-C(3)-C(2)	122.0(3)	C(9)-C(10)-C(11)	119.2(3)
C(4)-C(3)-H(3)	119.0	C(9)-C(10)-H(10)	120.4
C(2)-C(3)-H(3)	119.0	C(11)-C(10)-H(10)	120.4
O(2)-C(4)-C(3)	128.6(3)	N-C(9)-C(10)	123.0(3)
O(2)-C(4)-C(5)	112.2(3)	N-C(9)-H(9)	118.5
C(3)-C(4)-C(5)	119.2(3)	C(10)-C(9)-H(9)	118.5
F(4)-C(1)-F(5)	105.6(3)	C(9)-N-C(13)	117.3(2)
F(6)-C(1)-C(2)	113.5(3)	C(9)-N-Re	120.74(19)
F(4)-C(1)-C(2)	110.3(3)	C(13)-N-Re	121.98(19)
F(5)-C(1)-C(2)	111.4(3)	C(2)-O(1)-Re	127.52(19)
F(6)-C(1)-F(5)	106.8(3)	C(4)-O(2)-Re	128.08(19)
F(6)-C(1)-F(4)	108.9(3)	C(7)-Re-C(8)	87.17(12)
F(2)-C(5)-F(3)	107.9(3)	C(7)-Re-C(6)	89.37(13)
F(2)-C(5)-F(1)	106.7(3)	C(8)-Re-C(6)	89.37(13)
F(3)-C(5)-F(1)	107.2(3)	C(7)-Re-O(2)	93.63(10)
F(2)-C(5)-C(4)	110.6(3)	C(8)-Re-O(2)	179.17(9)
F(3)-C(5)-C(4)	112.9(3)	C(6)-Re-O(2)	91.73(11)
F(1)-C(5)-C(4)	111.2(3)	C(7)-Re-O(1)	175.00(10)
O(3)-C(6)-Re	177.5(3)	C(8)-Re-O(1)	94.62(10)
O(4)-C(7)-Re	178.8(3)	C(6)-Re-O(1)	95.33(11)
O(5)-C(8)-Re	179.1(2)	O(2)-Re-O(1)	84.56(8)
N-C(13)-C(12)	122.7(3)	C(7)-Re-N	92.72(11)
N-C(13)-H(13)	118.7	C(8)-Re-N	95.11(11)

C(12)-C(13)-H(13)	118.7	C(6)-Re-N	175.89(10)
C(13)-C(12)-C(11)	119.6(3)	O(2)-Re-N	84.62(8)
C(13)-C(12)-H(12)	120.2	O(1)-Re-N	82.48(8)
C(11)-C(12)-H(12)	120.2		

Table B.5:   Hydrogen coordinates (x 10^4) and isotropic displacement parameters (Å^2 x 10^3) for *fac*-[Re(HFA)(CO)$_3$Py].

	x	y	z	U(eq)
H(11)	5565	7109	-1662	26
H(9)	5839	2004	-345	25
H(3)	9430	2843	374	31
H(10)	5227	3823	-1590	27
H(12)	6513	8464	-453	29
H(13)	7069	6561	779	25

Table B.6:   Hydrogen bonds for *fac*-[Re(HFA)(CO)$_3$Py] [Å and °].

D-H...A	d (D-H)	d (H...A)	d (D...A)	D-H...A Angle
C3-H3...F3[a]	0.93	2.37	2.725(5)	102
C3-H3...F6[a]	0.93	2.39	2.737(5)	102
C13-H13...O1[a]	0.93	2.49	2.996(4)	114
C11-H11...O5[b]	0.93	2.55	3.196(4)	127

Symmetry transformations used to generate equivalent atoms:

a. x,y,z   b. x, -y + 3/2, z-1/2

APPENDIX C

The aqua substitution reactions of *fac*-[Re(Acac)(CO)$_3$(CH$_3$OH)] by Py was performed at different temperatures. A constant [Re(I)] of 1 x 10^{-4} M was used for all the reactions.

Table C.1.1: [Py] and k_{obs} data of the *pseudo*-first order reaction between *fac*-[Re(Acac)(CO)$_3$(CH$_3$OH)] and [Py] at different temperatures; [Re] = 1 x 10^{-4} M.

[Py] (M)	(x 10^3) k_{obs} (s^{-1})			
	15 °C	25 °C	35 °C	45 °C
0.01	0.073(3)	0.17(4)	0.391(2)	0.76(3)
0.03	0.181(4)	0.441(6)	1.09(2)	2.31(2)
0.05	0.325(4)	0.705(4)	1.67(6)	4.27(5)
0.10	0.63(3)	1.41(40)	3.27(5)	7.49(5)
0.15	0.918(2)	2.06(4)	4.96(6)	11.40(4)
0.20	1.21(2)	2.79(6)	6.40(2)	16.10(4)

Table C.1.2: Eyring plot data of the rate constant for the reaction between *fac*-[Re(Acac)(CO)$_3$(CH$_3$OH)] and [Py] at different temperatures; [Re] = 1 x 10^{-4} M.

1/T (x 10^3 K^{-1})	ln(k$_1$/T)
3.470	-10.773
3.354	-9.988
3.245	-9.169
3.143	-8.365

Table C.2: [Py] and k_{obs} data of the *pseudo*-first order reaction between *fac*-[Re(TFA)(CO)$_3$(CH$_3$OH)] and [Py] at 25 °C; [Re] = 1 x 10^{-4} M.

[Py]	(x 10^3) k_{obs} (s^{-1})
0.01	0.0191(3)
0.03	0.0246(3)
0.05	0.0409(4)
0.10	0.058(10)
0.15	0.0693(8)
0.20	0.0860(4)

Table C.3: [Py] and k_{obs} data of the *pseudo*-first order reaction between *fac*-[Re(HFA)(CO)$_3$(CH$_3$OH)] and [Py] at 25 °C; [Re] = 1 x 10^{-4} M.

[Py]	(x 10^3) k_{obs} (s^{-1})
0.01	0.0139(2)
0.03	0.0178(5)
0.05	0.0214(2)
0.10	0.0299(6)
0.15	0.0385(4)
0.20	0.0468(1)